Copyright is owned by the Author of the thesis. Permission is given for a copy to be downloaded by an individual for the purpose of research and private study only. The thesis may not be reproduced elsewhere without the permission of the Author.

INSTANT MILK POWDER PRODUCTION: DETERMINING THE EXTENT OF AGGLOMERATION

A thesis presented in partial fulfilment of the requirements for the degree of

Doctor of Philosophy
in
Chemical Technology

at Massey University, Palmerston North,
New Zealand.

Anna M Williams

2007

ABSTRACT

Agglomerated milk powders are produced to give improved properties such as flowability, dispersibility, reduced dustiness and decreased bulk density. A key function of these powders is to dissolve "instantly" upon addition to water and because of this they are also called "instant milk powders". They are produced by agglomerating the undersized fines that are returned to the top of the spray drier with milk concentrate droplet spray. Interaction occurs in a collision zone, often with multiple sprays and fines return lines. Agglomeration can be a difficult process to control and operators find it hard to fine tune the process to produce specific powder properties. This work aimed to understand the effects of key droplet and fines properties on the extent of agglomeration to allow a mechanistic understanding of the process.

Three scales of spray drier were investigated in this study with different rates of evaporation; a small scale drier (0.5 – 7 kg water h^{-1}), a pilot scale drier (80 kg water h^{-1}) and a range of commercial production scale driers (4 - 15 000 kg water h^{-1}). A survey of operators of commercial scale driers showed that control of instant milk powder production to influence bulk density is highly intuitive. Fines recycle rates were expected to be important in control of agglomeration processes and were estimated on a specific plant by using the pressure drop measured in the fines return line. A model based on pressure drop along a pneumatic pipeline under-predicted the experimental values for pressure drop due to solids, which means a calibration curve should be generated for each specific drier. Fines recycle rates were predicted to be significantly higher at 95 to 130 % of production rates compared to those expected by operators of 50%.

Experimental measurements agreed with existing models for the effect of temperature on the density and viscosity of milk concentrates. Experimental results showed that the surface tensions of concentrated milks were within the same range as literature values for standard milks below 60°C, but were significantly higher for milk above 60°C. This is thought to be linked to the mechanism of skin formation due to disulphide cross linking at high temperatures and concentrations. Powder properties were also established for selected products produced on the commercial scale driers. These powders were then used in experiments on the two smaller driers. Because collision frequency depends on the velocity and droplet size of sprays; these properties were measured for the small scale drier and estimated, where possible, for the pilot and commercial driers.

The small scale agglomerating spray drier was configured to alter droplet and particle properties when interacting a vertical fines particle curtain with a horizontal spray sheet. An extensive design and improvement process was carried out to ensure the system consistently delivered these streams in a controllable manner. The processes of collision and adhesion occur very quickly inside the spray drier. In order to assess the extent of agglomeration that has occurred, the feed streams must be compared to the final product stream. An ideal way to do this is to use an agglomeration index which

compares the particle size distributions of the feed (fines recycle and spray streams) and the particle size distribution of the product stream (the agglomerated powder). The index described changes between these steams across the particle size distribution and is called an agglomeration efficiency, ξ_g. However, it was found that the presence of fines in the product of the one-pass design obscured the agglomerates formed. The agglomeration efficiency, ξ_g, was modified to become ξ_h which subtracted the fines stream from the agglomerated product distribution. In this way ξ_h models industrial operation where the fines are recycled, by effectively just comparing the spray and product streams entering and leaving the process.

The small scale drier was used for an experimental study on natural and forced agglomeration, where the drier was operated with spray only, then with spray and fines. For natural agglomeration, SEM images of the product powder indicated that little agglomeration occurred between spray droplets. The product yield was unacceptably low (~ 40%) due to adhesion of spray droplets to the drying chamber wall opposing the horizontal spray. When the fines curtain was introduced in the forced agglomeration experiments, product yield increased above 50% because the fines acted as collectors for the spray droplets. However, the agglomeration performance of the modified spray drier was lower than expected. The equipment design was then optimised by considering three key issues; fines dispersion, droplet dispersion and stickiness, and agglomerate breakdown. Final experiments studied agglomeration at low fines to spray mass flux ratios and showed that increasing the fines size had a positive effect on agglomeration efficiency, ξ_h.

The agglomeration study at pilot scale identified the effect of key variables, total solids, concentrate and fines flow rate, and fines size on the agglomeration efficiency. A dimensionless flux approach was used to explain the experimental results. The fines to spray mass flux ratio and the projected area flux ratio (at constant concentrate flow rate) were found to be the most suitable to represent the physical processes during agglomeration. Experimental results showed that a higher dimensionless flux resulted in more agglomeration and as well as small fines size and atomising low solids concentrate. The critical Stokes number highlighted the importance of particle size and collision velocity on the outcome of the collision as well as the importance of stickiness on adherence following the collision. A statistical analysis established a relational model for predicting the agglomeration efficiency based on fines size, total solids and the fines to spray mass flux ratio.

This thesis has gained insight into agglomeration processes during spray drying and knowledge about how to define the extent of agglomeration. Practical findings from this research can have a significant impact on successful spray drying operation for instant powders. There are some practical steps to be taken industrially to promote the control of agglomerating spray driers. The first step is to measure and control the flow of fines recycled to the top of the spray drier. The next step is to validate the findings at industrial scale and link the agglomeration index to the bulk powder properties. However, there are many challenges that remain to be tackled in the area of milk powder agglomeration. Milk powder agglomeration at the top of the spray drier is a complex process involving many different variables. A more detailed study of the micro processes that occur during agglomeration will give increased understanding of the relationships between key operating variables and agglomerate properties.

ACKNOWLEDGEMENTS

"Particles can't read" so just writing the word agglomeration on a piece of equipment will not necessarily ensure this is the process that will happen inside. This quote certainly sums up my thesis, which would have told quite a different story if only particles could read.

A PhD is a rollercoaster ride of success and failure, however this journey is never completed alone. There are many people who deserve to be thanked for the part they have played along the way. Of course, I would like to thank all of my supervisors for their contributions; your discussions, guidance and patience was appreciated.

Firstly, thanks to my primary supervisor Dr. Jim Jones, for convincing me to do this project and for helping me seize opportunities. I have truly valued the support, advice and encouragement that you have given me. Also thanks go to Associate Professor Tony Paterson for your enthusiasm and general support and for challenging my ideas. Finally to my industry supervisor Dr. David Pearce, thank you for all of your assistance and practical advice; it was invaluable.

Special thanks to Associate Professor John Abrahamson and Mr Trevor Berry from the University of Canterbury for their assistance with the high speed camera for capturing the size and velocity of sprays.

Thanks to the staff in the Institute of Technology and Engineering at Massey University. I am also grateful for the other postgraduate students who helped me survive the process, especially Adi, Amsha, Craig, Jarod, Jeremy, Jenny, Kelly, Rachel, Ros, and Stephen.

There are so many people at Fonterra Palmerston North that I would like to thank for their help and assistance in this project whether it was in the lab, for strange requests or just general friendliness. Thank you all: Amy Yang, Brenda Bowie, Giao Truong, Skelte Anema, Marcel Hollenstein, Robyn Hirst, Liz Nickless, and Barabara Kuhn-Sherlock. Special thanks to Colin Knight for his helpful ideas, kiwi ingenuity and No. 8 wire. Also thanks to Susan Adams, John Grant, Dennis Dugmore and Bill Barnes for their time and humour. At Fonterra Whareroa, thanks to Jason Stevenson and Daniel Parker for their assistance.

I am grateful for the support of my friends and family (the Williams' and the Young's) throughout this project; I certainly could not have done it without you all. Special thanks to my parents and sisters for giving me your love, support and encouragement. Last but not least, thanks to Glen, without your love and understanding, this would not have been possible, thank you for your unconditional support.

TABLE OF CONTENTS

LIST OF FIGURES

LIST OF TABLES

NOMENCLATURE

$\dot{A}$	area flux of powder traversing the spay zone	$m^2\ s^{-1}$
A	area	m^2
A_t	total cross sectional nozzle area	m^2
A_p	particle surface area	m^2
A_{spray}	spray on foot print area of the nozzle onto the powder bed	m^2
Ca	Capillary number	–
C_D	drag coefficient of particle	–
C_D'	modified drag coefficient	–
C_p	specific heat capacity at constant pressure	$J\ kg^{-1}\ K^{-1}$
D	diameter	m
D_0	initial droplet diameter	m
D_{12}	sum of colliding particle radii	m
$D_{3,2}$	Sauter mean diameter	m
$D_{4,3}$	volume weighted mean diameter	m
D_{BET}	BET diameter	m
D_{bridge}	diameter of sinter bridge	m
D_f	diffusion coefficient	$W\ m^{-1}\ K^{-1}$
D_{max}	maximum diameter of droplet	m
DoA	degree of agglomeration	–
$D_{particles}$	volume mean particle diameter of the particles	m
$D_{primary}$	diameter of initial particles	m
D_v	diffusion coefficient of water vapour in air	$W\ m^{-1}\ K^{-1}$
D_w	diffusion coefficient of water vapour through the droplet	$W\ m^{-1}\ K^{-1}$
e	coefficient of restitution	–
E_{in}	heat in inlet air	kW
E_{loss}	heat loss	kW
E_{out}	heat in outlet air	kW
f	frequency	–
F	fines flow rate	$kg\ s^{-1}$
FN	flux number	–
f_n	number of fines particles	–
F_N	total number of fines particles	–
f_p	solids-pipe friction factor	–
F_{PA}	projected area of fines	m^2
F_{pw}	solids-pipe friction force	$Pa\ m^{-1}$
F_t	impact force	$Pa\ m^{-1}$
g	acceleration due to gravity	$m\ s^{-2}$
h	convective heat transfer coefficient	$W\ m^{-2}\ K^{-1}$
h_a	height of granule surface asperities	m
H_{amb}	enthalpy of ambient air	$kJ\ kg^{-1}$
H_{fus}	latent heat of fusion	$J\ kg^{-1}$
H_{in}	enthalpy of inlet air	$kJ\ kg^{-1}$

h_m	convective mass transfer coefficient	W m^{-2} K^{-1}
H_{out}	enthalpy of outlet air	kJ kg^{-1}
k	constant or ratio of specific heats	–
K	consistency coefficient	N s m^{-2}
KD	constant × particle diameter	M
KE_1	kinetic energy before impact	J
KE_2	kinetic energy after impact (droplet is at maximum	J
k_l	thermal conductivity of liquid	W m^{-1} K^{-1}
L	length	m
L_e	equivalent length	m
l_v	friction loss	m^2 s^{-2}
l_w	wetted length of Wilhelmy plate	m
m	mass loading = ratio of M_p to M_g	–
M_A	mass rate of air	kg s^{-1}
M_{atm}	mass flow rate of air through the atomiser	kg s^{-1}
M_c	mass flow rate of concentrate	kg s^{-1}
M_{chute}	mass flow rate of air through the chute	kg s^{-1}
M_f	mass flow rate of fines	kg s^{-1}
M_g	mass flow rate of gas	kg s^{-1}
M_{in}	mass flow rate of inlet air	kg s^{-1}
M_{leak}	mass flow rate of air in due to leakage	kg s^{-1}
m_{obs}	mass of powder added over observed time	kg
M_{obs}	mass flow rate of fines (observed)	kg s^{-1}
M_{out}	mass flow rate of outlet air	kg s^{-1}
M_p	mass flow rate of particles	kg s^{-1}
M_{prod}	mass flow rate of powder production	kg s^{-1}
M_s	mass flow rate of spray	kg s^{-1}
m_t	total mass added	kg
n	power law index	–
$\hat{N}$	number concentration of particles	m^{-3}
$\dot{N}$	number flow rate	s^{-1}
N	number of particles per kilogram	kg^{-1}
Nu	Nusselt number	–
Oh	Ohnesorge number	–
p	mass proportion in the powder	–
P_1	inlet nozzle pressure	Pa
P_2	exit nozzle pressure	
Pr	Prandlt number	–
P_w	Wilhelmy force	N
ΔP	pressure drop	Pa
ΔP_{fg}	pressure drop due to friction of gas	Pa
ΔP_{fs}	pressure drop due to solids friction	Pa
ΔP_g	pressure drop due to gas	Pa
Δp_{hug}	pressure drop due to hold up of gas	Pa

ΔP_{hus}	pressure drop due to hold up of solids	Pa
ΔP_s	pressure drop due to solids	Pa
Q_a	volumetric air rate	$m^3 s^{-1}$
$Q_{a.c}$	volumetric flow rate of curtain air	$m^3 s^{-1}$
Q_{atm}	volumetric flow rate of atomising air	$m^3 s^{-1}$
q_b	binder spray rate	$kg s^{-1}$
Q_l	liquid flow rate	$kg s^{-2}$
r	particle or granule radius	µm
Re	Reynolds number	–
RH	relative humidity	$kg kg^{-1}$
S	spray flow rate	$kg s^{-1}$
Sc	Schmidt number	–
SE_1	the surface energy before impact	J
SE_2	surface energy after impact	J
S_g	geometric standard deviation	–
Sh	Sherwood number	–
s_n	number of spray droplets	
S_N	total number of spray droplets	–
S_{PA}	projected area of spray	m^2
SSA	specific surface area	$m^2 g^{-1}$
St^*	critical Stokes' number	–
Ste	Stefan number	–
St_V	viscous Stokes' number	–
T	temperature	°C
T_{amb}	ambient temperature	°C
T_1	air temperature under sonic conditions	°C
t	time	s
t_{exp}	exposure time	s
T_g	glass transition temperature	°C
T_m	droplet melting temperature	°C
TS	total solids concentration	–
$T_{w.1}$	initial substrate temperature	°C
U	velocity	$m s^{-1}$
u_0	initial relative granule collision velocity	$cm s^{-1}$
U_0	droplet impact velocity	$m s^{-1}$
U_A	velocity of air	$m s^{-1}$
U_{A1}	predicted air exit velocity from the nozzle	$m s^{-1}$
U_{A2}	predicted velocity 50mm from nozzle of air and spray	$m s^{-1}$
$U_{air\ only}$	measured air velocity 50 mm from nozzle without spray	$m s^{-1}$
U_c	collision velocity	$m s^{-1}$
UD	constant, D and overall heat transfer coefficient U	$W K^{-1}$
U_d	droplet velocity	$m s^{-1}$
u_e	excess gas velocity	$m s^{-1}$
U_g	interstitial gas velocity	$m s^{-1}$

U_s	velocity of particles	m s^{-1}
U_T	terminal velocity	m s^{-1}
u_z	velocity of entrained air	m s^{-1}
$u_{zmax\infty}$	centre velocity of the air in the equilibrium state	m s^{-1}
$\dot{V}$	volumetric spray rate of the binder liquid	m^3 s^{-1}
v	specific volume of mixture	m^3 kg^{-1}
V_b^*	dimensionless bridge volume	–
V_b	pendular bridge volume	m^3
V_d	droplet volume	m^3
v_f	specific volume of fat	m^3 kg^{-1}
V_g	volume of gas	m^3
v_i	specific volume of component i	m^3 kg^{-1}
v_{nw}	specific volume of native whey protein	m^3 kg^{-1}
v_{rel}	relative velocity between liquid and air	m s^{-1}
V_s	volume of solids	m^3
v_s	velocity of a single particle	m s^{-1}
$v_{s\infty}$	terminal velocity of a single particle	m s^{-1}
v_z	velocity of the particle in the powder jet	m s^{-1}
$v_{zmax\ infin}$	centre velocity of the particle in the equilibrium state	m s^{-1}
w	width	m
W^*	dimensionless rupture energy	–
W	pendular bridge rupture energy	J
We	Weber number	–
W_{vis}	work done in deforming a droplet against viscosity	J
x	curtain width	m
X_c	dry matter content of concentrate	kg kg^{-1}
X_{casein}	mass concentration of casein	kg L^{-1}
X_{dw}	mass concentration of denatured whey protein	kg L^{-1}
X_{eq}	equilibrium moisture content	kg kg^{-1}
X_{fat}	percentage of fat	–
x_i	percentage of component *i* in the mixture	–
x_l	dry matter fraction of lactose	kg kg^{-1}
X_{milk}	dry matter content of standard milk	kg kg^{-1}
X_{nw}	mass concentration of native whey protein	kg L^{-1}
y	curtain length	m
Y_g	dynamic yield stress	Pa
Z_{12}	collision rate between two particles	m^{-3} s^{-1}

Greek Letters

μ	viscosity	Pa s
μ_g	viscosity at the glass transition temperature	Pa s
μ_l	viscosity of lactose solution	Pa s
μ_{ref}	viscosity of the serum	Pa s
α	shape factor	–

γ	rate of strain	s^{-1}
ε	voidage	–
θ	contact angle	°
θ_a	advancing contact angle	°
ζ_g	agglomeration efficiency using *g* distribution	–
ζ_h	agglomeration efficiency using *h* distribution	–
ρ	density	kg m^{-3}
σ	surface tension	N m^{-1}
σ_l	surface tension of saturated lactose	N m^{-1}
τ	shear stress	Pa
Φ	volume fraction of concentrate	–
Φ_{max}	the maximum volume fraction	–
Φ_{milk}	volume fraction of milk	–
ψ	dimensionless time	–
Ψ_a	dimensionless spray flux	–
δ	thickness of the liquid layer	m

Subscripts

0	before
1	after
a	air
agg	agglomerates
c	concentrate
d	droplet
AE	entrained air
f	fines
g	gas
p	particle or product
s	spray, dried droplets
skim	skim milk
whole	whole milk

Acronyms

AF	agglomeration factor
AP	agglomeration parameter
BET	Brunauer, Emmett, & Teller
DoA	degree of agglomeration
GAB	Guggenheim-Anderson-de Boer
ISMP	instant skim milk powder
IWMP	instant whole milk powder
PSD	particle size distribution
SEM	scanning electron microscopy
SMC	skim milk concentrate
SSA	specific surface area
SSM	standard skim milk
SWM	standard whole milk
WMC	whole milk concentrate

CHAPTER 1

INTRODUCTION

1.1 Problem Definition

Agglomerated or instantised milk powders are produced by the dairy industry to give improved physical properties such as flowability, dispersibility, reduced dustiness and decreased bulk density. Instantised milk powder is obtained by size enlargement using agglomeration and the addition of lecithin (for whole milk powders) to improve wettability. Agglomeration is achieved by returning fines to the top of the spray drier and contacting them with milk concentrate droplets, followed by evaporative drying. This allows small particles to combine and form large, porous, open structures. Instantised milk powders have been produced by Fonterra Co-operative Ltd (Fonterra) for a number of years, however little knowledge has been gained to adequately describe the agglomeration process. Some qualitative relationships have been introduced but they are not widely understood. Therefore, agglomeration can be difficult to control and operators find it hard to fine tune the process to produce specific powder properties and this often results in a low quality product.

The sale price of instant milk powder is dictated by product quality, measured according to a number of key indicators. Reconstitution performance and bulk density are two of these. Neither can be directly related to the operation of the drier but both are related to the structure of the powder. Large porous open agglomerates reconstitute well, have low bulk density and good flowability compared to powder containing single milk powder particles. Therefore standards of reconstitution performance and bulk density have been set and it is in the operator's interest to meet the highest standards as often as possible. Achieving this is difficult without a good knowledge of how the operating variables affect the key indicators of product quality. This thesis assumed that the key indicators of product quality are all related to the structure of the powder defined by the extent to which it is agglomerated. Therefore, this thesis aims to relate the operating conditions of an agglomerating drier to the extent to which the powder is agglomerated.

1.2 Proposed Solution

Currently the operating conditions required to make an acceptable instant milk powder product are assessed qualitatively, without reference to interacting variables. Parameters such as atomisation pressure, air flow or solids concentration are adjusted intuitively to manipulate the physical properties of the product. Traditionally, the processing conditions to manufacture a specific product are determined by trial and error. This approach to optimise bulk density, performance (i.e. reconstitution) and strength can be time consuming and expensive.

An alternative is to take a mechanistic approach to understand the mechanisms responsible for agglomeration at the top of the spray drier. By understanding the mechanisms of collision and adhesion between droplets and particles, an attempt can be made to control the degree of agglomeration. A mechanistic study better lends itself to a laboratory investigation, away from a production environment but still has industrial significance. Identification of practical tools to control agglomeration processes industrially will ensure powders are produced with consistent product properties.

1.3 Economic Benefit

Bulk density control is important for a number of reasons which all have an impact economically:

1. mass of powder in bag vs. size of bag (i.e. consumer perception of head space)
2. influences flow properties
3. wetting during reconstitution

A small but important source of downgrades is from bulk density. To investigate the economic need for this investigation, powders produced at one Fonterra site were investigated. No figures are given for the cost of downgrades due to commercial sensitivity but analysis showed that 25% of all downgrades at this site are due to product not complying with the bulk density specified. This project aims to improve knowledge of agglomeration and reduce the level of bulk density downgrades and to realise the lost opportunity cost due to these downgrades.

1.4 Thesis Objectives

The objective of this research was to identify and understand the important operating parameters that influence the production of agglomerated milk powders in spray driers. To do this requires a deeper understanding of the relevant mechanisms affecting agglomeration at the top of a spray drier. The specific aims of this research are:

1. Benchmark current agglomeration practise by monitoring plant performance
2. Identify the physical properties that impact agglomeration and understanding the physical mechanisms of collision and adhesion
3. Design a spray device and curtain device to study agglomeration at small scale
4. Establish appropriate analysis methods for determining whether agglomeration has occurred and to what extent
5. Determine the influence of droplet and fines properties on the extent of agglomeration
6. Validate these findings at pilot scale
7. Develop useful guidelines to enable improved operation of spray drying and agglomeration equipment to improve product quality and plant productivity.

Due to the complex nature of the agglomeration process, research is required in a number of areas to improve understanding of this process (Verdurmen et al., 2004). Although there is little existing work which specifically addresses agglomeration at the top of the spray drier there is a range of literature in the area of atomisation, droplet drying, collision and adhesion, coalescence and granulation which is discussed in the following chapter.

1.5 Thesis Summary

The thesis is structured in the traditional manner with a detailed literature review, followed by a series of chapters to address each of the objectives listed above. Each chapter also contains literature relevant to the area of investigation; some of this may not be addressed in the initial literature review. Each chapter is outlined briefly below.

Chapter 1 introduces the topic of study by defining the problem and explaining the thesis objectives, as well as the economic benefit and a brief thesis outline. Chapter 2 gives a general review of literature and explains the process of agglomeration in depth. A micro-process approach is taken to ensure all the relevant areas of agglomeration are discussed, from droplet formation and drying, to collision and adhesion of droplets and fine particles, the stickiness phenomenon and final agglomerate properties.

Chapter 3 outlines the current accepted practise for instant milk powder production and knowledge regarding agglomeration processes that exist in industry. This chapter also estimates fines recycle rates in one Fonterra plant and produces a calibration curve of pressure drop vs. mass flow rate. A key aspect of this chapter was the selection of two instant milk powders to investigate in this thesis.

Chapter 4 presents the relevant physical properties of milk concentrates (including density, surface tension and viscosity) used to manufacture the previously selected instant milk powders. The properties of the milk concentrate sprays (droplet size and velocity) were also investigated.

Chapter 5 uses information from previous chapters to design the spray and curtain devices in order to study the relevant operating variables to agglomeration performance. This required extensive modification of an existing small scale spray drier to allow delivery of a curtain of fines particles and a sheet of spray droplets. Experiments were performed to quantify performance as a function of the operating variables.

Chapter 6 develops methods for analysis for agglomeration performance using an agglomeration index. A parameter called the agglomeration efficiency is defined which quantifies the changes between the particle size distributions of droplets, fines and agglomerates and allows comparison between all processing scales

Chapter 7 details the small scale study using the modified design presented in Chapter 5. A series of experiments were carried out to fine tune this equipment to determine the optimum setup for investigating agglomeration. The analysis methods developed in Chapter 6 were used to compare results.

Chapter 8 describes the pilot scale study which includes the effect of total solids, concentrate and fines flow rates, and fines size on agglomeration efficiency. A dimensionless flux was used to discuss the key mechanisms and a statistical analysis described how interaction variables affect agglomeration efficiency.

Chapter 9 summaries the key conclusions of the thesis. Practical findings are also discussed with application to industry. It also includes recommendations for further work and addresses the final objective to provide useful guidelines for operation of industrial agglomeration spray driers.

CHAPTER 2

LITERATURE REVIEW

Agglomeration is a term used to describe the size enlargement process where single particles become bonded to form a product with a larger mean particle size. Agglomeration at the top of a spray drier involves contact between milk concentrate droplets and recycled fine milk powder particles to produce open, porous structures. This size enlargement process is a proven method to transform small particles (30 to 50 μm) into larger aggregates (150 to 200 μm) which are easy to handle due to their desirable bulk properties (Hogekamp, 1999b). This process improves the functionality of the powder, giving enhanced flowability, wettability and dispersibility, reduced dustiness and decreased bulk density. This powder is termed "instant" as it has specific applications that are usually related to its dispersibility in water.

Many of the size enlargement methods employed by the food industry are proven methods that have been studied widely. The literature provides few guidelines for operation of agglomerating spray driers and the effect of design and processing parameters on size enlargement is relatively unknown. The process of agglomeration is complex and is best understood as a series of micro-level processes of droplet formation, impact, coalescence and drying. However, it is difficult to isolate and study each of these individual steps within the industrial situation. Due to the complexity of interacting variables (Figure 2.1) which influence the agglomeration process, Retsina (1988) claims it is impossible to predict product properties from operating parameters.

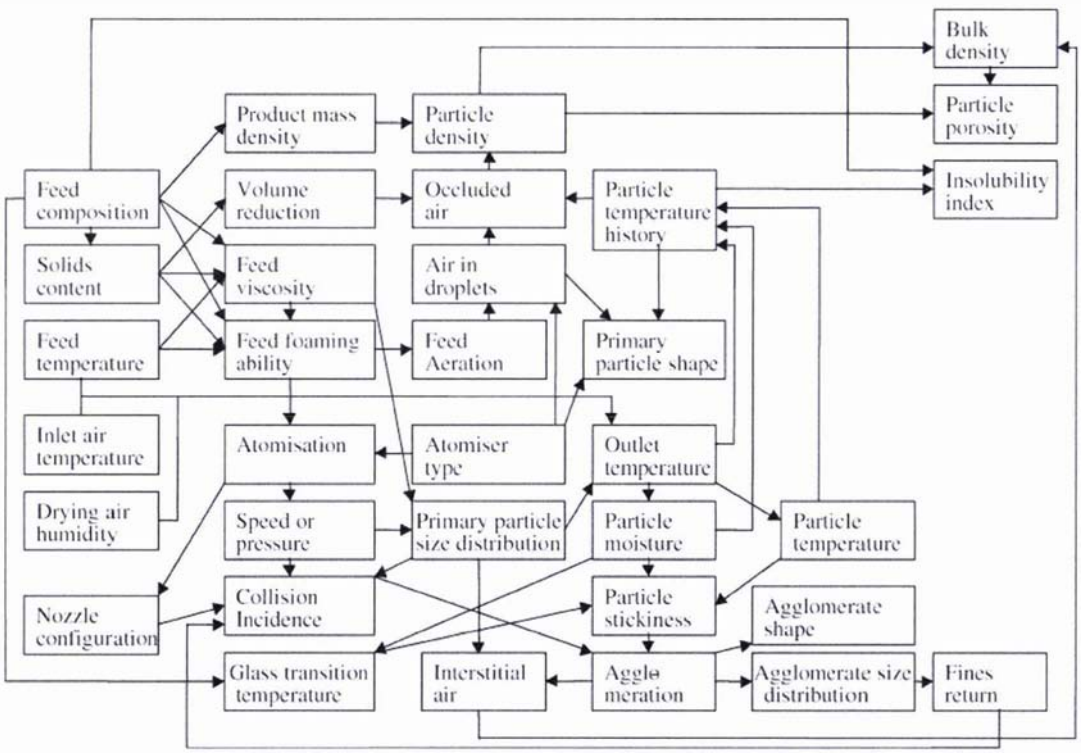

Figure 2.1: The effect of parameters on the agglomeration process (Pisecky, 1997).

Schubert (1987) Schuchmann and Schubert (1993), Schuchmann et al. (1993), Hogekamp (1999b) and Hogekamp (1999a), have investigated the process of steam jet agglomeration which has similar mechanisms to agglomeration at the top of a spray drier. The main difference is that the surface of powder particles are partly dissolved by the condensing steam environment, this allows the formation of liquid bridges following collision with other wetted particles. Agglomeration is often considered to be a type of granulation requiring agitation and a liquid binder. The mechanisms of agglomeration can be compared to those established for granulation processes although agglomeration is faster, smaller forces act on the particles and shape of the agglomerates can be more variable and more porous compared to granules. Studies on high-shear granulation of milk powder have been performed recently by Field-Mitchell (2002) who found that milk powder granules had better flowability than standard spray dried powder but exhibited poor wettability. A mechanistic approach to the granulation process identified three regimes: nucleation and wetting, growth and coalescence, and attrition and break-up (Iveson, Litster, & Ennis, 1996). The granulation mechanisms have been reviewed by Iveson, Litster, Hapgood and Ennis (2001) and depicted in Figure 2.2.

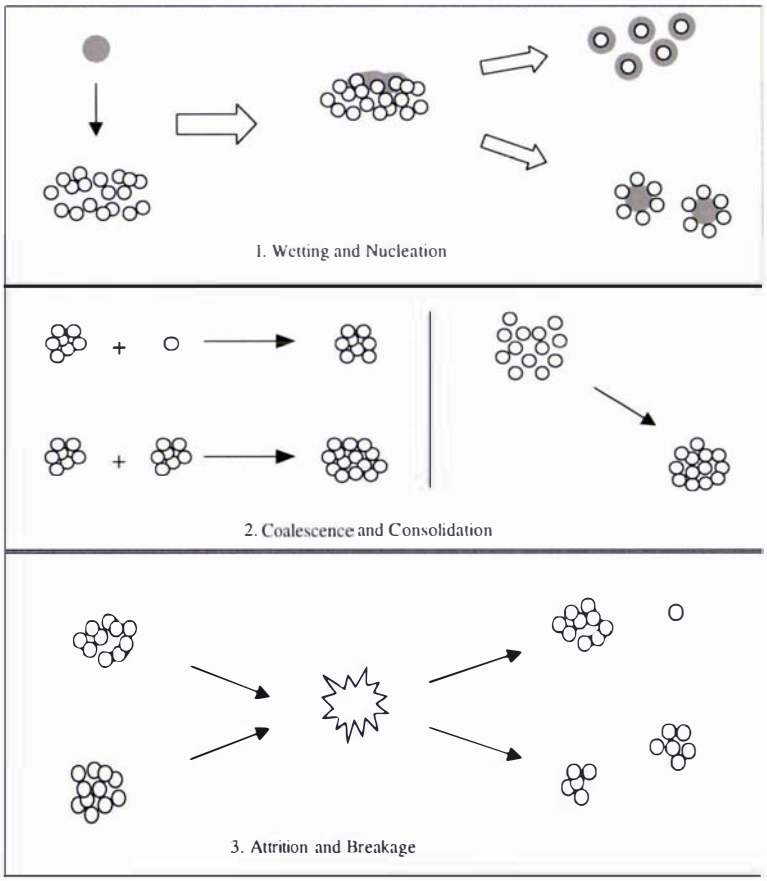

Figure 2.2: Granulation mechanisms (Iveson et al., 2001).

Granulation has been widely researched, including experimental studies focussing on each granulation mechanism, techniques for modelling granulation (Cryer, 1999; Goldschmidt, Weijers, Boerefijn, & Kuipers, 2003), and assessment of granule properties such as structure and strength (Iveson, Beathe, & Page, 2002).

Mujumdar (2004) suggests that higher production rates and the need for uniform particle size distributions are likely to be two key issues driving research in drying technology. Particle engineering can add value to food powders by ensuring they maintain their stability and functionality (Fitzpatrick & Ahrne, 2005). Spray drying research is being market driven as production becomes more technically difficult (Masters, 2004). Developing new products on existing spray driers can be difficult; this reinforces the need for development at small, pilot and plant scale to understand the mechanisms of agglomeration to ensure relevant powder properties are optimised depending on market requirements (Masters, 2004; York, 2003).

There are a range of studies which look at the effect of spray drying conditions on food powder properties (Birchal, Huang, Mujumdar, & Passos, 2006; Birchal, Passos, Wildhagen, & Mujumdar, 2005; Chegini & Ghobadian, 2005; Goula, Adamopoulos, & Kazakis, 2004; Huntington, 2004; Nijdam & Langrish, 2005). The authors show that air inlet temperature, drying air flow rate and atomisation air flow rate all affect the moisture, solubility, particle size, wettability and density of powders. Huntington (2004) gives a review of the entire spray drying process including a summary of the possible agglomeration mechanisms. However none of these venture further to assess how spray drier operation influences agglomeration performance. Most of these studies are carried out on lab scale equipment (~ 100 mm drier diameter) where droplet residences times are very short and the particle trajectory is unlikely to imitate the conditions of industrial powders.

There have been several studies carried out on pilot scale driers (0.8 m diameter) which use computational fluid dynamics (CFD) modelling to simulate the drying process looking specifically at milk powders (Fletcher et al., 2006; Harvie, Langrish, & Fletcher, 2002; Langrish & Fletcher, 2001; Langrish & Kockel, 2001; Ozmen & Langrish, 2003b). Huang (2006) also used CFD to model drying performance in a pilot scale drier and validated these results experimentally. Nijdam et al. (2003) and Nijdam et al. (2004) investigated the challenges of simulating droplet coalescence within the spray zone of a spray drier. Maa et al. (1998) has identified problems with collection of particles < 5 μm in a cyclone and modified a laboratory scale spray drier to improve the design resulting in an increased production yield. Although the EDECAD project reported by Verdurmen et al. (2004) has attempted to simulate the entire agglomeration process, more understanding of particle agglomeration is needed to translate this to industrial operating guidelines.

2.1 Instant Milk Powder Production

Milk has high nutritional value and is a complex emulsion consisting of a suspension of fat globules, colloidal proteins and sugars. The main benefit of milk powder manufacture is that it converts this perishable liquid into a powder which can retain its quality during storage (Walstra, 1999). First the raw milk is delivered to the evaporator, where the preheated milk is concentrated in stages or "effects" from around 9% total solids content for skim milk and 13% for whole milk, and up to 45 – 52% total solids to produce “milk concentrate”.

Spray drying involves atomising the milk concentrate from the evaporator into fine droplets. This is done inside a large drying chamber in a flow of hot air (up to 200°C) using either a spinning disk atomiser or a series of high pressure nozzles. The milk droplets are cooled by evaporation and the surface of the droplets never reaches the temperature of the air (Buma, 1970; Reineccius, 2004; Truong, Bhandari, & Howes, 2005a) The concentrate may be heated prior to atomisation to reduce viscosity and most of the remaining water is evaporated in the drying chamber, leaving a fine powder of around 6% moisture content. Final or "secondary" drying takes place in a fluid bed, or in a series of beds, in which hot air is blown through a layer of fluidised powder removing more water to give product with a moisture content of 2 – 4%. Kelly (2006). has outlined that milk powder production has a strong position in the market and that innovation that will be required to take advantage of further opportunities. Due to the large amount of energy required in spray drying there is a move to develop plants which are more energy efficient (Caric, 2002).

Milk powders are more stable than fresh milk but protection from moisture, oxygen, light and heat is needed in order to maintain their quality and shelf life. Milk powders readily take up moisture from the air, leading to a rapid loss of quality and caking or lumping. Standard powders do not dissolve well, so "agglomerated" or "instant" powders were specifically developed to counter this problem. Instant powders must wet, sink and disperse quickly, when added to water. Ideally, after reconstitution in water, the resulting milk should be similar in composition to natural milk while retaining the sensory and nutritional properties.

The manufacture of an agglomerated powder follows the standard process of evaporation and drying where small powder particles (the "fines") leaving the drier are recovered in cyclones (or a bag house) and are returned to the drying chamber near the atomiser. The concentrate droplets collide with the recycled fines and stick together, forming agglomerates. Skim milk powder manufactured this way can be termed "instant", however, with whole milk powder (WMP), an extra step is needed after agglomeration to ensure the powder is "instant". A small amount of surfactant (lecithin) is sprayed on the powder in a fluid bed to overcome the hydrophobic nature of the fatty powder surface. Alternatively, milk powder can be agglomerated in a fluidised bed by returning fines to the well-mixed and vibrating fluid beds following the spray drier otherwise known as rewet agglomeration; a process which has been well reviewed by Mackereth (1983).

Industry investigations provide evidence that the properties of both the milk concentrate and the powder particles impact the agglomeration process. Buma (1971) suggests that maintaining the moisture content of fines above 5% is necessary to initiate agglomeration. Mackereth (1985) established that the effect of fines return flow rate varied depending on the fines size distribution and that increasing the mean particle size of the returned fines increased bulk density. A later study carried out by Jones (1992) indicates that the extent of agglomeration (measured by particle size distribution) can be influenced by the fines return location. This identified that agglomerate structure is sensitive to the moisture content of the droplets at the point of collision with fines particles.

Chen (1992) found that a number of factors affect the agglomeration process including nozzle orientation and height, nozzle spray angle, returned fines concentration, particle size distribution of fines, concentrate flow rate and concentrate viscosity. The fines return system for a nozzle configuration drier has been included in Figure 2.3. A small degree of concentrate overlap between nozzles will help to improve the mechanical stability of the product while still achieving the desirable functional properties. Chen (1992) observed that inter-particle collisions primarily among concentrate droplets can worsen the dispersibility of the product compared to collisions between droplets and particles. This is likely due to the ease of dissolution of a bridge between particles as opposed to large or merged particles. It is important to investigate the degree of agglomeration due to droplet collision without any fines return.

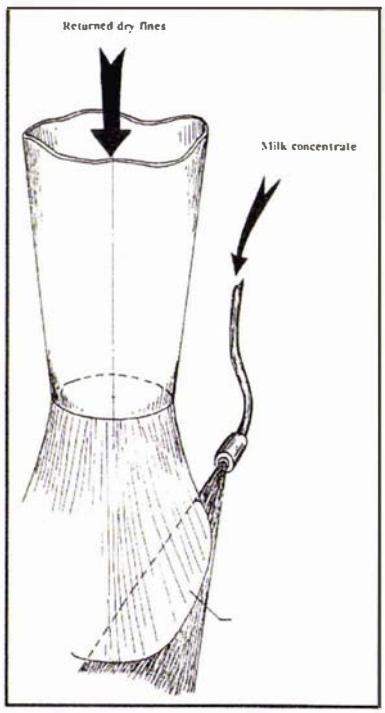

Figure 2.3: Agglomeration of milk powder using a nozzle atomiser (Chen, 1992).

2.2 Agglomeration Theory

The science of agglomeration is young and began with the development of common theories which evolved from many fields of science (Pietsch, 2003) . Research into the process of agglomeration at the top of a spray drier is a relatively new challenge. Currently, there is little understanding of the processes of collision and adhesion that occur during agglomeration. Collisions can result from aerodynamic turbulence or mechanical agitation. Adhesion depends on the existence of attractive forces and the energy involved in the collisions (Hogg, 1989). Forces acting on fine particles and agglomerates include gravity, hydrodynamic forces, thermal energy, and van der Waals', electrical, chemical, solvation and capillary forces. The energy involved in the collision and the mechanical properties of the agglomerates affect rebound, deformation and fracture.

Two types of agglomeration exist: primary agglomeration and secondary agglomeration (Pisecky, 1997). Primary agglomeration involves collisions between atomised droplets. Secondary agglomeration involves collisions between droplets and dry particles, and can be forced or spontaneous. Spontaneous agglomeration refers to fine particles being dragged into the agglomeration zone by aerodynamic recirculation. Forced agglomeration refers to the spraying of atomised droplets on to a fines recycle stream that enters the top of the drier. The appearance of agglomerates has been described as onion, raspberry or grape-like (Pisecky, 1997). An onion is created when small droplets of high moisture (i.e. low viscosity) contact the fine particles and spread over the surface. A raspberry is formed when large droplets of high moisture collide with a large amount of fines. The fines adhere to the outer surface but do not penetrate the droplets. When dried, raspberry and onion structures may have high mechanical strength but are often difficult to dissolve. A grape is created by the collision of similar quantities of droplets and fine particles. Higher moisture content droplets result in a compact grape and lower moisture content droplets result in a loose grape structure. The optimum to achieve a dissolvable powder with good mechanical strength lies between the loose grape and the compact grape.

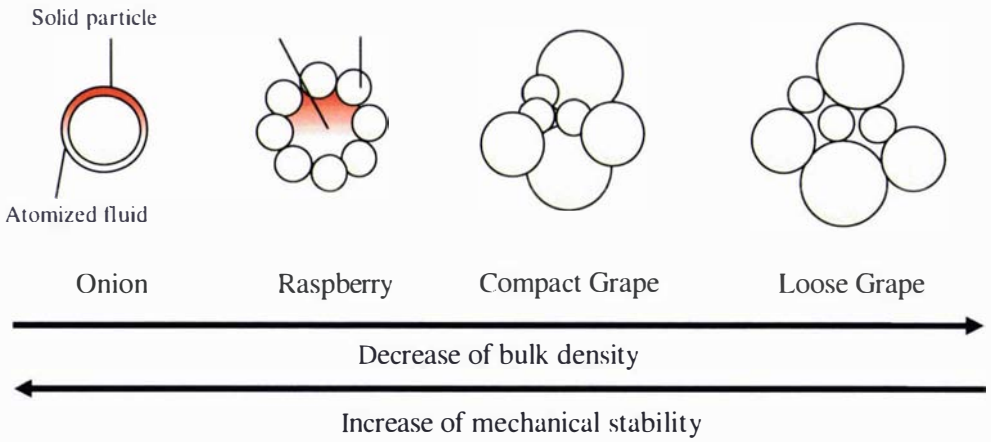

Figure 2.4: Agglomerate morphology.

Industrially agglomeration occurs in three separate zones of a fluidised spray drier (FSD) as indicated in Figure 2.5. In zone 1 near the atomiser weak agglomerates can be formed by droplet coalescence and contact between wet droplets and fine particles (forced agglomeration). In zone 2, fine dried particles are re-circulated near the initial collision zone before the exhaust so that dry and sticky particles can collide to form agglomerates. Schwartzbach and Masters (2001) state that zone 3 is possibly the most important zone where agglomerates are formed and stabilised. Zone 3 is within the fluid bed itself and includes the area just above it. In zone 3 particles undergo mixing due to fluidisation which promotes particle contact. Air temperature and velocity can be manipulated to affect agglomerate structure through further granulation, however as the fluid bed also provides extra drying to adjust the product moisture it is often not desirable to manipulate these variables.

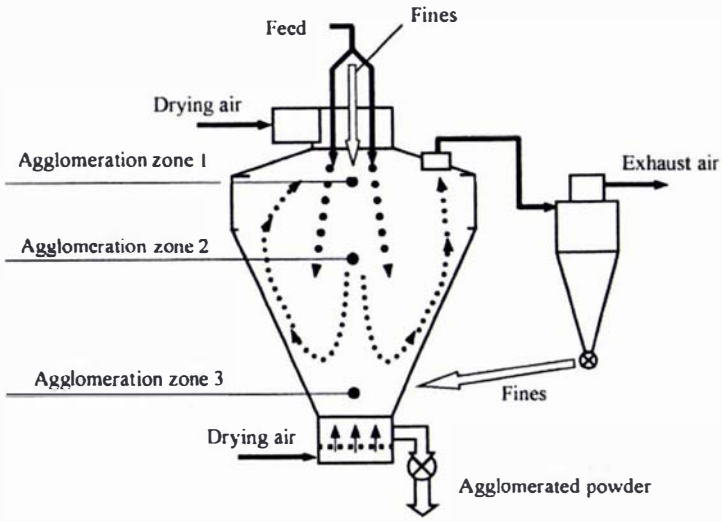

Figure 2.5: Agglomeration zones in a FSD (Schwartzbach & Masters, 2001).

2.3 Micro Processes of Agglomeration

In investigating milk powder agglomeration the interaction zone between the powder particles returned to the top of the spray drier and the milk concentrate droplets is of interest. During atomisation a large number of concentrate droplets are produced in a very small space near the top of the spray drier. The collisions among droplets and recycle fines particles are enhanced under the conditions of hot air turbulence increasing the statistical chance of agglomeration of concentrate particles. The properties of the spray and the particles, as well as the drying environment will determine the effectiveness of agglomeration in this interaction zone.

These steps are considered to be primary agglomeration in this thesis, in which all the droplets and the particles involved have just entered the drier. This is different from the definition by Pisecky, given above. Secondary agglomeration is regarded here to involve droplets, particles or agglomerates that have had some life history inside the drier and occurs away from the collision zone, i.e. in the mid and base of the drier and subsequent fluidised beds (zones 2 and 3 in Figure 2.5). This thesis only investigates the effect of primary agglomeration on product properties. Primary agglomeration under this definition can then be divided into natural and forced agglomeration. Natural agglomeration refers to the process of droplet-droplet collision. In industrial driers, these collisions result from the milk concentrate spray streams overlapping. This can be achieved by directing multiple nozzles so that their spray patterns cross over. However, even one nozzle in a small scale spray drier is likely to produce droplet-droplet collisions. A high number of droplet-droplet collisions are likely to result in the product agglomerates having large bondage areas, high mechanical strength and poor functional properties. Chen (1992) states that the degree of agglomeration due to concentrate droplet collision (natural agglomeration) should be established before optimising any agglomeration process where fines are returned (forced agglomeration).

Figure 2.6 defines simplified steps for agglomeration from a particles point of view and is a clearer description of the process than Pisecky's diagram in Figure 2.1. Drying occurs constantly and needs to be considered at every step. Initially, the concentrate stream is atomised creating droplets and these have a defined size, velocity and moisture content. During flight, a droplet both decelerates and evaporates, which changes its moisture content and size over time. After the droplet has travelled some distance, it enters a stream of particles, and it may collide with one or more particles as it travels through the stream. Some of these particles will adhere to the droplet and a degree of wetting will occur depending on the surface interaction properties. Other collisions, involving droplets, particles and agglomerates, will also occur because of the high turbulence within the collision zone. The liquid bridges that will be formed between particles will quickly dry to form an agglomerated particle with a defined size, moisture and particle density. Each step is reviewed further in the following sections with regard to how each micro process can be studied more closely to allow the performance of the agglomeration process to be improved.

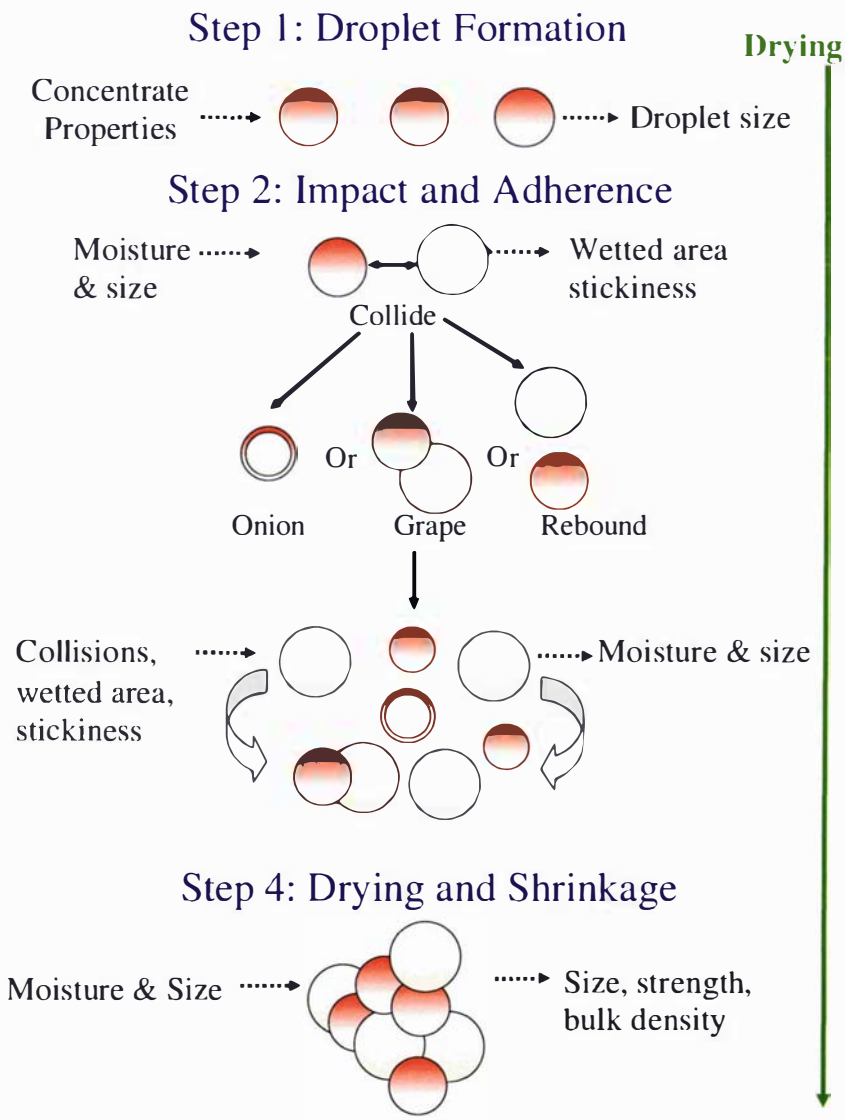

Figure 2.6: Separating the micro processes.

2.4 Droplet Formation and Drying

The first step in agglomeration involves the formation and drying of droplets prior to the collision zone. The formation of droplets is influenced by altering the concentrate properties such as viscosity, surface tension, density and temperature (Mujumdar, 1992). During atomisation, fluids deform under the influence of an applied stress; Newtonian fluids will produce a flow in proportion to the shear stress experienced. A dilatant non-Newtonian fluid will increase in viscosity with an increased shear rate (n >1) and a pseudoplastic (or shear-thinning) non-Newtonian fluid will decrease in apparent viscosity with increased shear rate (n < 1). Most milk products are shear-thinning and this behaviour is correlated by the power law in equation (2.1). Some properties of two milk concentrates have been included in Table 2.1:

$$\tau = K\gamma^n \tag{2.1}$$

where K = consistency coefficient [N s m^{-2}], τ is the shear stress [Pa], γ = rate of strain [s^{-1}] and n = power law index [–].

Table 2.1: Rheological properties of two milk concentrates (Mujumdar, 1992).

Concentrate	Total Solids	Density	Viscosity	Power law index	Surface tension
	(wt%)	(kg m^{-3})	(Pa s)	n	(N m^{-1})
Whole	54	1020	0.030	0.60	0.034
	56	1050	0.030	0.52	0.035
	58	1030	0.030	0.44	0.036
Skim	47	1196	0.015	0.90	0.053
	48	1197	0.022	0.75	0.041
	50	1199	0.022	0.75	0.037

2.4.1 Atomisation

Atomisation involves a series of processes which can be divided into three different regimes; internal flow, break up and droplet dispersion (Mao & Tate, 1997). Internal flow determines the initial liquid disturbances which subsequently affect the break-up and droplet dispersion phases. During atomisation a number of disruptive forces influence droplet formation including kinetic energy, friction, gravity, interface shearing and pressure fluctuations. Cohesive forces within the liquid include molecular bonding, viscosity and surface tension. The consolidating effect of surface tension pulls the liquid into a form that exhibits minimum surface energy while the stabilising effect of viscosity opposes any change in the geometry of the liquid (Liu, 2000). It is the balance between disruptive and cohesive forces which determines the extent of disintegration.

There can often be two phases to the droplet break-up process, primary disintegration/atomisation and secondary disintegration/atomisation. The initial break-up of the liquid due to oscillations is considered to be the primary phase, often larger droplets can become unstable above a certain droplet size and can disrupt further by secondary disintegration. Break-up of a fluid during atomisation depends on the physical properties of the fluid and is commonly characterised by the following dimensionless groups.

$$Re = \frac{D\rho U}{\mu} = \frac{inertial\ forces}{viscous\ forces} \quad (2.2)$$

$$We = \frac{\rho U^2 D}{\sigma} = \frac{inertial\ forces}{surface tension\ forces} \quad (2.3)$$

$$Oh = \frac{\mu}{\sqrt{\sigma\rho D}} = \frac{viscous\ forces}{(inertial\ forces \times surface tension\ forces)^{1/2}} \quad (2.4)$$

where Re = Reynolds number, We = Weber number, Oh = Ohnesorge number, D = drop diameter [m], ρ = density of liquid [kg m^{-3}], U = droplet velocity [m s^{-1}], μ = viscosity of liquid [Pa s] and σ = surface tension of liquid [N m^{-1}].

The atomisation/drying of milk can be divided into the following stages

- milk concentrate
- liquid film
- film break-up into large irregular shaped liquid drops
- spherical liquid drops
- zone of rapid drying
- substantially dried particles

In a real system there is irregular liquid break-up due to stresses within each droplet caused by the interaction between the atomized spray and the surrounding air. Various mechanisms have been proposed to account for liquid break-up in a real system including Rayleigh mechanism, Weber theory, Ohnesorge criteria, Castleman hypothesis and Taylor mechanism. The four regimes classified by Ohnesorge are the most commonly applied and have been included in Table 2.2. These regimes depend on the relative importance of inertial, surface tension, viscous and aerodynamic forces.

Table 2.2: Classification and criteria of break-up regimes of liquid jets (Liu, 2000).

Regime	Classification	Break-up Mechanism	Criteria
I	Rayleigh Jet Break-up	Surface Tension Force	$We_a < 0.4$
II	First Wind-Induced Break-up	Surface Tension Force, Dynamic Pressure of Ambient Air	$1.2 + 3.41Oh^{0.9} < We_a < 13$
III	Second Wind-Induced Break-up	Dynamic Pressure of Ambient Air	$13 < We_a < 40.3$
IV	Atomisation	Unknown	$We_a > 40.3$

Nozzle atomisers and disc atomisers are the two types of atomisation equipment used in the dairy industry in New Zealand. Pressure nozzles are commonly used in most modern systems. The principle behind nozzle atomisation is to convert the energy of pressure into the kinetic energy of a moving liquid. The liquid sheet breaks up under the influence of the liquid's physical properties and due to the frictional effects from the medium into which the sheet is discharged. Masters (1979) reports that mean droplet size is thought to increase with increasing flow rate, viscosity and solids content and decreasing pressure and surface tension. Figure 2.7 depicts the break-up of a liquid sheet propagated by a pressure nozzle.

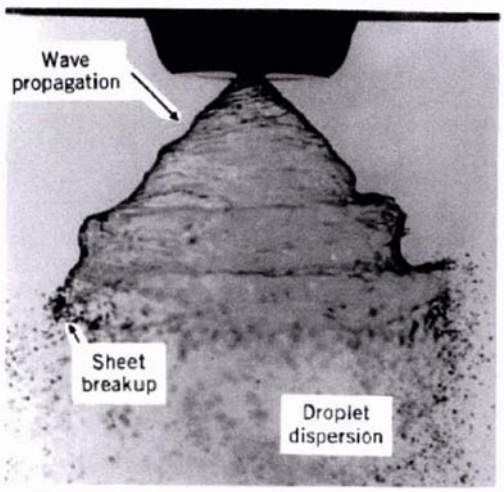

Figure 2.7: Wave formation and break-up of a sheet (Mao & Tate, 1997).

Masters (1979) and Liu (2000) explain the fundamentals behind atomiser operation and the processes of droplet formation. Iveson et al. (2001) found a strong relationship between droplet size and the particle size distribution of nuclei formed in a fluid bed granulator. Maa (1996) observed that high particle to droplet size ratios result in the lowest level of agglomeration in spray coating. Control of droplet size is important to control agglomeration as this property will also affect the rate of drying and ultimately the outcome of any droplet-particle collisions that occur in the interaction zone.

Control of droplet size and size distribution during spraying is not easy. Total solids levels and atomiser pressure are all adjustable for any given nozzle design however the concentrate flow rate will determine production rates. Correlations are available to predict droplet sizes from fluid properties for high pressure and laboratory-scale pneumatic nozzles; however, many of these apply to particular nozzles over narrow operating ranges, and usually only apply for water. Clement et al. (1997) reports an experimentally correlated droplet size equation for a milk disc drier as:

$$D_{3,2} \propto \frac{[M_c(1+X_c)]^{0.15}\mu^{0.1}}{U\rho^{0.5}} \tag{2.5}$$

where $D_{3,2}$ = Sauter mean particle diameter [m], M_C is the mass rate of concentrate [tonnes h^{-1}], X_c = total solids content [wt%], U = peripheral speed [m s^{-1}] and μ and ρ are the viscosity [Pa s] and milk concentrate density [kg m^{-3}].

The Sauter mean particle size is suitable to describe the droplet size during spray drying as it represents the surface to volume weighted mean significant for the process of drying a droplet. The $D_{4,3}$ or volume weighted mean particle diameter is used to represent the mean size of particles measured using laser diffraction and this is relevant when estimating the number density of particles in volumetric space.

For nozzle driers the Sauter mean diameter has a similar relationship as disc driers but also has an extra dependence with the feed rate:

$$D_{3,2} \propto \Delta P^{-0.375} \tag{2.6}$$

Dewettinck and Huyghebaert (1998) have given the following relationship for pneumatic nozzles to predict the Sauter mean droplet size, $D_{3,2}$:

$$D_{3,2} = \frac{585 \times 10^3 \sqrt[3]{\sigma}}{v_{rel}\sqrt{\rho}} + 597\left(\frac{\mu/1000}{\sqrt{\sigma\rho}}\right)^{0.45}\left(\frac{1000Q_l}{Q_{atm}}\right)^{1.5} \quad (2.7)$$

where σ = surface tension [N m^{-1}], Q_l = liquid volumetric flow rate [m^3 s^{-1}], and Q_{atm} = atomising air volumetric flow rate [m^3 s^{-1}], v_{rel} = relative velocity between fluid and air. Such a prediction is likely to be inaccurate unless the atomisation air flow rate and relative velocity between the fluid and the air are precisely known.

2.4.2 Droplet Drying

Following atomisation, droplets travel through the drying air towards the curtain of recycled fines particles. These droplets must impact with the particles before the surface moisture content becomes so low that they are no longer sticky enough to adhere. The mechanism of moisture flow through a droplet during spray drying is mostly diffusional and is supplemented by capillary flow (Masters, 1979). The drying rate affects the appearance, porosity, surface and friability of the agglomerate. Evaporation of a liquid droplet involves heat transfer by conduction and convection from the surrounding gas to the drop surface. The rate of transfer is a function of the temperature, humidity and transport properties of the gas as well as the diameter, temperature and relative velocity of the droplet. Evaporation from a drop has been studied by Ranz and Marshall (1952), however very little accurate data exists on drying of milk droplets, particularly the compositional influence upon evaporation and the change in diameter of milk droplets (Lin & Chen, 2002).

Lin and Chen (2004) have studied the effect of the composition of milk droplets on evaporation and the change in diameter of the milk droplets. Several authors have developed mathematical models to predict the momentum, heat and mass transfer processes that occur during spray drying (Zbicinski, 1995). From a design point of view, prediction of droplet drying rates will be useful in determining the optimum nozzle position relative to the fines return. The surface moisture profile is useful for predicting the stickiness state of the surface for lactose-containing droplets.

Evaporation from the droplet has two steps, the constant rate drying period and the falling rate drying period. In the first step, diffusion of moisture from inside the droplet ensures the surface remains saturated. After the surface moisture content drops below saturated conditions this is deemed the critical point and a shell begins to form on the surface. After this time the evaporation is dependent upon the rate of moisture diffusion through this shell. As drying progresses over time the thickness of the surface shell increases and this causes a decrease in the rate of evaporation. Important dimensionless groups for evaporation from droplets when considering both mass and heat transfer include the Reynolds, Schmidt, Sherwood, Nusselt and Prandlt number:

$$Re = \frac{D\rho U}{\mu} = \frac{inertial\ forces}{viscous\ forces} \quad (2.2)$$

$$Sc = \frac{\mu}{\rho D} = \frac{momentum\ diffusivity}{mass\ diffusivity} \quad (2.8)$$

$$Sh = \frac{h_m D}{D_f} = \frac{convection\ mass\ transfer\ flux}{diffusion\ mass\ transfer\ flux} \quad (2.9)$$

$$Nu = \frac{hD}{k_l} = \frac{convection\ heat\ transfer\ flux}{conduction\ heat\ transfer\ flux} \quad (2.10)$$

$$\Pr = \frac{C_p \mu}{k_l} = \frac{momentum\ diffusivity}{thermal\ diffusivity} \quad (2.11)$$

where D_f = diffusion coefficient [$Wm^{-1}\ K^{-1}$], h_m = convective mass transfer coefficient [$Wm^{-2}\ K^{-1}$], h = convective heat transfer coefficient [$Wm^{-2}\ K^{-1}$], k_l = thermal conductivity of the liquid [$Wm^{-1}\ K^{-1}$] and C_p = specific heat capacity at constant pressure [$J\ kg^{-1}\ K^{-1}$].

Until recently, the most widely applied heat and mass transfer equations are those determined by Ranz and Marshall (1952). For Reynolds number range of 0 to 200 the following equations hold for heat transfer and mass transfer respectively:

$$Nu = 2.0 + 0.60 \mathrm{Re}^{1/2} \Pr^{1/3} \quad (2.12)$$

$$Sh = 2.0 + 0.60 \mathrm{Re}^{1/2} Sc^{1/3} \quad (2.13)$$

However, radiative heat transfer is ignored and the droplet's internal structure is assumed to be stable with no internal circulation or surface distortion. These two assumptions are likely to impact upon the validity of the model significantly. Also, droplets are assumed to be in a stable air flow. In real systems the air flow is likely to be swirling; this would result in a reduced boundary layer, meaning higher evaporation rates than predicted.

Zbicinski (1995) developed models to predict the momentum, heat and mass transfer process which occurred during spray drying. Zbicinski's work assumes a spray boundary region and a spray core region exist, and assumes that the spray is monodispersive with a constant temperature and humidity across the cross section. A more recent model uses finite element methods to quantitatively calculate flow data for transport of moving droplets through a suspending fluid and can predict the terminal velocity and shape of droplets (Petera & Weatherley, 2001). Wesselingh and Bollen (1999) use a dimensionless approach for all variables relating to a reference variable which depends on the physical properties of the particle (or drop) and the fluid phase. Their method aims to eliminate the iterative velocity calculations often required to predict mass transfer coefficients using traditional methods. Nijdam and Langrish (2006) confirm the findings of others that during droplet drying a skin forms, and a vacuole and the inflation and shrinkage of the particle occurs. Kentish et al. (2005) studied skin formation of milks during drying and showed that skin thickness affected mass transfer during drying.

Lin and Chen (2002) aimed to improve the current correlations for drying kinetics of liquid droplets by using a glass filament method as the supporting mechanism. The vapour flux values were approximately 10 times greater than the Ranz-Marshall investigation. The correlations were obtained for operating conditions which can apply to the production of milk powders:

$$Nu = 2.04 + 0.62\,\mathrm{Re}^{1/2}\,\mathrm{Pr}^{1/3} \tag{2.14}$$

$$Sh = 1.63 + 0.54\,\mathrm{Re}^{1/2}\,Sc^{1/3} \tag{2.15}$$

Droplet shrinkage can be estimated using by:

$$\frac{D_p}{D_d} = \left(\frac{\rho_c}{\rho_p} \times \frac{X_c}{X_p} \right)^{1/3} \tag{2.16}$$

where D_d = droplet diameter [m], D_p = particle diameter [m], ρ_c = density of the concentrate [kg m^{-3}], ρ_p = density of the particle [kg m^{-3}], X_c = weight fraction solids per total weight of concentrate [kg kg^{-1}], X_p = weight fraction solids per total weight of product [kg kg^{-1}].

Werner (2005) used a mathematical model to predict the drying kinetics of a single droplet during coating of particles in a Würster coater. This calculated the surface moisture content of a droplet at the point of impingement on a particle surface. The surface moisture content and droplet diameter are of interest to both coating and agglomeration studies. Werner (2005) proposed that a droplet will shrink ideally until the surface has enough mechanical strength to resist deformation and it is suggested that the point when the surface becomes rigid depends on the droplet temperature and its proximity to the glass transition temperature, T_g (to be defined in §2.4.3). Figure 2.8 gives a diagram of the possible internal structures during droplet drying. In agglomeration processes the information can be used to optimise the proximity of the nozzle to the powder flow and the drying air conditions to ensure droplets are sticky at impact and agglomeration is optimised.

Models of spray drier performance have been reviewed by Oakley (2004) including the prediction of product properties such as product moisture. Ozmen and Langrish (2003b) used an equilibrium based model where simple heat and mass balance models can be used for prediction of heat loads, however particle sizes are small, drying kinetics are fast and residence times are long. The product powder is not always expected to be in equilibrium with the outlet air which makes predicting the powder moisture content more difficult. Rate based models are recommended but these require experimental data on the drying kinetics of the particular material. Langrish and Kockel (2001) and Oakley (2004) suggest the use of characteristic drying curves for prediction of product properties during spray drying.

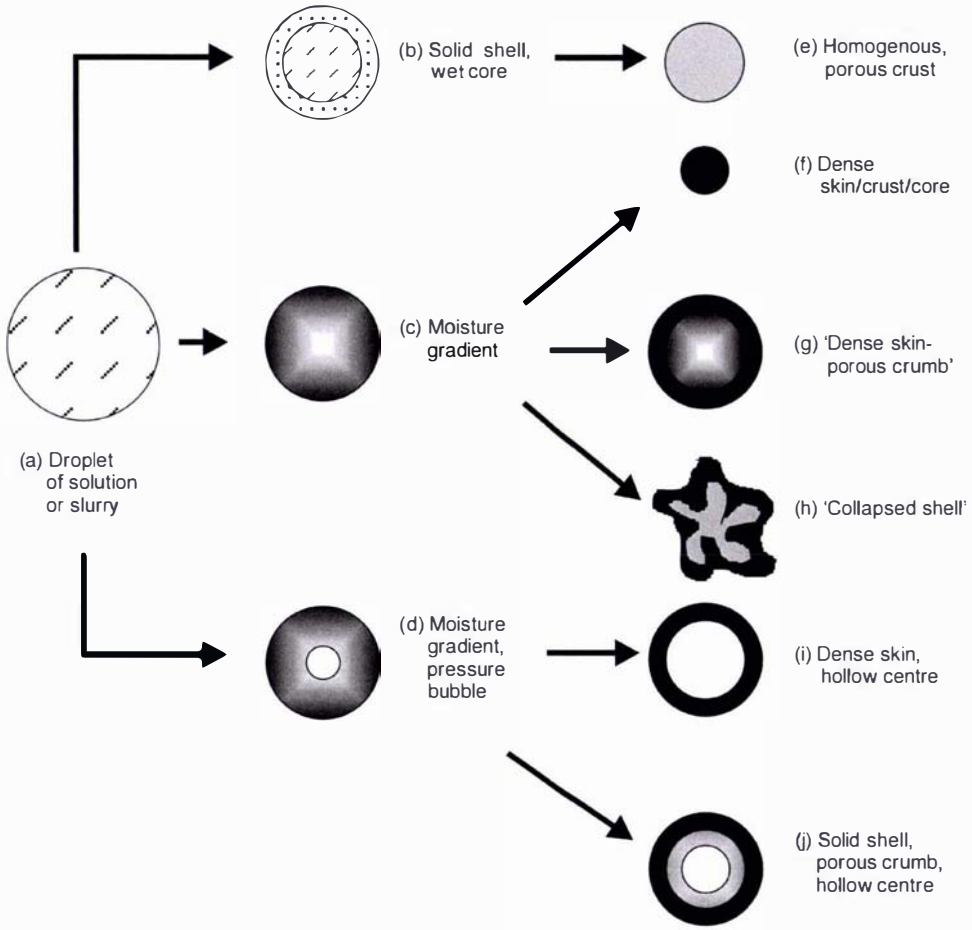

Figure 2.8: Possible internal structures during droplet drying (Werner, 2005).

2.4.3 Stickiness

For agglomeration to occur, it is essential that a droplet adheres to a fines particle following contact in the collision zone. For adherence to occur the droplet must satisfy the surface conditions required to have the appropriate level of tack or stickiness. Stickiness is the tendency of a substance to adhere to a surface, and is an issue affecting the entire food industry. In milk powder manufacture, stickiness is used to describe the processes of particle-particle cohesion and particle-wall adhesion in spray drying (Truong et al., 2005a). If a spray drier is designed to be large enough there should be no deposition of material on the wall, however drier size is limited by economics which means that deposition may occur. This deposition is an issue which costs the dairy industry due to loss of quality, reduced yield, plant shutdowns as well as cleaning and safety issues (Adhikari, Howes, Lecomte, & Bhandari, 2005; Hennings, Kockel, & Langrish, 2001; Kudra, 2003; Papadakis & Bahu, 1992). In instant milk powder production, the stickiness phenomena is a desirable parameter but must be controlled to certain limits. It is ideal that droplets and particles exhibit an optimum level of stickiness in the collision zone to produce bonded agglomerates, and sufficient drying of these agglomerates must occur before collision with the drier wall.

Stickiness is affected by temperature, moisture content, humidity and composition (Downton, Flores-Luna, & King, 1982). It occurs by the mechanism of viscous flow; upon the collision of two particles, adhesion will occur only if there is sufficient viscous flow to build an inter-particle bridge that is capable of resisting mechanical deformations. When in the glassy state, a material has a high viscosity, 10^{12} Pa s, after the material undergoes a transition to the rubbery state (due to the influence of moisture and/or temperature) the viscosity drops to below 10^{8} Pa s and material flow between particles can occur, resulting in adhesion. Downton et al. (1982) also defined a critical viscosity for sticking and this will differ for each material depending on the composition and the moisture content of each powder.

$$\mu = \frac{k\sigma t}{KD} \tag{2.17}$$

where μ = viscosity [Pa s], t = time [s], k = a constant, σ = surface tension [N m^{-1}] and KD = constant × particle diameter [m].

In adhesion science, stickiness is termed pressure sensitive adhesion or tack (Adhikari, Howes, Bhandari, & Truong, 2003a). Adhikari et al. (2001) reviewed the phenomenon of stickiness and current measurement techniques. There are many techniques which can be used to investigate powder stickiness including mechanical stirring method (Hennings et al., 2001; Ozmen & Langrish, 2002), volume change (Lloyd, Chen, & Hargreaves, 1996), hardness test, shear cell method, cohesion tests (Chen, Rennie, & Mackereth, 2004), cyclone stickiness test (Boonyai, Howes, & Bhandari, 2006), the dynamic sticky point using a fluidised bed (Verdurmen, Houwelingen, Gunsing, Verschueren, & Straatsma, 2006) and using the particle gun technique (Chatterjee, 2004; Murti, 2006; Zuo, 2004).

Solutions containing sugar, in particular, become sticky as the temperature increases towards glass transition temperature (Chen et al., 2004; Chuy & Labuza, 1994; Lloyd et al., 1996; Rennie, Chen, Hargreaves, & Mackereth, 1999; Roos, 2002) Milk powders produced by spray drying have a large amount of amorphous lactose present and distinctive properties are associated to this through the sticking mechanism (Ozkan, Walisinghe, & Chen, 2002). Until recently, few attempts were made to quantify the tack of sugar rich foods during drying operations; however Adhikari et al. (2003) designed an apparatus to study this. Since then many studies have aimed to characterise the stickiness of sugar-rich droplets as drying occurs (Truong et al., 2005a; Truong, Bhandari, & Howes, 2005b; Werner, Jones, & Paterson, 2007b). This apparatus was improved by van der Hoeven (2006) who studied the surface tack of droplets with application to agglomeration processes during spray drying.

Kim et al. (2002) investigated the composition of milk powder by comparing the bulk and surface compositions of two spray dried dairy powders (Table 2.3). Kim et al. (2003) identified that solid/solute segregation occurred before the formation of a crust during the drying process. They also concluded that the protein absorbed preferentially to the air/liquid interface during droplet formation. During drying both protein and fat accumulate at the surface of a droplet (Nijdam & Langrish, 2006). Nijdam and Langrish proposed that skin formation hinders the process of protein accumulation at the surface and as drying temperature increases, protein accumulation decreases, resulting in high lactose coverage on the surface. The percentage of fat, lactose and

protein present on the surface of the dried or drying particle will influence adhesion and therefore agglomeration (Ozkan et al., 2002). In general, skim milk powders form weaker agglomerates which could be attributed to the degree of adhesion or sticking that occurs during agglomeration.

Table 2.3: Bulk and surface composition of milk powders (Kim et al., 2002).

Powder	Bulk Composition (%)			Surface Composition (%)		
	Lactose	Protein	Fat	Lactose	Protein	Fat
Skim Milk	58	41	1	36	46	18
Whole Milk	40	31	29	2	0	98

Several authors have identified mechanisms for sticking in dairy powders (Chatterjee, 2004; Foster, 2002; Ozkan et al., 2002). The glass transition temperature (T_g) can be used to describe these properties. The T_g concept indicates the physical changes in the viscous behaviour of a material. The transition can be characterised by a release in thermal energy detected by DSC as the change in state occurs from glass to rubber. This change is not instant and T_g can be reported as the onset or midpoint temperature. When the material temperature is below T_g, a material is in the glass state characterised by a high viscosity and above T_g the material transforms and the viscosity decreases. In amorphous powders the presence of water can change the glass transition temperature.

Foster (2002) found that increasing the temperature of powders to temperatures where surface fat became molten, fatty liquid bridges could form between particles. Similarly, stickiness can occur between particles due to exceeding the glass transition temperature of the sugars present on the powder surface. Stickiness is dependent on the amount the glass transition temperature of the powder is exceeded by ($T-T_g$). Figure 2.9 includes a diagram of the amorphous lactose caking mechanism, due to the formation of liquid bridges by the mechanism of viscous flow. Foster (2002) developed a model to predict the T_g for dairy powders and these have been validated experimentally for different compositions.

Palzer (2005) identified that three different adhesion processes can occur between particles depending on the contact time: liquid bridging, viscous bridges built by viscous flow (sintering) and increased contact area due to viscoelastic deformation. Palzer combined the Williams-Landel-Ferry (WLF) equation, Navier-Stokes and viscoelastic knowledge to predict the $T - T_g$ depending on the contact time available for adhesion. This relationship can be applied in several ways to determine the storage temperature of a powder in a bag/vessel, contact time for particles to agglomerate in a fluidised bed or the $(T - T_g)_{critical}$ for a spray dried particle as it hits the chamber wall.

$$t = \left(\frac{5D_p^{\,2}\pi}{4\sigma_l a\pi + 2F_t} \right) \mu_g \left(\frac{D_{bridge}}{D_p} \right)^2 10^{[C(T-T_g)]/[B+(T-T_g)]} \tag{2.18}$$

where σ_l = surface tension of saturated lactose [N m^{-1}], F_t = impact force [N], μ_g = viscosity at the glass transition temperature [Pa s], D_{bridge} = diameter of sinter bridge [m], C, B = WLF constants, T = temperature [°C], T_g = glass transition temperature [°C].

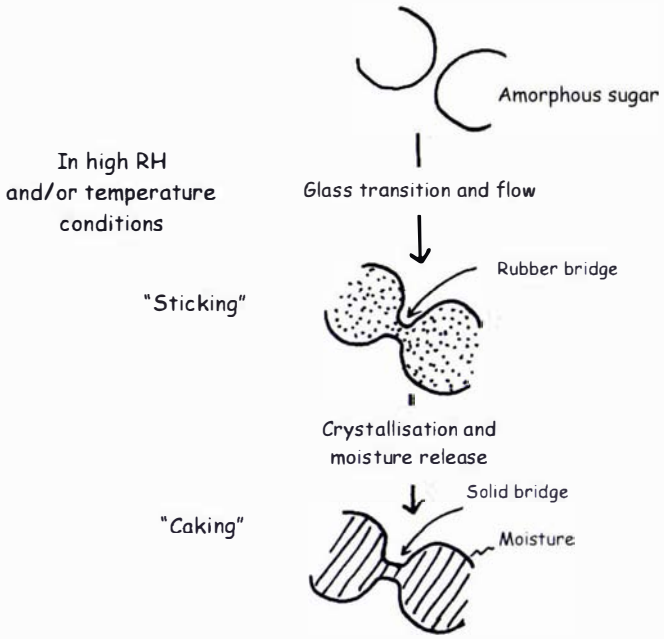

Figure 2.9: Amorphous lactose caking mechanism (Foster, 2002).

2.5 Droplet-Particle Collisions

The successful collision between a droplet and a particle is the first step necessary to achieve coating, granulation and agglomeration (Link & Schlünder, 1997). The key mechanisms of agglomeration are the processes of collision and adhesion, which can also be referred to as coagulation and sintering (Palzer, 2005; Schmid, Al-Zaitone, Artelt, & Peukert, 2006). It is the frequency of these collisions and the likelihood of adhesion which determines whether agglomeration is successful (Schuchmann et al., 1993).

Link and Schlünder (1997) also describe this process as similar to dust collection which occurs by a two step process: particle transport to the surface followed by particle adhesion on the surface. This process can be considered as having a collection efficiency comprised of an impingement efficiency (which determines the number of droplets that reach the surface of the particles) and an adhesion efficiency (which determines whether droplets adhere to particles following collision). Depending on the droplet and particle sizes and each of their relative velocities, interception, inertia or diffusion will occur during collection (see Figure 2.). The impingement efficiency depends on droplet density, size and shape and flow rate compared to collector particles. In agglomeration at the top of a spray drier, it is likely that both inertia and interception play significant roles during the collection of droplets by fines particles. For this reason it is essential that the trajectories of the droplets and the recycled fines particles intersect at the top of the spray drier. Jones (2005) assesses the probability that droplets and particles interact by assuming the trajectories cross paths. The probability that a droplet and particle will collide in the collision zone depends on the size and velocity of droplets and particles as well as the frequency they enter the interaction zone.

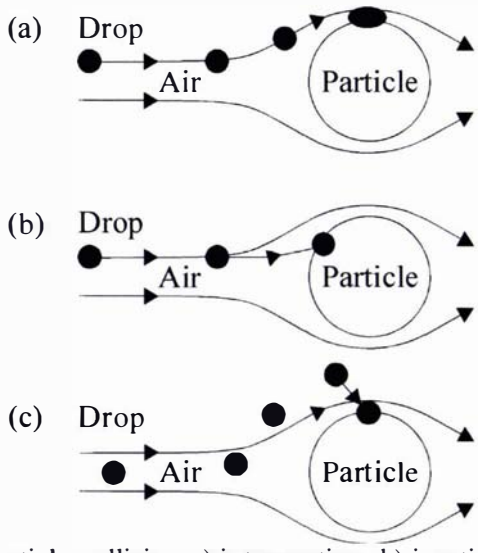

Figure 2.10:Droplet-particle collision a) interception, b) inertia, c) diffusion (Guignon, Duquenoy, & Dumoulin, 2002) .

Several authors have investigated the implications of droplet-particle impact in relation to air-suspension particle coating (Guignon et al., 2002; Guignon, Regalado, Duquenoy, & Dumoulin, 2003; Link & Schlünder, 1997; Werner, 2005). Coating and agglomeration involve many of the same processes; however the desired outcome is the opposite. In coating, the aim is to optimise spreading and layering of particles and to avoid agglomeration. In forced agglomeration fines pass through the spray zone only once and coating/layering of fines with no coalescence is not desirable. Agglomeration cannot occur if no particle collisions take place. Abrahamson (1975) developed a method to calculate collision rates in turbulent flows based on the kinetic theory of gases and this has been expanded (Ho & Sommerfeld, 2002; Sommerfeld, 2001). Verdurmen et al. (2004) calculated the probability of collisions during milk powder agglomeration using the approach of Sommerfeld (2001). The collision rate in the mixing zone is difficult to predict and relies on the properties of the droplet, particle and agglomerate and their velocities. Abrahamson (1975) has suggested that the collision rate can be calculated using the following equation:

$$Z_{12} = 5\hat{N}_1\hat{N}_2 D_{12}^2 \sqrt{\overline{U}_1^2 + \overline{U}_2^2} \tag{2.19}$$

where Z_{12} = collision rate between two particles [m^{-3} s^{-1}], $\hat{N}$ = number concentration of particles [m^{-3}], D_{12} = sum of colliding particle radii [m], U_1, U_2 = average velocity of particles relative to the mean fluid velocity [m s^{-1}].

Boerefijn and Hounslow (2005) discuss the use of the flux number (FN) which can be used as a guide to determine whether granulation or coating occurs in fluidised beds. This approach indicates that at high flux number (solids to spray ratio) there is a border between granulation and coating. This suggests that the number of collisions between droplets and particles will influence agglomeration. This study found that for granulation to occur the flux number (FN) needs to be below 3.5 and above 2.

The flux number allows for scale-up of growth rates from batch to continuous granulation:

$$FN = \log_{10}\left(\frac{\rho_p u_e A_{spray}}{q_b}\right) \tag{2.20}$$

where ρ_p = the particle density [kg m^{-3}], u_e = the excess gas velocity [m s^{-1}], q_b = the binder spray rate [kg s^{-1}], and A_{spray} = is the spray footprint area on the powder bed [m^2].

A similar approach was earlier developed by Hapgood et al. (2003) and Litster et al. (2001) which uses a binder spray flux to understand the influence of spray rate on nucleation. If the solids to spray ratio is decreased, or if the binder spray flux is increased it is more likely that agglomeration will occur. Since time for droplet/particle contact is short a large number of droplets are required to contact the moving powder curtain for agglomeration to occur between particles.

$$\Psi_a = \frac{3\dot{V}}{2\dot{A}D_d} \tag{2.21}$$

where $\dot{V}$ is the volumetric spray rate of the binder liquid, D_d is the droplet size and $\dot{A}$ is the area flux of powder traversing the spray zone.

2.5.1 Droplet Impact and Adhesion

Single droplet–particle collision is a two-step process of collision (or impact) and adhesion. The collision rate is affected by the nozzle position, the number density of droplets, the droplet velocity and the geometry of the spray with respect to the particle stream. There must be collisions between droplets and particles and wet particles must have a sticky surface to ensure adhesion results to produce agglomerates (Kudra, 2003). It is essential that, for successful particle coalescence to occur, the kinetic energy of the particle before the collision is dissipated in the liquid bridge (Ennis, Tardos, & Pfeffer, 1991; Hogekamp, 1999a, 1999b; Tardos, Khan, & Mort, 1997; Tardos & Talu, 2000). Therefore if the kinetic energy is too large or viscous forces in the liquid bridges are too weak particle rebound will occur. Bridges that have high solids contents, high viscosity, and are between small particles are likely to be the strongest.

Currently there is little understanding of the processes of collision, adhesion, rebound, deformation, fracture and coalescence that occur during agglomeration. Collisions between particles can result from motion or turbulence and adhesion of particles following collision depends on the existence of attractive forces (Hogg, 1989). Forces acting on fine particles and agglomerates include gravity, hydrodynamic (drag) forces, thermal energy, van der Waals forces, electrical forces, chemical forces, solvation forces and capillary forces.

The process of droplet deposition followed by coating and granulation are mechanisms which are not yet fully understood (Panda, Zank, & Martin, 2001), however experimental investigations in this area are increasing. Panda et al. (2001) indicate that drop velocity has little effect on the growth rate of agglomerates. However Link and

Schlünder (1996) have shown that there is a critical droplet velocity, which results in droplets bouncing back from the surface. For droplets impacting a surface, velocity initiates spreading and surface tension forces pull the droplet back towards the centre (Aziz & Chandra, 2000). Droplet impact on a surface is often accompanied by break-up of large droplets or splashing. Immediately after a droplet impinges on a surface a thin liquid film jets out radially, waves form along the edges of the film and if the growth of these waves is not damped out by viscosity or surface tension they can detach producing small satellite droplets (Shakeri & Chandra, 2002). Although the mechanism that causes splashing is not entirely understood, it is proposed to be caused by Rayleigh-Taylor instability on the edges of the spreading liquid film. Recent work in the area has found this theory can be applied well experimentally.

Figure 2.11 below depicts some possible outcomes for the process of droplet impact and spreading taken from Werner (2005) with reference to spray coating. Figure 2.11(a) represents rebound, droplet velocity is too high or drying has occurred; Figure 2.11(b) is the case of limited spreading after impact and adherence. If the droplet impact velocity is too high, splashing may occur (Figure 2.11(d)) or if recoil velocity is too high, the droplet may be ejected from the surface (Figure 2.11(e)).

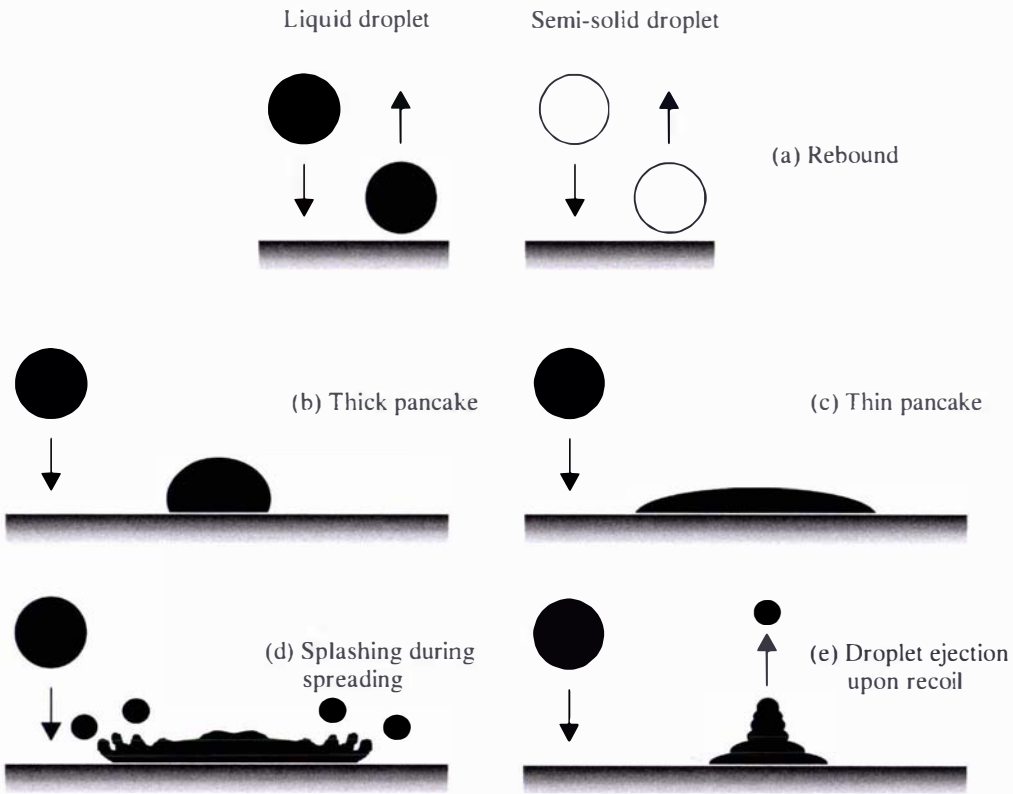

Figure 2.11: Possible outcomes of the impact of a droplet on a flat, dry surface: (a) liquid and solid droplet rebound; (b) thick pancake; (c) thin pancake; (d) splashing during spreading; (e) droplet ejection upon recoil (from Werner (2005)).

Chemical forces can contribute to agglomerate strength but are not important during the formation and growth of agglomerates. Interaction forces are important in most aspects of agglomeration including the formation and growth of agglomerates from discrete particles and in the structure and mechanical strength of the agglomerates produced.

The capillary pressure can be estimated for concentric liquid bridges between two particles determined by Rumpf (1990). If the calculated pressure within the liquid is less than the external pressure it adds to the adhesion. The attractive force can be calculated to quantify the van der Waals force based on Hamakers microscopic theory (Rumpf, 1990). When two solid surfaces come in contact electrostatic forces of attraction arise as a result of the charged surface of the particles.

Rumpf's classification of particle-particle bridging has been summarised by Capes and Darcovich (1997) although a number of bonding mechanisms are likely to occur. The four major groups are intermolecular and electrostatic forces, liquid bridges, solid bridges and mechanical interlocking. The regimes of liquid contact which can exist in an agglomerate are shown in Figure 2.12. For each state a different agglomerate strength can be calculated as the adhesion of particles together with a liquid affects the interfaces at the agglomerate surface which impacts upon the strength of the bonds formed.

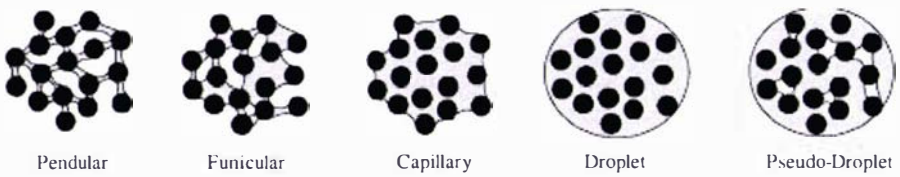

Figure 2.12: States of liquid content in bonding (Iveson et al., 2002) .

The granulation literature states that, if the kinetic energy of the collision is known, together with the liquid layer thickness and the deformation properties of (spherical) granules, then the criteria for successful coalescence can be determined (Liu et al., 2000). The growth process is known to be driven by surface tension and viscous forces as well as the wetting behaviour of the liquid. Surface tension forces promote compaction and coalescence; however they also give rise to frictional forces acting between particles which make up the agglomerates.

Ennis et al (1991) proposed that viscous forces prevent rebound and allow particles to stay in contact long enough for coalescence to occur. This theory is applied best to rigid particles and does not account for the energy of dissipation by internal deformation. Other authors (Keningley, Knight, & Marson, 1997) supported this theory and emphasised the role of viscous forces during coalescence, particle bonding and growth. The Stokes' number highlights the importance of viscosity. Limiting values of the Stokes' number (equation (2.22)) can be defined for the type of coalescence and rebound that will occur if the Stokes' number exceeds the limit. In practice, it is not possible to measure the sizes and velocities of all the particles involved in the collision and it is not reasonable to assume that the surface is uniformly covered by a viscous layer.

$$St_V = \frac{8\rho u_0 r}{9\mu} \tag{2.22}$$

where St_V = viscous Stokes' number, ρ = granule density [g cm^{-3}], u_0 = initial relative granule collisional velocity [cm s^{-1}], r = particle or granule radius [μm] and μ = binder viscosity [Pa s].

Ennis et al. (1991), and Liu et al. (2000) have investigated collisions between two spherical particles with wetted surfaces and the forces involved. Following successful droplet-particle impact it is essential to establish what conditions are required for coalescence to occur. If it is considered that all of the kinetic energy of the collision is dissipated in the pendular liquid bridge formed between particles, the minimum velocity required for particles to rebound (or maximum velocity required for particle capture to occur) can be determined. Practically, both capillary and viscous dissipation mechanisms can occur simultaneously, however viscous dissipation is dominant. The critical Stokes number, St^*, for rebound is:

$$St^* = \frac{8\rho u_0 r}{9\mu} = \left(1+\frac{1}{e}\right)\ln\left(\frac{\delta}{h_a}\right) \tag{2.23}$$

e = coefficient of restitution [–], δ = thickness of the liquid film on granule surface [m], and h_a = height of granule surface asperities (i.e. surface roughness) [m].

Some particles may absorb the collision energy by deformation and Iveson et al. (2001) use a Stokes deformation number to describe the threshold for deformation adherence. This number measures the ratio of impact kinetic energy to the plastic energy absorbed per unit strain. This may be important for semi-dried droplets that may exhibit a yield stress upon impact.

$$St_{def} = \frac{\rho_p U_c^2}{2Y_g} \tag{2.24}$$

where U_c is the collision velocity [m s^{-1}], ρ_p is the particle density [kg m^{-3}] and Y_g is the dynamic yield stress.

An alternative approach is that of Simons (1994) who developed a model to provide a value of the rupture energy of pendular liquid bridges. Fairbrother and Simons (1998) expands on this work and directly measures bridge rupture energies between particles as small as 3 μm in diameter. The viscous forces do not always dominate and a simple expression for the energy required to rupture a pendular liquid bridge was derived for the case of perfect wetting (i.e. zero contact angle).

$$W^* = cV_b^{*0.5} \tag{2.25}$$

where W^* = dimensionless rupture energy [–], ($W^* = W/\sigma r^2$, where W = pendular bridge rupture energy [J] and r = particle radius [m]), c = constant [1.8] and V_b^* = the dimensionless bridge volume [–], ($V_b^* = V_b/r^3$ where V_b = volume of the pendular bridge [m^3]). The approximation of the rupture energy of a liquid bridge can be made with knowledge of the bridge volume, the particle size and the surface tension of the coating solution.

2.5.2 Droplet Spreading

After successful collision and adhesion between a droplet and particle, droplet spreading may occur, resulting in a wetted particle surface. The phenomenon of spreading has been studied by several authors with a variety of applications including particle coating, spray painting, combustion, spray cooling and inkjet printing (Aziz & Chandra, 2000; H. Liu, 2000; Werner, Jones, & Paterson, 2007a). In coating applications Figure 2.11(c) results in the best spreading conditions. For agglomeration a thick pancake (b) is likely to enable the formation of liquid bridges to produce a grape-like structure.

The extent of spreading depends upon the properties of the droplet such as size, temperature, impact velocity, viscosity and the interfacial energies (Aziz & Chandra, 2000; Link & Schlünder, 1996; Pasandideh-Fard, Chandra, & Mostaghimi, 2002; Pasandideh-Fard, Qiao, Chandra, & Mostaghimi, 1996). If the droplet spreads easily, it may coat the particle and produce the "onion" structure (see Figure 2.4). If the droplet does not spread well or retains its shape as it dries, typical grape-like agglomerates are obtained. Werner et al. (2007a; 2007b; 2005) investigated droplet spreading on anhydrous milk fat (AMF) with the aim of maximising spread diameter. They found that high impact velocities and droplets with lower viscosities experienced more spreading.

Pasandideh-Fard et al. (1996) established a simple model to estimate the maximum droplet spread diameter which assumes the sum of the kinetic energy and the surface energy of the droplet before a collision is equal to the sum of the energy dissipated and the surface energy after collision (equation (2.26)).

$$KE_1 + SE_1 = KE_2 + SE_2 + W_{vis} \tag{2.26}$$

where KE_1 = kinetic energy before impact, SE_1 = the surface energy before impact, KE_2 = the kinetic energy after impact when the droplet is at the maximum diameter (KE_2 = 0), SE_2 = surface energy after impact and W_{vis} = the work done in deforming the droplet against viscosity. These terms are included in the following equations:

$$KE_1 = \left(\frac{1}{2}\rho U_0\right)\left(\frac{\pi}{6}D_0^3\right) \tag{2.27}$$

$$SE_2 = \pi D_0^{\,2}\sigma \tag{2.28}$$

$$SE_2 = \frac{\pi}{4}D^2{}_{\max}\sigma(1-\cos\theta_a) \tag{2.29}$$

$$W = \frac{\pi}{3}\rho V_0^{\,2} D_0 D_{\max}\frac{1}{\sqrt{Re}} \tag{2.30}$$

where ρ = droplet density [kg m^{-3}], U_0 = droplet impact velocity [m s^{-1}], D_0 = initial diameter of the spherical droplet [m], σ = surface tension [N m^{-1}], D_{max} = the maximum diameter of the droplet [m], θ_a = advancing contact angle [°].

2.6 Agglomerated Product

The final stage in the production of instant milk powder is further drying and shrinkage, which occurs once the surface moisture of the agglomerates is so low that no further adhesion occurs. Their final size, density and moisture content influence bulk properties of the powder such as flowability, bulk density and reconstitution performance. Powder flowability directly influences powder behaviour during handling. Bulk density will determine the packaging, storage and transportation costs for a powder and reconstitution performance is an indication whether an agglomerated milk powder can dissolve instantly in water and therefore determines the powder's applications. Agglomerate structure is defined by the extent of agglomeration and Pisecky (1997) defined an agglomerate efficiency as the percentage of agglomerates in the powder before the fines are separated. By controlling the extent of agglomeration, or agglomeration efficiency, the bulk density and agglomerate strength may also be controlled.

While the process of spray drying has been widely investigated there have been few studies that focus on the prediction of product physical properties. Yu, et al. (1995) investigated the effect of operating parameters on the agglomeration and packing behaviour of coal and showed that particle size and bulk density were largely influenced by initial properties. More recently, several experimental studies aimed to link product properties or powder quality to the controllable operating parameters during spray drying for a variety of products (Birchal et al., 2005; Goula et al., 2004; Huntington, 2004; Kwapinska & Zbicinski, 2005; Nijdam & Langrish, 2005). Most of these studies are carried out on laboratory scale spray driers where the atomised droplets may not be exposed to the same drying environment as the industrial scale due to very short residence times.

Milk powder properties were characterised by Caric and Milanovic (2002) to be physical, functional, biochemical, microbiological and sensory and all have an impact on powder quality. In particular the physical and functional properties will have a large impact on the performance of an instant milk powder intended for use as a food ingredient requiring hydration.

2.6.1 Physical Properties

The significant physical properties of agglomerates include particle size, shape, density and strength which link to the bulk properties of flowability and bulk density. The shape and size of the particles will affect their packing and powder bulk density. Agglomeration also results in powder with better flowability, which is the ability of a power to flow freely without forming lumps or arching. Larger particles flow more easily than fine particles and particles with a narrow size distribution flow more freely than for a broad size distribution. The moisture content, size, distribution and morphology will affect the bulk density and flowability of the powder and particle strength will also need to be considered during handling/transport. Walton and Mumford (1999) identified that particle morphology related clearly to the above mentioned product properties. Ilari (2002) points out that the flowability of dairy powders can vary significantly depending on both composition and structure.

The bulk density of milk powders is influenced by the particle density and the particle size (Pisecky, 1978). Hogekamp and Pohl (2003) found that the porosity of whole milk powder is lower than that of skim milk powder agglomerates and that porosity increases with increasing particle size. The particle density of a powder is affected by the amount of occluded air in the powder particle; this is mainly due to the inclusion of air into the concentrate feed. Verhey (1973) established that vacuole formation occurs during the atomisation stage due to air incorporation. Gas bubbles are entrained into the feed when it accelerates inside the atomiser, these bubbles are then dispersed during droplet formation and some small bubbles remain entrapped resulting in the formation of vacuoles. Pisecky (1978) theorised that occluded air content is due to air bubbles in the concentrate heating and expanding. The specific occluded air volume can be calculated and has been included for some common milk powder particles in Table 2.4:

Increasing the spray drier air temperature and air flow rate as well as increasing the concentrate total solids and concentrate feed rate can cause a decrease in particle density and bulk density of the powder. Masters (1979) states that pressure nozzles with low capacity have negligible vacuole formation whereas high capacity pressure nozzles aerate the milk concentrate to a similar extent to rotary atomisers. Atomizer type is not the only parameter to be considered when trying to control bulk density, concentrate properties and drier operating conditions are also important.

Table 2.4: Particle density for some dairy powders (Chen, 1994)

Product	Particle Density	True Density	Specific Occluded Air Volume
	($g\ ml^{-1}$)	($g\ ml^{-1}$)	($ml\ g^{-1}$)
SMP	1.28	1.53	0.13
WMP	1.21	1.28	0.05
Instant WMP	1.25	1.28	0.02

Agglomerate strength is a parameter which must be optimised for instant milk powder manufacture as the agglomerates formed have relatively weak bonds. This is essential and is driven by the milk powder function or end use as it must break up and dissolve easily upon reconstitution. However, it is also essential that the weak agglomerates formed are not broken up during transportation. The bond strength of agglomerates is a key issue for both the manufacturer and end user of the product. Ideally, milk powder agglomerates should meet the customers expectation with regard to dispersibility (an indicator of powder quality) while meeting packaging requirements (bulk density) and surviving storage and transport. Therefore, these powders need have an "optimum" agglomerate strength meaning that the bonds within the agglomerate need to be weak enough to allow dispersion in liquid but strong enough to prevent attrition during processing and transportation. Industrially, agglomerate strength is inferred and instead of measuring bond strength directly, powder strengths are compared using a fluidised bed technique (P.Webby, personal communication, 2005). Agglomerate strength can also be determined by the extent of breakage which can be estimated using a variety of methods which usually relate some impact velocity to a loss in mass or size (Boerefijn & Hounslow, 2005). Samimi et al. (2003) showed that agglomerate strength depends largely on the method of manufacture and also showed that drying strengthens agglomerates.

Beekman (2002) defined breakage using four terms: (i) attrition – small force in normal direction resulting in removal of asperities on a particle surface, (ii) abrasion – small force in tangential direction leading to polishing of particle surface, (iii) fragmentation – high force in normal direction results in breakage, (iv) chipping – high force in tangential direction leading to roughness (Figure 2.13). Reynolds (2005) carried out a review on agglomerate breakage and testing methods. Van Laarhoven et al. (2006) use an abrasion tester to separate the tangential and normal components.

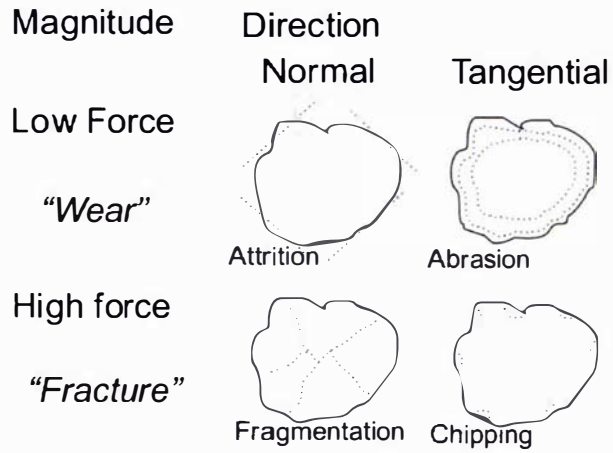

Figure 2.13: Breakage mechanisms (van Laarhoven et al., 2006)

Particle size has a significant influence on the cohesive and adhesive strength of a particulate system. Cohesion is an internal property and a measure of force holding two similar particles together while adhesion is an interfacial property and a measure of force holding different particles together. The cohesive or adhesive forces are inversely related to the particle size (Buma, 1971; Rennie et al., 1999). A zone diagram showing the strength of agglomerate bond as a function of particle size is given in Figure 2.14. Schubert (1987) also found that large particles exhibit the worst mechanical stability.

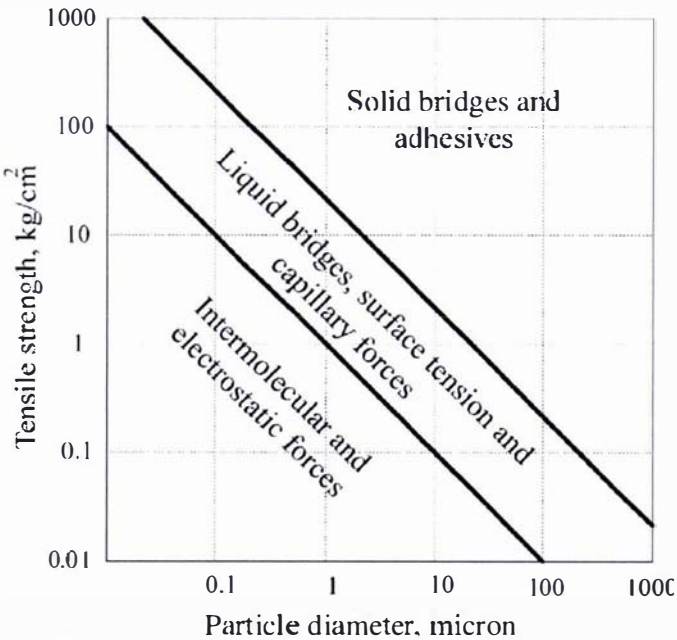

Figure 2.14: Strength of bridges to hold particles together (Rumpf, 1990).

The solid bridges binding the particles within the agglomerates will ultimately affect the attrition and breakage performance of the powder. The solid bridges are formed when the liquid bridges dry. In general, it is assumed that bonds holding the skim milk particles together are weaker than for whole milk powder agglomerates (Renner, 1989) and industrial evidence supports this. However the findings of Ozkan et al. (2002) indicate SMP bonds are stronger than WMP bonds above the glass transition temperature. It is unclear why SMP are more prone to breakage upon handling. A possible reason is due to the compositional differences in the bridges. The high fat content of the WMP bridges are likely to be mobile and rubbery, the bridges in the SMP agglomerates have a lower fat content and are likely to be rigid and more brittle resulting in breakages during handling.

2.6.2 Functional Properties

The functional properties of milk powder agglomerates link primarily to the reconstitution performance. Reconstitution refers to the process of recombining milk powder with water to give its original composition (Walstra, 1999). However, some loss of nutrients and flavour changes will result due to the manufacturing process. The following steps make up the process of reconstitution:

1. immersibility
2. wettability
3. dispersibility
4. solubility

Immersibility relates to the powder's ability to break water surface tension and submerge into the liquid. Wettability is the penetration of the liquid into the pores of the powder particle and depends on the surface activity of the particle's surface area, surface charge, particle size, density and porosity (Caric & Milanovic, 2002). Dispersibility refers to the ability of particles to disperse and mix in the water forming a homogenous emulsion. Dispersibility is improved by agglomeration and minimising the holding time and temperature of the concentrate. The solubility is the process of forming and maintaining a stable emulsion in water and depends on the three previous steps. The solubility index is a measure of the un-dissolved residue of milk powder and is often a key indicator of product quality which represents the suitability of the agglomerated product to be reconstituted. Poor solubility is often due to denaturation of milk proteins so heating of milk concentrate needs to be minimised.

The powder structure and particle size distribution will have a big impact on these processes and it is considered that a particle size of 150 – 200 μm is the best for reconstitution (Caric & Milanovic, 2002). Fitzpatrick and Cuthbert (2004) have found that the immersibility or "sinkability" of the powder is the most limiting factor when reconstituting using mixing. Hla and Hogekamp (1999) state that for most instantised powders the wettability is the critical, rate controlling step of the re-dispersion process. Both statements are correct as step one must be performed before the others can occur however step 2 may be the most time dependent step and are likely to influence whether a powder can be termed "instant".

2.6.3 Biochemical, Microbiological and Sensory

The physical and functional properties will all contribute to the quality of the powder. The biochemical, microbiological and sensory properties of the powders are just as important when considering the suitability of a powder. Flavour, composition, colour and the presence of scorched particles can all be considered as sensory properties. Scorched particles are overheated or burnt particles that have undergone Malliard reactions which result in browning and undesirable flavours.

Milk powder composition can also affect the physical and functional properties of a powder. The presence of fats on the surface of agglomerates can prevent wettability during reconstitution and lecithin is sprayed on the surface of instant whole milk powder to overcome the surface hydrophobicity. Milk powders with high amorphous lactose contents are also likely to have reduced flowability due to lumping and caking during storage resulting in handling problems if not dried sufficiently before storage.

Storage conditions are also important for powder stability, specifically powder moisture content, water activity, storage temperature and humidity. The term 'water activity' describes the amount of water available for hydration of materials. Roos (2002) states the water activity of dairy powders must be below 0.37 to retain quality. Figure 2.15 demonstrates the effect of water activity on the rate of transformation processes that can occur during storage of dairy powders. Powders can become sticky and lactose may exhibit crystallisation which may enhance the deterioration of the dairy powders resulting in browning and oxidation. The growth of moulds, yeast and bacteria are processes which specifically need to be avoided during storage to ensure that milk powders are suitable for human consumption.

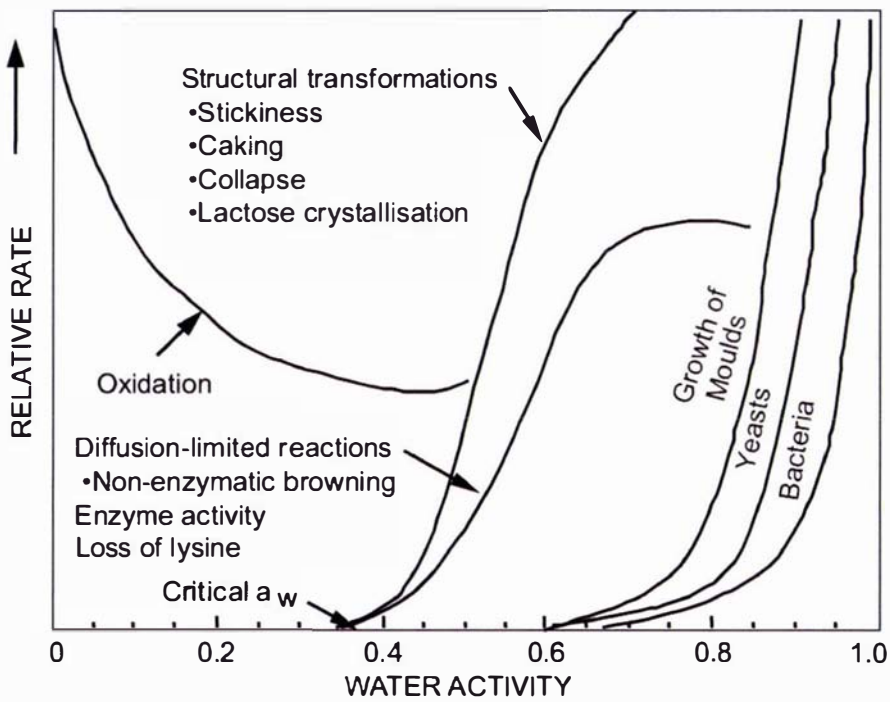

Figure 2.15: Stability map for dairy powders containing amorphous lactose (Roos, 2002).

2.7 Chapter Conclusion

In this chapter the phenomenon of agglomeration was introduced and discussed in relation to the existing literature. Agglomeration is still a relatively new area of research, and still needs to be described completely. Agglomeration is a complex process with many interacting variables that influence product properties. Granulation is a topic which has been widely studied, and spray drying has also been well researched, but little emphasis has been placed on investigating agglomeration during spray drying.

During agglomeration, the many complex processes occurring can be simplified into a few micro-processes; droplet formation; impact and adherence followed by drying and shrinkage. The literature has defined the conditions for adhesion following collisions but need to be validated for forced agglomeration. The structure of the agglomerate formed will depend on the above processes which will influence the final properties of the product. Physical and functional properties such as particle size, shape, density, and reconstitution performance are intertwined although there is limited knowledge of how they influence each other.

CHAPTER 3

BENCHMARKING INDUSTRY PERFORMANCE

To study agglomeration with the aim of improving bulk density control, a clear understanding of the scale of the problem is required. This chapter benchmarks the performance of some Fonterra spray drying plants that produce agglomerated or 'instant' milk powders. It also outlines the currently accepted practise for instant milk powder production and the knowledge that exists in industry regarding agglomeration processes. There were five main objectives in this benchmarking investigation:

- Determine the level of downgrades where product does not meet target bulk density and 'instant' properties.
- Identify how operators control the bulk density of instant milk powders
- Identify plant configurations for instant milk powders using pressure nozzles
- Investigate the effect of operating parameters on agglomerate properties
- Estimate fines recycle flow rates for one powder on one spray drier

These objectives were carried out on several plants at one Fonterra site. The fines recycle study was performed on the low capacity drier which has only one fines recycle line and therefore required less powder to imitate the fines recycle mass flow rates. The findings of the benchmarking study were later used as a guide for the equipment and experimental design in the experimental part of this project.

3.1 Powder Selection and Level of Downgrades

It was essential to select industry powders to use as a reference for the experimental study. To keep the scope of this investigation as narrow as possible, plant operation was investigated for two instant skim milk powder (ISMP) and five instant whole milk powder (IWMP) using high pressure nozzles. Table 3.1 lists the downgrades due to product not meeting the target bulk density for instant whole and skim milk powders at one Fonterra site. Due to the high percentage downgrades for powders that are produced at a high rate of production an ISMP A and an IWMP E produced at one Fonterra site were selected for further study.

Table 3.1: Bulk density downgrades for one Fonterra site.

Powder	Specification	Bulk Density Downgrades (tonnes)	Total Production (tonnes)	% Downgrades (%)
ISMP	A	H	H	2.9
ISMP	B	L	L	1.2
IWMP	C	L	H	0.1
IWMP	D	L	L	0.8
IWMP	E	H	H	1.5
IWMP	F	H	L	23.7
IWMP	G	L	H	0.2

3.2 Operator Knowledge

The procedure used to control bulk density of agglomerated milk powders was assessed by surveying plant operators at several Fonterra sites. The survey asked operators a number of questions relating to bulk density control; however the actual results have not been included as they are commercially sensitive. The questions asked have been included below.

When controlling the bulk density of an agglomerated bulk powder:
1. what operating parameters do you change and what is your first step?
2. does your first action always work?
3. would you change each parameter individually?
4. do these steps increase or decrease the mass flow rate of fines?
5. what operating parameters would you avoid changing?

Control of bulk density is difficult as Fonterra has a range of plant types, some of which have been modified since installation and each plant has its own idiosyncrasies. For this reason there are no standard operating procedures for controlling bulk density and operators usually act from their own experience. This means the steps taken to manipulate bulk density vary from plant to plant and also change between shifts. The surveys results often produced conflicting answers; for example, some operators would avoid altering the total solids of the milk concentrate while for others this would be the first step to take when controlling bulk density. All operators agree that increasing total solids results in an increase in bulk density. Because of the different responses, it is speculated that different drier types and configurations affect which operating parameters are effective in controlling bulk density during instant milk powder production.

In general, the next step taken by operators to change the bulk density is to alter the fines recycle rates. This is currently achieved by increasing or decreasing the air to the fluid beds to change the level of "fines stripping". "Fines stripping" is the term used to describe the process where particles leave the powder bed and are carried with the air stream to the cyclones. Increasing the air flow rate to the fluid beds will increase the size (and therefore the amount of particles) that can be transported by the air stream. However, no current measurement of recycle fines flow rates is performed on any spray driers continuously.

Bulk density is currently measured hourly by taking a small sample prior to packaging and, therefore, it is difficult to determine how bulk density actually fluctuates from bag to bag. This makes it difficult to assess when changes have occurred and by what magnitude. Continuous bulk density measurement of powder, would allow a correlation between the measurable operating parameters and powder bulk density.

An increased understanding of the important mechanisms that influence agglomeration and therefore powder bulk density will lead to standardising operations. However, before agglomeration and therefore bulk density can be controlled, both the recycled fines and milk concentrate properties need to be measurable and controllable.

3.3 Drier Configuration

Early spray driers had only a single drying stage and there were several disadvantages associated with this, a large chamber, high outlet temperature, low feed flow and therefore low capacity and because of the high inlet temperature particles could experience heat damage. Most modern plants are now designed to incorporate a second stage drying through the use of static and/or vibrating fluid beds following primary drying in the chamber. A secondary drying stage extends the residence time available for drying and improves on all of the disadvantages of single stage drying. The moisture content of the product exiting the spray drying chamber can be higher which means the drier is more flexible and more efficient. The powder quality is usually better, the powder cools and some level of agglomeration can occur which can help with bulk density control. There are several types of secondary stage drier:

- Vibrating fluid bed (VFB)
- Well-mixed fluid bed
- Integral or static fluid bed (IFB or SFB)
- Niro multi-stage drier (MSD)

3.3.1 Fonterra Palmerstone North Plants

Fonterra Palmerston North has two pilot scale driers, the De Laval and the Integral Fluid Bed (IFB). The De Laval is a tall form drier and has a diameter of 2.134 m and a production rate of 150 kg h^{-1}. The fines are returned through 2 inch pipes and expand to 3 inch at the top of the drier where a nozzle line flows inside this pipe. The IFB has a diameter of 2.9 m and can produce ~ 75 kg h^{-1} of powder. The fines flow pipes are 2 inches and expand to 3 inches at the top of the drier where fines are returned tangentially. Three lances are positioned evenly around this fines return point and are directed towards the centre of the drier and each other.

3.3.2 Fonterra Manufacturing Plants

Two different Fonterra plants were selected to benchmark the current practice with respect to instant milk powder production; a Stork Wide Body drier and a Niro Compact drier. The Niro Compact is similar in configuration to the IFB at Fonterra Palmerston North and this drier produces ISMP A at a product rate of ~ 3500 kg h^{-1}. This drier has a swirling air flow that enters the drier tangentially at approximately 125 000 m^3 h^{-1}. At the top of the drier are 6 nozzles positioned, around the central fines return point. The fines from the vibrating fluid beds and the drier exhaust are collected in a bag house where they are returned to the top of the drier.

The Stork Wide Body drier is similar to the De Laval at Fonterra Palmerston North. A concentrate flow rate of ~ 35 000 L h^{-1}, and air flow into the drier of ~ 300 000 m^3 h^{-1} was used to produce IWMP E. At the top of the drier are 6 venturis; each has a bank of 8 lances with a central fines return point jacketed by cooling air. The Stork Wide Body has an external well mixed bed and two trains which each have two vibrating fluid beds and a sifter. There are three sources of fines, from the fluid beds (one from each train) and from the drier exhaust cyclones. Four inch lines deliver fines to the top of the drier where each line splits into two 3 inch lines.

3.4 Investigating Specifications ISMP A and IWMP E

The key operating parameters that operators believe influence bulk density when manufacturing instant milk powder were discussed in §3.2. An investigation was carried out to confirm the relationship between operating parameters and powder properties for the Niro Compact producing ISMP A and the Stork Wide Body spray drier producing IWMP E. The study on the Niro Compact measured the properties of samples taken from the static fluid bed (SFB) and the 2nd vibrating fluid bed (VFB), sifter and one packaging sample. Only one sample was taken because it was not possible to track the location of each powder following the sifter as the powder was stored in bins before packing. After, changing operating parameters, the drier was allowed to reach steady state before repeating the sampling.

The study on the Stork Wide Body drier only assessed the influence of total solids on powder properties and this variable was only changed slightly (indicated by concentrate density). This was due to the high cost risk of falling outside the functional standards required for specification IWMP E. Hence, a different assessment approach was taken. Two sets of samples were taken one hour apart. Samples were taken from the well-mixed bed, sifters A and B, the packaging line and fines were sampled from above the vibrating beds because it was unsafe to sample at the cyclones. This fines sample was not an actual representation of the fines returned to the top of the drier because it ignores fine collected by the cyclones mounted near the top of the drier.

The particle sizes of all powders were measured according to the method in Appendix A using the Mastersizer 2000. Agglomerate strength can be assessed in several ways; in terms of powder survival in the transportation system after exiting the drier chamber and also by its "breakdown' or strength which is only implied. It is the change in BD experienced by each powder under standardised shear conditions and this is what allows the comparison. Breakdown was measured using a fluidisation device (P. Webby, personal communication, 2005), and the procedure for using this is included in Appendix B. Survival in the transportation system can be assessed by comparing the bulk densities of the powder after leaving the drier (at the well mix or SFB) with the bulk density of the powder at packaging. The methods for determining the moisture content and bulk density of the samples are included in Appendix C.

3.4.1 ISMP A Results and Discussion

Table 3.2 records the moisture, particle size, and bulk density of the powders sampled for ISMP A produced on the Niro Compact at varied fines flow rates and concentrate total solids levels. The results indicate that the increase in bulk density is within the bounds of error and there is no relationship between bulk density and the operating parameters investigated. However, agglomerate strength appears to decrease slightly with increasing total solids; this opposes current operator belief. The "survival" of the powder in the transportation line from SFB to the sifter is consistent between experimental conditions and can be expressed in terms of a bulk density decrease of 0.06 – 0.08 g m^{-3} from the SFB to packaging. The moisture levels were consistent between experiments, and the fines were ~ 1% higher than the powder from the SFB and ~ 1.5% higher than the powder sampled at the point of packaging.

Table 3.2: Powder properties for ISMP A collected from the Niro Compact.

Time	Point	Fines Flow	Total Solids	Bulk Density (loose)	Bulk Density (tapped)	Moisture	$D_{3,2}$	Break-down
			(%)	(g m^{-3})	(g m^{-3})	(%)	(µm)	(g m^{-3})
10:45	SFB	Base	43	0.37	0.42	4.4	113	
	VFB			0.39	0.45		124	
	Sifter			0.40	0.44		120	0.227
	Fines					5.6	54	
11:30	SFB	Base	44	0.37	0.42	4.4	119	
	VFB			0.39	0.44		119	
	Sifter			0.39	0.45		121	0.230
	Fines					5.4	55	
12:30	SFB	Base	46	0.36	0.41	4.4	125	
	VFB			0.39	0.44		123	
	Sifter			0.39	0.44		121	0.234
	Fines					5.4	53	
1:30	SFB	High	45	0.38	0.43	4.1	119	
	VFB			0.40	0.45		130	
	Sifter			0.39	0.45		125	0.235
	Fines					5.3	56	
2:00	Packaging				0.49	4.0	121	0.199

SFB = static fluid bed, VFB = vibrating fluid bed, error for TS ± 0.3, error for moisture ± 1% of the measurement e.g. 4.4 % ± 0.044, error for loose bulk density ± 0.03, error for tapped bulk density ± 0.01

3.4.2 IWMP E Results and Discussion

The properties of IWMP E powder at the various collection points are included in Table 3.3. The results indicate there is no link between a small increase in total solids (indicated by concentrate density) and the bulk density of the powder. IWMP E powder from the Stork Wide Body Drier has a high level of breakdown in the transportation line, indicated by an increase in bulk density from 0.39 to 0.50 g m^{-3} from the well mix to the packaging. This is similar to the breakdown experienced by ISMP A in the Niro Compact transport system. The IWMP E appears to have a higher agglomerate strength (breakdown = 0.060) than ISMP A (breakdown = 0.199). The IWMP E product has moisture of ~ 2.9% (compared to 4.0% for ISMP A) and fines moisture of ~ 4.7% (compared to 5.3 to 5.6% for ISMP A). The particles sizes for both powders are in a similar range; however ISMP A fines have a mean particle size of approximately 55 µm compared to around 114 µm for IWMP E. This difference could be due to the sampling point. While on the Niro Compact fines were sampled before being returned to the top of the drier, on the Stork Wide Body they were sampled above the fluid beds.

These results do not confirm current operator belief related to how operating parameters affect the bulk density of instant milk powders. As the variations in agglomerate strength and bulk density are very small, the differences are not significant enough to show a relationship between operating parameters and powder properties. It should be noted that the powder has a residence time of ~ 30 minutes in both plants.

Table 3.3: Properties of IWMP E instant whole milk powder.

Time	Sample	Conc Density	Bulk Density (loose)	Bulk Density (tapped)	Moisture	$D_{3,2}$	Breakdown
		(kg m^{-3})	(g m^{-3})	(g m^{-3})	(%)	(µm)	(g m^{-3})
14:00	Well Mix	1108	0.33	0.39		108	
14:00	Sifter A		0.34	0.4		122	
14:00	Sifter B		0.36	0.42		116	
14:00	Packaging		0.40	0.5	2.9	109	
14:00	Fines				4.7	112	
15:00	Well Mix	1109	0.34	0.40		109	
15:00	Sifter A		0.34	0.41		113	
15:00	Sifter B		0.34	0.41		121	
15:00	Packaging				2.9	130	0.060
15:00	Fines				4.6	116	

Error for moisture is ± 1% of the measurement e.g. 4.4 % ± 0.044, error for loose bulk density ± 0.03, error for tapped bulk density ± 0.01

3.5 Droplet size estimation

The droplet size distribution of industrial sprays is difficult to measure, but they can be back calculated by measuring the particle size distributions of non-agglomerated milk powders, assuming limited natural agglomeration. The mean droplet size for the sprays used to produce ISMP A and IWMP E have been estimated by using standard (non-agglomerated) whole and skim milks produced on the Niro Compact and Stork Wide Body and are included in Table 3.4. The droplet size was calculated using two different methods, that of Lin and Chen (2002) (referred to as the L & C method) and Masters (1979). Lin and Chen (2002) report D/D_0 values of 0.78 and 0.8 using a drop suspended from a glass filament. The method of Masters (1979) back calculates size by mass balance using the droplet and powder solids contents using equation (2.16):

$$\frac{D_p}{D_d} = \left(\frac{\rho_c}{\rho_p} \times \frac{X_c}{X_p} \right)^{1/3} \tag{3.1}$$

where D_d = droplet diameter [m], D_p = particle diameter [m], ρ_c = density of the concentrate [kg m^{-3}], ρ_p = density of the particle [kg m^{-3}], X_c = solids fraction in concentrate [kg kg^{-1}], X_p = solids fraction in product [kg kg^{-1}].

The Sauter mean drop size was calculated to be from 64 to 67 µm for the Niro Compact. This agrees with that from nozzle suppliers (Spraying Systems) who estimate a drop size of 70 µm for water. However, spray drier operators of the Niro Compact suggest these estimates are high, and Harvie et al. (2002) state droplets in industrial driers are typically 50 µm. In contrast, the Sauter mean drop sizes for the Stork Wide Body were calculated to range from 117 to 151 µm. These are high and may be due to the age of the samples, where caking or agglomeration due to droplet-droplet collisions may have occurred resulting in an increase in particle size.

Table 3.4: Droplet size calculation for two Fonterra plants.

Powder	Plant	Particle Size	Particle Density	Shrinkage D/D_0	Shrinkage D_ρ/D	Drop Size (L & C)	Drop Size (Masters)
		(μm)	(kg m^{-3})	(L & C)	(Masters)	(μm)	(μm)
SMP	Niro	50	1430	0.78	0.75	64	67
WMP	Stork	94	1260	0.80	0.76	117	124
WMP	Stork	115	1260	0.80	0.76	144	151

SMP and WMP are standard spray dried powders, manufactured on the Niro Compact and Stork Wide Body driers by spray drying milk concentrate with no fines return.

3.6 Powder Properties

The physical properties of the two selected powders (ISMP A and IWMP E) have been included in Table 3.5. These properties include the Sauter mean particle size, bulk density, particle density and agglomerate breakdown. The changes in particle size and bulk density between the sifter and packaging indicate the breakdown that occurs over the packaging lines. During transport to packaging the ISMP A powder increases in size. However both the powder transported in lines A and B on the Stork Wide Body experience a similar level of breakdown. The ISMP appears to have a slightly lower mean particle size, a higher bulk density and a much higher breakdown (or lower agglomerate strength) than the IWMP.

Table 3.5: Properties of powders ISMP A and IWMP E.

Powder	Sample Point	Particle Size	Bulk Density	Breakdown	Particle Density
Units		(μm)	(g cm^{-3})	(g cm^{-3})	(g cm^{-3})
ISMP A (Niro Compact)	Sifter	118	0.45	0.24	1.42
	Packer	121	0.49	0.20	
IWMP E (Stork Wide Body)	Sifter A	135	0.40		1.23
	Packer A	125	0.47	0.09	1.23
	Sifter B	131	0.39		1.25
	Packer B		0.47	0.09	1.22

The gross composition of both powders has been included in Table 3.6. Powder composition affects the storage behaviour of powders (as explained in §2.4.3) and this will limit the outlet temperature for operation of a spray drier as explained in §5.1.3. These compositions are used in §4.2 to manufacture milk concentrate with a similar composition to measure the relevant physical properties.

Table 3.6: Composition of IWMP E and ISMP A powders.

Powder	IWMP E	ISMP A
Fat	28.8%	0.8%
Lactose	36.4%	53.8%
Ash	5.6%	8.3%
Protein	26.7%	33.3%
Moisture	2.5%	3.8%

3.7 Fines Properties

It was important to measure fines properties to align the design of the small scale agglomerator in Chapter 5 with industry scale production. However, the characterisation of the fines was limited by the sampling ability of the plant. Fines samples were taken from the bag house on the Niro Compact Drier with ease. The Stork Wide Body Drier fines were sampled from the weirs above the vibrating fluid beds which, as mentioned previously; do not represent the fines collected at the cyclones. Collection from the cyclones was unsafe and so was not carried out. Table 3.7 includes the measurements made for the fines and product when running at standard operating conditions for both ISMP A and IWMP E powders. As §3.5 previously established, industrial droplet sizes range from 50 to 70 μm so a fines size of 55 μm falls in the same range, indicating that fines are non-agglomerated dried droplets. On both plants, the fines moisture content was higher than that of the product. Buma (1971) recommends the fines moisture content should be > 5% to promote agglomeration.

Table 3.7: Fines and product characterisation.

Powder	Sample	Moisture (wt %)	Particle Size (μm)
ISMP A	Product	4.0	121
ISMP A	Fines	5.4	55
IWMP E	Product	2.9	130
IWMP E	Fines	4.6	116

The scanning electron microscopy (SEM) images of product and fines samples were used to characterise the shape and structure of the fines and products. The SEMs of the ISMP (Figure 3.1) indicate that the fines are mostly small particles and there appears to be no fractured or broken particles. The product agglomerates seem to be fairly strong indicating a high degree of concentrate overlap or droplet/droplet collisions during formation. The SEM's of the IWMP (Figure 3.2) shows clearly the individual droplets and particles which have joined to form an agglomerate. There does not appear to be as much concentrate overlap as the instant skim milk powder. The fines powder appears to have agglomerates of a similar size to the product powder. Some fractured agglomerates are visible and more small particles are present.

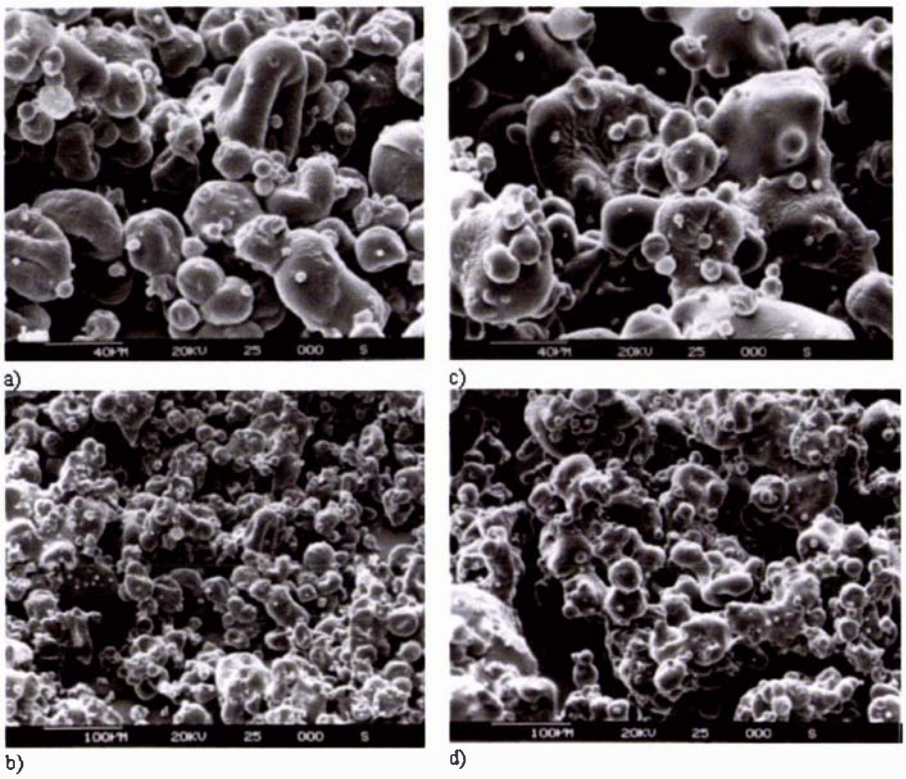

Figure 3.1: ISMP A a) fines 500x; b) fines 200x; c) product 500x; d) product 200x.

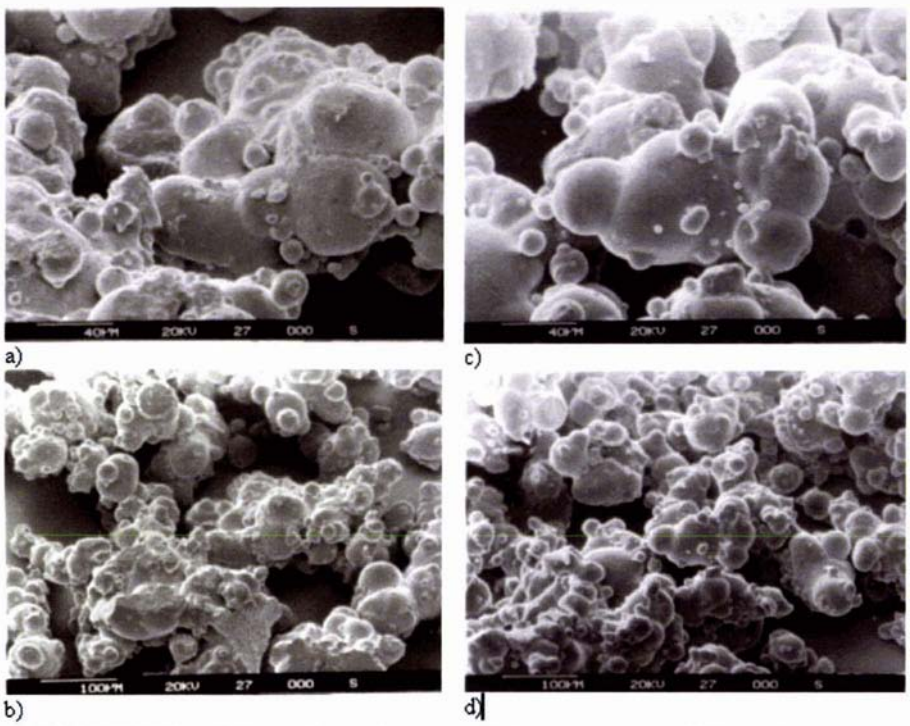

Figure 3.2: IWMP E a) fines 500x; b) fines 200x; c) product 500x; d) product 200x.

3.8 Fines Flow Estimation

Operators believe that the flow rate of fines delivered to the top of the drier is important for bulk density control. However, recycle rates of fines are currently not measured on spray driers producing agglomerated (or instant) milk powders. Despite this, they were anecdotally thought to vary from 5 to 50% of production. In order to investigate agglomeration on a small scale in a way that relates to the industrial situation an estimation of these fines recycle rates was needed.

There are a number of measurement methods available to define powder flow rates in a pneumatic line. Pressure drop measurement is inexpensive but is generally regarded as unreliable for determining solid particulate flow rates, due to large fluctuations that occur in pneumatic pipelines. More reliable methods are available (Tallon & Davies, 2000) but, because of the ease of measurement, pressure drop was used in this work. During production of instant milk powder on the Niro Compact drier, fine powder particles are carried by air from the drier or fluidised beds to the bag house where they are collected. They are then dropped via a rotary valve into a pneumatic line to be recycled to the top of the spray drier.

Instant skim milk powder (ISMP A on the Niro Compact) is currently produced at a rate of 3500 kg h^{-1}. During operation the pressure drop in the fines line is consistently 21 kPa, and fluctuates from ~ 18 to 25 kPa. This study established a calibration curve between pressure drop and fines mass flow rate for the Niro Compact drier, and uses this to investigate the suitability of the approach of Lech (2001). It is acknowledged this is not necessarily the best method available as discussed in Appendix D, and Yan (1996) gives an detailed review of the measurement techniques for solids flows in pneumatic pipelines. However, the use of pressure drop was employed here because of the easy access and low cost of taking pressure measurements. The work of Venkatasubramanian (2000) confirmed that the pressure drop-based mass flow meter of Cabrejos and Klinzing (1992) gives satisfactory results for dilute phase conveying systems suggesting this is a valid method for fines flow rate estimation.

3.8.1 Engineering Theory

Pressure drop in a vertical pipe line can be estimated using experimental correlations which relate the pressure drop to the mass loading of particles. Henthorn (2005) reports that Reynolds number, mass loading and particle shape and size can affect the pressure drop in a vertical pneumatic line. A range of studies found that an increase in mass loading will increase the total pressure drop (Hettiaratchi, Woodhead, & Reed, 1998; Klinzing, 1980; Konno & Saito, 1969; Namkung & Minyoung, 2002; Rautiainen, Stewart, Poikolainen, & Sarkomaa, 1999). However, Klinzing (1980) established that an increase in fines loading may result in a decrease of pressure drop for fine particles and at low Reynolds numbers.

There have been a range of studies investigating vertical gas-solids conveying (reviewed by Rautiainen et al. (1999)). Rhodes (1998) gives a description of the fundamentals for flow of gas and particles in a vertical pipe. The equations that govern the steady-state fully developed flow of a gas–solid suspension in a vertical pipe may be derived from relatively simple conservation laws. One of the most fundamental

concepts used in the derivation of these equations is that of a control volume. The notation and parameters associated with the control volume are in Figure 3.3. Rautiainen et al. (1999) gives a full explanation of how this control volume can be used to derive the relationships in Equation (3.2) and (3.3). The total pressure can be divided into four components; the gas and solid phase hold up pressure and the gas and solid phase frictional pressure.

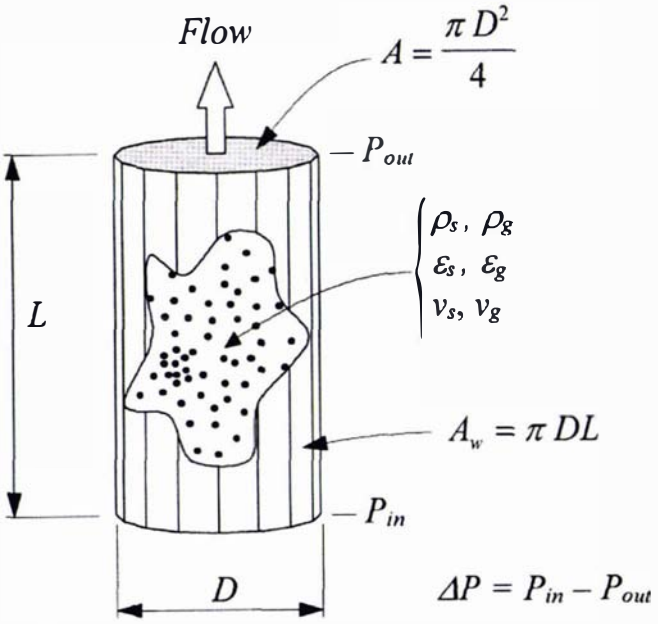

Figure 3.3: Notation for the control volume (Rautiainen et al., 1999).

$$\Delta P_T = \Delta P_s + \Delta P_g \tag{3.2}$$

$$\Delta P_T = \Delta P_{fs} + \Delta P_{hus} + \Delta P_{fg} + \Delta P_{hug} \tag{3.3}$$

where ΔP_{fs} = pressure drop due to solid friction [Pa], ΔP_{hus} = pressure drop due to hold up of solid [Pa], ΔP_{fg} = pressure drop due to friction of gas [Pa] and ΔP_{hug} = pressure drop due to hold up of gas [Pa]. Pressure drop of gas is estimated by recording the pressure losses when only air is transported. The difference between ΔP_T and ΔP_g is the loss due to solids. Lech (2001) used the Fanning equation to establish pressure drop as a function of mass flow rate for vertical transportation (see Appendix E):

$$\Delta P_s = \frac{M_p U_p g L}{A}\left(\frac{f_p}{2Dg} + \frac{1}{U_p^2}\right) \tag{3.4}$$

where M_p = solids mass flow rate [kg s^{-1}], U_p = velocity of particles [m s^{-1}], L = length between pressure transducers, A = cross sectional area of the pipe [m^2], f_p = solids – pipe friction coefficient [–], D = diameter of the pipe [m], and g = acceleration due to gravity [m s^{-2}].

Equation (3.5) relies on a friction coefficient f_p, which Lech (2001) approximated from the work of Yang et al. (1980) to be a linear relationship with the solids volume fraction, for vertical transport in a pipeline:

$$f_p = 0.0108 + 0.066(1 - \varepsilon) \tag{3.5}$$

where the solids volume fraction can be approximated by $1-\varepsilon \approx M_t/(U_t A \rho_p)$, where ρ_p is the solids particle density [kg m^{-3}].

The approximation assumes $\rho_p >> \rho_g$ and is calculated from $\varepsilon = V_g/(V_g+V_s)$ where V_g and V_s are the volumes of air and solid passing a plane in a given time. This correlation is just one of many correlations used to predict the solids friction factor (Rautiainen & Sarkomaa, 1998). The pipe line in this study is much more complicated than that used by Lech (2001) with many additional bends and horizontal sections between the fines inlet and the top of the drier. Due to particle inertia around bends and saltation in horizontal sections, the friction coefficient is expected to be greater in this work.

The correlation of Konno and Saito (1969) is a commonly used approach to relate the solids friction force to mass loading for vertical transport:

$$F_{pw} L = 0.057 m \rho_g U_g \sqrt{\frac{g}{D}} L \tag{3.6}$$

where F_{pw} = solids-pipe friction force [Pa m^{-1}], m = mass loading = ratio of the mass flow rate of particles to the mass flow rate of gas [–], U_g = interstitial gas velocity [m s^{-1}], ρ_g = density of the gas [kg m^{-3}].

For horizontal transport the solids-pipe friction force can be determined from equation (3.7) where U_p is found using equation (3.8) and f_p is determined using the correlation of Hinkle (1953) in equation (3.9).

$$F_{pw} L = \frac{2 f_p (1 - \varepsilon) \rho_p U_p^2 L}{D} \tag{3.7}$$

$$U_p = U_g (1 - 0.0638 D_p^{0.3} \rho_p^{0.5}) \tag{3.8}$$

$$f_p = \frac{3}{8} \frac{\rho_g}{\rho_p} \frac{D}{D_p} C_D \left[\frac{U_g - U_p}{U_p} \right]^2 \tag{3.9}$$

where C_D = the drag coefficient between the particle and the gas [–], and D_p = particle diameter [m].

Hinkle's analysis assumes that particles lose momentum by collision with the pipe walls and the pressure loss due to solids-pipe friction is the gas pressure loss as a result of reaccelerating the solids.

3.8.2 Experimental

The drier studied produces skim milk powder and a schematic of the Niro Compact drier studied is shown in Figure 3.4. Calibration experiments were carried out with the drier turned off. Powder was manually poured at a controlled rate into the top of the bag house. A fixed speed rotary valve [NU-CON CV [4"] 1250 DEM Round] then delivered it into the pneumatic blow-line. It is 100 mm in diameter; the radii of the bends had not been measured. The powder used for these experiments was "start-up" powder with a $D_{3,2}$ measured at 108 µm (see Table 3.8). "Start-up" powder refers to the product collected at the start of a run before the drier has reached equilibrium in relation to solids concentrations and levels of fines recycle so agglomeration is low.

The pressure gauge used was a Rosemount type 113. Readings were recorded manually off the control room screen only when changes in the trend line of pressure occurred. The pressure recordings for all trials have been included in Appendix F. Figure 3.5 shows an example of the pressure readings recorded with time and includes lines to indicate t_1 and t_2 which are the start and finish points for the measurements. The baseline was determined to be 4 kPa to account for pressure drop in the pipeline due to gas only. The pressure recordings outside of this measurement time indicate transients associated with powder entering the blow line and tailing off during powder addition. The drier fans were turned off during these experiments to avoid re-circulation of fines to the bag house, meaning the chamber was not under vacuum. Normal operating pressure is -4 mmWg (-40 Pa), which is insignificant compared to the ~20 kPa delivered by the blower (Robuschi, type SRB41/2P, 11.3 kW).

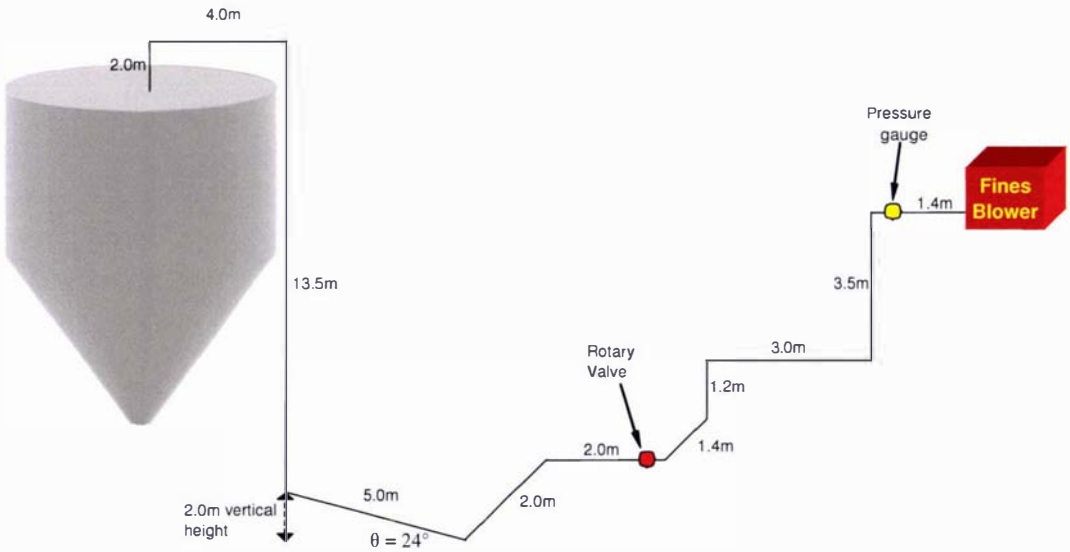

Figure 3.4: Schematic of pneumatic line showing pressure gauge and rotary valve.

Table 3.8: Comparing fines, start-up and product particle sizes.

Powder	$D_{0.5}$	$D_{3,2}$
Units	(µm)	(µm)
Fines	76	55
Start-up	161	108
Product	160	120

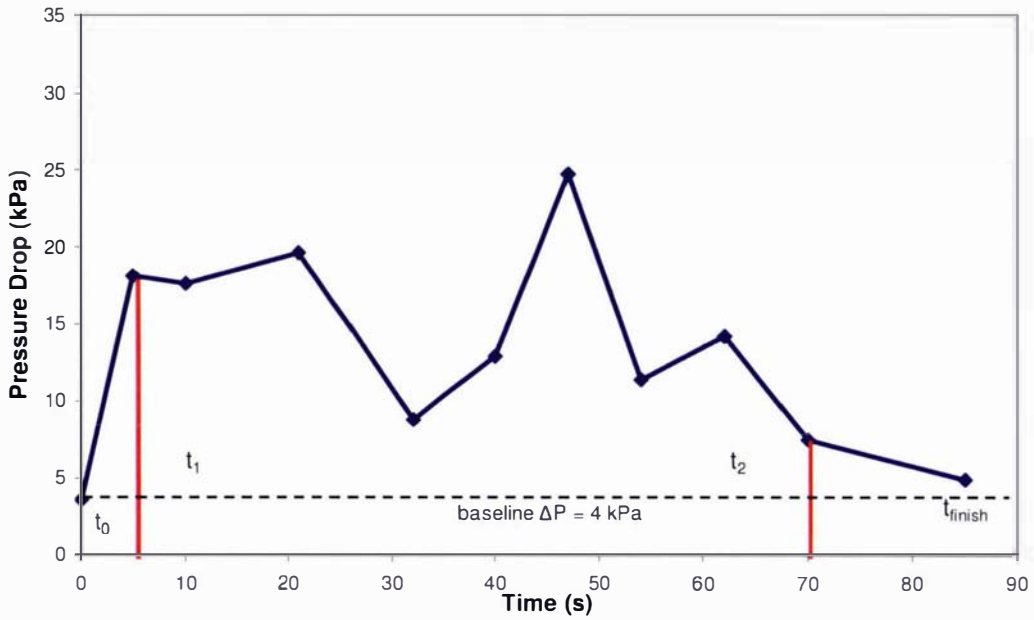

Figure 3.5: Trial 4 Pressure vs. time for manual addition rate of 61% of capacity.

3.8.3 Results and Discussion

Figure 3.6 compares the addition rate and the observed fines flow rate of the powder in the fines return line. The addition rate is the amount of powder added to the bag house during an experiment divided by the time taken for powder addition:

$$M_{add} = \frac{m_t}{t_{finish} - t_0} \tag{3.10}$$

Where M_{add} = addition rate of powder to the bag house [kg s^{-1}], m_t = total mass added [kg], t_{finish} = the time at the last pressure reading [s] and t_0 = the time at the first pressure reading [s].

The pressure gauge readings differ significantly over the recording time in some trials (Figure 3.5), indicating that powder flow through the rotary valve was not even, despite attempts to manually add powder at an even flow rate. The initial increase in pressure as powder enters the blow line and the tail-off as the last of the powder was cleared by the rotary valve constitutes transients, as do fluctuations over the (supposed) continuous feeding of the rotary valve. The observed rate was calculated by:

$$M_{obs} = \frac{m_{obs}}{t_{obs}} \tag{3.11}$$

where M_{obs} = observed fines flow rate [kg s^{-1}], t_{obs} = the time between the t_1 (the first time pressure is observed to increase after the start) and t_2 (the time when pressure is observed to decrease (see Figure 3.5) [s] and m_{obs} = mass of powder added over observed time [kg]. m_{obs} is determined by dividing the area under the plot between t_1

and t_2 by the total area (equation (3.12)). The baseline pressure drop due to gas in the pipe line of 4 kPa is subtracted from this area.

$$m_{obs} = \frac{\int_{t_1}^{t_2} \Delta P_s \, dt}{\int_{t_0}^{t_{finish}} \Delta P_s \, dt} m_t \qquad (3.12)$$

Generally, the observed delivery rate was lower than the manual addition rate due to powder hold-up in the hopper feeding the rotary valve. The rotary valve was not feed rate limited over the range investigated in this work.

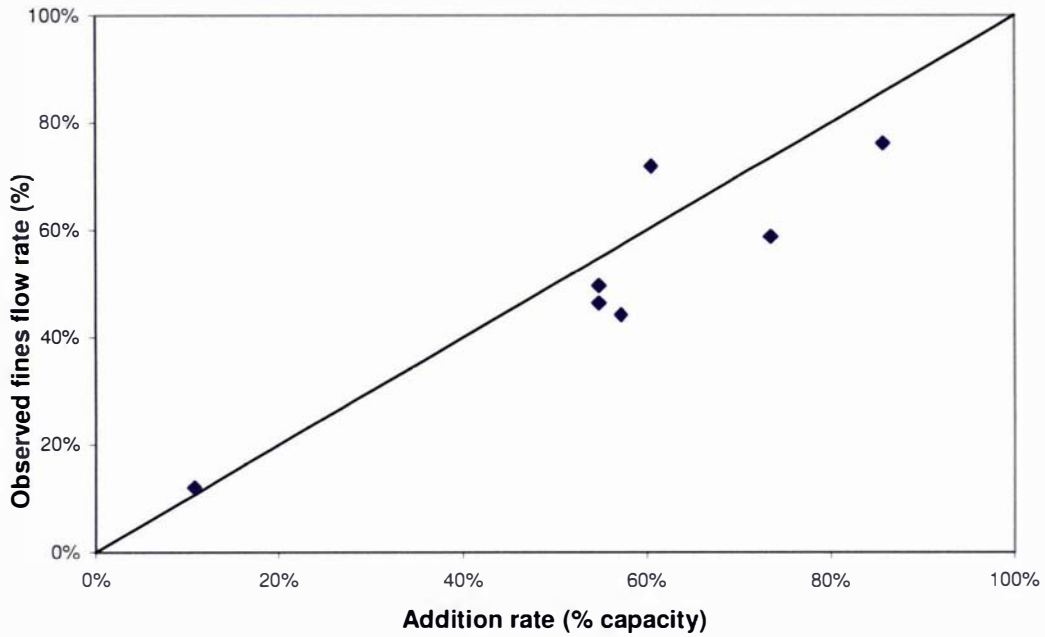

Figure 3.6: Observed fines flow rate vs. the addition fines flow rate expressed as a percentage of production capacity of the plant.

The Robuschi blower used to transport fines to the top of the drier delivers an air rate that varies as a function of the delivery pressure head. For each fines mass flow rate, Table 3.9 lists the mean pressure drop, the air rate, and solids volumetric loading using $1-\varepsilon = M_p/(Q_a \rho_p)$ where Q_a = air flow rate [$m^3\ s^{-1}$], ε = voidage [–], and ρ_p of 1280 kg m^{-3}. Particle velocity, U_p, was calculated using equation (3.8) and is used to predict the pressure drop due to solids in the discussion below.

Table 3.9: Estimated solids volumetric loadings and particle velocities.

Fines Mass Flow rate (M_f/M_{prod}) (% capacity)	Average pressure ΔP (kPa)	Air Delivery Rate $Q_a \times 3600$ ($m^3 h^{-1}$)	Volumetric Solids 1-e (-)	Air Velocity U_g $m s^{-1}$	Particle Velocity U_p $m s^{-1}$
12%	2.3	558	0.0006	19.7	16.4
44%	7.9	550	0.0022	19.5	16.1
76%	15.8	539	0.0039	19.1	15.8
72%	11.5	545	0.0036	19.3	16.0
59%	8.1	550	0.0029	19.5	16.1
50%	7.4	551	0.0025	19.5	16.1

Air delivery rate was found from the performance test curves of the Robuschi blower for a shaft speed of 2960 rpm (Appendix G), M_{prod} = the powder production mass flow rate of the drier.

Figure 3.7 compares the measured and predicted pressure drops using the correlations from §3.8.1. All predictions consider the pipe length to be from the point of fines addition into the blow line from the rotary valve. The combined predictions include an estimation of pressure drop due to bends, particle acceleration, and the inclined section of pipe line. Fan and Zhu (1998) state that inclined sections of pipe have a high pressure drop (compared to vertical and horizontal transport) to convey the solids by overcoming the forces associated with horizontal conveying and also the material's tendency to slide down the incline. It is suggested that if an inclined pipe has an angle of <15° or > 80° then the pipe can be treated as horizontal or vertical. In this case the incline has an angle of 24° as indicated on Figure 3.4, so here the vertical and horizontal components of the pipe line are used to estimate pressure drop although this approach is likely to underestimate the pressure drop for the incline

Rhodes (1998) states that there are no reliable methods for predicting the pressure drop in a bend other than by experimentally measuring the pressure drop at the specific operating conditions. The pressure drop in a bend is usually high due to particles slowing down and requiring re-entrainment and re-acceleration following a bend. Industrially, the pressure drop is approximated by using the correlations for prediction of vertical transport and assuming an equivalent length of 7.5 m per bend for a given pip diameter, which is considered to give a conservative estimate.

All correlations under-predict the actual pressure drop in this system for each fines addition rate to the pipe. The Konno and Saito (1969) expression for vertical flow compares well to the expression of Lech (2001) (which is also for vertical transport). The combined predictions which predict the pressure drop for each section of pipe agree well using either prediction for vertical pressure drop, and are better predictors than using just vertical flow but still under-predict the pressure drop. It is apparent that the correlations do not predict pressure drop due to solids for this system and they cannot be used to predict mass flow rates of fines. This reinforces the need to determine a calibration curve of mass flow rate vs. pressure drop for the specific plant.

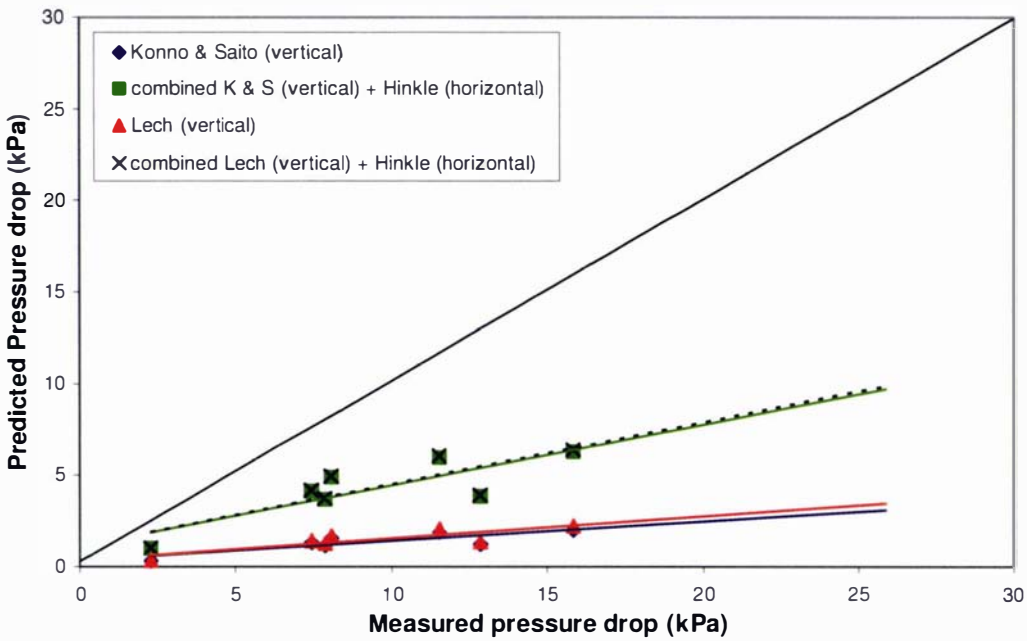

Figure 3.7: Predicted vs. measured pressure drop using four different approaches.

There are several explanations to account for the under-prediction of pressure drop for this system using the correlations. Firstly, the expression used to calculate U_p assumes that particle velocity is independent of the solids loading, which may not hold for this system. Also, this pipe work has many bends and the pressure drop across these bends has been estimated using the suggested approach of Rhodes. Figure 3.8 shows that the combined approaches (to incorporate bends) predict the pressure drop well when increasing the equivalent length, L_e, of the bends from 7.5 m to 35.5m.

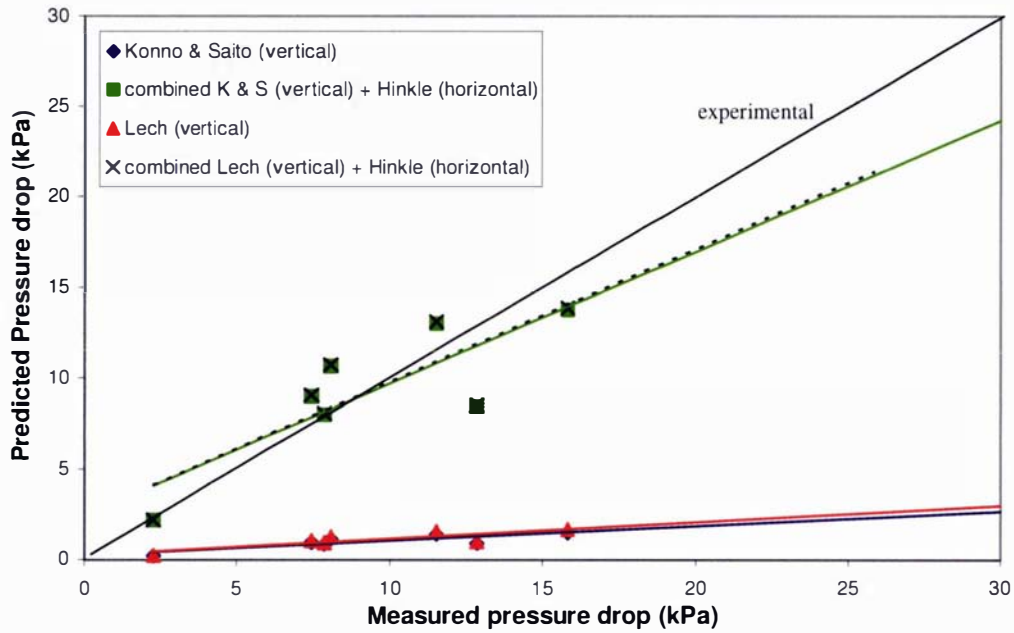

Figure 3.8: Predicted vs. measured pressure drop equating L_e for bends to 35.5 m.

The presence of bends in the pipe work means that friction coefficients are unknown and are calculated here to be significantly higher experimentally than calculated by Lech (2001) or Hinkle (1953) and shown in Table 3.10.

Table 3.10: Comparison of experimental and predicted f_p values.

Fines Mass Flow rates	Average Pressure Drop	Experimental Friction Coefficient	Lech (2001) Friction Coefficient	Hinkle (1953) Friction Coefficient
$M_f \times 3600$	ΔP	f_p	f_p(Lech)	f_p(Hinkle)
(kg h^{-1})	(kPa)	(–)	(–)	(–)
423	2.3	0.057	0.011	0.009
1549	7.9	0.055	0.011	0.009
2668	15.8	0.067	0.011	0.009
2517	11.5	0.049	0.011	0.009
2058	8.1	0.041	0.011	0.009
1738	7.4	0.045	0.011	0.009
1626	12.9	0.091	0.011	0.009

Average pressure drop is calculated from the correlation in Figure 3.9.

Figure 3.9 shows the average pressure drop versus the observed delivery rate which is essentially a calibration chart for the Niro Compact drier. The calibration curve does not cover the range of pressure drops experienced during production (18 to 25 kPa). However, extrapolation predicts that fines recycle rates vary from 95% to 130% of production or 3325 kg h^{-1} to 4550 kg h^{-1}. This is much higher than the expected recycle rates of 5 to 50%. Care should be taken when interpreting these extrapolated values and it is recommended that measurements are made at higher experimental fines mass flow rates.

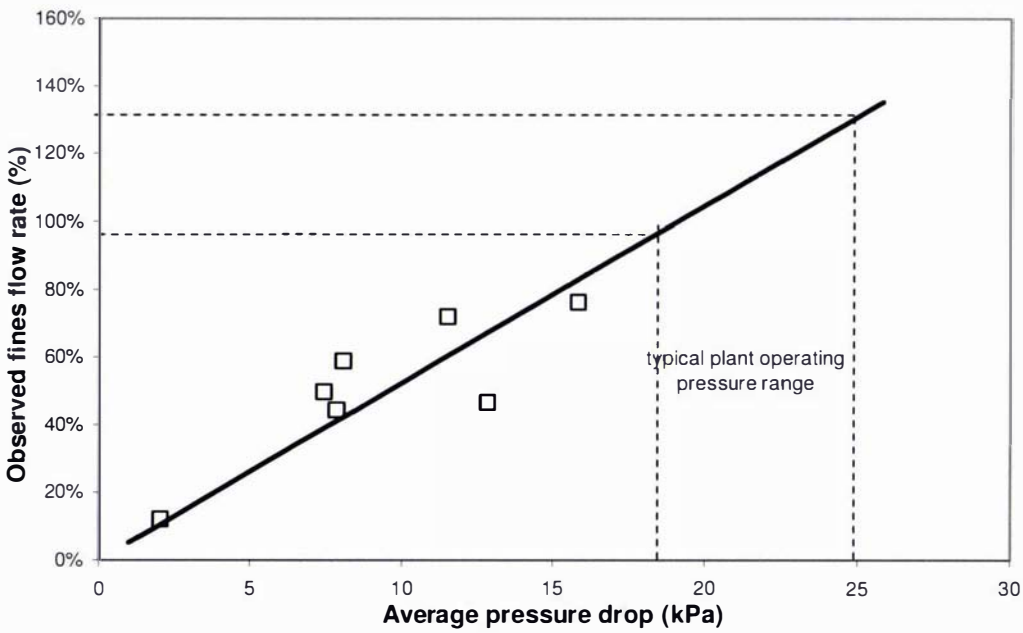

Figure 3.9: Calibration curve for average pressure drop vs. observed fines flow rate as a percentage of production capacity.

3.9 Chapter Conclusion

This chapter identified that current practice is highly intuitive with respect to influencing bulk density of instant milk powders. It is especially dependent on the type of drier, and the culture of the operating environment. These two factors indicate the need for a more precise way of controlling bulk density by understanding the processes that occur during agglomeration. A range of plant configurations were identified. At a single particle level the conditions experienced by an individual particle in the Niro Compact are similar to those experienced by a single particle in the Palmerston North IFB. Similar comparison can be drawn between the conditions experienced by an individual particle in the Stork Wide Body and the Palmerston North De Laval.

The variation in bulk density due to different operating conditions is small and it is difficult to draw conclusions. These findings demonstrate the difficulty of precise measurements on industrial driers which have many interacting and often only semi-controllable variables. The measurements themselves indicate some differences in the expected response of the powder properties to changes in operating variables. This supports the need for further investigation into agglomeration processes.

Fines recycle rates are not currently measured in spray driers. Anecdotally, it was expected that recycle rates would correspond to 5 – 50% of production. The results show otherwise with predicted recycle rates between 95 – 130% of production. The plant recycle rates predicted were extrapolated, indicating a need for further experimental work. Fines flow rate was modelled by accounting for the pressure loss due to friction of solids, using the equations of Konno and Saito (1969), Hinkle (1953) and Lech (2001). These correlations under-predict the pressure drop for this pipe line. The complex pipe work means that the experimental friction factors were significantly greater experimentally than predicted. Thus, the predictive equations can only be used in conjunction with system calibration. A major problem with these trials was the fluctuation in pressure readings due to poor delivery of fines to the blow line via the bag house and rotary valve.

CHAPTER 4

PHYSICAL PROPERTIES

An instant skim milk powder (ISMP) and an instant whole milk powder (IWMP) were selected previously in §3.1. Chapter 4 describes how the physical properties of their solution or corresponding concentrates were measured. These properties affect atomisation as discussed in §2.4.1 and therefore the processes of collision and adhesion between droplets and particles in the top of a spray drier. The concentrate properties measured in this chapter include viscosity, density, and surface tension presented in §4.1 and the droplet size and velocity of skim milk concentrate sprays presented in §4.6.

4.1 Measurement Methods for Density, Viscosity and Surface Tension

Milk concentrates were produced using the pilot plant research evaporator at Fonterra Palmerston North. The milk concentrate flow rate was measured using a Micromotion D12 mass flow meter with an attached density transducer (DMS-2-NA-1-CS, Micromotion Inc., Boulder, Colorado, USA). This was calibrated using sugar solutions which established that a correction factor of + 11 kg m^{-3} was required. Viscosity was measured using a viscometer (Paar Physica MC1) operating with US200 software (v2.30) the method is included in Appendix H. The sample was held at the appropriate temperature (20, 50, 60, 75, and 80°C) over the measurement period using a jacketed sample vessel. Surface tension can be measured a number of ways, these include the Wilhelmy plate, Du Noüy ring, bubble pressure, sessile drop and falling drop methods.

In these experimental measurements the Wilhelmy plate method was employed using a commercial apparatus, the Krüss K12 Tensiometer (Krüss GmbH, Hamburg, Germany). The Wilhelmy plate method uses a vertical platinum plate with known geometry that has been roughened to improve its wettability. The plate is brought into contact with the sample liquid and the force on the plate is measured. The technique is depicted in Figure 4.1.

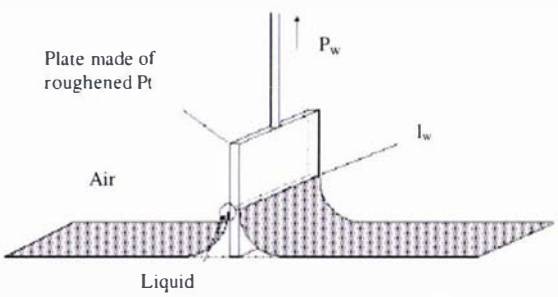

Figure 4.1: Factors affecting the calculation of surface tension for a plate.

The liquid surface tension is calculated from this force using Equation (4.1).

$$\sigma = \frac{P_W}{l_w \cos\theta} \tag{4.1}$$

where σ = surface tension [N m^{-1}], P_w = Wilhelmy force [N], l_w = wetted length [m] and θ is the contact angle between the tangent at the wetting line and the plate [°]. The plate surface has been treated to improve wettability, so θ is assumed to be zero.

A calibration, measurement and cleaning procedures are described in Appendix I. Glass vessels are usually used for surface tension measurements as certain types of plastic containers can contaminate the sample upon heating. Due to the difficulty of reliably cleaning the glass vessels, specific disposable plastic vessels were used that were suitable for the temperature range required.

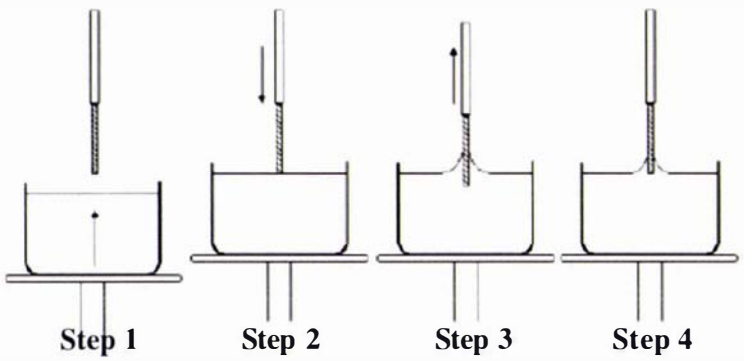

Figure 4.2: Wilhelmy plate measurement of surface tension.

Figure 4.2 depicts the movement of the plate and vessel prior to a surface tension measurement. Approximately 30 ml of solution was poured into a plastic container and placed in the jacketed measurement block. A plate speed of 2 mm min^{-1} was used to perform the following movements. The vessel was first raised until the plate was level with the liquid level in step 2. The plate was lowered until it was submerged by 2 mm, as shown in step 3, after which it was raised again until it was level with the liquid surface, as shown in step 4. This process took ~ 2 minutes to complete and the measurement of surface tension commenced at step 4. Initial tests on water gave accurate and repeatable results in the temperature range from 20 to 80°C: specifically 20°C, 72.8 ± 0.7 mN m^{-1}; 50°C, 67.9 ± 0.5 mN m^{-1} (Appendix J).

Single measurements were taken for the measurements made on water. Surface tension measurements of milks were made using a series of measurements. This was due to the slow time dependency of wetting of the plate and subsequent gravity flow of the solution which results in a fall in surface tension reading (Appendix K). The high viscosity of the liquid causes this effect. A film of liquid will stick to the plate causing an increased load on the force measuring system which directly translates to an increased surface tension. As the film of liquid flows back into the sample vessel over time, the surface tension then decreases to the 'actual' value. Due to this effect it is best to wait until an equilibrium value is reached, especially for samples with a high viscosity. One measurement was taken every 10 s for up to 90 readings or until the readings reached a plateau. This is discussed further in §4.5.

4.2 Milk Composition and Experimental Plan

The compositions of the milk concentrates used in these physical property measurements were based on the compositions of the previously selected ISMP and IWMP. These compositions are listed in Table 4.1 alongside the standard milks used for these experiments. WMC and SMC refer to whole and skim milk concentrate (40 to 53 wt% solids concentration) and SWM and SSM are standard whole and skim milk (10 to 12 wt% solids concentration). The concentrates were produced using the Fonterra PN pilot plant research evaporator (feed ~ 300 kg h^{-1}) and were tested 'fresh' immediately following evaporation. One extra sample was prepared by reconstitution using ISMP A and compared to fresh SMC. A scraped surface heat exchanger was used to heat the milk concentrates. The residence time in the heat exchanger was approximately 180 s for Run A, and 36 s for later runs. The standard milks were heated using a coil placed in a water bath with a residence time of ~ 10 s.

Table 4.1: Composition on a dry basis for IWMP E and ISMP A.

Spec/Run	IWMP E	Run A	Run C	Run Da	Run Db	ISMP A	Run B	Run E
Product	WMC	WMC	WMC	SWM	SWM	SMC	SMC	SSM
Fat	29.5	27.8	29.2	27.6	28.1	0.8	1.0	5.6
Lactose	37.3	38.5	37.6	39.5	38.8	55.9	57.0	48.4
Ash	5.7	5.6	5.9	6.0	6.1	8.6	7.2	7.8
Protein	27.4	28.2	27.3	27.0	27.0	34.6	34.9	38.2

WMC, SMC = whole, skim milk concentrate, SWM, SSM = standard whole, skim milk

The experimental runs performed to measure the physical properties are included in Table 4.2 for WMC and SWM and SMC and SSM. For each set of variables, the density, viscosity and surface tension were measured. These experimental conditions aim to imitate the range of solids concentrations, and temperatures used to manufacture ISMP A and IWMP E industrially.

Table 4.2: Experimental plan for WMC, SWM, SMC and SSM.

Run	Total Solids	Temp	Rep	Run	Total Solids	Temp	Rep
Units	**(wt%)**	**(°C)**			**(wt%)**	**(°C)**	
A1	47	50	a,b	B1	40	50	a
A2	47	80	a,b	B2	40	60	a
A3	53	80	a,b	B3	40	80	a
A4	53	50	a,b	B4	47	80	a
C1	47	50	a	B5	47	60	a
C2	47	60	a	B6	47	50	a
C3	47	80	a	E1	10	20	a
C4	53	80	a	E2	10	50	a
C5	53	60	a	E3	10	60	a
C6	53	50	a	E4	10	75	a
D1	12	20	a,b	D3	12	60	a,b
D2	12	50	a,b	D4	12	75	b

A, C = whole milk concentrate experiments, B = skim milk concentrate experiments, D = standard whole milk experiments, E = standard skim milk experiments.

4.3 Density Results and Discussion

The density of milk concentrate affects many aspects of the agglomeration process: in atomisation it influences droplet size and size distribution, it affects the rate of drying, and it affects the spreading rate when droplets impact on a surface. The density of milk is a function of composition, solids content and temperature. Middleton (1996) also found the thermal history of the milk impacts upon the density of both skim and whole milks. However, little published work predicts the relationship between total solids and the density of milk concentrates. A number of authors report how density is affected by temperature at different fat contents (Bertsch, Bimbenet, & Cerf, 1982; Houska, 1994; Wood, 1996). Bertsch et al. (1982) used Equation (4.2) to predict density as a function of temperature at two fat contents (Figure 4.3).

$$\rho = -2.307x10^{-3}T^2 - 0.266T + 1040.5 - 100X_{fat}(-47.8x10^{-6}T^2 + 9.7x10^{-3}T + 0.967) \quad (4.2)$$

where T = temperature [°C], X_{fat} = mass fraction fat [kg kg^{-1}] and ρ = density [kg m^{-3}].

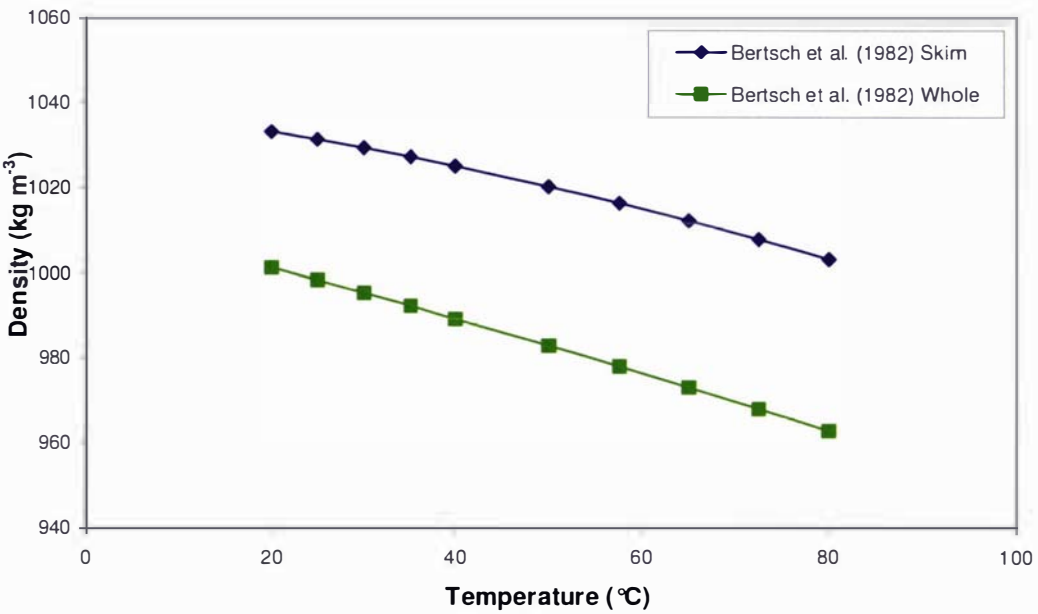

Figure 4.3: Effect of temperature on the density of skim and whole milks.

The density of a mixture can be determined as the inverse of the specific volume of the mixture, which is the sum of the volume of each component in the mixture:

$$\rho = \frac{1}{v} \quad (4.3)$$

$$v = \sum_i x_i v_i \quad (4.4)$$

where ρ = density of the mixture [kg m^{-3}], v = specific volume of the mixture [m^3 kg^{-1}], v_i = specific volume of component i, and x_i = the percentage of component i present in the mixture.

The specific volume of water is a function of temperature and can be easily calculated (Irvine & Liley, 1984). Table 4.3 gives the constant values used for the specific volumes of milk components including casein, whey, lactose, sucrose, glucose, galactose and ash. The fat specific volume is also a function of temperature and calculated using equation (4.5) (K. Pearce, personal communication, 1995).

$$v_f = \frac{1}{928.75 - 0.677803 \times T + 1.89394 \times 10^{-4} \times T^2} \tag{4.5}$$

where v_f = the specific volume of fat [m^3 kg^{-1}] and T = temperature [°C].

Table 4.3: Constant values of specific volume for components of milk.

Component	Specific Volume
Units	($L\ kg^{-1}$)
Casein	0.71429
Whey	0.74074
Lactose	0.62854
Sucrose	0.62972
Glucose	0.64103
Galactose	0.64103

Figure 4.4 compares the experimental results obtained by measuring density at 50°C with the expected values calculated using the approach outlined above. The predicted and measured values show good agreement. Equations (4.6) and (4.7) are the trend lines for the density of IWMP E (Run C) and ISMP A (Run B) at 50°C on the plot.

$$\rho_{whole} = 222TS + 1011 \qquad R^2 = 0.9536 \tag{4.6}$$

$$\rho_{skim} = 480TS + 965 \qquad R^2 = 0.9821 \tag{4.7}$$

where ρ_{whole} = density of whole milk concentrate [kg m^{-3}], ρ_{skim} = density of skim milk concentrate [kg m^{-3}], and TS = total solids [wt%].

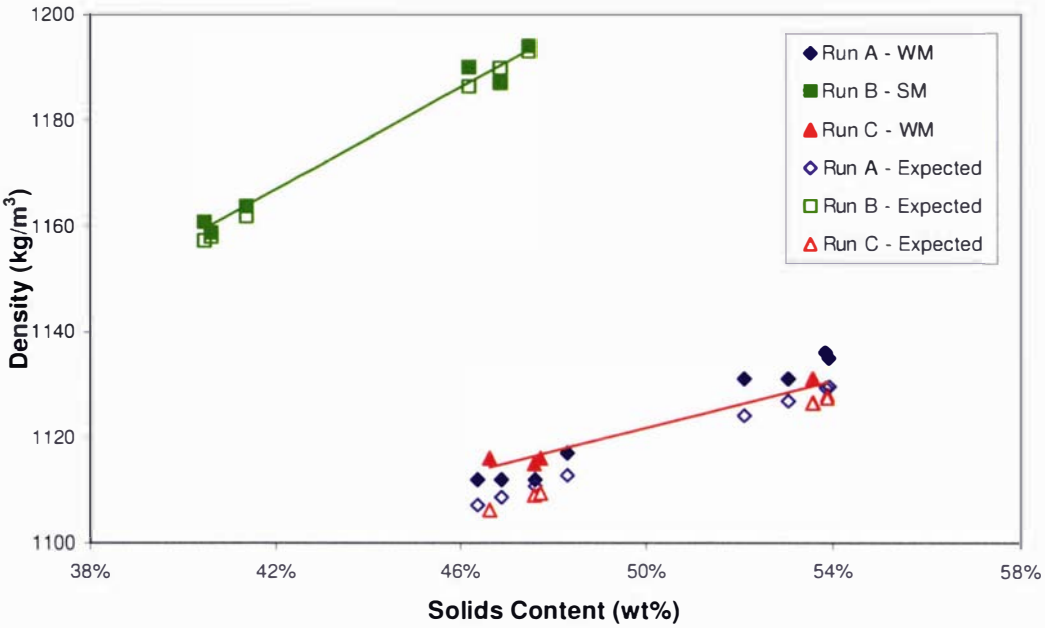

Figure 4.4: Density vs. solids content for Runs A, B and C at 50°C.

4.4 Viscosity Results and Discussion

Processing milk concentrates is limited by viscosity which depends on the composition, pre-treatment, temperature, solids content and evaporator holding time (Wood, 1996). Bloore and Boag (1981) state that the achievable solids concentration level during evaporation is restricted by concentrate viscosity. A number of sources have discussed the effect of temperature on viscosity (Bertsch & Cerf, 1983; Houska, 1994; Wood, 1996).

Snoeren et al. (1982) have proposed a model of milk concentrate viscosity. The viscosity depends on the volume fraction of the molecular material and the viscosity of the milk serum. The molecular material consists of casein and whey proteins whereas the milk serum is made up of lactose and salts. The theoretical relationship between viscosity and volume fraction is given below (Eilers, 1941):

$$\mu = \mu_{ref}\left(1+\frac{1.25\Phi}{1-\Phi/\Phi_{max}}\right) \tag{4.8}$$

where μ = the viscosity of the mixture [Pa s], μ_{ref} = the viscosity of the serum and Φ = the volume fraction of the molecular material. Φ_{max} = the maximum volume fraction.

The viscosity of the serum, μ_{ref}, is a function of the lactose and salt content and can be easily established. The volume fraction of milk can be affected by the amount of casein, denatured whey protein and native whey protein present:

$$\Phi_{milk} = X_{casein} v_{casein} + X_{dw} v_{dw} + X_{nw} v_{nw} \tag{4.9}$$

where X_{casein} = the mass concentration of casein [kg L^{-1}], v_{casein} = specific volume of casein [L kg^{-1}], X_{dw} = the mass concentration of denatured whey protein [kg L^{-1}], v_{dw} = specific volume of denatured whey protein [L kg^{-1}], X_{nw} = the mass concentration of native whey protein [kg L^{-1}], v_{nw} = specific volume of native whey protein [L kg^{-1}].

The volume fraction of protein in a concentrate can be related to the volume fraction of protein in milk by:

$$\Phi = \Phi_{milk} \times \frac{X_c}{X_{milk}} \times \frac{\rho_c}{\rho_{milk}} \tag{4.10}$$

where X_c = solids content of concentrate [kg kg^{-1}], X_{milk} = solids content of standard milk [kg kg^{-1}], ρ_c = concentrate density [kg m^{-3}], ρ_{milk} = milk density [kg m^{-3}].

From Eilers' relation the viscosity of concentrate depends on the protein content, composition, and hydration, as well as the degree of concentration and the concentrate temperature. Experimental results confirmed that Eilers' relation may be used to predict the viscosity of milk concentrates, but further work showed that viscosity increases during storage regardless of preheat treatment, and that the structure build-up can be disrupted by agitation. Snoeren et al. (1982) suggest viscosity should be measured at a shear rate as high as that occurring at a wheel or nozzle to achieve practical measurements. For this reason, in this thesis all viscosities are measured at a shear rate of 1000 s^{-1} which is the maximum shear rate of the Paar viscometer.

Figure 4.5 shows the viscosity results obtained for each run compared to the calculated or expected values. The increase in viscosity at higher solids contents may be explained by the closer interaction between components in the concentrated milk solution. The experimental results agree with the predicted data at low solids contents, but at high solids the expected values using Snoeren's approach over predicts viscosity. This was also observed by Paramalingam et al. (2002) who developed a model based on the approach of Snoeren et al. (1982) for the viscosity of whey concentrates and applied this model to successfully predict viscosity of whole milk concentrates up to 50 wt% with less than 10% error. In this model by Paramalingam et al. (2002) the viscosity of the solvent, μ_s, is replaced by the viscosity of lactose plus the salt solution and the regression model for the viscosity of the lactose solution was generated from experimental data ((Buma, 1980; Fernandez-Martin, 1972):

$$\mu_l = aT^{-1.3156}(TSx_l)^3 - bT^{-0.949}(TSx_l)^2 + cT^{-0.6414}(TSx_l) + dT^{-0.7142} \tag{4.11}$$

where, μ_l = viscosity of lactose solution, a = 0.0095, b = 0.0736, c = 0.484, d = 8.7033, T = temperature [°C], TS = total solids concentration [kg kg^{-1}], and x_l = dry matter fraction of lactose [-].

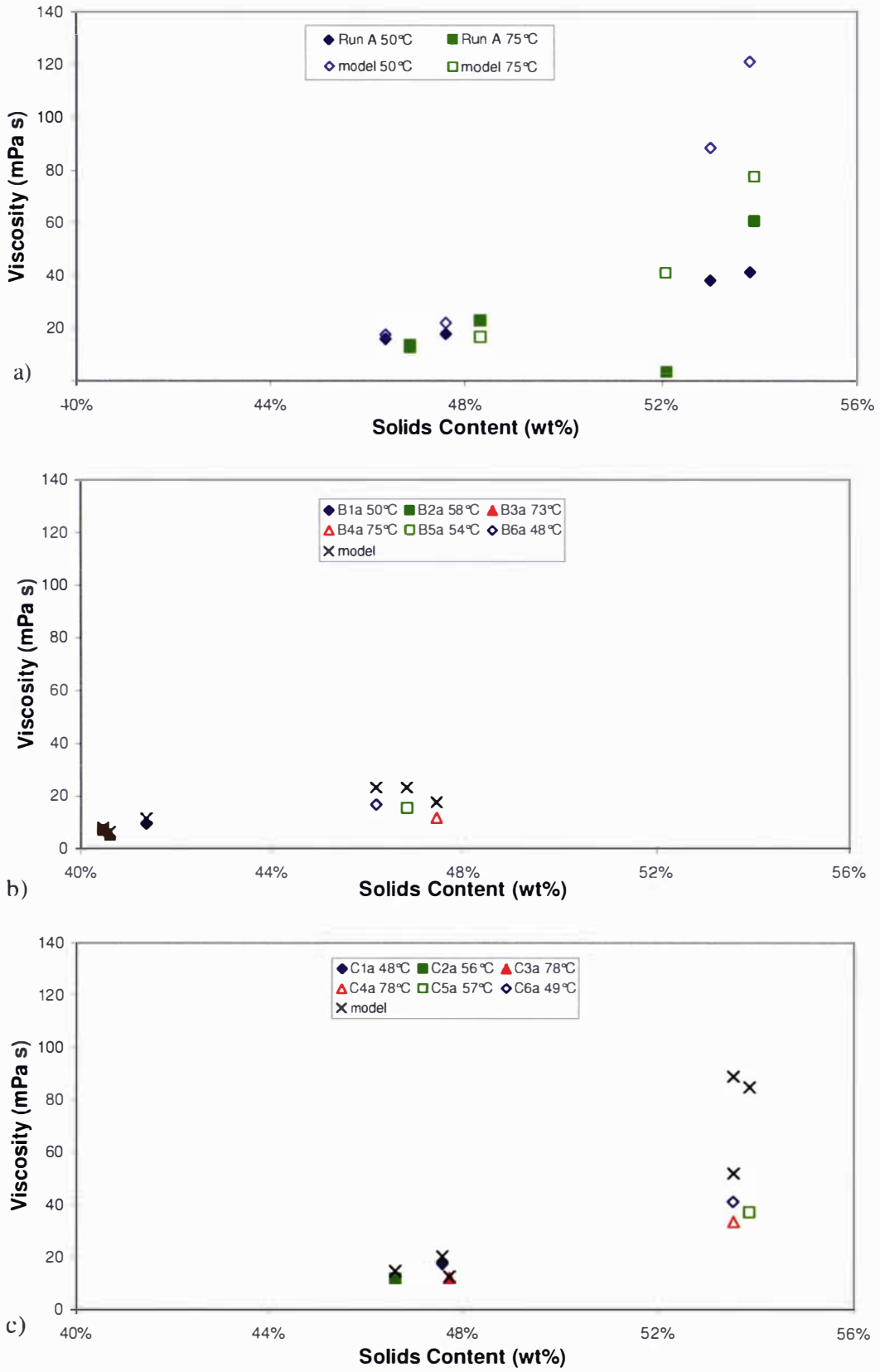

Figure 4.5: Viscosity vs. solids contents (shear rate of 1000 s^{-1}) a) WMC Run A b) SMC Run B, c) WMC Run C.

4.5 Surface Tension Results and Discussion

Figure 4.6 is a collection of surface tension data from the literature for whole and skim milk, measured using a range of techniques. These include the vibrating jet method (Whitnah, Conrad, & Cook, 1949), the falling drop method (Bertsch, 1983), the Wilhelmy plate method (Kristensen, Jensen, Madsen, & Bird, 1997) and the Du Noüy ring method (Janal, 1975; Kuk, 1955; Watson, 1958). Although the work of Kuk (1955) has been reported in two separate sources (Houska, 1994; Wood, 1996); it is unclear what method was used to obtain these results. The regression formulae for skim milk and whole milk included below are sourced from Houska (1994) but were formed using many of the other data points listed in Figure 4.6.

$$\sigma_{Skim} = 4.74\times10^{-2} - 9.02\times10^{-5}T - 3.79\times10^{-7}T^2 \tag{4.12}$$

$$\sigma_{Whole} = 5.21\times10^{-2} - 1.52\times10^{-4}T - 1.97\times10^{-7}T^2 \tag{4.13}$$

where σ_{Skim} = surface tension of skim milk [N m^{-1}], σ_{Whole} = surface tension of whole milk [N m^{-1}] and T = milk temperature (0 – 80) [°C].

The regressions apply for standard whole and skim milks only; the surface tension of milk concentrates has only been reported by Parker (1978) who observed lower values than those reported for standard milks. Paramalingam et al. (2002) measure surface tension as a function of solids content for whole milk but the temperature is not reported. The measurements made for standard milks generally agree with the Houska (1994) correlations. The measurements made by Bertsch et al. (1983) using the falling drop method are higher than those obtained by other techniques.

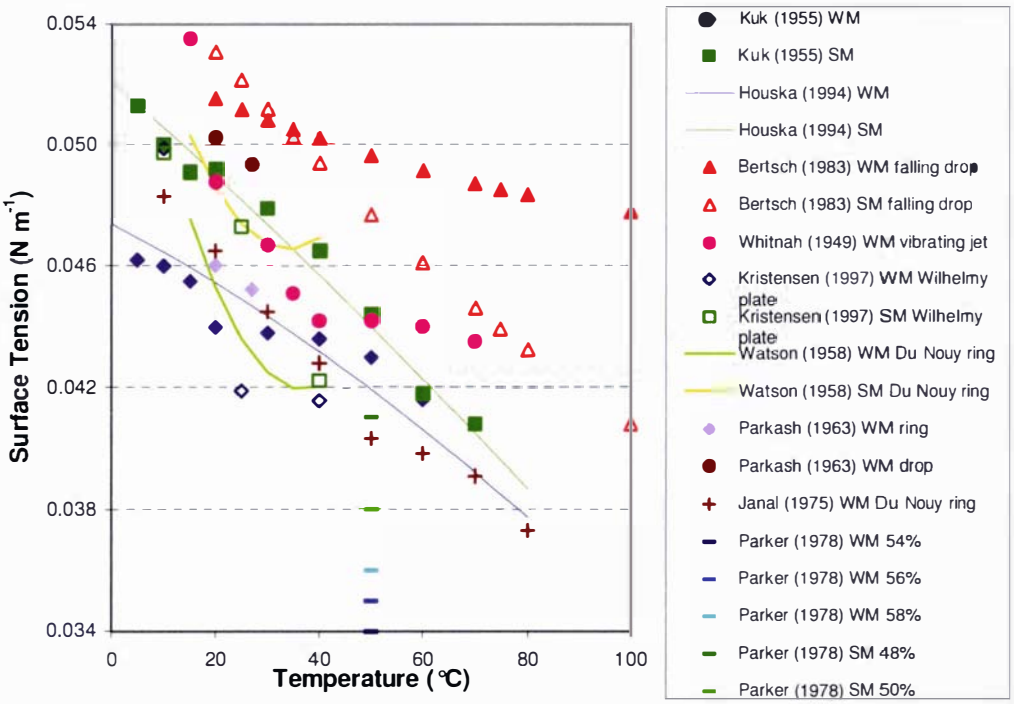

Figure 4.6: Surface tension of whole milk and skim milk as a function of temperature.

The Wilhelmy plate method is influenced by a number of factors (Appendix K) with the most important being the viscosity of the sample. The liquid viscosity affects the rate of drainage from the plate. Therefore, the force recorded may include liquid that has not yet drained away. The effect of drainage is observed as a decrease in force with time as shown in Figure 4.7. The force profile is affected by the initial amount of liquid drawn up the plate and the rate of drainage of the liquid back into the sample vessel.

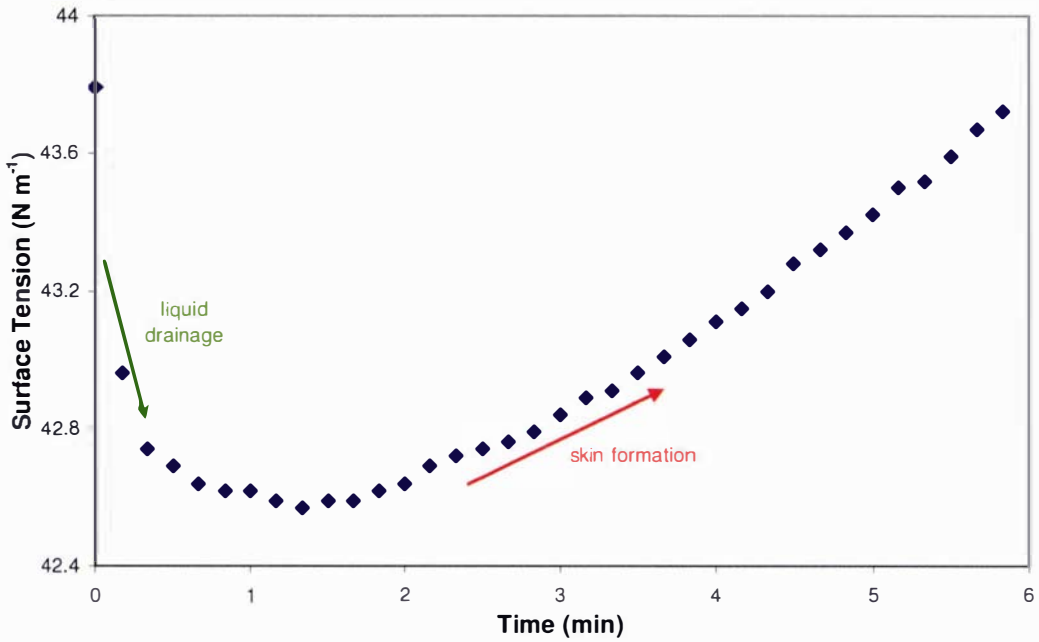

Figure 4.7: Force–time profile of whole milk concentrate, 46.4% solids and 47.4°C.

Figure 4.7 shows that after some time, an increase in force on the plate also occurs. This subsequent rise can be associated with the formation of a skin on the surface, which is observed during measurement. Hassan and Mumford (1993) showed that during drying a skin appears on the surface of skim milk droplets. Skin formation is proposed to be due to drying and evaporation, and cross-linking of fat globules due to protein denaturation (Newstead, 1994) . In this context, denaturation refers to the heat-induced changes in protein structure. The ambient conditions when these measurements were taken are given in Table 4.4. The process of drying and evaporation can explain why a skin may form over time. As discussed in Appendix L, the evaporation rate from the sample surface appears to be constant over a range of sample temperatures. However, control of humidity in the sample chamber could be made using a saturated salt solution with an excess of solids.

Table 4.4: Ambient conditions during surface tension measurement.

Sample Temperature	Air Humidity (RH%)		Air Temperature (°C)	
(°C)	Room	Chamber	Room	Chamber
20	47.5	49	20.9	20
50	45.4	54	22	26.1
60	47	61	21.5	28.3
75	45.9	80	21.1	28

Knowledge of milk chemistry can aid understanding of how the process of skin formation can be affected by solids concentration, fat content and temperature. Milk proteins, milk fat and free fatty acids are the principal surface-active components that affect the surface tension of milk (Whitnah, 1959). An increase in these components at the surface will result in a decrease in surface tension. Conversely, denaturation of the milk proteins on the surface of fat globules will increase surface tension as the protein is no longer an effective surface-active agent (Wong, 1988).

Denaturation starts between 60 and 70°C and disulphide bridges form on the surface of fat globules resulting in aggregation. The formation of a skin due to micellar aggregation is likely to be faster at higher solids concentrations and fat contents as micelles are more tightly packed. Although denaturation is retarded at high solids concentrations, possibly because of increased lactose concentrations, a sufficient degree of denaturation may occur to allow aggregation (Anema, 2000). The competing effects of viscous drainage and skin formation mean it is not possible to distinguish the end of drainage from the start of skin formation. Therefore, the minimum force in Figure 4.7 was used to calculate the surface tension. The error in these minimum values obtained is difficult to estimate.

Figure 4.8 reports surface tension for both whole milks, standard (SWM) and concentrated (WMC) and compare these results with Houska's correlations. Figure 4.9 reports the same but for skim milks (SSM) and concentrates (SMC). In both plots below 60°C, the experimental values are scattered about Houska's correlations. Above 60°C, the surface tension of concentrated milks increases markedly. This trend is similar for standard milks although the deviation is not as great. Whole milks (Figure 4.8) appear to exhibit a greater increase in surface tension above 60°C than skim milks. Reconstituted skim milk concentrate of the same composition compares well to fresh measurements. The reason for the increasing surface tension is likely to be due to denaturation of proteins which causes disulphide linking of micelle particles above 60°C resulting in an increase in skin formation and the apparent surface tension. This is clearly influenced by the concentration of proteins in solution. There is also a difference between whole and skim milks but the mechanism for this is unknown.

Muhkerjee et al. (2005) also measured the surface tension of homogenised milks of similar compositions to the standard whole and skim milks measured in this work. Measurements were made using both capillary rise and Wilhelmy plate techniques at 20°C and were found to be higher than those values obtained in this study. Surface tension measurements were reported to be 52.7 – 54.0 mN m^{-1} for 'dark blue milk' (similar to standard whole milk) and 64.3 – 67.4 mN m^{-1} for 'light green milk' (similar to standard skim milk).

Masters (1979) gave the following relationship between surface tension and droplet size (Equation (4.14)). This can be used to perform an error analysis of the surface tension on the droplet size prediction.

$$D_d \propto [\sigma]^{0.25} \tag{4.14}$$

where D_d = droplet size [m] and σ = surface tension of fluid [N m^{-1}].

Considering that the maximum and minimum experimental values recorded are 51.1 and 40.57 mN m^{-1} (57.1 mN m^{-1} for whole milks is an outlier), the error, ε, is (51.1 – 40.57)/40.57, or 26%. Consequently, the error with respect to the droplet size is +5.9% or –7.3%. As this is below 10%, the uncertainty in the surface tension values due to the competing effects of drainage and skin formation can be considered acceptable for future calculations.

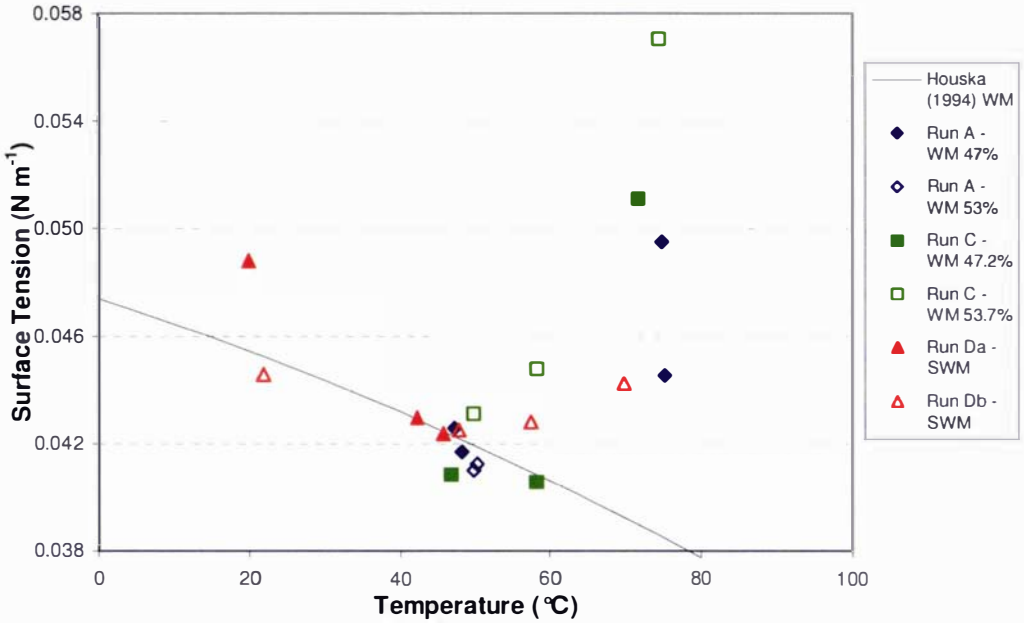

Figure 4.8: Comparing surface tension of whole milks with Houska's equation (4.13).

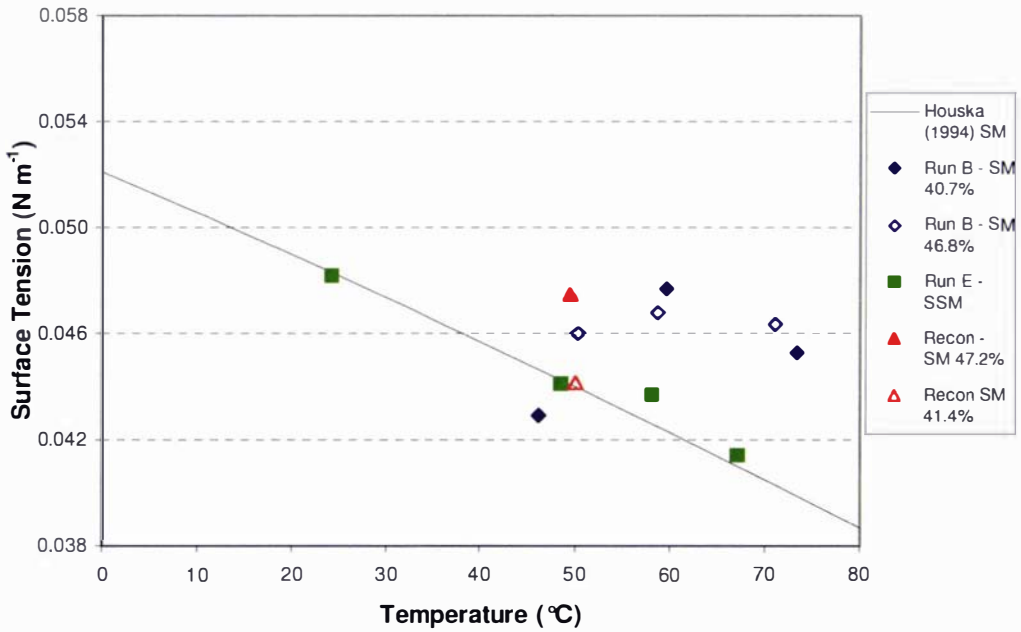

Figure 4.9: Comparing surface tension of skim milks with Houska's equation (4.12).

4.6 Droplet Size and Velocity Measurement of Skim Milk Concentrate Sprays

Atomisation is the most widely used process for droplet generation and refers to a process in which bulk liquid is disintegrated into small droplets. During atomisation a number of disruptive forces influence droplet formation including kinetic energy, friction, gravity, interface shearing and pressure fluctuations. Counteracting these are cohesive forces which include molecular bonding, viscosity and surface tension. The surface tension pulls the liquid into a shape (sphere) that exhibits minimum surface energy while the stabilising effect of viscosity opposes any change in the geometry of the liquid (H. Liu, 2000). Droplet formation is discussed in more detail in §2.4.1

The atomisation of milk generally occurs in a hollow cone pressure nozzle and can be divided into the following stages (Chen, 1992)

- milk concentrate
- liquid film
- film break-up into large irregular shaped liquid drops
- spherical liquid drops
- zone of rapid drying
- substantially dried particles

In this work a two-fluid self-cleaning nozzle was used rather than a hollow cone nozzle. The two fluid nozzle produces smaller droplets than a pneumatic nozzle and is more suitable for experiments in a small pilot scale drier where the droplet residence time for drying is significantly shorter than in a large industrial drier. However, there is the same need to establish droplet size and velocity for agglomeration studies.

Droplet Size

Droplet size is able to be measured by a range of commercial laser diffraction devices including a Malvern Mastersizer X (Elversson, Millqvist-Fureby, Alderborn, & Elofsson, 2003), Malvern Spraytec, Malvern Mastersizer E (Nguyen & Rhodes, 1998) and Phase-Doppler Particle Analyzer (PDPA) (W. T. Kim, Mitra, Li, Prociw, & Hu, 2003; Panchagnula & Sojka, 1999; Schelling & Reh, 1999). The difficulty with spray sizing is to obtain a representative population of droplets from the spray, both across the spray and with distance from the nozzle to ensure droplet break-up has occurred and other factors such as evaporation, coalescence, and spray coating of the lens have not affected the size distribution.

An alternative implicit method of droplet sizing is to run a single spray nozzle within a spray drier without any fine powder recycled. The sprayed droplets are dried and then collected. These dried droplets can be regarded as particles formed without any of the design or operating features that enhance agglomeration. Experiments with multiple nozzles and fines recycle can then be compared against this base case. In this work, the base case dried droplets were collected and sized for comparison against the spray droplets measured using laser diffraction and photographic techniques. Lin and Chen (2004) have related the final size D to the droplet size D_0, finding D/D_0 values for skim milks from 0.67 (20% TS) and 0.76 (30% TS). Masters (1979) proposes that droplet sizes can be calculated from equation (2.16).

Droplet Velocity

Velocity is more difficult to ascertain because of the turbulence needed to cause droplet break-up in a two-fluid nozzle. Calculations involving turbulence are difficult and still need to be validated against experiments. Therefore a direct measurement tool for velocity in the collision zone between droplets and recycled powder particles was needed. Non invasive velocity measurement is difficult for droplets in air. High-speed photography was used here but needed careful placement of the spray in the focal length of the camera, and required good shielding of the lens from droplet deposition. Such placement means the technique was essentially invasive to the flow field created by the atomiser and spray. Also the depth of field about the focal length was small and care was taken to obtain a representative population of droplet velocities. The air velocity at the exit of the nozzle was measured using a turbine anemometer (Testovent 4000, Testoterm, Germany) with no liquid supplied to the nozzle.

4.6.1 Methods and Materials

Measurements for droplet size and velocity were carried out for water and skim milk concentrates at a range of solids concentrations, atomising air pressures and flow rates. The nozzle used was a self-cleaning, two-fluid flat spray nozzle (Spray Systems 2850 fluid cap, 67228-45 air cap). Reconstituted milk concentrates were prepared by milk powder addition to 50°C water for 20 minutes followed by a 10 minute hydration period. A Malvern Mastersizer S was used for droplet size measurements and a High Speed B/W CMOS Camera, Model # CPL MS50 K was used to determine droplet size and velocity. Droplet size was also measured using a Mastersizer 2000 for particles collected after the spray had been dried inside the drier without the presence of a powder recycle.

Malvern Mastersizer S

A Malvern Mastersizer (Model S, Malvern Instruments Limited, Malvern, Worcestershire, UK) unit was modified to allow a spray to pass between the beam expander and the lens as shown in Figure 4.10. The 1000 mm focal length lens was used with at least 5000 sweeps. The lower and upper obscuration bounders were set at 2 and 40% and obscuration was observed to be 5 – 15%. Care was taken to avoid droplet deposition on the lens by blowing purge air on either side of the spray. Beam alignment and measurement of the background signal received by the detector was checked between each measurement and the lens was cleaned if necessary. The spray was positioned so that the laser beam was directed through the centre of the spray. Droplet size varies with the position sprays. Bakker (1988) found that particles are larger in the centre; measurements were made in the centre to see the trend for changing fluid properties and no measurements were made at the edge of the spray.

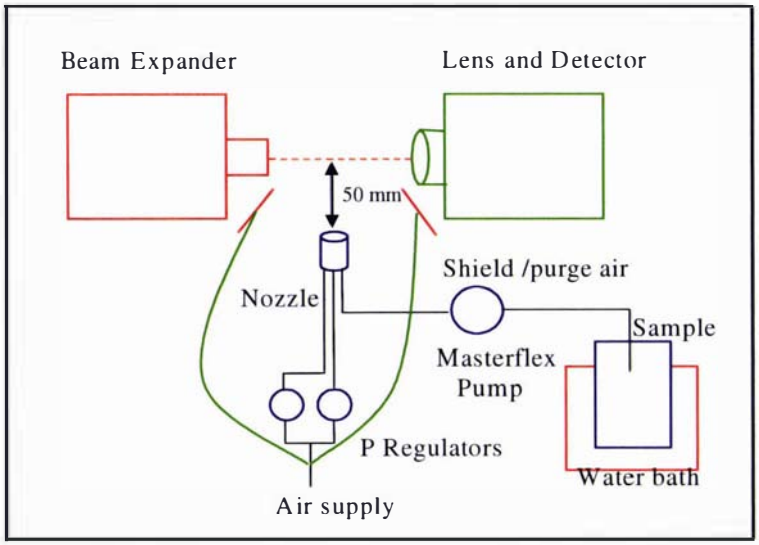

Figure 4.10: Experiment setup for Mastersizer S.

Figure 4.11 shows the relationship for water between the surface weighted mean droplet size, $D_{3,2}$, and distance of the nozzle from the beam. Three replicates were measured at each distance. The plot indicates the level of break-up at each position from the nozzle exit, and shows that, at 10 mm, droplet break-up was incomplete. The smallest mean size occurs at 25 mm. When the nozzle was moved further from the beam, droplet coalescence results in larger mean sizes. Also, increasing the distance causes more lens splatter which was detected by the intensity of the background signal. Further experiments with skim milk used a nozzle to beam distance of 50 mm which has been used by several authors (Elversson et al., 2003; Nguyen & Rhodes, 1998).

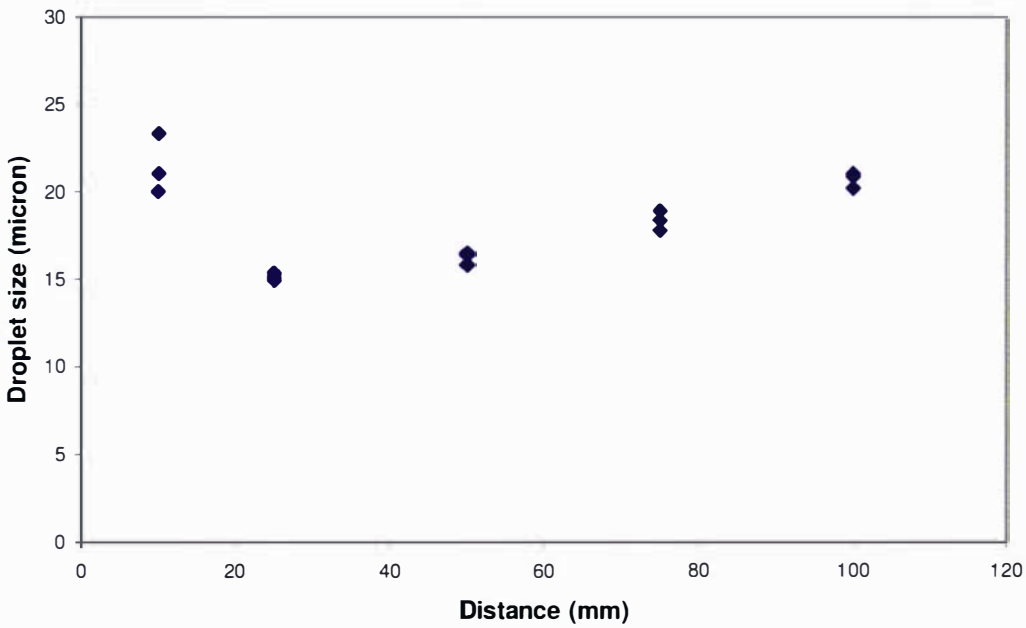

Figure 4.11: Droplet size vs. distance for water at 50°C, 1 bar and 3.8 kg h^{-1}.

Mastersizer 2000

The Malvern Mastersizer (Model 2000) was used to measure the particle size distribution of the powders produced in the 0.8 m diameter Niro spray drier modified as explained in Chapter 5. When measuring particle size 10 000 sweeps were used and the lower and upper obscuration boundaries were set at 1 and 5%. The measurement method used to operate the Mastersizer 2000 has been included in Appendix A.

High Speed B/W CMOS Camera

A high speed camera [B/W CMOS, Model # CPL MS50 K] was used to produce video records at a high frame rate to determine the droplet velocity. The camera used was situated in the laboratory of Dr John Abrahamson at Canterbury University in Christchurch, New Zealand. Individual frames were used to extract images of the droplet path as demonstrated in Figure 4.12. The droplet is silhouetted on a black field so that light streaks of width, w and length, L occur. The width of the droplet was used to estimate droplet size and the droplet velocity was estimated using L and the camera exposure time:

$$U_d = \frac{L}{t_{exp}} \tag{4.15}$$

where U_d = velocity of droplets [m s^{-1}], and t_{exp} = exposure time [s].

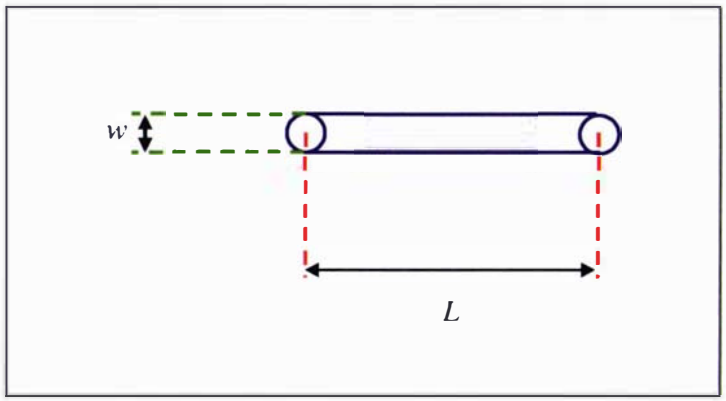

Figure 4.12: Simplistic view of particle motion recorded in on a single frame over the exposure time of the high speed video.

Figure 4.13 shows the experimental set up for producing and capturing images of the milk concentrate spray. The PC connected to the camera used the program, Mega speed MS50K Version 8.0, to capture the images. Water was used to focus the camera and establish the appropriate lighting and camera positioning which has been included in Figure 4.14. The lens was used to focus light at the position of the image required for capture. The camera aperture of F8, and an exposure time of 100 µs were used for all experiments. A photograph of the camera set up is shown in Figure 4.15. The camera had 21, 31 and 13 mm lenses and recorded at 1037 frames per second capturing a total of 2.097 s of footage. An example frame has been included for water in Figure 4.16.

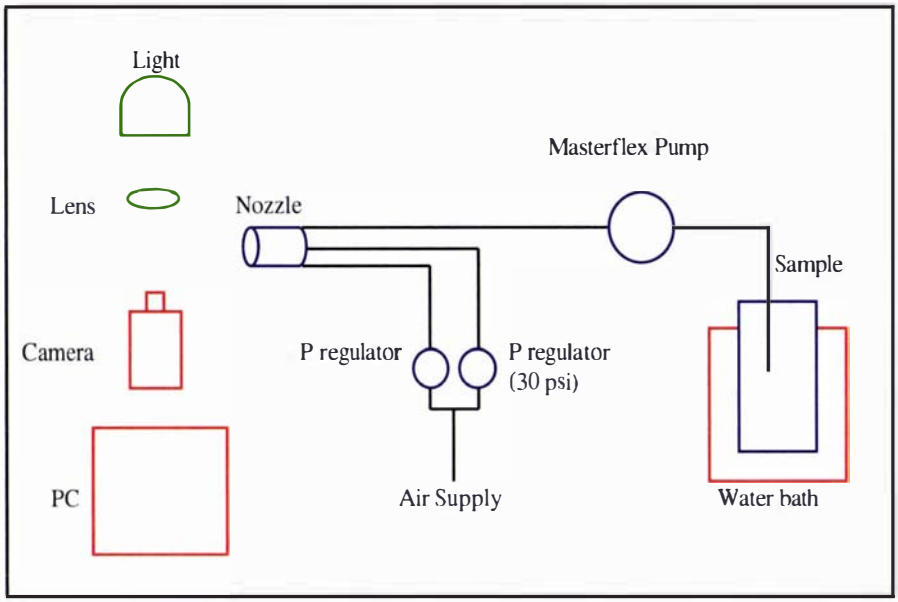

Figure 4.13: Schematic of experimental set up using high speed camera.

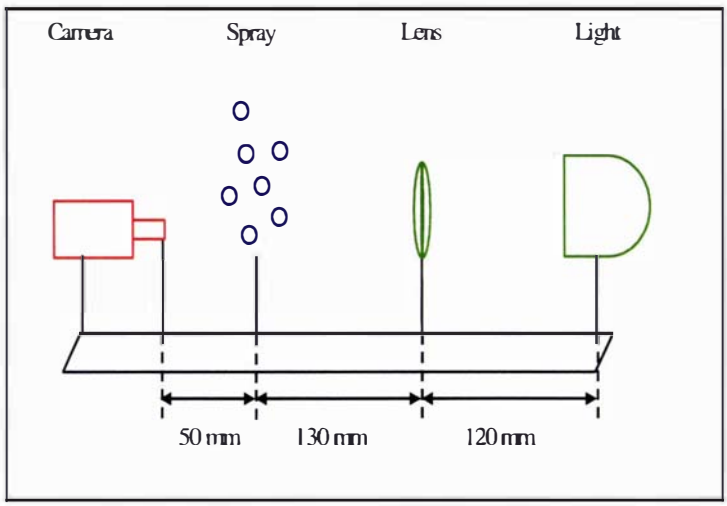

Figure 4.14: Schematic of camera, spray, lens and light position on the optical bench.

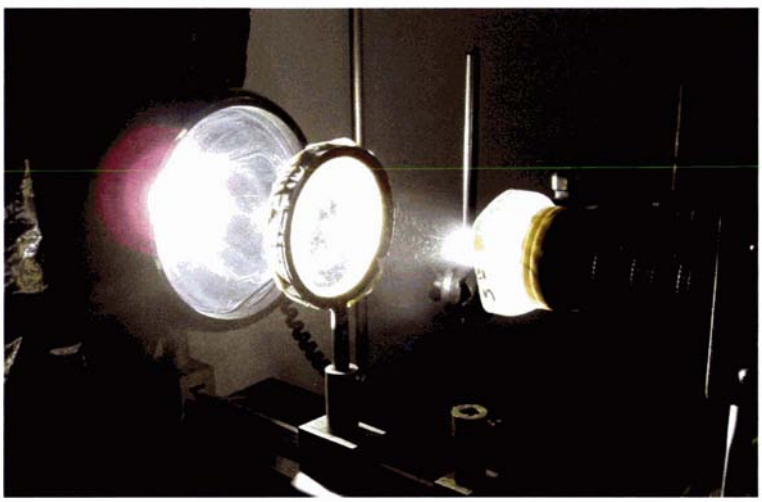

Figure 4.15: Equipment set up to capture spray images.

Figure 4.16: Example frame for water at 0.5 bar atomization pressure and 1.8 kg h^{-1}.

A mesh grid with an aperture size measuring 1 × 1 mm was situated at the position of the image (50 mm) to focus the camera and to calibrate the distance of each frame. An average of 20 measurements was used to determine that on average 78.6 pixels is equal to 1 mm. To determine the size and velocity measurements for one experiment, 10 frames were sampled and 10 streaks were randomly selected from each frame to determine an average value per frame. For each experiment the mean and 95% confidence interval were calculated.

4.6.2 Droplet Size Results and Discussion

Droplet size distributions were obtained for a range of flow rates, total solids and atomisation pressures. Figure 4.17 shows the mean droplet size as a function of atomisation pressure for four flow rates of 47 wt% skim milk concentrate (SMC). Only mean sizes are reported because of data loss, fortunately sauter mean sizes were recorded in a laboratory book however analysis of the distributions cannot be made. Two SMCs of different compositions were investigated, SMC A was reconstituted using ISMP A and SMC X was a standard SMC taken from the Fonterra Palmerston North pilot plant evaporator. The lowest atomisation pressure produces a large range of droplet sizes, probably because atomisation was incomplete. Above an atomisation pressure of 1.0 bar, the range of mean sizes was much narrower. Concentrate flow rate has little effect on the mean droplet size, which is expected as the atomising itself in the two-fluid nozzle is done by the air. The SMC A concentrate generally shows a larger droplet size measurement than SMC X possibly due to a higher viscosity because of a difference in temperature, composition and manufacturing process. Repeatability was investigated by the three replicates for SMC A at 2.5 kg h^{-1} at three different atomisation pressures; these show good repeatability. Figure 4.18 shows the mean droplet size for water at one flow rate and two atomisation pressures. This reveals that the water droplet size, 12 µm, was not dissimilar to that of the 47 wt% concentrate, 15 µm. This indicates that the effect of concentration on droplet size was small.

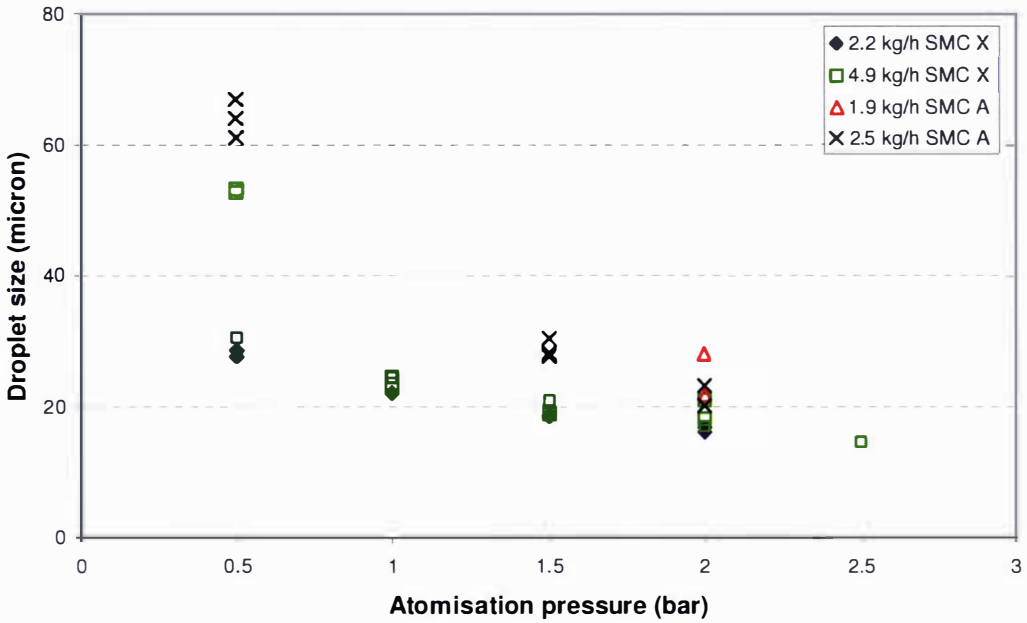

Figure 4.17: Sauter mean droplet size for 47 wt% SMC X at 40°C and 47 wt% SMC A at 50°C from Mastersizer S.

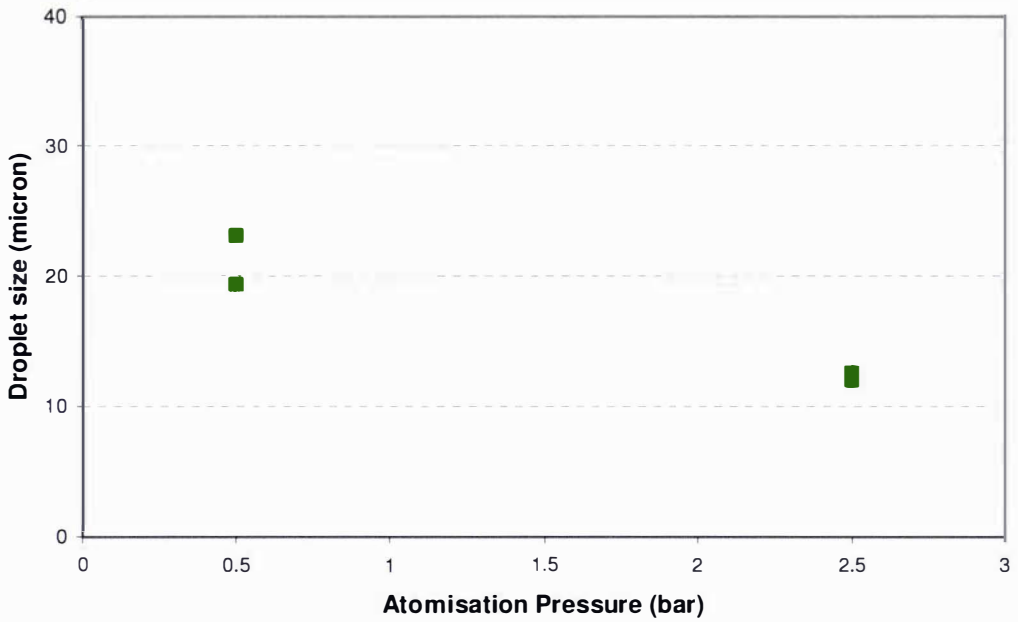

Figure 4.18: Sauter mean droplet size for water at 3.8 kg h^{-1} and 50°C.

Figure 4.19 shows size measurements made using the high speed camera by measuring the width of the particle trace. These size measurements were made on 41 wt% skim milk concentrate A at two flow rates. They are compared to the mean sizes obtained for water from the laser diffraction method. The observed sizes were similar; indicating the effect of viscosity on droplet size was small. The error in determining droplet size using this technique is larger than the differences between repetitions with the Mastersizer S.

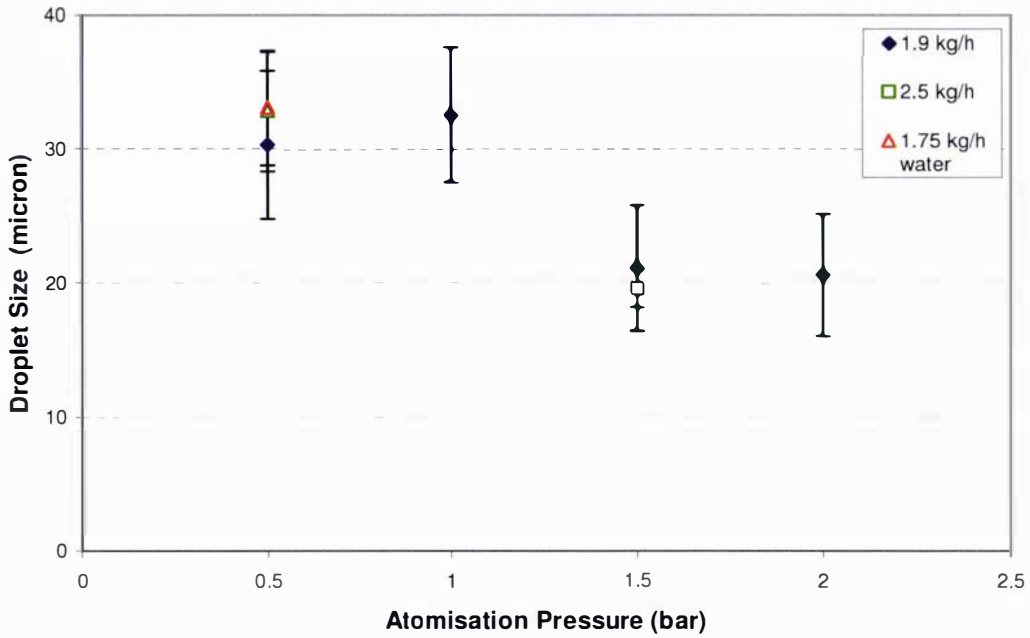

Figure 4.19: Droplet size for 41 wt% SMC A at 50°C from camera.

Droplet size was also measured implicitly by measuring dried powder from the nozzle. Figure 4.20 and Figure 4.21 shows the mean dried sizes compared to the mean obtained for the droplets from laser diffraction for two total solids contents, 41 wt% and 47 wt%. The D/D_0 ratios are compared in Table 4.5. The shrinkage rates using the approaches of Masters (1979) and Lin and Chen (2004) fit well to the experimentally determined ratios at 47 wt% solids. For droplets with an initial solids concentration of 41 wt% the shrinkage rates calculated are too large; in reality the droplets reduce in size by half, which is smaller than predicted.

This demonstrates that droplets with low total solids shrink more than droplets with higher total solids. At high solids concentrations, droplets have lower surface moisture contents so a skin can quickly form which inhibits size reduction and moisture diffuses though this skin as drying occurs. At low solids concentrations a droplet has higher surface moisture content so it takes more evaporation (in the constant rate period) and hence more time for a skin to form and shrinkage to occur.

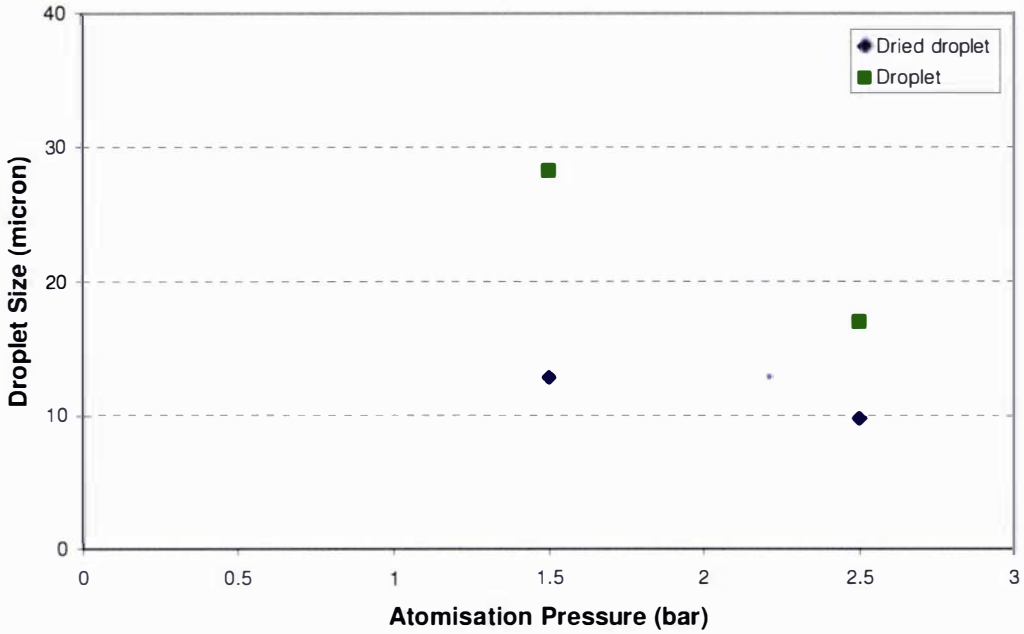

Figure 4.20: Comparison dried droplet size and droplet size (from Malvern Mastersizer S, (Figure 4.17) for 41 wt% SMC A at 2 kg h^{-1}.

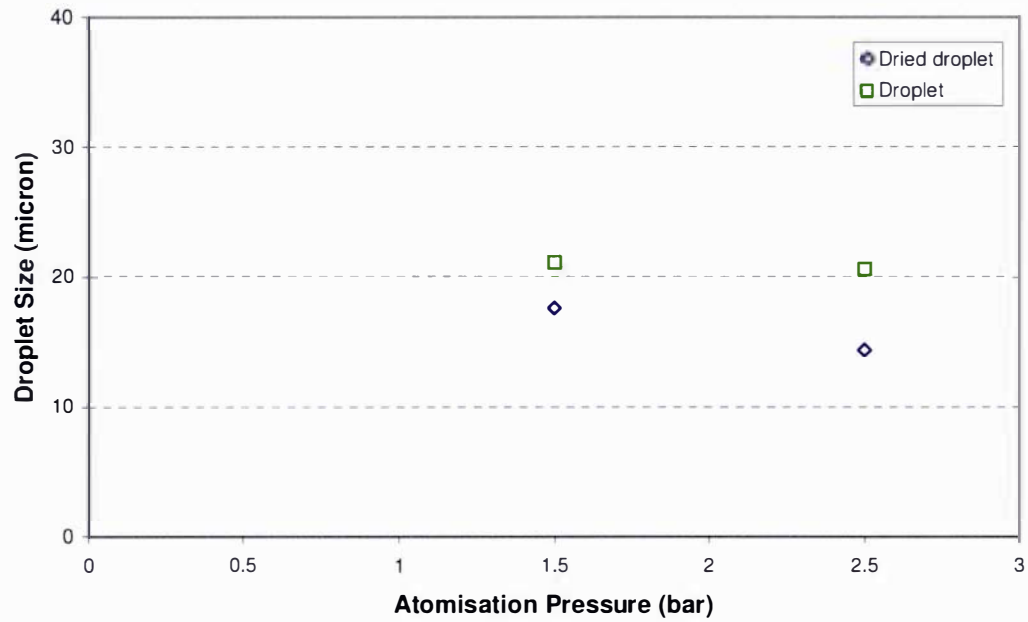

Figure 4.21: Comparison dried droplet size and droplet size (from Malvern Mastersizer S, (Figure 4.17) for 47 wt% SMC A at 2 kg h^{-1}.

Table 4.5: Comparing calculated and experimental shrinkage rates for SMC A.

Total Solids	Atomisation Pressure					
	1.5 bar			2.5		
wt%	L and C	Masters	SMC A	L and C	Masters	SMC A
41	0.76	0.71	0.45	0.76	0.71	0.58
47	0.76	0.75	0.84	0.76	0.75	0.70

4.6.3 Droplet Velocity Results and Discussion

Table 4.6 lists the liquid flow rate and air pressure conditions used to measure the droplet velocity using the high speed camera. The air velocities were also measured at the nozzle exit using a turbine anemometer for each air pressure with no liquid flow. The air loses momentum to both the liquid during atomisation and to entrained air. If conditions upstream of the nozzle = 0, at the exit of the convergent nozzle = 1 and 50 mm downstream of the nozzle = 2, the following momentum balance from 1 to 2 will hold:

$$M_A U_{A1} = (M_A + M_{AE}) U_{A2} + M_S U_{A2} \tag{4.16}$$

where M_A, M_S, M_{AE} = mass rate of air, spray, entrained air [kg s^{-1}]; U_A, U_S, U_{AE} = velocity of air, spray, entrained air [m s^{-1}]. At position 2 the velocity of the droplets, atomising air and entrained air are assumed to be equal because the droplets are small and the slip velocity will be small compared to the bulk velocity, i.e. $U_{A2} = U_S = U_{AE}$ [m s^{-1}]. For the experiment without spray, the anemometer measurements of air velocity can be used to determine the mass flow rate of entrained air:

$$M_{AE} = \frac{M_A (U_{A1} - U_{A2})}{U_{A2}} \tag{4.17}$$

where U_{A2} equals the anemometer measurements, $U_{air\ only}$, in Table 4.6. To determine M_{AE}, the velocity of the atomising air leaving the convergent nozzle is required, U_{A1}, which then can be used to determine the mass flow rate of atomising air M_A given the cross sectional area at the throat of the convergent nozzle, A_t = 1.37 x 10^{-6} [m^2], where $M_A = U_{A1} \rho_{A1} A_t$. The atomising air velocity is obtained from standard equations for compressible flow from Street et al. (1996):

$$\frac{U_{A1}^2}{2} = \frac{k}{k-1} \frac{P_1}{\rho_A} \left[1 - \left(\frac{P_1}{P_0} \right)^{\frac{k-1}{k}} \right] \tag{4.18}$$

Assuming that the outlet pressure P_1 is atmospheric (1 bar) and that the ratio of specific heats, k =1.4, and that the air density at the nozzle exit is $\rho_{A1} = P_1/RT_1$. The limiting condition of choked flow is where the velocity equals the speed of sound $= \sqrt{(kRT_1)}$ = 313 m s^{-1}. The gas constant for air is R = 287 J kg^{-1} K^{-1} and T_1 [K] = the outlet temperature which can be approximated by the critical temperature for choked flows (as all flows are close to choked), $T_1 = 2T_0/(k-1)$ where T_0 = 20°C.

With U_{A1} and M_{AE} determined, the droplet and air velocity U_{A2} can now be estimated from equation 4.16 and compared to the measured values using the high-speed camera. The predicted quantities U_{A1}, M_A, and M_{AE} necessary to complete the above calculations are also contained in Table 4.6. Comparison of the measured U_d and predicted U_{A2} show that they are of similar magnitude. It must be noted that this analysis is simplistic and does not account for possible losses at the sudden divergence of the gas leaving the nozzle, nor does it account for radial variations in momentum that will be present.

Table 4.6: Comparison of measured U_d with predicted droplet velocity U_{A2}.

measured				predicted			
M_S (×3600)	ΔP_{air}	U_d	$U_{air\ only}$	M_A (×3600)	M_{AE} (×3600)	U_{A1}	U_{A2}
(kg h^{-1})	(bar)	(m s^{-1})	(m s^{-1})	(kg h^{-1})	(kg h^{-1})	(m s^{-1})	(m s^{-1})
1.9	0.5	6.81	20	0.30	3.11	231	12.84
1.9	1.0	6.91	25	0.15	1.61	296	12.01
1.9	1.5	8.77	30	0.18	1.81	313	15.35
1.9	2.0	7.49	40	0.24	1.62	313	19.79
2.5	0.5	6.80	20	0.12	1.25	231	7.08
2.5	1.5	6.44	30	0.18	1.81	313	13.30
Average			7.20				

where M_s = measured spray flow rate, ΔP_{air} = measured pressure difference across nozzle, U_d = measured spray droplet velocity 50 mm from nozzle, $U_{air\ only}$ = measured air velocity 50 mm from the nozzle without spray, M_A = predicted atomising air mass rate, M_{AE} = predicted entrained air mass rate, U_{A1} = predicted atomising air exit velocity from the nozzle. U_{A2} = predicted velocity 50 mm from nozzle of air and spray.

Figure 4.22 shows the droplet velocities measured using the high speed camera. It is possible these vales are artefacts of the measurement method used. Streaks indicating droplets caught in the exposure are limited to those that appear with each frame for the 100 µs exposure time. Therefore faster droplets will not appear and may appear too faint to see. Figure 4.22 demonstrates that the mean velocity of the droplet is not affected significantly by atomisation pressure, flow rate or fluid viscosity. The average droplet velocity in the spray at 50 mm from the nozzle exit was found to be 7.20 m s^{-1} however, individual droplet velocities ranged from 2 m s^{-1} to 35 m s^{-1}.

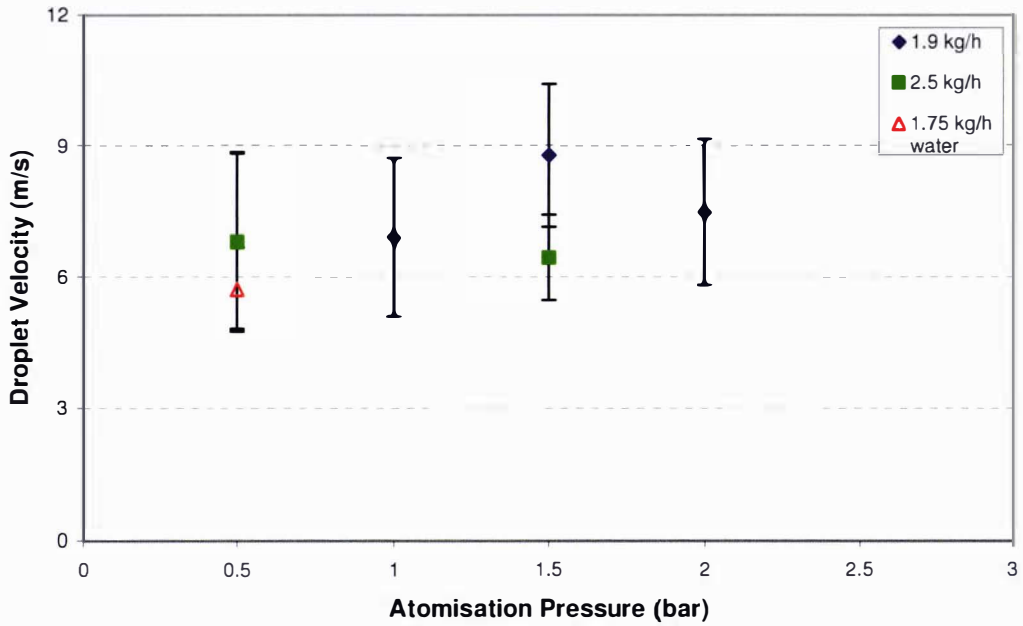

Figure 4.22: Droplet velocity for 41 wt% SMC A 50°C and water 20°C at various liquid flow rates.

4.7 Chapter Conclusions

Density of concentrates can be accurately predicted for a specific temperature and solids content. Concentrate viscosity is also predicted using a model based on Snoeren et al. (1982); however it is only accurate at low solids contents. Few literature values for the surface tension of concentrated milks exist, but a wide range of data is available for standard concentration milks over a range of temperatures. The values are scattered, which appears to relate to the measurement technique employed. The experimental results reported here showed that the surface tensions of concentrated milks (fresh and reconstituted) were within the same range as literature values below 60°C, but were significantly higher for milk above 60°C. This behaviour was exhibited by standard whole milks using the same technique. The Wilhelmy plate technique requires time to lower and raise the plate, which introduces problems. The solution must drain from the plate; this particularly affects viscous milk concentrates. Also, the time taken allows a skin to form. The mechanism that causes this is not known precisely but relates to disulphide cross linking for the increased tendency for skin formation at high temperatures and concentrations. Although an error analysis of the influence of surface tension on droplet size indicated less than 10% error, a more rapid measurement technique than the Wilhelmy plate method may avoid these problems.

This work showed that nozzle placement from the measurement device was crucial in spray characterisation. Atomisation pressure on a two fluid nozzle had only a small effect on droplet size particularly at lower air pressures. Fluid flow rate has little effect on the mean droplet size and SMC A generally shows a larger droplet size. Size measurements made using the high speed camera were similar to those determined by the Mastersizer S. For the droplet velocity calculated using the high speed camera no relationship between atomisation pressure or fluid type was seen within the error limits.

CHAPTER 5

EQUIPMENT AND EXPERIMENTAL DESIGN

This chapter describes the process taken to design a mini agglomerator to study the effect of relevant variables on agglomerate properties. Agglomeration is a rapid process and, for agglomerates to be collected, subsequent drying is also a necessity. Therefore, it makes most sense to study agglomeration inside a commercial spray drier, which can simulate the typical moisture and temperature gradients, and the air, droplet and particle interactions. However, manipulating operating variables does not isolate individual micro process or the variables that affect them; instead, they provide changes that may have multiple influences. For this reason, industrial spray driers are ill-suited to the sort of experiments required to fully investigate the agglomeration process. Instead a small scale spray drier was used which had the flexibility to vary process parameters without having to consider the impact on production and product quality.

The variables that affect droplet-particle impact and adhesion, as identified in Chapter 2, have been listed in Table 5.1, alongside the operating parameters which influence them. While the variables in the left hand column represent operating parameters available using a small scale drier they are not available to industrial operators because of upstream recycle and downstream process considerations. Therefore in this work when the words operating parameters are used, they refer to those available in the small scale drier. The variables listed in the right hand column relate to those identified in Chapter 2 as important to the micro processes of agglomeration. A trade-off exists between the micro processes that occur during agglomeration and the experiments that can be conducted. Experimentally, operating parameters can be incorporated into a statistical design while maintaining as constant the drying rate, inlet air temperature and the temperature of the droplet.

Table 5.1: Key variables affecting agglomeration.

Parameter	Units	Description	Variable affected
M_p	kg s^{-1}	particle flow rate	$\dot{N}_p$
x	m	curtain width	$\dot{N}_p$
$Q_{a.c}$	m^3 s^{-1}	curtain air flow rate	$\dot{N}_p$, U_p
D_p	m	size of particles	D_p
M_c	kg s^{-1}	concentrate flow rate	$\dot{N}_d$, D_d
P	bar	Atomising air	$\dot{N}_d$, D_d
TS	%	total solids of	$\dot{N}_d$, D_d, μ, X_d

d,p subscripts = droplets and particles, $\dot{N}$ = number flow rate [s^{-1}], U = velocity [m s^{-1}], D = diameter [m], μ = concentrate viscosity [Pa s], X = moisture content [kg kg^{-1}].

Earlier discussions identified the interaction zone in the top of a spray drier as being the most important for agglomeration; a simplified agglomerating system was investigated as a sheet of spray droplets interacting with a curtain of powder particles, shown in Figure 5.1. This system utilised a two fluid nozzle positioned to spray horizontally onto

a curtain of particles delivered through a narrow opening in the top of a small scale Niro drier which imitated the conditions of an industrial plant (see Figure 5.2). This system makes it possible to vary and study the effect of droplet and powder properties on the degree of agglomeration. A key issue with this design is ensuring droplets are dried to produce a powder.

To construct equipment suitable for studying each variable, it was necessary to consider the project in four parts. The first selected the appropriate drier and established its capacity; the second focused on the design of the curtain generator, and its performance; the third involved constructing the spray device and an acceptable procedure to manufacture milk concentrate; and the final design area focused on the agglomeration experiments and the design of experimental plans. Each of these parts is discussed in the sections below.

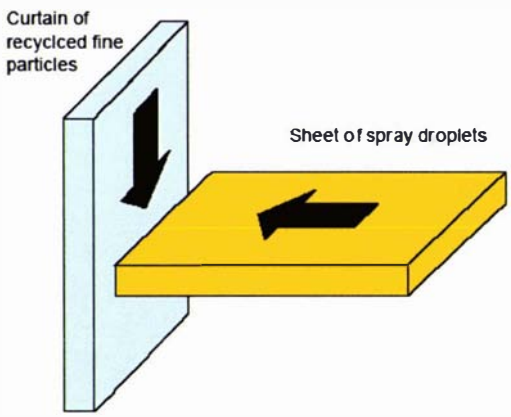

Figure 5.1: Sheet of spray droplets approaching a curtain of powder particles.

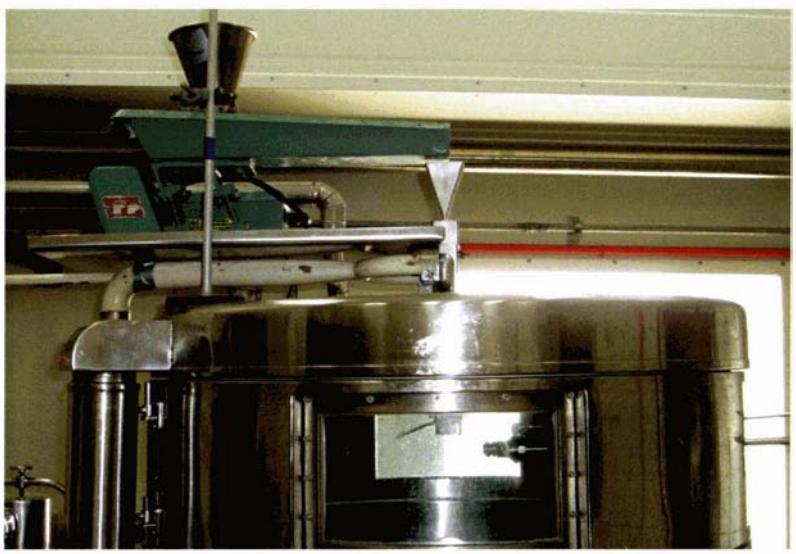

Figure 5.2: The final agglomerator design.

5.1 Drier Selection

One of the main advantages of using a small scale drier is that it provides a suitable chamber for drying and contacting the concentrate spray. It is also directly comparable with the situation in industry; the diameters and capacity of each scale have been included below:

1. laboratory scale (BUCHI B-290, D = 0.15 m, 0.5 kg h^{-1} water evaporation)
2. small pilot scale (Niro, D = 0.8 m, 0.5 – 7 kg h^{-1} water evaporation)
3. pilot scale drier (IFB, D = 2.9 m, ~ 80 kg h^{-1} water evaporation)
4. industrial scale (Niro Compact, D = 6.5 m, ~ 15 000 kg h^{-1} water evaporation)

A small drier was required to contain the agglomeration experiments and several options were considered. Goula et al. (2004) recently identified the benefits of using laboratory scale spray driers for investigating aspects of spray drying. They state the main advantage is that the drying conditions are easy to control and experiments can be performed quickly. However, laboratory scale spray driers are not able to produce powders with the same bulk properties as those generated on a larger scale because finer droplets are dried over shorter residence times. In this case, laboratory scale driers were considered too small to perform an agglomeration study effectively. The sizes of the droplets and particles would need to be scaled down significantly from the industrial situation and particles would not experience the same drying trajectories. A small pilot scale drier (referred to as the small scale drier in the rest of the thesis) can be used to study the collision and adhesion between particles and droplets due to their flow trajectories and surface stickiness properties as opposed to other forces, such as electrostatics, that may result in agglomerate formation.

Nijdam and Langrish (2005) also established that small scale spray driers are ideal for studying milk powders as very little natural particle agglomeration occurs due to low number concentrations, which is essential for this study which aims to understand forced agglomeration. One of the main advantages is that small amounts of powder can be produced. One of the main disadvantages is that the drier required alteration to allow the introduction of fines into the system. The small scale drier also had difficulties drying high fat products as deposition occurred on walls, pipes and cyclones due to fat melting (Sowersby, 2004). As there was no secondary drying, the powder will exit with higher moisture content compared to industrial driers. High moisture content can lead to shelf life problems and also result in sticking and clumping in the collection jar since there is no fluid bed to cool the powder prior to collection. This issue is discussed in §5.1.3 to determine the operating conditions required to produce powder at an acceptable moisture content to avoid problems during production, storage and testing.

Four small scale spray drying units were available for the agglomeration study. Five criteria were used to evaluate the suitability of the spray drying chambers; these criteria have been discussed in more detail in Appendix M. The drier selected as the most appropriate (Niro Atomiser Mobile Minor Spray Drier, Niro A/S, Soeberg, Denmark) was because it is easy to modify and it was readily accessible for use. A schematic of the selected drier is included in Figure 5.3.

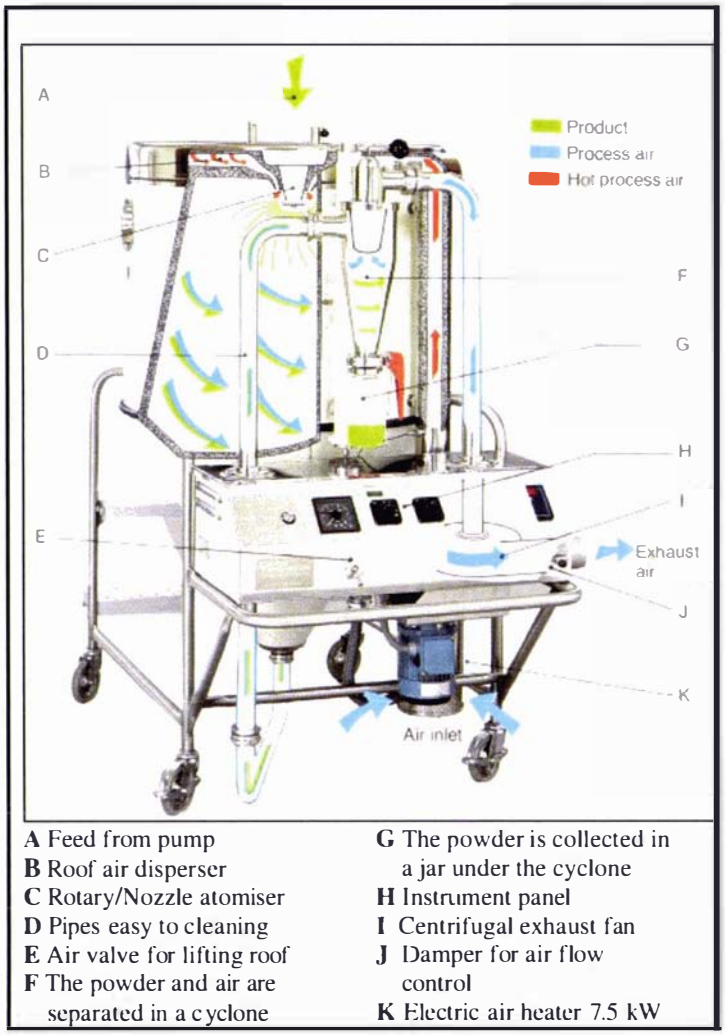

A Feed from pump
B Roof air disperser
C Rotary/Nozzle atomiser
D Pipes easy to cleaning
E Air valve for lifting roof
F The powder and air are separated in a cyclone
G The powder is collected in a jar under the cyclone
H Instrument panel
I Centrifugal exhaust fan
J Damper for air flow control
K Electric air heater 7.5 kW

Figure 5.3: Niro Atomiser Mobile Minor Drier.

The drier was modified to allow the addition of a powder curtain (2 x 60 mm gap as discussed later in §5.2.2). The capability of the Niro drier at different inlet temperatures is included in Table 5.2. These performance data were obtained without any powder addition but with the powder chute open. A two fluid nozzle (Spray Systems 2850 fluid cap, 67228 - 45 air cap) was used to atomise water at 22°C. Therefore the inlet air temperature only represents the air that passes over the air heaters; other air enters through the chute opening and with the atomiser air. The remainder of this section characterises the performance of the selected drier, establishing the drying air flow, outlet conditions and limits of the system that will affect the design of other parts of the agglomerator as well as the agglomeration study.

Table 5.2: Capability of modified Niro drier for water at ~ 22°C.

Inlet Temperature (°C)	Water Flow rate (kg h^{-1})	Outlet Temperature (°C)
195	1.75	61.5
200	1.75	64.2
205	1.75	67.4

5.1.1 Determination of Drying Air Flow

In standard operation of the Niro drier, the exhaust fan draws air through the air inlet, past the heaters and into the drying chamber. A key parameter responsible for the amount of drying that occurs is the hot inlet air flow rate. In this Niro drier the inlet air flow rate was difficult to measure directly. The hot inlet air flow rate can be inferred by measuring the outlet air flow rate. However, with a modified fines inlet, the exhaust fan also draws air through the chute opening. A third air stream also enters the drier as atomisation air from the two fluid nozzle. A turbine anemometer was used to measure the inlet and exhaust duct air velocities and the chute velocity. The atomising airflow measurement was made as near to the nozzle as possible while operating without liquid at the same pressure drop.

A heat balance was used to calculate the hot inlet air flow rate by equating the heat lost to evaporation to the heat gained by the air streams. Equations (5.1) to (5.3) were used to calculate the flow rate of hot air into the drier; this was calculated using the measurements in Table 5.3. These measurements were made by spray drying 41% total solids skim milk concentrate at 50°C, at a flow rate of 1.7 kg h^{-1}, and an atomising air pressure of 2.5 bar. The hot air flow rate was calculated to be 60.5 kg h^{-1} (80.7 m^3 h^{-1}), at the measured outlet air flow rate of 109.8 m^3 h^{-1}. There is 26.2 m^3 h^{-1} of extra air which may be from some level of error in the measurements and calculations or leakage through the seals.

$$E_{out} = E_{in} = M_{out}(H_{out} - H_{amb}) \tag{5.1}$$

$$M_{in} = \frac{E_{in}}{H_{in}} \tag{5.2}$$

$$M_{out} = M_{in} + M_{chute} + M_{atm} + M_{leak} \tag{5.3}$$

where E_{out} = heat in outlet air [kW], E_{in} = heat in inlet air [kW], M_{out} = mass flow rate of outlet air [kg s^{-1}], M_{in} = mass flow rate of inlet air [kg s^{-1}], H_{out} = enthalpy of outlet air [kJ kg^{-1}], H_{in} = enthalpy of inlet air [kJ kg^{-1}], H_{amb} = enthalpy of ambient air [kJ kg^{-1}], M_{chute} = mass flow rate of air through the chute [kg s^{-1}], M_{atm} = mass flow rate of air through the atomiser [kg s^{-1}], and M_{leak} = mass flow rate of air in due to leakage [kg s^{-1}].

Table 5.3: Measurements on drier air streams to calculate the hot air inlet flow rate.

Air Stream	T (°C)	RH (%)	U (m s^{-1})	Q (m^3 h^{-1})	ρ (kg m^{-3})	M (kg h^{-1})	AH (kg kg^{-1})	H (kJ kg^{-1})
Chute	20	48.9	6.75	2.9	1.20	3.5		
Cool inlet	20	50.2	0.46	54.5	1.20	65.4	0.008	37
Hot inlet	195			**80.7**		**60.5**	0.008	220
Exit outlet	40	62.2	3.52	**109.8**	1.12	123.3	0.030	120
Drier outlet	72			109.8	1.02	111.8	0.030	156
Leak	20	50.2		**26.2**				

T = temperature, RH = relative humidity, U = velocity, Q = volumetric flow rate, ρ = density, M = mass flow rate, AH = absolute humidity, H = enthalpy and E = energy.

5.1.2 Prediction of Outlet Conditions

Outlet temperature and product moisture content are crucial indicators of product stability. Maintaining these within acceptable limits determines the drying capacity of the spray drier. Models of spray drier performance have been discussed extensively by Oakley (2004). An equilibrium based model, such as that used by Ozmen and Langrish (2003b) is recommended when particle sizes are small, drying kinetics are fast and residence times long. Simple heat and mass balance models are recommended for prediction of heat loads, and for preliminary process design. When equilibrium is not expected, more complex, rate based models are recommended but these require experimental data on the drying kinetics of the material. Langrish and Kockel (2001) and Oakley (2004) suggest the use of characteristic drying curves for spray drying. This approach assumes a specific drying rate at each moisture content independent of external drying conditions. The simplest case requires some knowledge of the system and the complex case requires a detailed understanding of gas flow and particle motion.

In this study a mass and heat balance in Excel was used to estimate the outlet conditions of humidity and temperature. Equilibrium was assumed to estimate product moisture content based on the work of Ozmen and Langrish (2003b). The calculations incorporated various air inlets through the air heaters, the chute, the atomiser and some leakage of air into the drier. The equilibrium moisture content of the particle is a function of the temperature and relative humidity of the gas environment and the nature of the solid. Two isotherms are listed below which can be used to predict the equilibrium moisture content; Equation (5.4) is recommended by Papadakis et al. (1993), for relative humidities below 21.4%; and, the Guggenheim-Anderson-de Boer (GAB isotherm) (Equation (5.5)) is used for higher humidities. Constants A, B, K_1, K_2 and K_3 are empirical and depend on the solid and liquid materials; the values used here are those determined by Kockel et al. (2002) for skim milk powder.

$$X_{eq} = A\exp\left[-BT\ln\left(\frac{1}{RH}\right)\right] \tag{5.4}$$

$$X_{eq} = \frac{K_1 K_2 K_3 RH}{(1-K_2 RH)(1-K_2 RH + K_2 K_3 RH)} \tag{5.5}$$

where X_{eq} = equilibrium moisture content [kg(water) kg^{-1}(water free solid)], RH = relative humidity [–], A = 0.1499 [kg(water) kg^{-1}(water free solid)], B = 2.306 x 10^{-3} [K^{-1}], K_1 = 0.19662 [kg(water) kg^{-1}(water free solid)], K_2 = 0.26244 and K_3 = 4.6167.

Foster (2002) formulated a prediction model for the moisture sorption isotherms of dairy powders which combined the isotherms of all of the components present. In contrast to the work above, this allows prediction of moisture content for powders with a specific composition that may differ from a typical skim milk powder. Including the composition in moisture prediction is crucial for accurate moisture content prediction, especially as measuring the moisture sorption isotherm for a specific powder is time consuming. Foster's model was validated with a number of powders and predicts the glass transition temperature at a specific water activity. This information is used in §5.1.3 to determine the maximum acceptable moisture content during storage.

To calculate the heat losses from the system the following equation was used:

$$E_{loss} = UD(T - T_{amb}) \tag{5.6}$$

where UD = constant = area × overall heat transfer coefficient [W K^{-1}] and T_{amb} = ambient temperature [°C]. UD does not change significantly with temperature and T_{amb} can be taken as 25°C. UD is determined by fitting existing data to the model, for experiment 1 a UD value of 0.0337 kW K^{-1} was obtained and this was used to predict the outlet conditions for experiment 2. Table 5.4 compares the predicted and measured values of outlet temperature, outlet humidity, equilibrium moisture content and percentage moisture for experiments 1 and 2 and the composition of this milk powder is given earlier in §3.6.

Table 5.4: Comparing measured and predicted outlet conditions for skim milk drying.

Experiment	Units	1		2	
		Predicted	Measured	Predicted	Measured
Concentrate flow rate	(kg h^{-1})	1.7	1.7	1.7	1.7
Total Solids	(%)	41.2	41.2	41.2	41.2
Outlet Temperature	(°C)	71.5	71.5	72	67.8
Outlet Humidity	(%)	8.1	13.4	7.1	13.1
O & L (2003) moisture	(%)	1.00	5.42	0.87	5.19
Foster (2002) moisture	(%)	1.52	5.42	1.74	5.19

O & L = Ozmen and Langrish (2003). Powder composition used to calculate Foster (2002) moisture: fat = 0.8%, lactose = 53.8%, protein = 33.3%, ash = 8.3%, and moisture = 3.8%.

The Foster (2002) moisture content prediction in Table 5.4 is similar to Ozmen and Langrish's to using the predicted outlet air humidity (in the predicted column). However using the GAB isotherm and the measured outlet humidity gives a moisture content that is closer to the actual moisture content (in the measured column). The difference between predicted and actual moisture content indicates that equilibrium is not reached and means that rate based modelling is needed to predict moisture content. Two reasons contribute to this discrepancy, the short residence time, and the high solids concentration of the feed. The residence time is shorter than designed for the drier because the droplet trajectory following atomisation is horizontal instead of vertical and is directed perpendicular to the hot air. This minimises contact between the spray and the drying air. The insufficient mixing in the atomisation zone can result in a low residence time (as well as wall/roof impingement). The solids concentration used by Ozmen and Langrish (2003) was 8.8% milk solids which, when atomised, produces a porous particle and meant that the equilibrium assumption was a valid predictor for their system. Here, the solids concentration is much higher and drying produces a different particle (more dense or hollow) the drying rate becomes limited by the moisture transport and the particle does not reach equilibrium in the time available for drying.

In this study it is desirable to be able to estimate the moisture content of the product at specific operating conditions. Experimental data for this system is shown in Figure 5.4 demonstrates the relationship between outlet temperature and product moisture content. The inlet temperature and total solids levels were held constant at 195°C and 41 wt% respectively to generate this plot by spray drying milk concentrate at a range of flow rates and atomisation pressures. Once the maximum acceptable product moisture content has been established, this can be used to find the minimum outlet temperature which will be a useful guide when conducting experimental work.

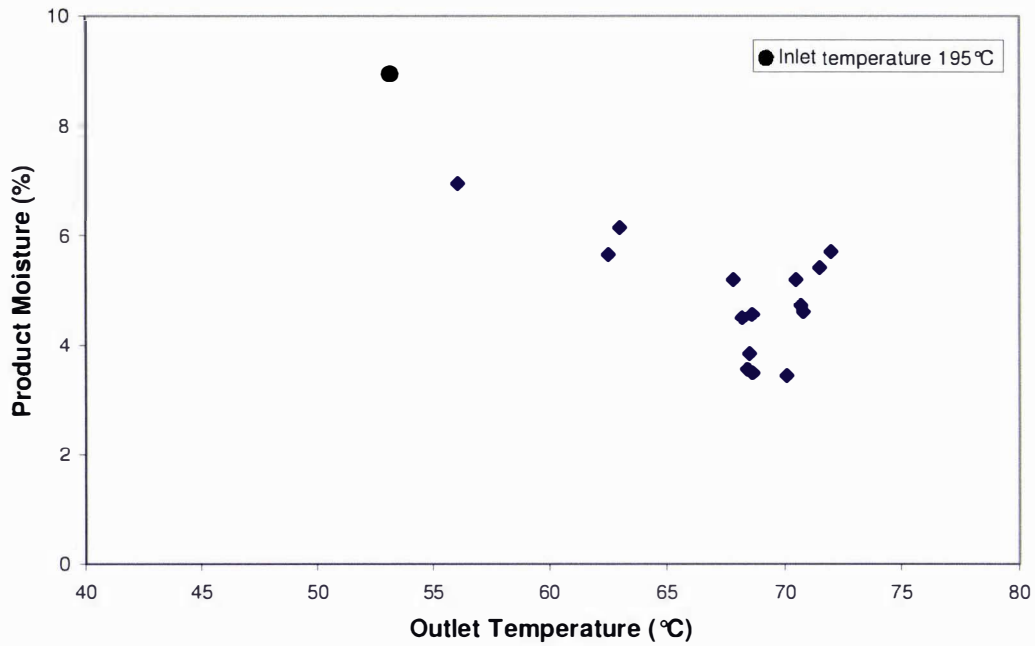

Figure 5.4: Moisture vs. outlet temperature for skim milk powder.

5.1.3 Maximum Acceptable Moisture Content

In terms of production for sale there is a maximum allowable moisture content for a spray dried milk product to be classed as a milk powder (5% according to (CODEX, 1999)) and this will also ensure product stability. If the exit conditions are such that powder particles can stick together, not only will further agglomeration take place but agglomerates will adhere to the walls of the collection vessel. Roos (2002) states that the water activity of dairy powder must be below 0.37 and Wewala (1992) states water activity must be below 0.3 otherwise lactose crystallisation will occur which releases water resulting in plasticization, and lowering of the glass transition temperature which will lead to powder caking. Also, crystallisation of the liquid bridges that may be formed between particles will cause the formation of strong solid bridges (Brooks, 2000). Bronlund (1997) states that when a small amount of amorphous lactose is present, later crystallisation will cause caking when lactose crystals are stored above 0.25 a_w. However, when high amounts of amorphous lactose are present in the powder (53.8 wt% in this case, see Table 3.6) the amorphous lactose acts as a buffer for moisture movement so a value of 0.3 a_w is selected.

This upper limit storage water activity is determined by the drier outlet conditions both for product moisture content and temperature. These may or may not be at equilibrium as already explained. If not, then the approach temperature of the particles to that of the exit air is needed. A range of opinions are presented in the literature, from Reineccius (2004) who states that particles never exceed the exit air temperature in a co-current drier to Buma (1970) who more precisely estimates the particle temperature to be ~ 10°C below the exit air temperature to Truong (2005a) who qualify that, for droplets less than 40 µm, particle temperature rises above 100°C then decreases as the outlet air is cooled by evaporating the larger droplets.

To check the approach temperature in this work, thermocouples were placed in the collection vessel at the bottom of the cyclone shown in Figure 5.5. Figure 5.6 shows the temperature profile over time at these various positions, for both powder temperature and also the outlet air temperature. The green and red lines indicate the start (7 minutes) and finish (22 minutes) of the trial and the blue dashed line indicates where the vessel was full and removed from the cyclone. The temperature probe at the top of the vessel remained to monitor powder temperature in the new vessel through the entire experiment. The highest powder temperature is 53.5°C at the top of the vessel when the outlet air temperature is 67.5°C, which is a difference of 14°C.

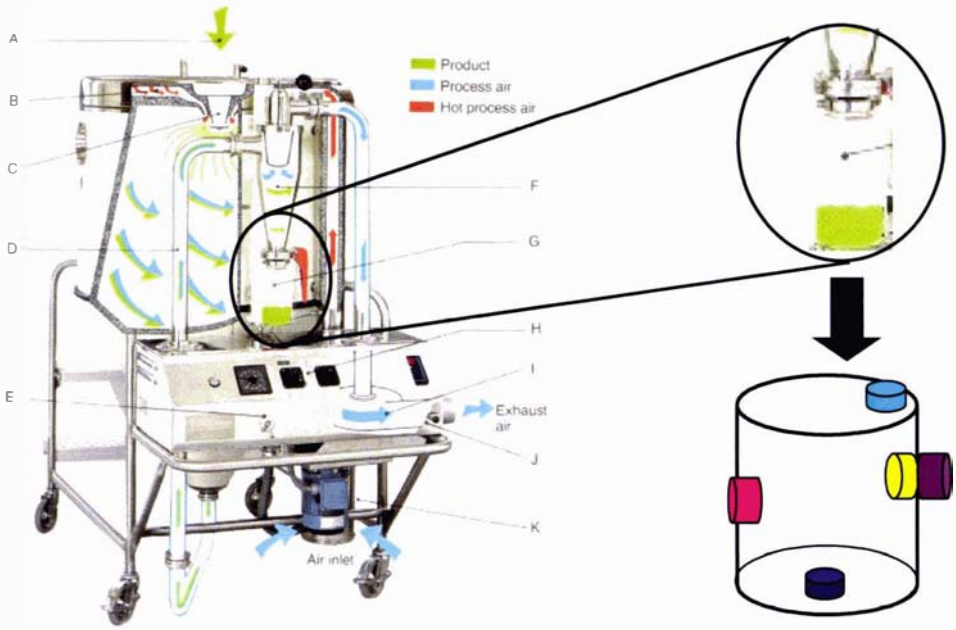

Figure 5.5: Diagram of temperature measurement positions in the collection vessel.

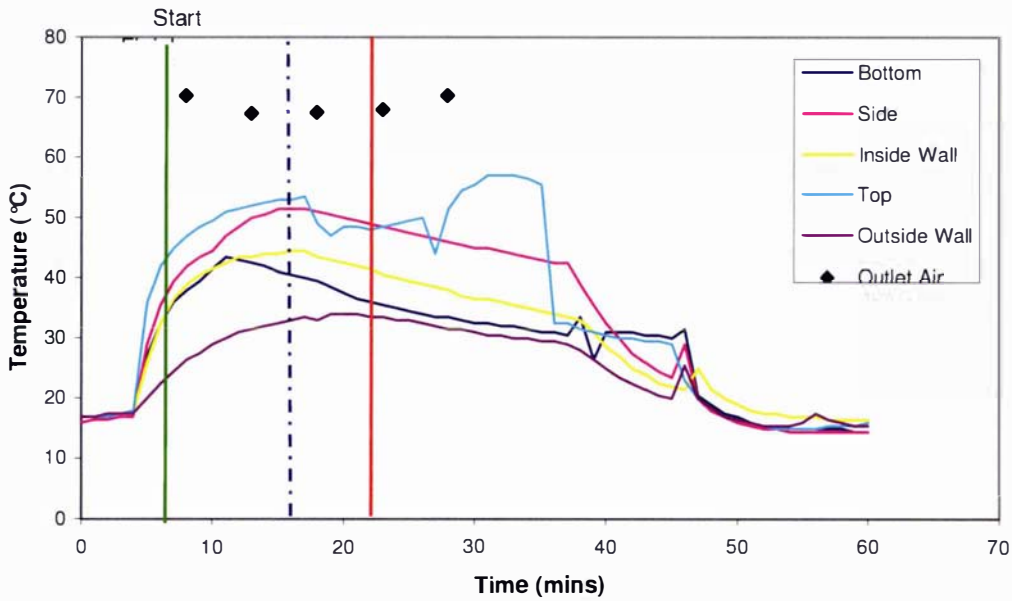

Figure 5.6: Temperature profile over time for an agglomeration run.

A stickiness curve showing the relationship between temperature and water activity can help determine whether the powder will become sticky during storage. The stickiness curve in Figure 5.7 is for an instant skim milk powder of a similar composition as ISMP A. The $(T - T_g)_{critical}$ (temperature above the glass transition temperature where sticking occurs) was found to be 40.3 ± 2°C using the particle gun technique employed by Zuo (2004) as discussed in Chapter 2. Murti (2006) also used the particle gun technique to capture stickiness data for a range of skim milk powders and improved the apparatus to investigate the effect of particle velocity on the sticky point temperature with a lower error of ± 0.8°C. The sticky point temperature is often applied to spray drying to determine the appropriate outlet drying conditions to avoid powder build-up inside the drier and periphery equipment such as cyclones. In this situation, the powder is travelling through the air and impacting a surface at a specific velocity.

Stickiness depends on environmental conditions that exceed the T_g of the powder and also the contact time available for viscous flow at the powder surface to form a liquid bridge between powder particles; this process is referred to as sintering (Palzer, 2005). The powder in the collection vessel is a static bed and the contact time between the powder particles is long and it is possible that sintering will occur between powder particles during collection/storage. Murti (2006) showed that decreasing the contact time available for adhesion also increased the $(T - T_g)_{critical}$ and also compared the results of the particle gun technique with a fluid bed technique and found that the fluid bed method gives lower $T - T_g$ values than obtained with the particle gun.

The approach of Foster (2002) was used to predict the glass transition temperature for this exact composition of skim milk powder. At a maximum water activity of 0.3 the glass transition temperature, T_g, would be 34°C. As the powder is in a static bed it is not suitable to apply the $(T - T_g)_{critical}$ values found using the particle gun technique. Applying a much lower $(T - T_g)_{critical}$ allows for the extended contact time between milk powder particles. Paterson et al. (2005) identified for amorphous lactose that as the time for adhesion decreases the $T - T_g$ increases. Palzer (2005) took this a step further and combined the Williams-Landel-Ferry (WLF), Navier-Stokes and viscoelastic knowledge to predict the $T - T_g$ depending on contact time for adhesion which was described earlier as equation (2.18).

$$t = \left(\frac{5D_p^{\,2}\pi}{4\sigma_l D_p \pi + 2F_t}\right)\mu_g\left(\frac{D_{bridge}}{D_p}\right)^2 10^{[C(T-T_g)]/[B+(T-T_g)]} \tag{2.19}$$

where σ_l = surface tension of saturated lactose , F_t = impact force, μ_g = viscosity at the glass transition temperature, D_{bridge} = diameter of sinter bridge, C,B = WLF constants, T = temperature, T_g = glass transition temperature.

Equation (2.18) was used with the values of Murti (2006) to calculate the expected $T - T_g$ level assuming the powder sits in the collection vessel for the duration of an experiment usually 15 minutes. Appendix N calculates a $(T - T_g)_{critical}$ value of 8.8°C. For an $a_w = 0.3$ where the glass transition temperature of the powder is 34°C, this means the temperature of the milk powder in the collection jar should therefore remain below 42.8°C and the outlet air temperature (+14°C) should be less than 56.8°C to avoid sintering. However, operating at this outlet temperature would result in high product

moisture content (~ 6.5%) as shown on Figure 5.4. This translates to a water activity that is higher than that specified, 0.3, to avoid lactose crystallisation.

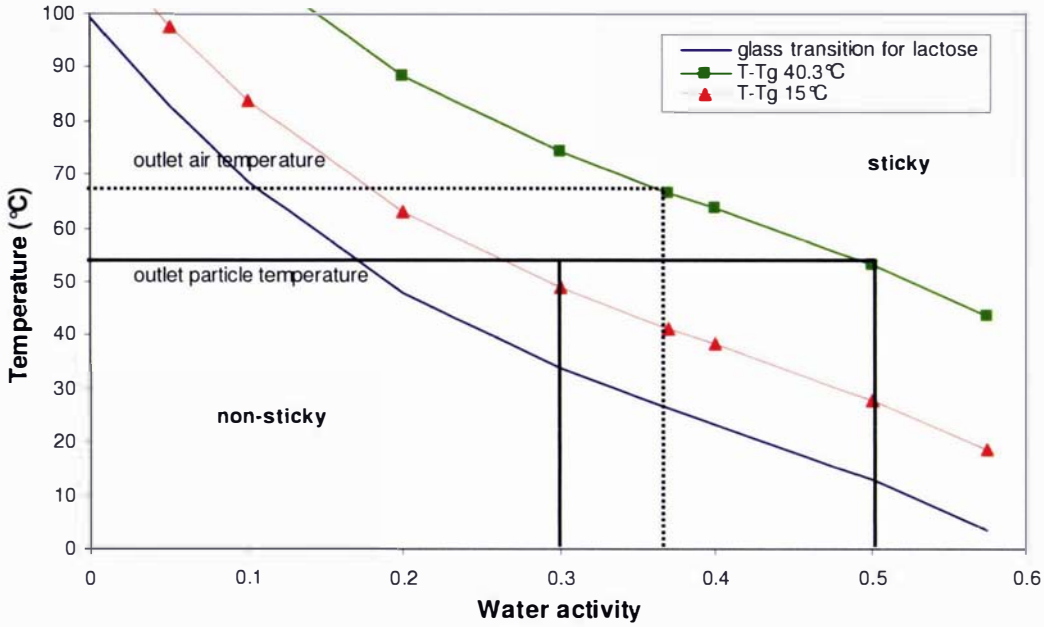

Figure 5.7: Glass transition for lactose and stickiness curve for ISMP.

Another approach is to use the suggested maximum water activity to determine the maximum suitable powder moisture content. In this case, production data has been used to determine the relationship between moisture content and water activity (Figure 5.8). The data points were generated by spray drying milk concentrate at a range of flow rates and atomisation pressures but a constant inlet air temperature of 195°C. Figure 5.8 shows a maximum product moisture content of ~ 5.7% is allowable for the agglomeration study. For an air inlet temperature of 195°C and for the additional inlet air flow rates of the chute, atomiser and leakage given in Table 5.3, this moisture translates to an outlet temperature of 63°C from the calibration curve of moisture content versus outlet temperature in Figure 5.4 and therefore an evaporation rate of 1.18 kg h^{-1}. These figures represent the maximum performance of the drier and affect the design of the spray and curtain design elements.

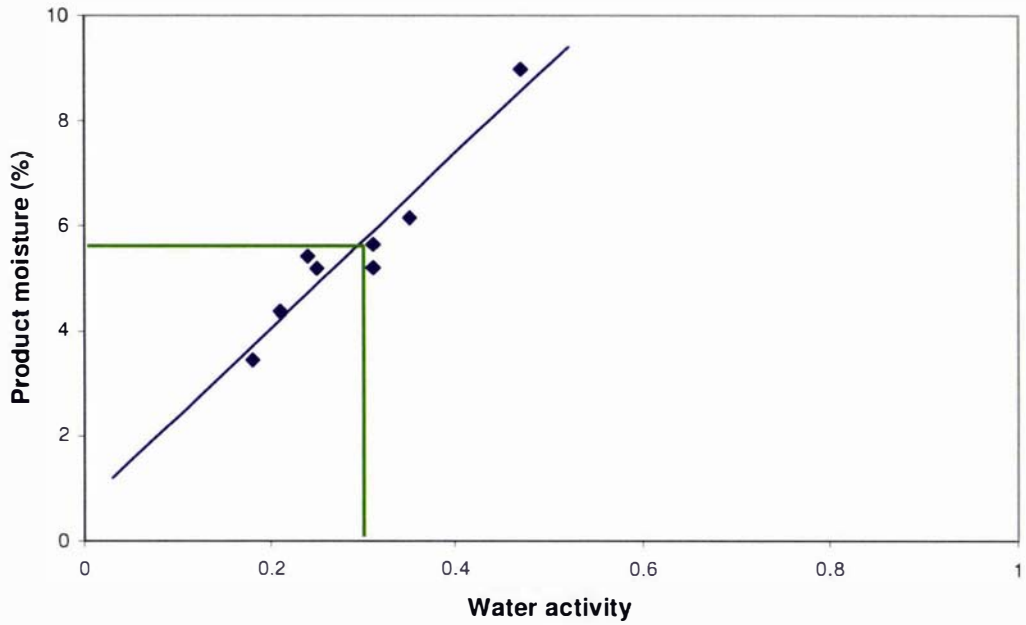

Figure 5.8: Product moisture as a function of water activity for ISMP A.

5.2 Particle Curtain Design

The aim of the small scale experiments is to study contact between a vertical flat curtain of powder and a horizontal sheet of spray droplets. Two issues are important to the curtain design: keeping an even, controllable flow of powder to the device and the distribution of the flow uniformly into a curtain and into the drier. Both are limited by the capacity of the drier and the design of the existing drier. Figure 5.9 shows the existing dimensions of the opening to the top of the small scale drier through which the curtain must pass.

The estimated fines recycle rates in industry affects the design of the curtain delivery device. Earlier work in §3.8 identified fines to spray mass flow rate ratios of between 0.43 and 0.59 industrially. As the modified drier has a maximum water evaporation rate of 1.18 kg h^{-1}, concentrate flow rates of up to 2 kg h^{-1} can be studied. This corresponds to design fines flow rates for the powder curtain in the range of 0.9 to 1.2 kg h^{-1}. To investigate a range of ratios the curtain delivery system must be able to provide flow rates of 1 – 2 kg h^{-1}.

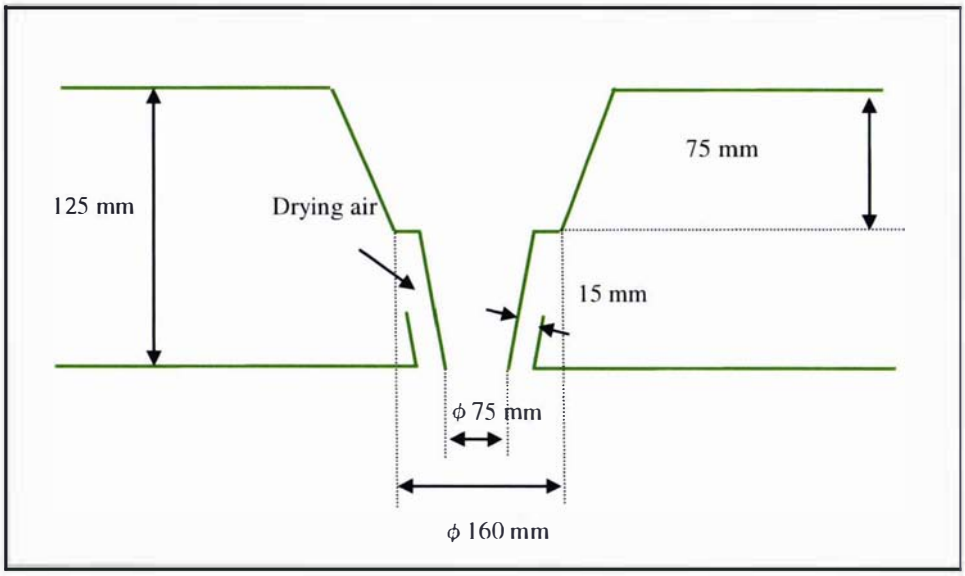

Figure 5.9: Drier size limitations.

5.2.1 Powder Feeder

A range of designs were considered for powder feeding including, a fluidised bed, a conveying belt, a hopper with a controllable discharge and a vibrating chute. The fluidised bed had several disadvantages; firstly, significant construction and design would be required to produce the equipment appropriate for this task, and secondly the air used to convey the particles to the top of the drier would reduce the evaporative capacity of the drier further. Even a small amount of introduced air has a significant effect on the evaporation rate of the drier. The hopper feeder required too small an orifice which would not consistently produce the required powder flow rate. The belt conveyor seemed a good option initially, but these devices are well known to be less effective than a vibrating chute. A vibrating chute was selected, with a chute width of 65 mm above one end of which a hopper was mounted as shown in Figure 5.10. Calibration was affected by the particle size of the powder and the exact clearance of the hopper above the vibrating chute. For this reason the actual powder flow rate was measured before each experiment.

Figure 5.10: Hopper and vibrating chute.

5.2.2 Curtain Distributor

The drier operates under vacuum so any openings for powder delivery will allow cool air to be drawn in. To avoid this as much as possible, the powder falling off the vibrating feeder drops through delivery chute with a 2 mm gap. This gap was calculated to restrict air flow to 3.5 kg h-1 (2.92 m3 h-1) as shown in Table 5.5 while allowing the production of powder with acceptable moisture content at a concentrate flow rate of 2 kg h-1. Chute dimensions of 30 x 60 mm were selected to fit in the top of the drier. Adjustable side panels meant the chute width could vary from 10 to 30 mm. A circular plate supports the unit into the top of the drier (Figure 5.11).

Table 5.5: Calculation of flow rate air through chute gap.

Variable	Units	Values
Air velocity	($m\ s^{-1}$)	6.75
Chute width	(m)	0.002
Chute depth	(m)	0.06
Air density	($kg\ m^{-3}$)	1.19
Volumetric air flow rate	($m^3\ h^{-1}$)	2.92

The chute length was such that it sat flush with the drier roof and particles travelled 80 mm before reaching the impact zone with droplets. This chute was lengthened a further 55 mm air to avoid fines dispersion, so that fines only travel 25 mm in the drying air before reaching the collision zone. Appendix O shows the complete drawings. This is the maximum length before droplets deposit on the delivery chute resulting in a build-up of concentrate and reduced running time. In addition, to further reduce dispersion by the drying air, wing deflectors were attached as shown in Figure 5.12. It was essential that the deflector wings did not extend past the fines curtain shroud to avoid coating from the spray.

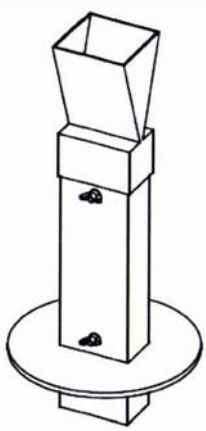

Figure 5.11: Powder delivery chute.

Figure 5.12: Powder delivery chute with deflector wings.

5.2.3 Selection of Fines Particle Size

The particle to droplet size ratio was one of the investigation variables identified earlier in Chapter 2. The range of fines to droplet size ratios are approximated to be 0.78 to 1.1 from the industrial benchmarking trials (§3.7). For the small scale experiments the fines particle size needed to imitate these ratios and the sizes selected for study were 15, 30 and 55 µm (Table 5.6). Table 5.15 later in this chapter shows the highest and lowest experimental fines to droplet size ratios were 0.57 and 3.33, which effectively covers the range of ratios experienced industrially by droplets exposed to fines particles from the extreme sizes in the particle size distribution. These selected sizes are significantly smaller than found in an industrial drier because the small scale drier uses a two-fluid atomiser which produces smaller droplets. Therefore the same ISMP A powder was milled and sieved giving the results shown in Figure 5.13. However, this was a time consuming process with the smallest fraction produced a $D_{3,2}$ of 30 µm.

Table 5.6: Industrial (Niro Compact) and experimental fines to droplets size ratios.

Particle size	Niro Compact fines	Niro Compact drops	Niro Compact Ratio	Exp drops $D_{3,2}$	Experimental Droplet Size for Ratio		
	(µm)	(µm)	(-)	(µm)	0.5	1.0	3.5
D (0.1)	30		0.4				
D (0.5)	75		1.1	15	8	15	53
D (0.9)	230		3.3	25	13	25	88
D (3,2)	55	70	0.8	35	18	35	123

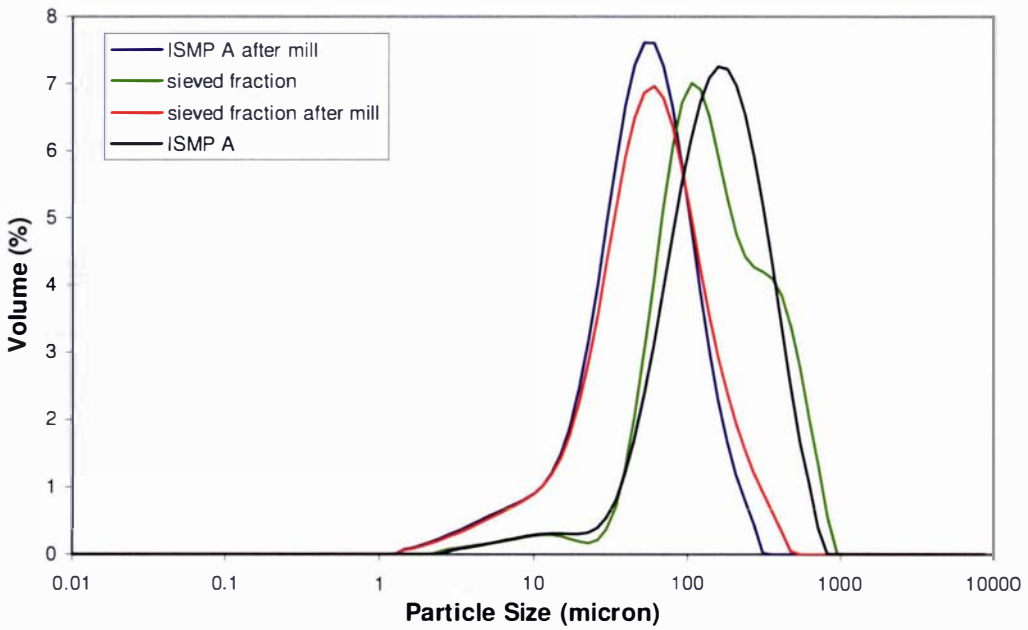

Figure 5.13: The effect of milling on ISMP A and a sieved fraction of ISMP A.

Powder was collected from the exhaust cyclone separately to the drier product using the Fonterra Palmerston North IFB pilot plant drier to produce very fine, spherical powder particles. Table 5.7 shows the operating conditions used to make this powder.

Table 5.7: Operating conditions used to produce small particle size powder.

Run	Collection	Conc P	Fluid Bed Air	Total Solids	$D_{3,2}$
		(bar)	($m^3 h^{-1}$)	(%)	(micron)
1	Drier	220	1500	47	51
	Cyclone				24
2	Drier	250	500	42	43

Nozzle type 63/20, concentrate flow rate = 90 – 100 L h^{-1}, 195°C drier inlet air temperature.

5.2.4 Calculation of Powder Curtain Velocity

In Chapter 2, it was established that the velocity of a particle will affect the probability of collision with a droplet in the collision zone. Also, the velocity of a particle at the point of impact is one of the variables that will influence the result of the collision, i.e., whether coalescence or rebound occurs. For this reason it is important to estimate the velocity of the particles in the powder curtain at the point of impact with the spray.

In this design the particles in the powder curtain fall freely into an air stream at the top of the drier. The air stream is drawn into the drier by the induction fan. The particles then travel approximately 375 mm before reaching the spray sheet of droplets. Hruby et al. (1988) and Ogata et al. (2001) observed that the velocity of particles in a powder curtain was larger than the free falling velocity of a single particle. Therefore the behaviour of the entire powder curtain should be considered rather than assuming the fine particles will behave like a single particle. Wardjiman et al. (2005) and Wardjiman and Rhodes (2006) determined the behaviour of a particle curtain falling into a horizontal gas stream. In these experiments, particles enter a vertical gas flow and air is also entrained into the curtain. From a force balance the acceleration of a single particle can be described by equation (5.7):

$$\frac{dv_s}{dt} = -\frac{3}{4} C_D \frac{\rho_a}{\rho_p D_p} v_s^2 + \left(1 - \frac{\rho_a}{\rho_p}\right) g \tag{5.7}$$

where t = time [s], v_s = velocity of a single particle [m s^{-1}], C_D = drag coefficient of particle [-], ρ_a = density of air [kg m^{-3}], ρ_p = particle density [kg m^{-3}].

Ogata et al. (2001) modified the above equation of motion for individual particles to those in a powder jet:

$$\frac{dv_s}{dt} = -\frac{3}{4} C_D' \frac{\rho_a}{\rho_p D_p} (v_z - u_z)^2 + \left(1 - \frac{\rho_a}{\rho_p}\right) g \tag{5.8}$$

where v_z = velocity of the particle in the powder jet [m s^{-1}], u_z = velocity of entraining air [m s^{-1}], C_D' = modified drag coefficient.

In this system $u_z > v_z$ in the acceleration phase. However, the particles used in this study are 20 – 50 µm and therefore are expected to quickly reach the air stream velocity then to assume a terminal velocity with respect to the air stream. By assuming this, no

acceleration occurs and equations (5.7) and (5.8) can be equated to find the velocity at the centre of the curtain:

$$v_{z\max\infty} = u_{z\max\infty} + v_{s\infty}\sqrt{\frac{C_D}{C_D'}} \tag{5.9}$$

where $v_{zmax\infty}$ and $u_{zmax\infty}$ = centre velocities of the particle and air in the equilibrium state and $v_{s\infty}$ = terminal value of a single particle.

Ogata et al. (2001) uses the correlation by Di Felice (1994) to find C_D':

$$C_D' = C_D\varepsilon^{-\beta} \tag{5.10}$$

Where the term $\varepsilon^{-\beta}$ is equivalent to the hindered settling correlation used in a gravity thickener. The power term is described empirically by:

$$\beta = 3.7 - 0.65\exp\left[-\frac{(1.5 - \log \mathrm{Re}_p)^2}{2}\right] \tag{5.11}$$

where ε = voidage of air curtain [–], Re_p = particle Reynolds number = $\rho_a v_{s\infty} D_p/\mu_a$ [–]. The voidage in the curtain was found from calculating the volume of solids present per unit volume of space as shown in Equation (5.12).

$$\varepsilon = 1 - \left[\frac{M_p}{\rho_f v_{s\infty} xy}\right] \tag{5.12}$$

where M_p = mass flow rate of particles [kg s^{-1}], x = curtain width [m] and y = curtain length [m].

For a free falling system Ogata et al. (2001) found that the entrained air flow rate increases with increasing mass flow rate of particles. In this system, the powder is not falling into stagnant air but falls into an air stream entering the drying chamber which is under a slightly negative pressure due to the induction fan on the downstream side of the drier. The air velocity through the chute was measured to be 6.75 m/s across an opening area of 30 mm x 60 mm, using an anemometer without fines flow. Bernoulli's equation calculates the pressure drop across this opening between the chute air inlet (v = 0) and the gap (equation (5.13)), where static head and frictional losses have been assumed to be negligible.

$$\Delta P = \frac{\rho V^2}{2} \tag{5.13}$$

where ΔP = pressure drop [Pa], ρ = air density [kg m^{-3}], and V = velocity of air [m s^{-1}]

This design restricts the air ingression to limit cooling of the drier by narrowing the slot width in the chute to 2 mm. Since the pressure drop will be the same across the opening irrespective of the size, the air velocity through this gap was calculated to be the same (6.75 m s^{-1}). Reducing the area of the opening to 2 mm x 60 mm reduced the cool air flow rate from 55 kg h^{-1} to 3.5 kg h^{-1}. This 2 mm gap expands to 10 mm, 20 mm or 30 mm depending on the experimental set up as shown in Figure 5.14. There are two plates inserted into the dispersion chute to reduce the gap (in this case to 20 mm) and these plates are held in place with a washer of a specific width and a wing nut.

Following Perry and Green (1997) 6-16 and using Equation (5.14) for frictional losses across expansion the velocity of the curtain air at the top of the chute after the 2 mm gap was calculated and this was found for each chute width. The centre velocity of the particles in the powder curtain was then calculated using equation (5.9). Figure 5.15 shows the effect of chute width on the air stream and particle velocity as it was found that the mass flow rate of particles and the size of those particles have a negligible effect on the curtain velocity. It must be noted that these calculations do not consider frictional effects due to the presence of the particles that may reduce the air velocity from 6.75 m/s at the 2mm slot.

$$l_v = \frac{V_1^2 - V_2^2}{2} = \frac{V_1^2}{2}\left(1 - \frac{A_1}{A_2}\right)^2 \qquad (5.14)$$

where l_v = friction loss [$m^2 s^{-2}$], V_1 = inlet air velocity [m s^{-1}], V_2 = velocity air chute [m s^{-1}], A_1 = area of entrance [m^2] and A_2 = cross-sectional area of chute [m^2].

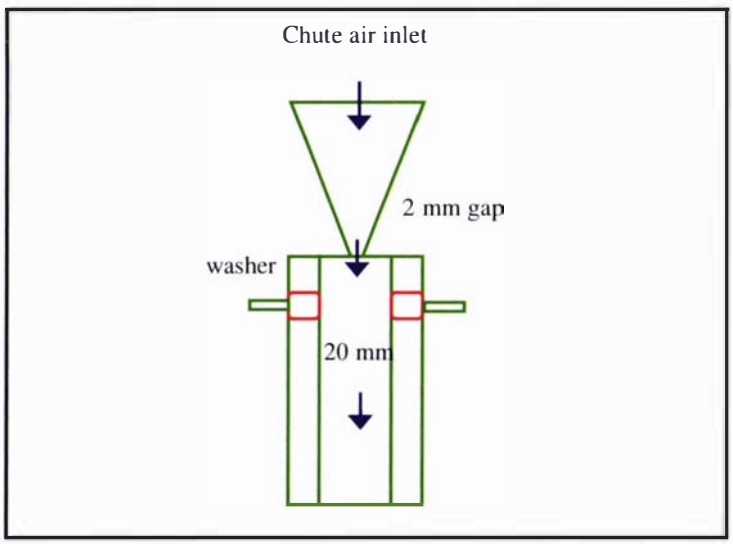

Figure 5.14: Diagram of curtain distributor.

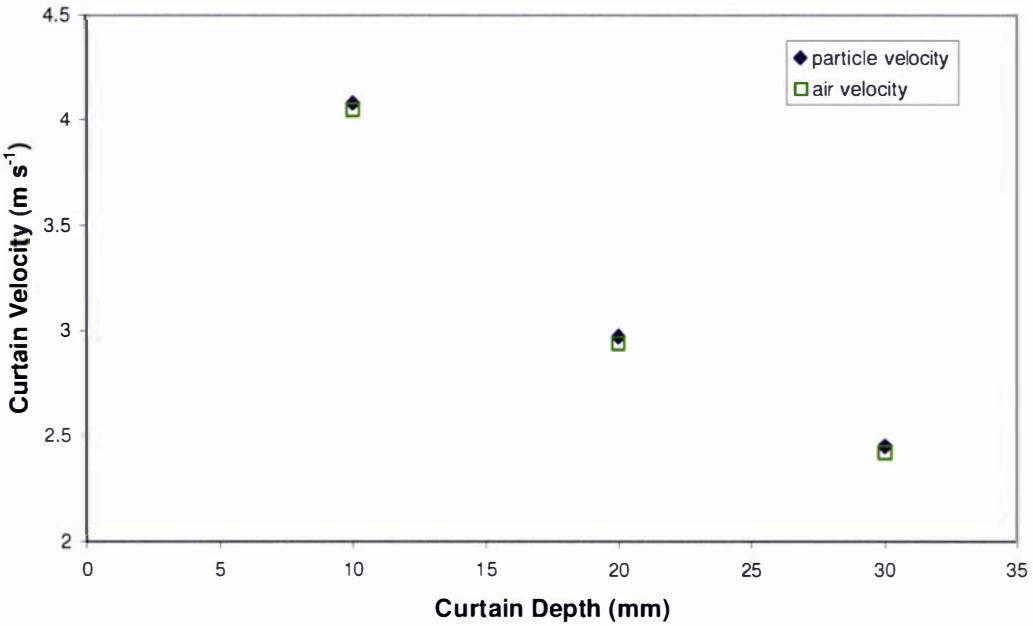

Figure 5.15: Effect of chute depth on calculated curtain velocity.

5.3 Generating a Sheet of Spray Droplets

A key challenge of this design was generating a suitable sheet of spray droplets for impact with the powder curtain inside the drier. It was necessary to consider all aspects of droplet generation including the selection of an appropriate atomiser, the attachment of this nozzle to the drier, the appropriate concentrate manufacturing technique and also commissioning of this nozzle to ensure it performed as required.

5.3.1 Selection of the Spray Nozzle

Industrially, high pressure hollow cone nozzles are used to atomise milk concentrate in spray drying (Figure 5.16). However, these nozzles are not suitable for concentrate delivered at low flow rates. In this work, a two-fluid nozzle was required for the following reasons: the flow rate was low, small droplets were required so that they dried in the residence time available, lower velocities were required and the energy of the air was required to effectively atomise the high solids concentration milk concentrate into a spray of droplets. A self cleaning, two-fluid spray nozzle (Spray Systems 2850 fluid cap, 67228 - 45 air cap) was selected to spray milk concentrate of 41 to 47 wt% solids content. The fluid cap, air cap, and the self-cleaning needle components are shown in Figure 5.17; the air cap has two extra air ports to produce a flat spray.

Figure 5.16: High pressure hollow cone nozzle.

a) fluid cap

b) air cap for flat spray

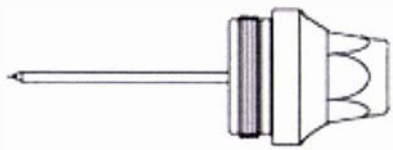

c) clean out needle assembly

Figure 5.17: Two fluid nozzle components.

The mechanism that occurs during two-fluid atomisation is one of a high velocity gas creating high frictional forces over liquid surfaces causing disintegration into droplets (Masters, 2002). Liquid disintegration involves liquid instability in two phases. The first phase involves the tearing of the liquid into filaments and large droplets; the second phase completes the atomisation into breaking these liquid forms into smaller droplets. The process is influenced by the liquid properties (surface tension, density and viscosity) and the gaseous flow properties of velocity and density. Droplet size is dependent on the type of atomisation and is difficult to both predict and measure industrially. The nozzle used in this work has been characterised with regard to droplet size and velocity at different flow rates, total solids and atomisation pressures in §4.6.

Spray drying milk concentrate of 47 wt% total solids using a two-fluid nozzle is not without complications and fouling of the nozzle exit means that a standard two-fluid nozzle with only the air and fluid cap blocked frequently (after approximately 5 minutes of running). T.A.G. Langrish (personal communication, 2004) suggested that when using two fluid nozzles for above 30 wt% solids a self-cleaning or ultrasonic atomisation system should be applied. A self-cleaning nozzle was purchased to fit the current fluid and air cap that had previously been characterised. This nozzle has a central needle which sits in the centre of the fluid line and can be retracted on applying a pressure (30 p.s.i.). By pulsing the air delivery the needle can move back and forth so that any exit fouling can be cleared from the nozzle. The solenoid was set so that a 1 s pulse of air was delivered every 3 s to reduce nozzle fouling. Blockages still occurred after approximately 20 minutes of atomisation; however this running time was assessed to be sufficient to produce enough powder for the tests required. The two-fluid self cleaning nozzle is pictured in Figure 5.18 and the set up for spraying with this nozzle is shown in Figure 5.19.

Figure 5.18: Two-fluid self-cleaning nozzle.

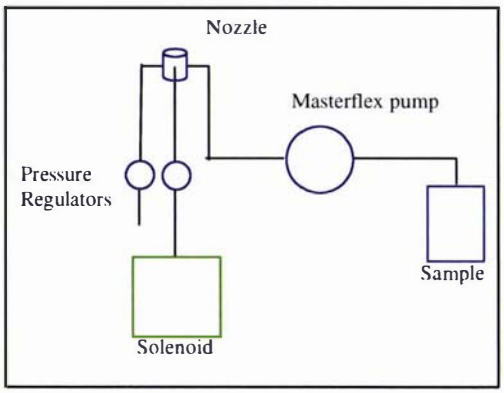

Figure 5.19: Schematic of nozzle setup.

Ultrasonic Nozzle

An ultrasonic nozzle (Sonotek RR5196 60 kHz) was used as part of the final experiments to understand the influence of spray properties on agglomeration processes. Ultrasonic nozzles have many benefits, including a low velocity spray, a wide range of fluid flow rates, the drops have a narrow size distribution and the system is non-clogging and very difficult to block. The ultrasonic nozzle was fitted with cooling ports and compressed air was delivered to the nozzle at 40 – 60 kPa to ensure the piezoelectric chip didn't exceed 125°C during operation. Figure 5.20 demonstrates the components inside an ultrasonic nozzle. The broadband ultrasonic generator supplied power to this nozzle; the power output was controllable using a dial. The piezoelectric transducers receive electrical energy and convert that into a vibratory motion at the same frequency. Two titanium cylinders magnify the motion and the liquid introduced onto the atomizing surface absorbs some of the vibrational energy.

The nozzle has optimum atomization performance at a limited power range. For each nozzle, fluid type, and fluid flow rate there is a 'stall point' where the nozzle will no longer atomise and a jet of liquid results. If the power is too high the liquid can be literally ripped apart resulting in very large droplets so that the nozzle only operates effectively over a narrow power input range. The manual suggests operating at one Watt above the stall point; this is determined by changing nozzle operating parameters and visually establishing when atomisation was incomplete. For water at 0.8 kg h^{-1} this stall point was 3 W and for 41 wt% milk concentrate at 1.2 kg h^{-1} this was ~ 6.5 W.

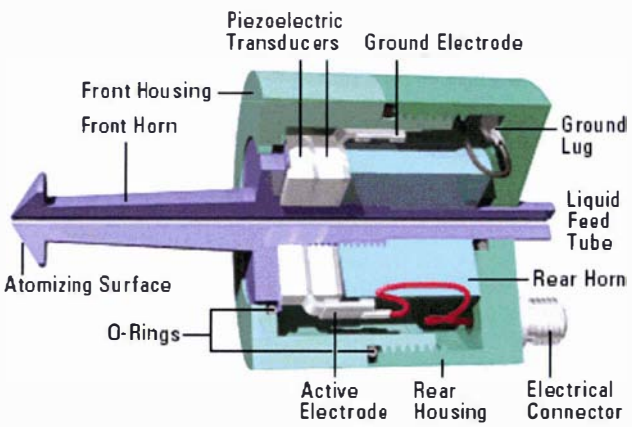

Figure 5.20: Cross-sectional view of a Sono-tek ultrasonic nozzle (www.sono-tek.com).

5.3.2 Attachment of the Nozzle

The two-fluid nozzle was attached to the side of the spray drier by constructing a stainless steel face plate to replace one of the sight glass windows (Figure 5.21). Drawings of this face plate have been included in Appendix P. Two air lines and a fluid delivery line were used to support the weight of the nozzle which was securely held in place by screws. In this design the distance from the spray relative to the curtain was adjustable. The trajectories of the droplets should overlap with the trajectories of the particles in the powder curtain. To achieve this overlap the nozzle was positioned as shown in Figure 5.22. The nozzle specification states a 45° spray angle, which is for water. It was observed that a milk concentrate spray has a larger spray angle, 62°, which means a spray width of 60 mm at a distance of 50 mm from the nozzle exit. This design assumes that the spray experiences a constant shape throughout the experiment.

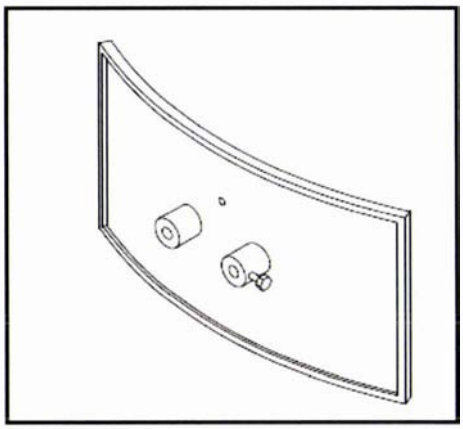

Figure 5.21: Niro face plate.

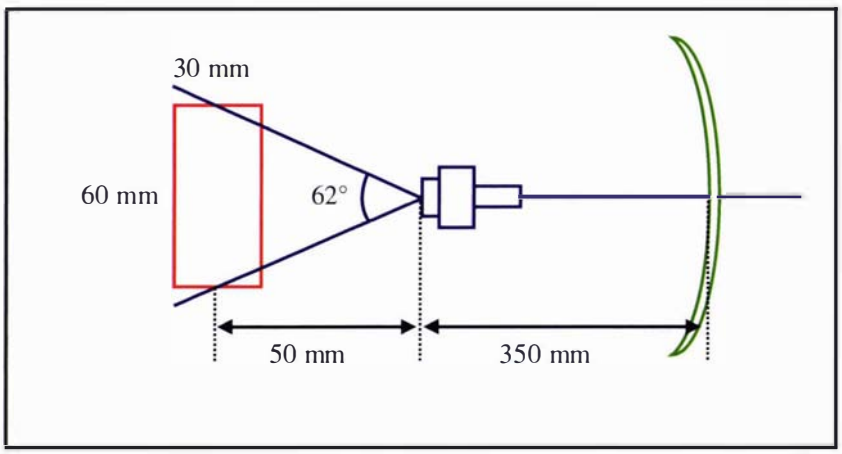

Figure 5.22: Plan view of nozzle position and spray trajectory relative to the curtain.

5.3.3 Commissioning the Self-cleaning Two-fluid Nozzle

Following nozzle selection and attachment to the drier wall, it was essential to test the nozzle's performance inside the drier. Figure 5.23 shows that the mean particle size, $D_{3,2}$, obtained from the powder collected when the drier was operated in spray mode only (without fines) decreases with increasing atomisation pressure. The extra data point at 1.5 bar does not follow the same trend and can be considered as an outlier. The collected powder size distribution was measured using a Malvern Mastersizer 2000 and the method for this is discussed in Chapter 6. It was shown previously (§4.6.2) that the dried droplet particle size relates to the measured droplet size. Mean droplet sizes were measured using a Malvern Mastersizer S (§4.6.2) showing a range of droplet sizes from 15 μm (at 2.5 bar) to 50 μm (at 0.5 bar).

Harvie et al. (2002) proposed that industrial droplet sizes are near to 50 μm, and industrial droplet sizes were estimated for the Niro Compact in §3.5 as ~ 65 μm. Therefore it is desirable to carry out small scale experiments using large droplet sizes to compare with industry. Figure 5.23 shows that dried droplets produced at 0.5 bar are larger than the product at 1.5 bar, which are not much larger than the dried droplets at 2.5 bar. It was found that below an atomising pressure of 1.5 bar the self-cleaning nozzle blocked more easily. This was also found by Ozmen and Langrish (2003b). The issue arises because the air orifices become blocked by wet droplets that land on the air cap (see Figure 5.17). These droplets dry forming thick layers and is referred to as "bearding". Non-bearding nozzle designs are available that change the air currents to avoid droplet deposition on the air cap. However, the possibility of using non-bearding nozzle was only realised after a significant amount of the work had already been completed. Since it is ideal to maximise running times by reducing nozzle fouling it was concluded that the range of sizes from 1.5 to 2.5 bar was sufficient to study the effect of droplet size on agglomeration performance.

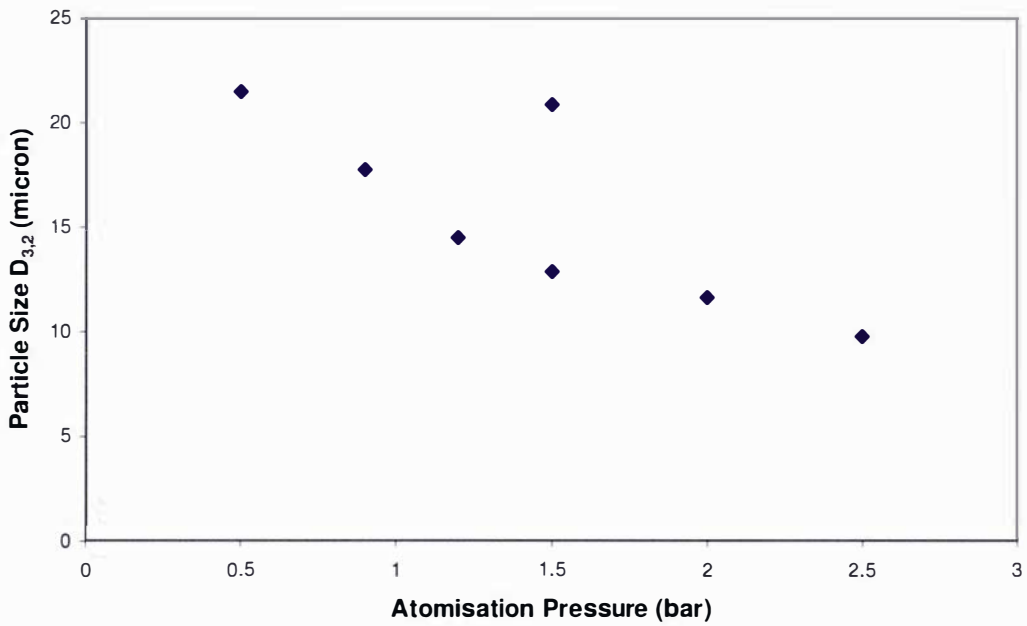

Figure 5.23: Dried droplet size vs. atomisation pressure at 41 wt % solids, 2 kg h^{-1}.

5.3.4 Method for Manufacture of Milk Concentrate

In Chapter 3, ISMP A and IWMP E were selected as the industrial milk powder specifications for study. Two options were available for the manufacture of milk concentrate for atomisation: reconstitution from instant milk powder, and concentrate produced from fresh milk by evaporation. The instant skim milk powder (ISMP A) was selected to eliminate any problems in concentrate manufacture due to the presence of fat (D.L. Pearce, personal communication, 2004). For each experiment only 2 kg of concentrate was required and so it was not practical to procure fresh farm supply milk for this small quantity and, additionally, the available research evaporator at Fonterra Palmerston North has a production rate of ~ 300 kg h^{-1} of milk flow. Instead, reconstitution of milk powder was selected as the most appropriate way to produce skim milk concentrate at specific solids concentrations. Nijdam & Langrish (2005) found that spray dried milk powders can be used to prepare milk concentrates for spray drying without affecting the glass transition temperature of the powder.

It is difficult to produce milk concentrate by reconstituting instant milk powder. The viscosity of milk concentrates in the range of 40 to 55 wt% total solids is non Newtonian and time-dependent according to Trinh et al. (2002). Trinh et al. (2002) designed a recombination system specifically for manufacturing reconstituted milk concentrates. It was identified that good control of air inclusion, temperature, shear rate and microbial contamination was essential to eliminating the onset of age thickening. This mechanism of age-thickening was earlier proposed to be due to the loosening of the casein micelles (Snoeren, Brinkhuis, Damman, & Klok, 1984). Although it is proposed that the presence of β-lactoglobulin affects the viscosity of a solution, possibly by stabilising casein micelles, it is unclear if this applies to the age-thickening phenomena observed in milk concentrates (Anema & Lugt, 1998). Bienvenue et al. (2003) investigated reasons behind the observed viscosity increase during storage and suggested that the phenomenon of age thickening exhibited by concentrated milks is actually due to the increase in calcium ion activity during the evaporation of milk (Nieuwenhuijse, Timmermans, & Walstra, 1988). The binding of calcium ions to the casein micelle surface leads to flocculation of micelles to form aggregates and result in an increased apparent viscosity.

Betteridge (1998) showed reconstituted skim milk gave similar viscosities to fresh skim if the sample is de-aerated. During reconstitution, it is essential to successfully mix the milk powder into water and this requires four steps:

- Wetting
- Sinking
- Dispersing
- Dissolving

Mixing powder into water becomes more difficult as the solids concentration (and viscosity) increases. Fitzpatrick and Cuthbert (2004) found that creating and maintaining a vortex in the solution improved the sinkability of the powder. However, there was a limit where the powder stopped sinking and the material behaved more like a solid than a liquid, preventing the formation of a vortex. Higher temperatures mean that high solids contents can be achieved before powder sinking stops and the effect of age thickening is also reduced. Trinh et al. (2002) aimed to reduce the amount of air inclusion in the sample by breaking the vortex.

Table 5.8 compares several procedures for reconstituting instant milk powder; the methods vary significantly because they are usually based on the specific needs of the manufacturer and relate to the end use of the concentrate. The method used in this work was selected by performing a number of measurements and optimising the production with respect to mixing speeds and times and reducing age thickening. In this study it was important to produce concentrate quickly at the appropriate temperature. The following procedure was used:

- Weigh out powder allowing 2% extra for losses on the sieve
- Add 55°C water into a 2 L stainless steel vessel
- Place this vessel into a water bath set at 50°C
- Insert the impeller (12 blade 80 mm diameter) into the water in the vessel and turn on the mixer (Heidolph 50111, type RZR1 Serial number 08234)
- At a mixing speed of 250 rpm add powder a spoonful at a time for 10 minutes using a spatula to break up any lumps
- At a mixing speed of 380 rpm continue to add powder for 5 minutes
- Increase mixing speed to 475 rpm for the final 5 minutes of powder addition
- Leave this concentrate to hydrate for 10 minutes on speed setting 0.
- Pour the concentrate through a 210 micron sieve into a 1 L stainless steel vessel
- cover with aluminium foil and return to water bath for storage (up to 2 hours)

Following manufacture the concentrate was immediately tested to determine the viscosity (using a Paar Physica MC1 viscometer). As the content of gas in the feed can directly relate to the particle density and therefore bulk density of the powder the dissolved oxygen was measured (using an Oxi 340i, CellOx® 325 sensor) for all reconstituted milk concentrates and ranged from 5.4 to 8.5 mg L^{-1}. This variation is oxygen level was quite consistent and for these small differences it is anticipated that there will be little effect on powder properties.

Table 5.8: Comparison of reconstitution procedures.

Procedure	Units	Betteridge (1998)	Trinh et al. (2002)	Field-Mitchell (1981)	This work
Water Temp	°C	55	35	50	50
Antifoam		Yes	No	No	No
Mixing time	min	10 s pulses	120	30	20
Hydration	min	No	30	30	10
Sieving	µm	No	No	210	210
Extra		De-aeration	No Vortex	180 rpm	250-475 rpm

The effect of mixing at the lowest speed (250 rpm) or no mixing on the viscosity of milk concentrate over time is shown in Figure 5.24. Mixing causes a significant increase in viscosity over 2 hours, whereas without mixing a small increase was observed. This effect is likely to be due to the incorporation of air and as a consequence all further studies did not have mixing during storage between the time of manufacture and running the experiment. Figure 5.24 uses ISMP B, which has a similar specification to ISMP A, due to availability. When the selected ISMP A was used, the initial viscosity and age thickening effect were reduced as shown in Figure 5.25. Antifoaming agents (30 wt% solution of Dow Corning Antifoam RD Emulsion) lower the surface tension and viscosity but were omitted from the reconstitution procedure. Figure 5.25 shows that the antifoam agent had no effect on viscosity or aging over time.

Reconstituted milk concentrate was used 1 to 1.5 hours following production. Over this time, Figure 5.25 shows some age thickening. However, it has been found by Snoeren et al. (2002) that structural viscosity can be completely broken down in an atomising wheel. In this work, the concentrate was sheared in a two-fluid atomiser. Bylund (1995) suggest shear rates of 10^3 s^{-1} in spraying. The shear is likely to be enough to breakdown such a small increase in structural viscosity. Bienvenue et al. (2003) also showed concentrated skim milks demonstrated shear thinning behaviour (where the viscosity decreases as shear rate increases), and that shear rates could collapse the structural viscosity for concentrates that had been stored for up to 8 hours for skim milk concentrate at 45 wt% solids concentration. However, above 8 hours the effects of age thickening were not reversible and it was proposed this was due to fusion of the casein micelles within that have aggregated following concentration (as previously explained) and results in an irreversible increase in the micelle size and therefore viscosity. Bienvenue et al. (2003) also showed that decreasing the level of soluble minerals in the milk reduced the apparent viscosity.

Shown on Figure 5.25 are two points for fresh ISMP A concentrate which have lower initial viscosities than the reconstituted concentrates. One is an experimentally measured point for trial B6a in §4.4; the other is the 'expected' value based on the composition according to the methodology of Snoeren et al. (1982) which is also discussed in §4.4. These are both significantly lower than the reconstituted concentrate initial viscosities. Later trials mainly used 41 wt% total solids rather than 47 wt% total solids concentrate. Table 5.9 shows the differences in viscosity between fresh and reconstituted concentrates are much reduced at 41 wt% solids concentration.

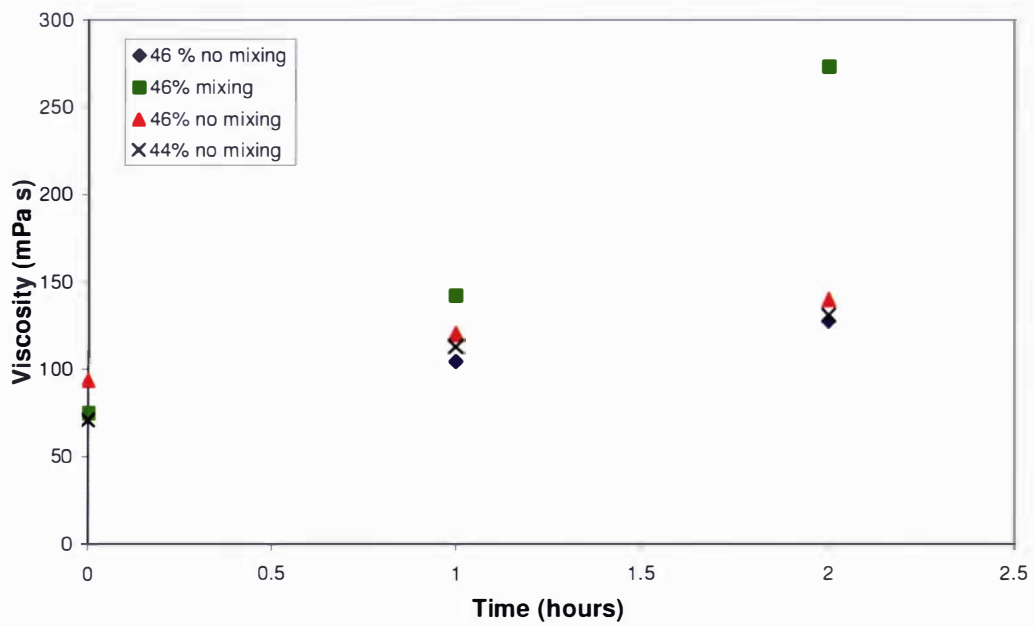

Figure 5.24: Viscosity vs. time for reconstituted ISMP B at 1000 s^{-1}.

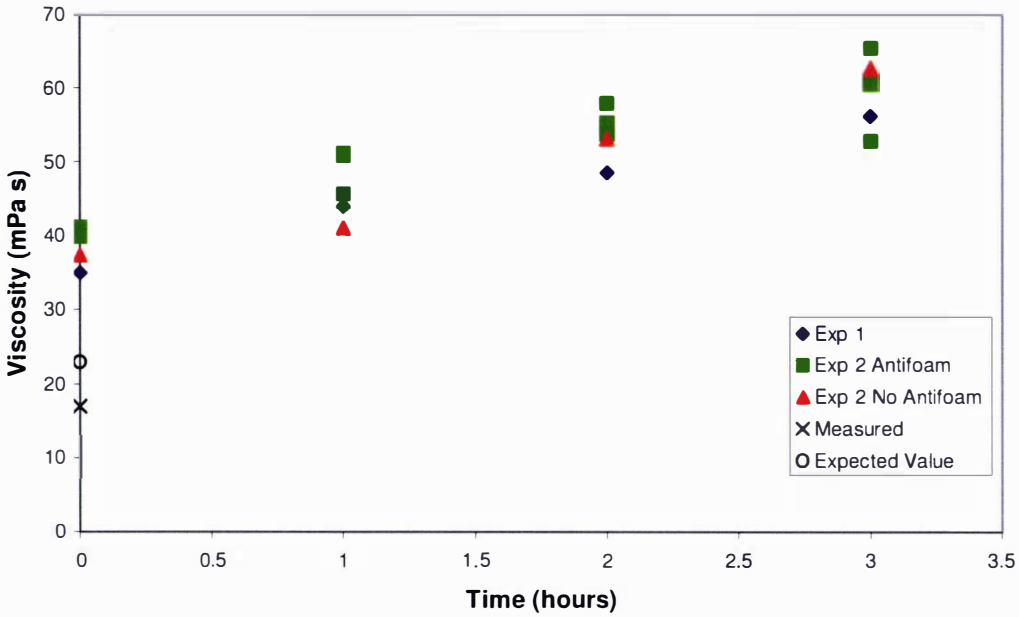

Figure 5.25: Viscosity vs. time for reconstituted 47 wt% ISMP A at 50°C at 1000 s^{-1}.

Table 5.9: Comparing viscosities for ISMP A SMC at 50°C.

Sample type	**Viscosity (mPa s)**	
Total Solids	**41%**	**47%**
Expected	11	23
Measured fresh	9	17
Reconstituted	15	35
	15	37
	14	32
	14	33

5.4 Experimental Design

This section discusses the design of experiments required to perform the agglomeration study using the small scale drier. This includes the experimental procedure used for the study of natural agglomeration (agglomeration without a powder curtain) and forced agglomeration (agglomeration with a powder curtain). Chen (Chen, 1992) states that the degree of agglomeration due to concentrate droplet collision should be established before optimising any agglomeration process where fines are returned. This process of agglomeration due to droplet-droplet collisions is referred to as natural agglomeration as explained in Chapter 2. The forced agglomeration experimental design is divided into two main sections, the preliminary experiments and those aimed at improving the design to increase the extent of agglomeration. Finally a comparison is made between the industrial conditions and those experienced in the small scale agglomeration experiments.

5.4.1 Natural Agglomeration

In this study on agglomeration, natural agglomeration without a fines curtain was used as the base case for later studies when a curtain was introduced. A full factorial design matrix is shown in Table 5.10 for the three adjustable variables of flow rate, total solids and atomisation pressure. Each variable was studied at two levels with one mid point investigated. The levels selected were limited by aspects of the agglomerator design. The concentrate properties were limited by the drier evaporative capacity and maximum acceptable powder moisture content outlined in §5.1. The atomisation pressure ranges were selected by determining the working range of the specific nozzle in §5.3.3. Variables held constant include flow rate of air into the drier, temperature of inlet air (195°C), and the temperature of concentrate (50°C).

Table 5.10: Design matrix for natural agglomeration using reconstituted ISMP A.

Variable	Concentrate Flow rate	Total Solids	Atomisation Pressure
	($kg\ h^{-1}$)	(%)	(bar)
S1	2	41	2.5
S2	2	41	1.5
S3	1.4	41	2.5
S4	1.4	41	1.5
S5	2	47	2.5
S6	2	47	1.5
S7	1.4	47	2.5
S8	1.4	47	1.5
S9	1.7	44	2

5.4.2 Preliminary Forced Agglomeration Experiments

Forced agglomeration occurs when a spray sheet interacts with a fines curtain. A series of preliminary experiments was carried out to ensure the system performed as required. During these experiments, minor operating and design changes were made to improve fines delivery and the droplet-particle interaction, the results of which are discussed in Chapter 7. The preliminary experimental conditions have been included in Table 5.11 in the order of changes made.

Table 5.11: Design matrix for preliminary experiments.

Exp	S	F	$D_{f,4,3}$	TS	P	D	FS	N	SC	W
	(kg h^{-1})	(kg h^{-1})	(μm)	(wt%)	(bar)	(mm)		(mm)		
P1	2.0	1.0	30	42.3	1.5	30	N	65	N	N
P2	2.1	1.1	30	40.9	1.5	30	N	50	N	N
P3	2.1	2.1	58.8	47.5	2.5	10	N	50	N	N
P4	1.4	1.0	30	41.2	2.5	30	N	50	N	N
P5	2.1	2.0	30	41.3	1.5	30	N	50	N	N
P6	1.4	1.1	30	41.6	2.5	30	Y	50	N	N

S = concentrate spray flow rate, F = fines flow rate, $D_{f,4,3}$ = volume weighted mean particle size of fines, TS = total solids of concentrate, P = atomisation pressure, D = curtain depth, FS = fines shroud, N = nozzle distance from centre of curtain, W = deflector wings, SC = sieve collector.

5.4.3 Improving the Design

The preliminary experiments identified that the small scale equipment designed did not appear to agglomerate to the extent required (see Chapter 7). A further set of experiments is shown in Table 5.12 to test added design features of a shroud, deflector wings and the inclusion of a sieve collector in the base of the drier. The design features are discussed in §5.2.2 and the sieve collector, which is an alternate powder collection method, is discussed along with the results of this study in §7.3. D1 and D2 are experiments that look at the shape of the fines curtain without any spray, and experiment D3 looks at agglomeration of fines by atomising water droplets.

Table 5.12: Design matrix for improving the design.

Exp	S	F	$D_{f,4,3}$	TS	P	D	FS	N	SC	W
	(kg h^{-1})	(kg h^{-1})	(μm)	(wt%)	(bar)	(mm)		(mm)		
D1	1.2	25	30	-		30	Y	50	N	N
D2a	1.2	25	30	-	1.5	30	Y	50	N	Y
D2b	1.2	25	30	-	2.5	30	Y	51	N	Y
D3	1.4	1.2	30	0.0	1.5	30	Y	50	N	N
D4	1.4	1.1	30	41.7	2.5	30	Y	50	Y	N
D5	1.4	1.1	30	41.6	2.5	30	Y	50	Y	Y
D6	2.1	1.1	20	47.3	1.5	10	Y	50	N	Y
D7	1.4	1.1	30	41.5	2.5	30	Y	50	N	N
D8	1.5	1.2	30	41.6	2.5	30	Y	50	N	Y

5.4.4 Forced Agglomeration Experiments

The nine operating and design variables are shown in Table 5.13. Three are kept constant which leaves six variables to be studied, meaning 64 separate experiments in a two level factorial design. An alternative was a ¼ fractional factorial requiring only 18 experiments; it can still study the main effects, as 2-way interactions with common centre points. Some of the experiments required for this matrix are included in the preliminary and design trials shown in Tables 5.11 and 5.12. The results of this study are discussed in §7.3. After analysing these results, coupled with the findings from Chapter 8 (pilot scale experiments) a few carefully selected further experiments were carried out to confirm the relationships predicted from the pilot scale experiments. The operating conditions used to carry out these experiments have been included in Table 5.14.

Table 5.13: Proposed experimental design for the two fluid nozzle.

Variable	Units	Base	High	Low
Concentrate Flow rate	(kg h^{-1})	1.7	2	1.4
Distance of Spray	(mm)	50	50	50
Powder Flow rate	(kg h^{-1})	1.5	2	1
Solids Concentration	(%)	44	47	41
Concentrate Temperature	(°C)	50	50	50
Curtain density	(mm)	20	30	10
Droplet Size	(bar)	2	1.5	2.5
Inlet Air Temperature	(°C)	195	195	195
Particle Size	(micron)	43	51	20

Table 5.14: Design matrix for final agglomeration experiments.

Exp	S	F	$D_{f,4,3}$	TS	P	D	FS	N	SC	W
	(kg h^{-1})	(kg h^{-1})	(µm)	(wt%)	(bar)	(mm)		(mm)		
A1	2.1	0.8	30	42	2.5	30	Y	50	N	N
A2	2.0	0.8	58.8	41	2.5	30	Y	50	N	N
U1	1.4	1.0	30	41.4	-	30	Y	50	N	N

S = concentrate spray flow rate, F = fines flow rate, $D_{f,4,3}$ = volume weighted mean particle size of fines, TS = total solids of concentrate, P = atomisation pressure, D = curtain depth, FS = fines shroud, N = nozzle distance from centre of curtain, W = deflector wings, SC = sieve collector.

5.5 Comparing Experimental Conditions at Small and Industrial Scales

The equipment and experimental programme designed and discussed in this chapter aimed to ensure an agglomeration study on a small scale would imitate the industrial situation. The data in Table 5.15 summarises the information gathered for the industrial Niro Compact spray drier when manufacturing the instant skim milk powder selected in §3.1, ISMP A. This data is compared with the experimental conditions for the lowest, base (or midpoint) case, and the highest ratios with regards to the key variables thought to affect agglomeration as outlined in Table 5.1. The key ratios are the fines to spray size ratio, the fines to spray flux ratio and the fines to spray number ratio, N_d:N_f. The ratios for the planned small scale experiments fit within the ranges observed industrially.

Table 5.15: Comparing industry with experimental conditions.

Variable	units	ISMP A	Exp base	Exp high	Exp low
Fines size $D_{3,2}$	(μm)	55	43	50	20
Droplet size $D_{3,2}$	(μm)	50 - 70	20	15	25
Concentrate flow	(kg h^{-1})	7670	1.70	1.4	2
Total solids	(%)	43-47	44	47	41
Spray velocity	(m s^{-1})	18.0	7.2	7.2	7.2
Air flow rate	(m^3 h^{-1})	125000	81	81	81
Curtain depth	(m)	0.1	0.02	0.03	0.01
Drying air velocity	(m s^{-1})	40	10	10	10
Fines flow rate	(kg h^{-1})	3325-4550	1.5	2	1
Fines air flow rate	(m^3 h^{-1})	592	2.94	2.94	2.94
Drying air temperature	(°C)	195	195	195	195
Fines:Spray size ratio	-	0.8 -1.1	2.15	3.33	0.80
Fines:Spray flux ratio	-	0.43-0.59	0.88	1.43	0.50
Fines air velocity	-	20.94	2.94	2.42	4.08
Fines particle velocity	(m s^{-1})	20.94	2.97	2.45	4.08
$\dot{N}_d$	(# s^{-1})	1.01E+10	9.55E+07	1.85E+08	5.85E+07
$\dot{N}_f$	(# s^{-1})	9.66E+09	7.70E+06	6.53E+06	5.10E+07
$\dot{N}_d : \dot{N}_f$	-	0.96	0.08	0.04	0.87

5.6 Chapter Conclusions

This chapter outlined the processes taken to design a mini agglomerator for a small scale study of agglomeration. Industrial spray driers are not able to manipulate the relevant variables to fully investigate the agglomeration process. The equipment and experimental programme designed and discussed in this chapter aimed to ensure that an agglomeration study at small scale would imitate the industrial situation. This required modification of an existing small pilot scale spray drier to include a vertical a particle curtain and flat spray sheet.

This chapter investigated four key areas, the selection of a suitable small scale drier, the delivery of a particle curtain, generation of a spray sheet and the experimental design. The delivery of the particle curtain required an understanding of the limitations in powder feeding, production of fines particles for use in the study and calculation of the particle curtain velocity. Atomiser selection and concentrate manufacture procedure were two key aspects considered when generating a sheet of spray droplets. The final equipment design fulfilled the necessary requirements to study agglomeration at small scale. An experimental program was designed to study the effect of spray and curtain variables on agglomerate properties. It is concluded that the small scale drier, modified as explained in this chapter, is a robust design that will allow controllable and repeatable experiments to be performed.

CHAPTER 6

DETERMINING AN AGGLOMERATION INDEX

During forced agglomeration, fine particles contact spray droplets and coalesce to form agglomerates that have a larger particle size distribution (PSD) than those of the two feed streams. The input size distributions change depending on the experimental conditions selected, so simply comparing product distributions of agglomerates between experiments is not the best way to assess how these conditions affect the level of agglomeration that has occurred. It is possible for two product particles to be the same size but made up of different primary particles; for example, one product powder may be comprised of large, single, spherical particles and the other product powder may contain agglomerate made up of many small particles. Information about the primary particles used to form the agglomerates must also be included to assess whether agglomeration has occurred.

To estimate the success of agglomeration, a quantifiable index is needed to link the two feed distributions (the fines and the droplets) with the product (agglomerates) distribution. This index can then be related to process conditions and particle and droplet properties, and can help in understanding the mechanisms of collision, adhesion and drying that occur to promote agglomeration. To be useful to operators of spray driers, the index must be easily obtained by standard techniques. Other performance indicators include the particle size, structure and shape, the moisture content, the bulk density, the agglomerate strength and the dispersion behaviour of the agglomerate. Process parameters that affect agglomeration are fines and concentrate flow rates, environmental factors of air flow rate, temperature and humidity. All need to be measured to monitor their affects on the agglomeration index or the other performance parameters.

Agglomeration occurs rapidly in the collision zone between spray droplets and recycled fine powder. It is not possible to selectively sample agglomerates within this collision zone because the agglomerates are sticky; however it is possible to measure the fine particle and spray droplet size distributions prior to agglomeration and the particle size distribution (PSD) of product exiting the spray drier.

The ideal milk powder agglomerate has a grape-like structure, because this gives good dispersion behaviour (Pisecky, 1997). Figure 6.1 shows a range of agglomerate structures. The size of the grape is a key measurement, along with the number of particles that constitute each agglomerate and the strength of the agglomerate. A number of measurement methods are available to obtain this information: light scattering provides a PSD, while scanning electron micrographs (SEMs) provide images of the agglomerates morphology and nitrogen adsorption and mercury porosimetry can provide specific surface area (SSA). Sieving was not used here because the agglomerated particles produced in these experiments were too small to be successfully characterized this way. Laser diffraction is widely used but calibration is essential as agglomerates are not crystalline or spherical and measurements will vary with morphology. Strength can be measured comparatively by fluidization, which breaks

down agglomerates (P. Webby, personal communication, 2005). Hogekamp (1999b) also found measuring agglomerate properties to be problematic and used modified or developed methods (including CCD video capture and image analysis) to characterise agglomerates produced using steam jet agglomeration.

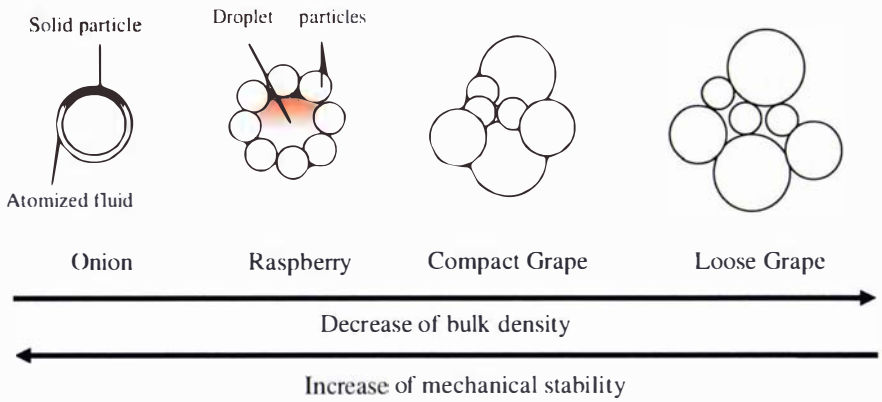

Figure 6.1: Agglomerate morphology.

Population balance modelling is used by many researchers to understand granulating and agglomerating systems as discussed in Chapter 2. While population balance model predictions can be compared to the data collected over time in a drum or high-shear granulating system, in spray drying systems, agglomeration occurs so fast that the only easily attainable information is at the start and the end of the process. Therefore, it is difficult to devolve the mechanisms of collision and coalescence that are needed to define the relationships used to construct the population balance models.

Using the fines and droplet particle size distributions, and the agglomerate PSDs, an agglomeration index can be defined in various ways. Several indices which currently exist in the literature are discussed below and two new indices are also proposed which are more suitable to describing agglomeration in spray drying. In this chapter the most suitable index to describe the extent of agglomeration is determined and developed to allow comparison between the processing scales.

6.1 Agglomeration Factor using Specific Surface Area

Several authors (Kammler, Beaucage, Mueller, & Pratsinis, 2004; Staiger, Bowen, Ketterer, & Bohonek, 2002) define an agglomeration index by relating the particle size to its specific surface area (SSA). The SSA is measured using nitrogen adsorption at 77 K, from which a BET diameter (Brunauer, Emmett, & Teller, 1938) is obtained assuming that the material is non-porous and is derived below by assuming a basis of 1 kg of particles:

$$\text{Mass} = N\rho\frac{\pi}{6}D_p^3 \tag{6.1}$$

where N = number of particles, ρ = density of particles and D_p = diameter of particles.

$$N = \frac{SSA}{\pi D_p^2} \tag{6.2}$$

where SSA = specific surface area = (surface area/kg particles). Substituting into a mass balance and rearranging gives:

$$D_{BET} = D_p = \frac{6}{\rho SSA} \tag{6.3}$$

Staiger et al. (2002) use D_{BET} to define an index they call the agglomeration factor, AF = $D_{0.5}/D_{BET}$, where $D_{0.5}$ is the median volume diameter of the starting powder. They claim that the AF can indicate the extent of agglomeration for a powder and discussed several methods available for PSD measurement. The problem with this index is that it only compares the fines to the agglomerates and ignores the droplet size distribution that is present in spray driers.

Alternatively, SSA can be measured by mercury porosimetry, although nitrogen adsorption is easier and more common (Allen, 1981). Nitrogen adsorption calculates an SSA for a monolayer of nitrogen molecules adsorbed at the surface, whereas mercury porosimetry calculates a pore surface area from a pore size distribution that is a function of pressure and the amount of ingressing mercury. Agreement between these two methods has been found under controlled conditions (Joyner, Barrett, & Skold, 1951; Westermarck, Juppo, Kervinen, & Yliruusi, 1998, 1999). However, mercury porosimetry best measures the diameter of pores from 7 nm to 14 μm and nitrogen adsorption best measures diameters from 3 to 200 nm. For this reason, comparison between the two techniques is often impossible.

6.2 Size Analysis Methods

Despite the conclusion of Staiger et al. (2002), particle size distributions are more easily obtained than surface area and so are therefore useful in constructing agglomeration indices. The specific surface area is the total surface area (internal and external). In agglomeration we are interested in the external area which BET does not measure. Three indices are discussed below; the agglomeration parameter is an existing index, while the number-based agglomeration index (DoA) and mass-based agglomeration efficiency (ζ) are proposed indices.

6.2.1 Agglomeration Parameter

An agglomeration parameter (AP) can be found by comparing the size of an agglomerate with the size of the primary particles; this method has been employed to determine the extent of sintering (D. M. Liu, Lin, & Tuan, 1999; Roosen & Hausner, 1984). Here, AP = $D_{particles}/D_{primary}$, where $D_{particles}$ refers to the volume mean particle size of the particles/agglomerates using laser diffraction and $D_{primary}$ is the size of the initial particles that form the agglomerates, determined using SEMs. Liu et al. (1999) used this AP to describe the extent of agglomeration that had occurred and linked it to the properties of the powder and the sintering behaviour. They also stated that it is

impossible to accurately determine an extent of agglomeration; however, this method is simple and physically meaningful. Like the agglomeration factor, this index doesn't consider the droplet size.

6.2.2 Number-Based Agglomeration Index

When the droplets are also considered, the simplest approach is to use the mean particle sizes to produce an agglomeration index that yield the number of particles and droplets that combine to form an agglomerate. The number of particles per kilogram (on a dry solids basis) can be calculated from the volume mean size of the fines, spray and agglomerates. This has been derived below for a generic particle. The specific number of particles on a dry solids basis is:

$$N = \frac{(\#\ particles)}{(kg\ of\ solid\ within\ the\ particle)} \tag{6.4}$$

This is obtained by first considering the more easily calculable:

$$\frac{(\#\ particles)}{(kg\ particles)} = \frac{6}{\rho \pi D^3} \tag{6.5}$$

where ρ = the particle density [kg m^{-3}] and D = the volume weighted mean particle diameter [m]. The (kg particles) can be divided into its water and solid components:

$$\frac{(\#\ particles)}{(kg\ particles)} = \frac{(\#\ particles)}{(kg\ water + kg\ solid)} \tag{6.6}$$

Multiplying through by (kg solid)/(kg solid) gives:

$$\frac{(\#\ particles)}{(kg\ water + kg\ solid)} = \frac{\#\ particles}{\left(\frac{kgwater}{kgsolid} + \frac{kgsolid}{kgsolid}\right) kgsolid} \tag{6.7}$$

Defining X = (kg water/ kg solid) and equation (6.7) is rearranged to obtain:

$$\frac{(\#\ particles)}{(kg\ solid)} = \frac{(\#\ particles)}{(kg\ particles)}(X+1) = \frac{6}{\rho \pi D^3}(X+1) \tag{6.8}$$

With respect to the fines, the number of fine particles per kilogram of dry solid, N_f, is obtained from the volume weighted mean particle size, D_f [m], the particle density, ρ_f [kg m^{-3}], and the fines moisture content, X_f:

$$N_f = \frac{6}{\rho_f \pi D_f^3}(1 + X_f) \tag{6.9}$$

Similarly, the number of agglomerated particles per kilogram of dry solid, N_{agg}, is obtained from the volume weighted mean particle size, D_{agg} [m], the particle density, ρ_{agg} [kg m^{-3}], and the agglomerate moisture content, X_{agg}:

$$N_{agg} = \frac{6}{\rho_{agg}\pi D_{agg}^3}\left(1 + X_{agg}\right) \tag{6.10}$$

The same relationships can be applied to the droplets:

$$N_s = \frac{6}{\rho_s \pi D_s^3}\left(1 + X_s\right) \tag{6.11}$$

Because this study investigated agglomeration due to the presence of fines and not agglomeration of the spray droplets themselves, D_s refers to the mean size of the powdered particles obtained when the spray has been dried alone, i.e. without fines recycle. Similarly, ρ_s and X_s refer to the density and the moisture content of the powder obtained by drying droplets. By proportioning droplets and fines according to their relative dry mass flow rates, the number of feed particles into the spray drier can be calculated per kilogram; this gives:

$$p_f N_f + p_s N_s \tag{6.12}$$

where p_f = F/(F + S) = mass proportion of fines in the agglomerated powder [–], p_s = S/(F + S) = mass proportion of spray in the agglomerated powder [–], F = solids flow rate of fines [(kg solid).(s^{-1})] and S = solids flow rate of spray [(kg solid).(s^{-1})]. The number of particles of fines and spray that combine to form an agglomerate is given by the ratio of the particle number before agglomeration to that after agglomeration. Here this is called the degree of agglomeration or DoA:

$$DoA = \frac{p_f N_f + p_s N_s}{N_{agg}} \tag{6.13}$$

If four fine particles and six droplets combine to make two agglomerates, the ratio equals 5 and this ratio has a number of interesting features. If no agglomeration or coating occurs, the expected number of particles per kilogram of dry agglomerated powder is $N_{agg} = p_f N_f + p_s N_s$ and $DoA = 1$. If onion-skinning occurs (see Figure 6.1 – droplets coat particles) then $N_{agg} = p_f N_f$ and $DoA = 1 + p_s N_s / N_{agg}$. If droplets are large and collect the smaller fine particles to form a raspberry type structure (see Figure 6.1), then $N_{agg} = p_s N_s$ and $DoA = 1 + p_f N_f / N_{agg}$. The differentiation between this and onion skinning depends on which stream contains the larger size. If significant agglomeration occurs, then DoA will be a larger number, with the lower limit being $1 + p_s N_s / N_{agg}$ or $1 + p_f N_f / N_{agg}$ depending on which stream contains the larger size.

The DoA relates agglomerate size to the number of droplets and fine particles that constitute the agglomerate. The concept is useful because it relates to the conditions within the collision zone that promote collision and adhesion. However, the DoA does not consider the distribution of sizes but uses a single value, the volume mean size, to calculate the index. This is not always representative of the size distributions, and

therefore some loss of accuracy is expected. More importantly a single mean value does not differentiate size dependent agglomeration. The following method considers the entire size distribution for this reason the next section proposes a method.

6.2.3 Mass Distribution Agglomeration Efficiency

Agglomeration means that smaller particles disappear from a size distribution to make larger particles. This process of death and birth in a specific size interval appears in the changed shape of the size distribution between the feed streams and the product agglomerates. If more deaths, and subsequently more births, occur then more agglomeration has also occurred. Therefore, an agglomeration efficiency can be defined as the mass proportion of all particle and droplets disappearing (or deaths) multiplied by the mass proportion of agglomerates appearing (or births). These two mass proportions are equal: the purpose of multiplying them together has an analogy in screening, where the screen efficiency is the proportion of particles larger than the screen aperture that pass to the overflow multiplied by the proportion smaller than the screen aperture that pass to the underflow. It must be noted that this definition is only valid if mass proportions are expressed on a dry solids basis and size distributions are adjusted to an equivalent particle density.

Rather than the droplet size distribution, the dried size distribution of droplets is used. This is because the agglomerates are made of fines and dried droplets. The base case for no agglomeration is when the spray drier is operated in spray only mode. The dried powder collected represents the dried droplet size distribution in this analysis. This does not necessarily represent the droplet size distribution in the spray but is better for studying the subsequent agglomeration. As discussed further in §7.1 this means that the remaining studies target agglomeration due to the presence of fines and exclude natural agglomeration that has occurred between droplets. In this work, this means that the particle densities of the dried droplets, fines and agglomerates are similar. The dry solid mass within a droplet, fine particle, and an agglomerate is:

$$\frac{\pi/6\, D_s^3 \rho_s}{1+X_s},\ \frac{\pi/6\, D_f^3 \rho_f}{1+X_f} \text{ and } \frac{\pi/6\, D_{agg}^3 \rho_{agg}}{1+X_{agg}} \text{ respectively.} \tag{6.14}$$

For the droplet the dry mass is equally given by defining D_s and ρ_s as the wet droplet size and wet density respectively, or as the dried droplet size and dried density. As explained above, the dry basis will be used here. The mass of particles in each size interval are only comparable (when assessing deaths and births) if the particles have equal density. Therefore, an adjustment to the distributions is needed to ensure density equivalence. By arbitrarily selecting the fines as the basis, the equivalent size of the droplet, D_s', is given by:

$$D_s' = D_s\left[\frac{\rho_s(1+X_f)}{\rho_f(1+X_s)}\right]^{1/3} \tag{6.15}$$

Therefore, each dried droplet size D_s within the discretized distribution is adjusted to size D_s'. This generally means that the equivalent droplet size distribution will shift to

smaller sizes, because in an operating drier, the fines moisture content is slightly lower than that collected from particles in the base of the drier. A similar equivalent size adjustment can be applied to the agglomerates:

$$D'_{agg} = D_{agg}\left[\frac{\rho_{agg}\left(1+X_f\right)}{\rho_f\left(1+X_{agg}\right)}\right]^{1/3} \tag{6.16}$$

However, in these experiments the moisture content and particle density of the fines, dried droplets and agglomerates are all very similar, meaning that the adjustment terms in equations (6.15) and (6.16) are approximately equal to 1 and hence $D_s' \approx D_s$ and $D'_{agg} \approx D_{agg}$.

Figure 6.2 illustrates how the agglomeration efficiency is calculated. Each measured size distribution (obtained on the Malvern Mastersizer 2000) is weighted to the proportional mass flow rates of the fines and spray on a dry solids basis. This means the area under each distribution represents the proportional dry mass flow of each feed stream. For mass frequency distribution data plotted in the typical way, i.e. normalized as $f(\log D_i)$ versus $\log D_i$ with size intervals equally separated on a log scale, the mass balance for the system can be plotted. For the recycled fines, it is $p_f \times f(\log D_{i,f})$ versus $\log D_{i,f}$, for the spray, it is $p_s \times f(\log D'_{i,s})$ versus $\log D'_{i,s}$, and, for the agglomerated powder, it is $f(\log D'_{i,agg})$ versus $\log D'_{i,agg}$. A mass balance means that the integrated distributions for fine particles and droplets add to 1.

$$p_f \int f\left(\log D_{i,f}\right) d\log D_{i,f} + p_s \int f\left(\log D'_{i,s}\right) d\log D'_{i,s} = \int f\left(\log D'_{i,agg}\right) d\log D'_{i,agg} = 1 \tag{6.17}$$

A difference plot is then obtained when the combined feed stream distributions are subtracted from the agglomerated product distribution (Figure 6.2(b)).

$$g\left(\log D_i\right) = f\left(\log D'_{i,agg}\right) - \left(p_f f\left(\log D_{i,f}\right) + p_s f\left(\log D'_{i,s}\right)\right) \tag{6.18}$$

Because the moisture contents and particle densities of all these streams are approximately the same, the correction terms can be ignored:

$$g\left(\log D_i\right) = f\left(\log D_{i,agg}\right) - \left(p_f f\left(\log D_{i,f}\right) + p_s f\left(\log D_{i,s}\right)\right) \tag{6.19}$$

As mass is conserved, the negative area equals the positive area, and multiplying them together gives an efficiency.

$$\xi_g = \left[\frac{1}{2}\int_{-\infty}^{\infty} |g| d\log D_i\right]^2 \tag{6.20}$$

The efficiency is subscripted g because it relates to the distribution function in equation (6.18). The difference plot can have a number of interesting limits that are attributable to different types of growth, such as no agglomeration, coating of fines, and droplet collection of fines or agglomerate formation. If no agglomeration occurs, the difference plot will be a flat line at zero and $\xi = 0$. If onion-skinning occurs (droplets coat

particles), the negative part of the plot will equal the mass of droplets in the system, and the positive part will reflect this mass layered on to the fines. There will be little size difference between the distributions of the fines and the agglomerates and $\xi = p_s^2$. This scenario is most likely when droplets are small compared with the fines and have low viscosity. If raspberry formation occurs (fine particles surround droplets), the negative part of the difference plot will equal the mass of fines in the system and the positive part will reflect this mass collected by the droplets. There will be little size difference between the distributions for the droplets and the agglomerates and $\xi = p_f^2$. This scenario is most likely when droplets are larger than the fines and have high viscosity.

In its simplest analysis, agglomeration is better as $\xi \to 1$, which occurs when there is no overlap between the agglomerate distribution and those of the droplets and fines. This implies a significant number of serial collision events. Some agglomeration occurs if $p_s^2 < \xi < 1$ when $D_f >> D_s$ or if $p_f^2 < \xi < 1$ when $D_s >> D_f$, but, when the sizes of the droplets and the fines are similar, some agglomeration can occur for ξ_g values below p_s^2 or p_f^2. Agglomeration efficiency can be used alongside the other indices such as the DoA; the following sections provide some experimental comparison of these agglomeration indices, the DoA and ξ, with those of other workers, the AP of Liu et al. (1999) and the AF of Staiger et al. (2002).

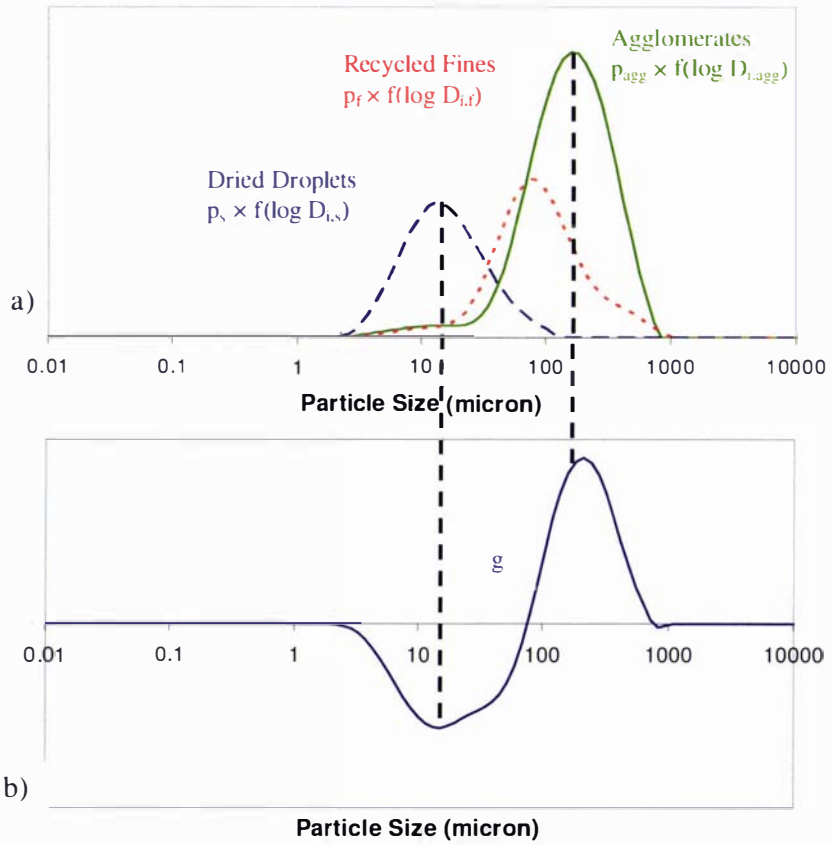

Figure 6.2. Mass-based agglomeration efficiency plots: (a) size distributions weighted by mass flow rate; (b) difference plot.

6.3 Experiments to Test Indices

The experiments listed in Table 6.1 provide a range of conditions intended to encourage or discourage agglomeration in order to compare the above indices. These experiments were conducted in the modified Niro drier (see Chapter 5) and were compared to a typical industrial agglomerated milk powder. Key measurements were particle size (Malvern Mastersizer 2000), SSA (Micromeritics ASAP 2010), particle density (Beckman Air Comparison Pycnometer Model 930) and SEMs for images.

Table 6.1: Design matrix for experiments.

Trial	Design Variables				Measured Properties			
	S	F	$D_{f,4,3}$	$D_{s,4,3}$	ρ_f	ρ_s	X_f	X_s
Units	(kg h^{-1})	(kg h^{-1})	(μm)	(μm)	(kg m^{-3})	(kg m^{-3})	(kg kg^{-1})	(kg kg^{-1})
1	1.7	1.9	47	23	1480	1470	0.04	0.041
2	2.1	1.0	47	34	1480	1470	0.04	0.039
3	1.4	1.1	30	14	1300	1400	0.03	0.033
4	2.1	2.1	59	33	1270	1400	0.03	0.038

S = concentrate spray flow rate, F = fines flow rate, $D_{f,4,3}$ = volume weighted mean particle size of fines, $D_{s,4,3}$ = volume weighted mean particle size of dried droplets, ρ_f = particle density of fines, ρ_s = particle density of dried droplets, X_f = moisture content of fines, X_s = moisture content of dried droplets.

6.4 Results and Discussion

Figure 6.3 shows the mass fraction weighted size distributions of the droplets, fines and agglomerates for experiment 4 (typical of the experiments) and Figure 6.4 shows the size distributions of a typical industry skim milk powder (ISMP A, the powder properties are included in §3.6). The values for the design variables and measured properties given in Table 6.1 for the typical industrial scale trial are S, F, $D_{f,4,3}$, $D_{s,4,3}$, ρ_f, ρ_s, X_f, and X_s. The results for all experiments are shown in Table 6.2. Two significant differences can be seen between these plots; for the small scale experiment 4, the dried droplets are significantly smaller than the fines and little change occurs between the fines and agglomerate PSD; whereas for the industrial drier, the dried droplets and fines are similar in size and the agglomerates are much larger than the fines. The indices for these two cases AP (0.99, 2.17), DoA (2.3, 10.4) and ξ (0.011, 0.148) clearly show that more agglomeration occurs in the industrial drier. Of the indices, the AP is the simplest index, being the ratio of the mean particle sizes of the agglomerates and the fines. It shows that agglomeration occurs in the industrial example but not in the small scale experiments.

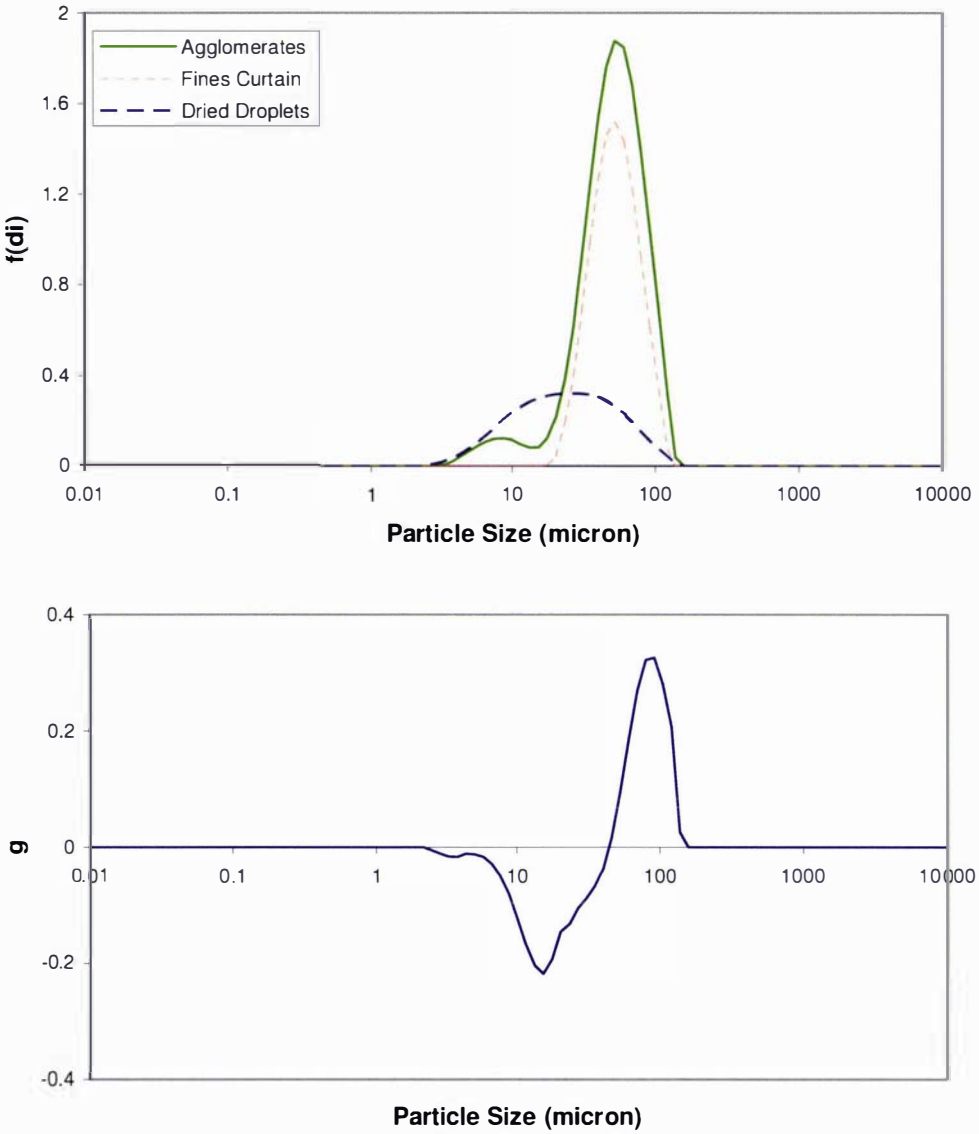

Figure 6.3: Experiment 4 a) comparison of PSDs b) difference plot.

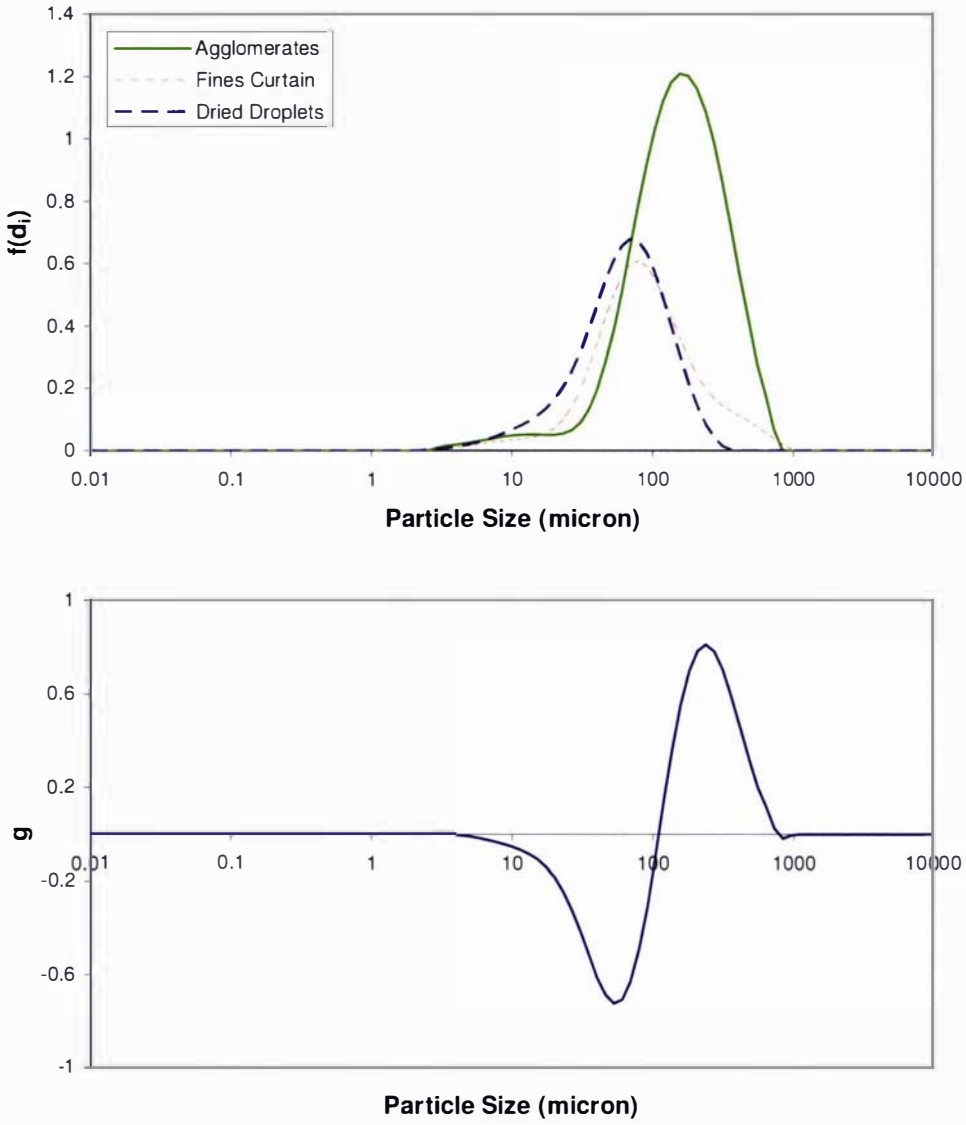

Figure 6.4: Industrial a) comparison of PSDs b) difference plot.

Table 6.2: Comparison of agglomeration indices.

Trial	$D_{agg,4,3}$	ρ_{agg}	X_{agg}	AP	DoA	ξ_g	SSA	D_{BET}	AF	$D_{agg,0.5}$
Units	(µm)	(kg m^{-3})	(kg kg^{-1})	(-)	(-)	(-)	(m^2 g^{-1})	(µm)	(-)	(µm)
1	45	1510	0.041	0.94	2.9	0.005	0.408	9.7	4.4	40
2	46	1470	0.039	0.96	1.6	0.040	0.565	7.2	5.9	41
3	30	1310	0.033	0.99	4.9	0.025				27
4	58	1320	0.038	0.99	2.3	0.011				55
Ind	202	1450	0.030	2.17	10.4	0.148				106

$D_{agg,4,3}$ = volume weighted mean particle size of agglomerates, ρ_{agg} = particle density of agglomerates, X_{agg} = moisture content of agglomerates, AP = agglomeration parameter, DoA = degree of agglomeration (number-based agglomeration index), ξ_g = mass-based agglomeration efficiency, SSA = specific surface area, D_{BET} = 6/SSA, AF = agglomeration factor, $D_{agg,0.5}$ = median agglomerate particle size, Ind = industrial.

The DoA detects agglomeration in a different way. It represents the mean number of fines and droplet particles that coalesce to form an agglomerate. The DoA values for the experiments are lower than expected for onion skinning (3.2, 2.1, 5.2 and 2.7 for experiments 1–4). This means that some coating is occurring but that other droplets do not coalesce with the particles. However, it must be remembered that the DoA is based on mean particle sizes, which are not always representative of the size distributions particularly if they are bimodal, and therefore some loss of accuracy is expected.

The agglomeration efficiency index (ξ_g) does interrogate the size distributions and is calculated from the difference plots of the PSDs shown in Figure 6.3(b) and Figure 6.4(b) for experiment 4 and the industrial example. For the small scale experiments, ξ is lower than expected for onion skinning (where p_s^2 = 0.08, 0.22, 0.14 and 0.11 for experiments 1 – 4), which also indicates that some coating is occurring but other droplets do not coalesce with the particles. The industrial drier produces an ξ_g that is also lower than expected for onion skinning (p_s^2 = 0.22) but is significantly larger than the small scale experiments.

Table 6.2 also contains the agglomeration factor, AF, an index based on the BET SSA for the product of experiments 1 and 2. The AF relates the volume weighted mean particle size and the equivalent particle size based on the calculated BET SSA. The surface areas found here, 0.41 and 0.57 $m^2\ g^{-1}$, are larger than those found by Berlin et al. (1964) using nitrogen adsorption (0.14 – 0.27 $m^2\ g^{-1}$ for instant and standard skim milk powder) but this is expected because the powders here are finer. The D_{BET} calculated from the SSA is much smaller than the $D_{0.5}$ of the agglomerates, which indicates that the SSA measured using nitrogen adsorption is much larger than the apparent combined surface area of the primary particles that make up the agglomerates. This indicates that the technique is also measuring the internal surface of these primary particles due to the porous nature of milk powder. Because of this reason, this approach of Staiger et al. (2002) using the AF is not a suitable agglomeration index for milk powder particles and so was not measured for experiments 3 and 4.

These indices should be used in conjunction with image analysis to establish the type of growth that has occurred. Figure 6.5 shows SEM images of agglomerated powder from experiment 4 and an industrial drier. It is clear that the agglomerated powder from the small scale experiments does not contain many primary particles in contrast to the industrial powder. The distinct differences between the powders originate from differences between the spray only mode of operation within each drier, i.e. when the drier is operated without fines recycle. In this operating mode, the industrial drier produces highly agglomerated powder whereas the small scale experiments do not. This illustrates the importance of investigating the spray angles in industrial driers with multiple spray nozzles. This work concentrates on additional agglomeration due to the presence of fines, and so these images alone do not indicate whether the presence of fines increases the extent of agglomeration. Image analysis needs to differentiate fines-dependent agglomeration, in addition to the other textural information that it can provide. Developing techniques of image analysis for application to agglomerates is an area of further work.

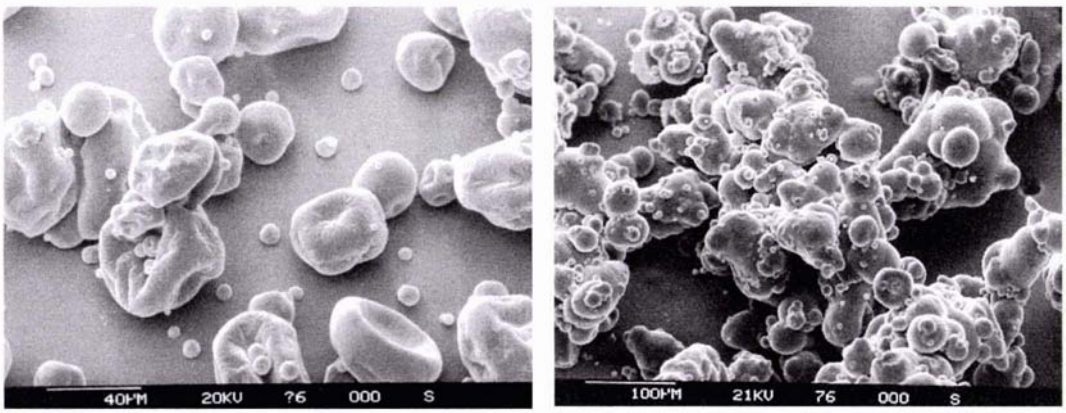

a) b)

Figure 6.5: SEM images of agglomerated powder (a) experiment 4 (b) industry.

In conclusion, the DoA and ξ_g are superior indices for agglomeration because they are inclusive of all streams, whereas AF and AP are not. Further, because DoA uses only the mean of each distribution, it is unsuitable if the size distributions are irregularly shaped. Therefore, ξ_g is the index of choice because it accounts for changes that occur across the entire particle size distributions. However, the above results show that little agglomeration occurred in the small scale experiments. It is postulated that the agglomerates that do form are obscured by a significant proportion of fines that appear directly in the product. This means that agglomeration is not detected as well as it could be using the current calculation method for the ξ_g index. The following section explores this postulate and proposes a refined index.

6.5 Development of the *h* Agglomeration Efficiency

Above, it is postulated that a significant proportion of fines pass straight to the product stream in the small scale drier. In doing so, they obscure the presence of any agglomerates which have formed in the collision zone. To remove some of this obscuration it is proposed that they be censored from the agglomerated powder stream to give a better "view" of the agglomerates. Censoring can be done when examining crystal size distributions, to select for or against fast or slow growing crystals (McLeod, Jones, & Paterson, 2006). Here, ideally only those droplets and fines that form agglomerates should be selected for calculating the index. There are several possibilities for removing the fine particles from the product, using a cut-off size (removing all product particles below a specific size), or imitating a cyclone efficiency (removing a distribution of fine particles from the product). The resulting agglomeration efficiency would be affected significantly by the cut-off size or cyclone efficiency selected (which would essentially be arbitrary). By considering the operation of a typical industrial agglomerating drier, a censorship regime can be established. Fines are always recycled and, at steady state operation, the flow rate, size distribution, and fluxes of spray droplets becoming fines and fines becoming product are all unchanged. Therefore it makes sense to subtract the fines distribution from the index calculation. At each size interval, the outgoing product mass minus the mass of fines is compared to the incoming mass of droplets. This new analysis is referred to as the *h* efficiency, ξ_h.

In this method a difference curve is produced by removing all the fine particles from the product and comparing this to the spray input to the drier. The difference curves are defined by the h distribution function which is dependent on the design of the drier, as shown in Figure 6.6; the division by p_s normalises the distributions so that, in a completely agglomerating system where all small sizes (droplets) disappear to be replaced by much larger sizes (agglomerates), the efficiency ξ_h is equal to 1. Efficiency is calculated in the same way, by equation (6.20) where the g distribution is replaced by the h distribution.

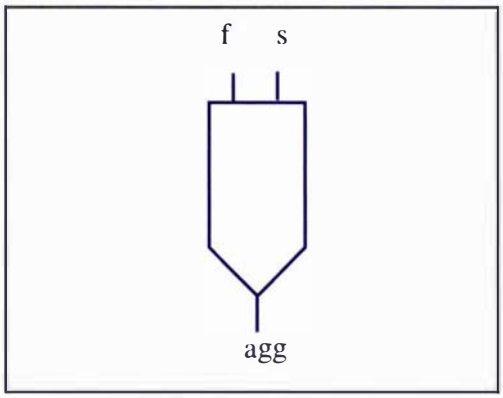

a) small scale agglomeration

$$h = \frac{(p_{agg} f_{agg} - p_f f_f) - p_s f_s}{p_s} \qquad (6.21)$$

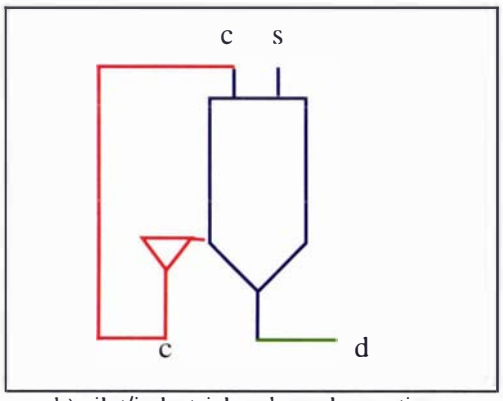

b) pilot/industrial scale agglomeration

$$h = \frac{(p_d f_d + p_c f_c - p_c f_c) - p_s f_s}{p_s} \qquad (6.22)$$

$$h = \frac{p_d f_d - p_s f_s}{p_s} \qquad (6.23)$$

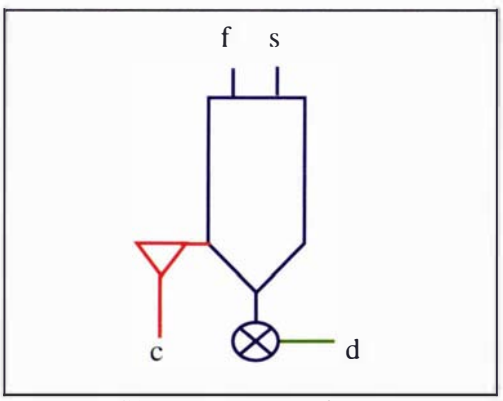

c) modified pilot scale agglomeration

$$h = \frac{(p_d f_d + p_c f_c - p_f f_f) - p_s f_s}{p_s} \qquad (6.24)$$

Figure 6.6: Comparison between processing scales/designs and the h efficiency.

Table 6.3 compares the new *h* efficiency with the *g* efficiency for the four small scale experiments and the industrial situation. The *h* efficiency better differentiates between the small scale experiments so that it is clearer which experiments exhibit agglomeration (3 and 4) and which conditions result in no agglomeration (1 and 2). This *h* efficiency is used when discussing the results of the experimental programme carried out at small scale (Chapter 7) and for the pilot scale study (Chapter 8). Although the ξ_h values for the small scale experiments are still much lower than experienced in the industrial drier, the following chapters, specifically Chapter 8, demonstrate that some agglomeration does occur on the small scale.

Table 6.3: Comparison of the *g* and *h* agglomeration efficiencies.

Trial	ξ efficiency	
	g	h
1	0.005	0.000
2	0.040	0.001
3	0.025	0.169
4	0.11	0.099
Industry	0.148	0.635

6.6 Chapter Conclusions

Agglomeration in spray driers is a rapid process and it is not possible to simply measure its progress with time. Instead, the extent of agglomeration must be determined using an index that relates the fines recycle and spray streams to the agglomerated powder. This chapter has reviewed a number of indices and proposes two new indices. The AF was found to be an unsuitable agglomeration index for milk powders because it measures internal surface area, which is not important for agglomeration which occurs at the external surfaces. The AP may be suitable because the ratio of mean sizes is sensitive to differences between the fines and the agglomerated product but it ignores the spray droplet size.

The indices proposed in this work, the DoA, ξ_g, and ξ_h include the spray droplet size, and can distinguish between the type and the extent of agglomeration, and are inclusive of all three streams in the process. DoA is insensitive to the shape of the size distribution and so ξ is the preferred index because it interprets change across the entire PSD whatever its shape. The agglomeration efficiency, ξ_g, was modified to ξ_h to remove obscuration of agglomeration by fines. Essentially the fines distribution is subtracted from the agglomerated product distribution. It therefore examines the transformation that occurs between the spray and the product, yet does not lose the fines information. This so called *h* efficiency is derived from the industrial situation and allows for better comparison between scales.

CHAPTER 7

RESULTS AND DISCUSSION OF SMALL SCALE EXPERIMENTS

This chapter reports the agglomeration studies conducted on the small scale Niro drier, as described in Chapter 5. Several different areas are discussed including the natural agglomeration that occurs even without fines addition, the preliminary experiments that determine the agglomeration performance, and incremental design improvements to address factors affecting the agglomeration. The performance of the improved design is then discussed relative to the fines and spray flux ratio. This work then leads into an experimental study on a larger pilot scale drier.

7.1 Natural Agglomeration without a Powder Curtain

During spray drying, natural agglomeration occurs due to droplet-droplet collisions even without a powder curtain (Chapter 2). Collisions between droplets will depend on droplet size, velocity, number density and flux. However, these are not independently controllable but are affected by three operating parameters, solids concentration, milk concentrate flow rate, and atomisation pressure. To determine the extent of natural agglomeration in the modified small scale drier, a series of experiments was conducted according to Table 5.10 in §5.4.1, which is repeated here as Table 7.1 for ease of interpretation of results. Variables held constant include the flow rate of air into the drier, the temperature of inlet air (195°C), and the temperature of concentrate (50°C).

Table 7.1: Design matrix for natural agglomeration using reconstituted ISMP A.

Experiment	**Concentrate Flow rate**	**Total Solids**	**Atomisation Pressure**
Units	**(kg h^{-1})**	**(wt %)**	**(bar)**
S1	2	41	2.5
S2	2	41	1.5
S3	1.4	41	2.5
S4	1.4	41	1.5
S5	2	47	2.5
S6	2	47	1.5
S7	1.4	47	2.5
S8	1.4	47	1.5
S9	1.7	44	2

The effect these three parameters have on the Sauter mean particle size of the dried droplet is shown in Figure 7.1. Increasing atomisation pressure decreased droplet size but increasing solids concentration increased dried droplet size; however concentrate flow rate had very little effect. The statistical software Minitab™ (v14.1) was used to generate the main effects plot in Figure 7.2 and shows the same trends as Figure 7.1.

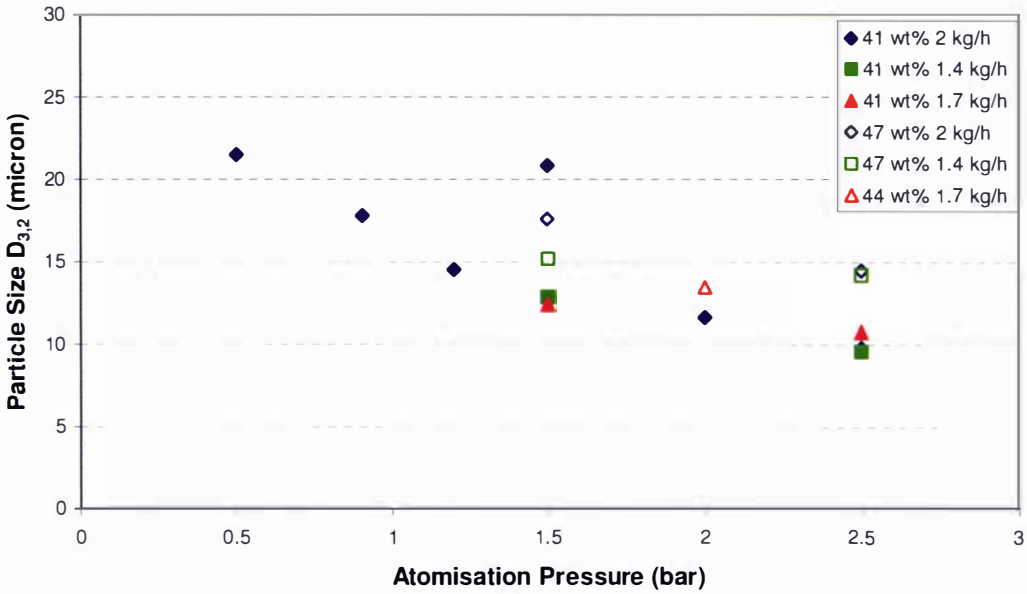

Figure 7.1: Particle size produced as a function of the atomisation pressure (bar), total solids (wt%) and concentrate flow rate (kg h^{-1}).

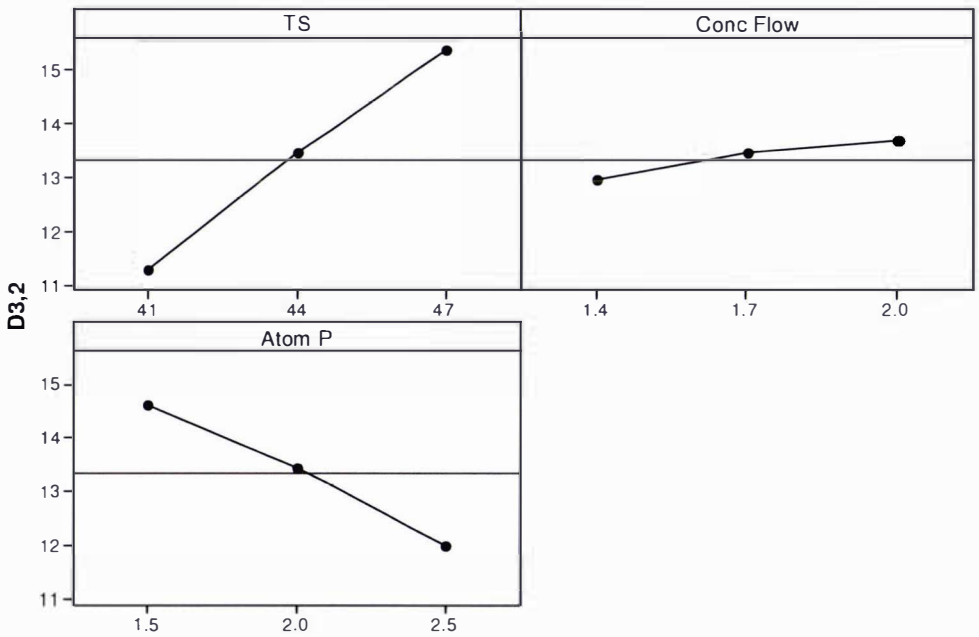

Figure 7.2: Plot showing the effect of total solids, atomisation pressure and concentrate flow rate on particle size, $D_{3,2}$.

A key indicator of agglomeration is particle morphology which can be observed a number of ways. Here scanning electron microscopy (SEM) plots are shown below in Figure 7.3 for S2 and in Figure 7.4 for S5. These depict milk powder particles produced from drying spray droplets. The particles are mostly spherical in shape with some puckered surfaces. Very little or no bonding between particles indicates that little natural agglomeration had occurred between droplets. This finding is significant for

later agglomeration studies when a powder curtain was included. The analysis methods presented in Chapter 6 determine agglomeration based on the difference between the size distributions for dried droplets with and without the presence of a fines curtain.

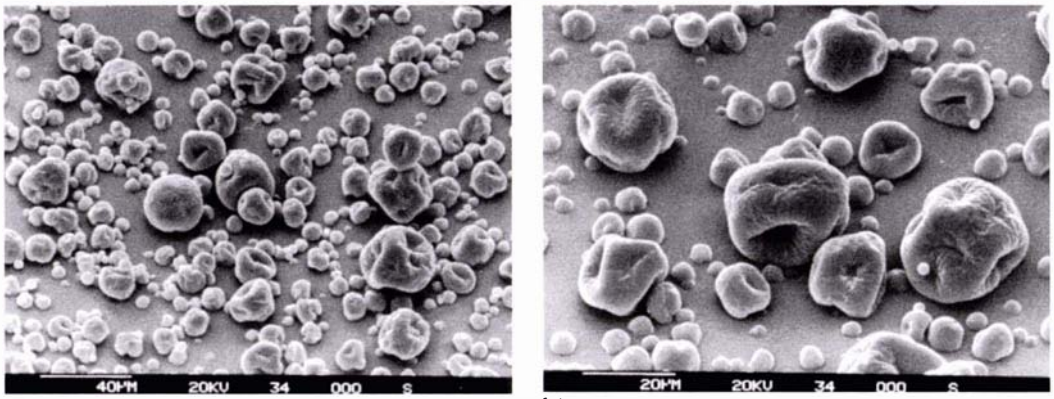

a) b)

Figure 7.3: SEMs of a) S2 at 500 x magnification b) S2 at 1000 x magnification.

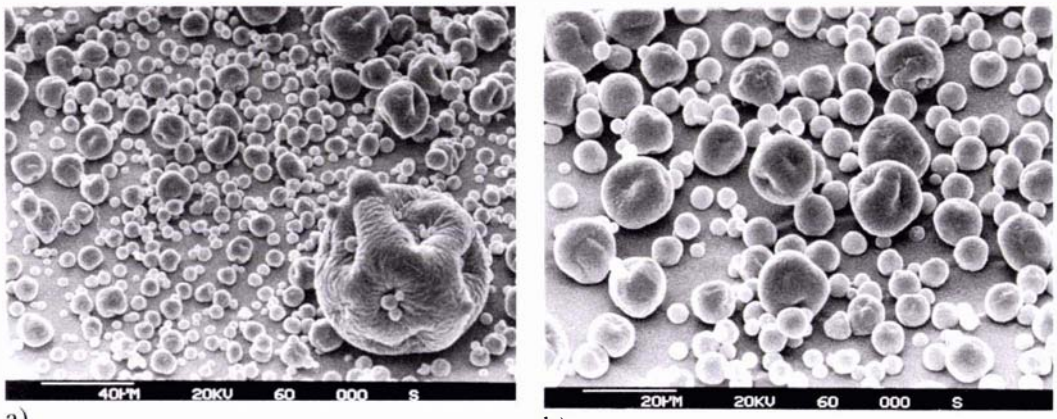

a) b)

Figure 7.4: SEMs of a) S5 at 500 x magnification b) S5 at 1000 x magnification.

Figure 7.5 compares the particle size distributions (PSD) for each experiment. The wider and larger size distributions are observed for experiments S5 and S6 which were obtained by atomising 47 wt% concentrate delivered at 2 kg h^{-1}. The geometric standard deviation can be used as an indicator of the width or span of a log-normal distribution. It can be determined by dividing the particle size at the 84.14% probability by the mass median particle diameter.

$$S_g = \frac{D_{84.14\%}}{D_{50\%}} \tag{7.1}$$

where S_g = geometric standard deviation [–], D_{50} = mass median particle diameter [µm], $D_{84.14}$ = diameter of the particle that is equal to or less than 84.14% of the particles present [µm]. Figure 7.6 shows that total solids (TS) has the largest effect on the span of the distribution when; higher solids concentrations the geometric standard deviation is higher. The geometric standard deviation also increases with increasing concentrate flow rate, and decreases with increasing atomisation pressure.

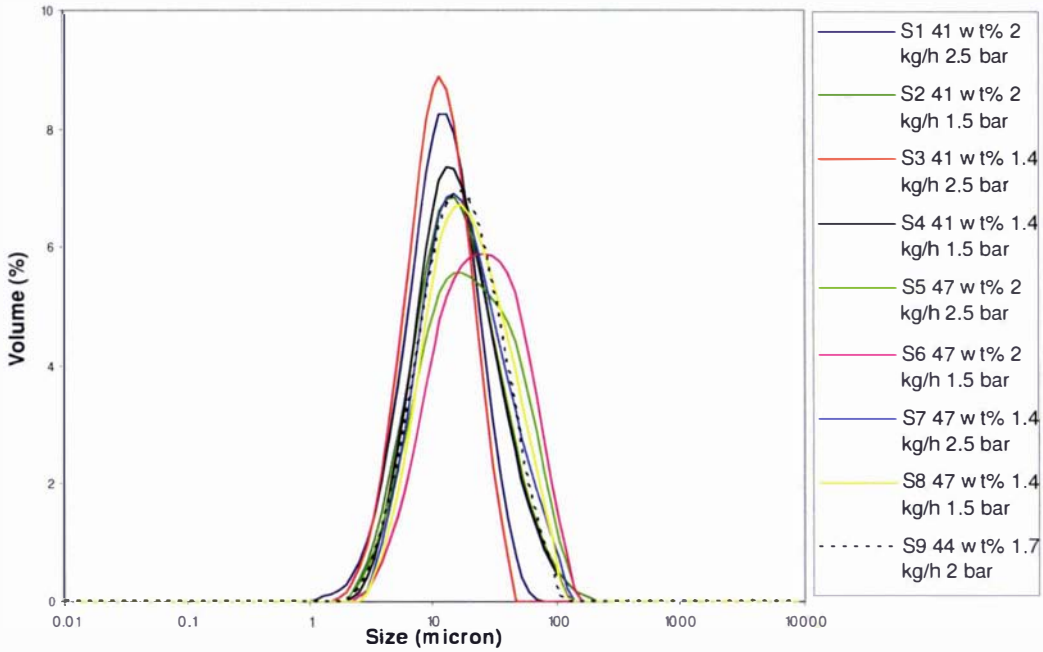

Figure 7.5: Comparing particle size distributions for experiments S1 to S9.

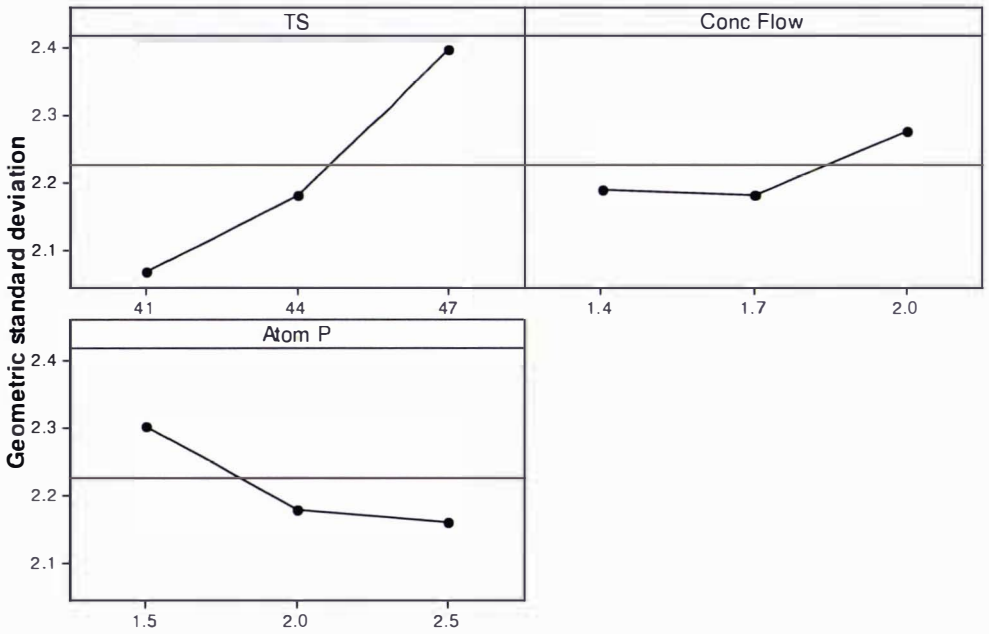

Figure 7.6: Effect of atomisation pressure (bar), total solids (wt %) and concentrate flow rate (kg h^{-1}) on the geometric standard deviation.

Figure 7.7 shows the relationship between bulk density and atomisation pressure for concentrates with different total solids and concentrate flow rates. The main effects plot in Figure 7.8 shows that bulk density decreases with an increasing atomisation pressure but increases as total solids increases. These are the same trends as observed in Figure 7.1 for mean particle size, which indicates that the mean particle size of an agglomerated powder may be related to its bulk density.

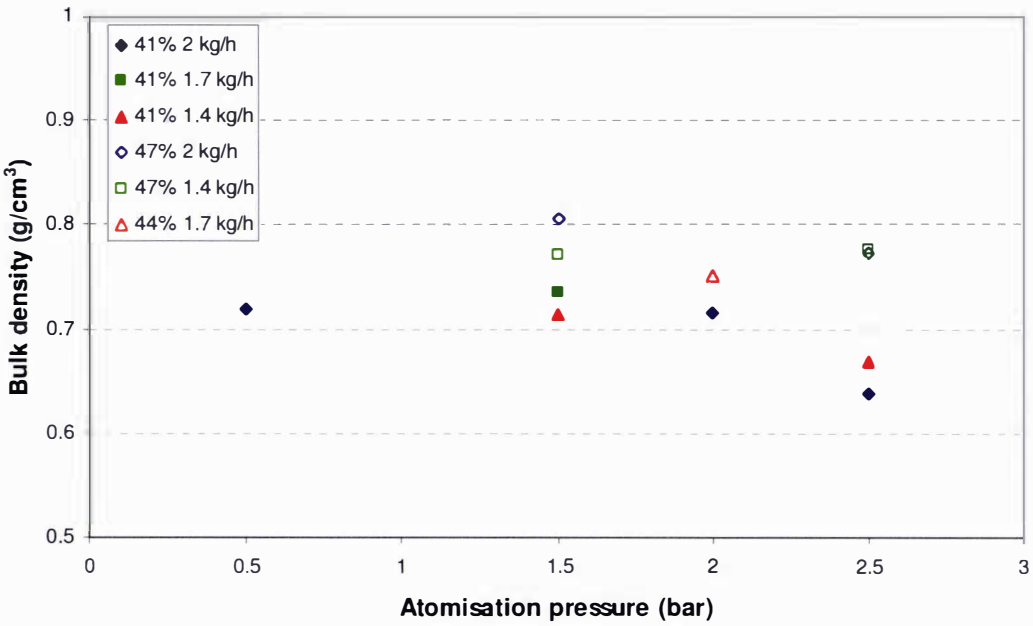

Figure 7.7: Effect of atomisation pressure (bar), concentrate flow rate (kg h^{-1}) and total solids (wt%) on bulk density.

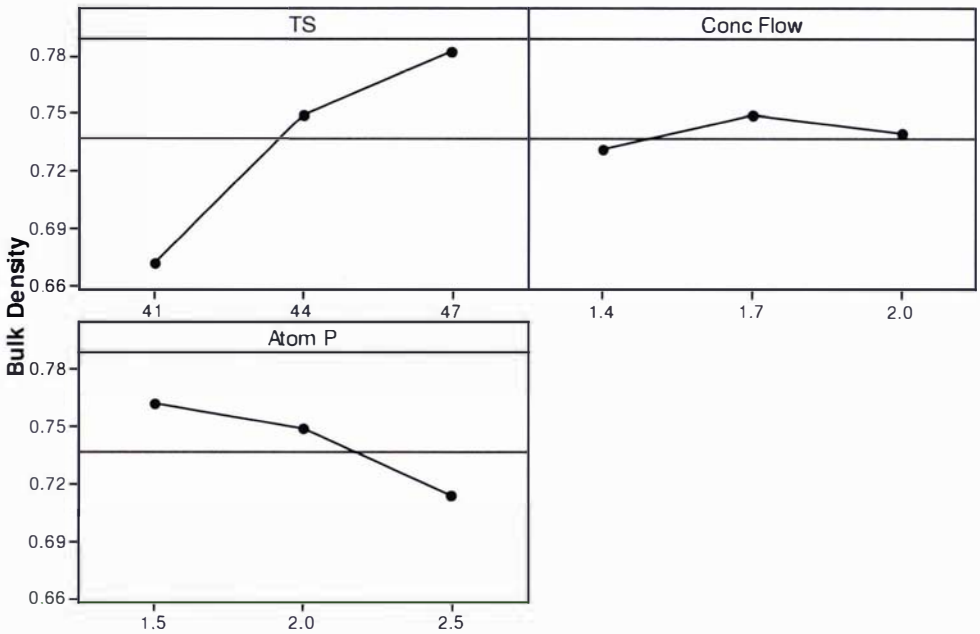

Figure 7.8: Effect of atomisation pressure (bar), concentrate flow rate (kg h^{-1}) and total solids (wt%) on bulk density.

Nijdam and Langrish (2005) found that reducing the drying temperature from 200°C to 120°C, decreased the mean particle size of a powder and resulted in an increase in bulk density which agrees with the findings of Buma (1971). Pisecky (1997) suggested that the particle porosity is more important than particle size when controlling bulk density. Figure 7.9 indicates that drying milk concentrate at one inlet air temperature (195°C),

bulk density increased with powder particle size and more concentrated milks produce larger and denser powder particles when the drier is operated in spray only mode.

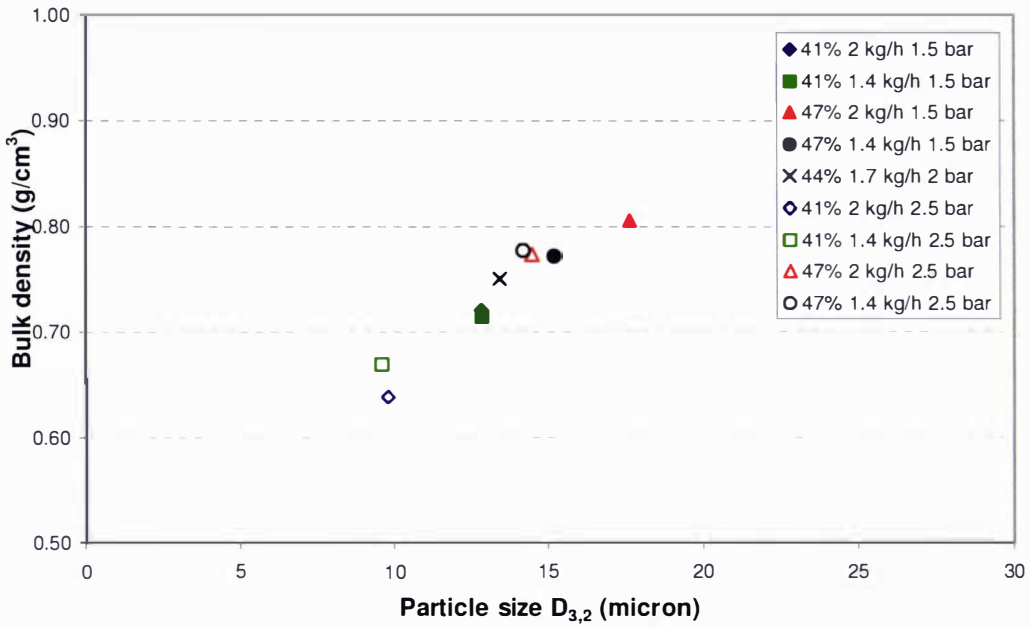

Figure 7.9: Bulk density vs. mean particle size for different spraying conditions.

Product yield is the percentage of solids collected at the cyclone compared to the amount sprayed into the drier. The flat spray meant that droplets adhered onto the opposite wall resulting in low yields of ~ 40% (Figure 7.10). It is difficult to predict how this low yield affects the particle size and results must be interpreted with this in mind.

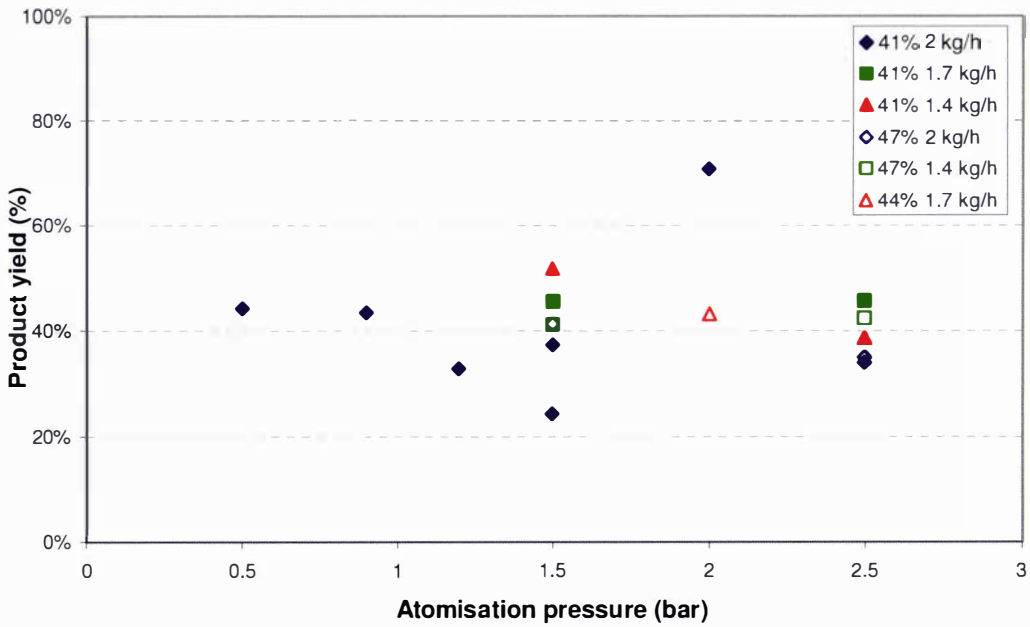

Figure 7.10: Product yield vs. atomisation pressure for different spraying conditions.

Natural agglomeration is not only affected by the collision rate but also by the adhesion efficiency, which is determined by the surface stickiness of droplets. Adhikari et al. (2003b) and Adhikari et al. (2005) use a dimensionless time ψ to determine the degree of difficulty for a drop to enter the safe drying regime. The dimensionless time is a ratio of the time required to enter the safe drying regime to the time needed to reach the final moisture content. When $\psi > 1$ the drop is not in the safe regime, and when $\psi < 1$ the droplet is in the safe regime so that $\psi = 1$ is the cut off point for safe drying. This safe drying regime is determined by the time required to dry the droplet so that the surface stickiness is low enough that product will not adhere to the drier walls.

Ozmen and Langrish (2003a) state that wall deposition is determined by whether the particles approach the walls and they stick to the walls. In these experiments, despite the natural swirl of the inlet air, the nozzle is mounted to give a horizontal spray. This means that droplets are transported towards the opposite drier wall. The fact that ~ 60% adhere to the wall indicates that droplets are both transported to the walls and are relatively sticky. In addition, ψ can also be related to the practical level of difficulty in spray drying, which can be interpreted as product yield.

This approach has been used by several authors Truong (2005b) and Bhandari et al. (1997) to indicate spray drying performance and Bhandari et al. (1997) defined 50% recovery as marginally successful in a pilot scale spray drier. Using the definition of ψ = 1 when recovery is 50%, a yield above 50% indicates successful drying and below is considered marginally successful. The spray trials average yield indicates unsuccessful spray drying. The small particle size means adherence to the walls will occur by mechanisms other than stickiness, e.g. deposition, electrostatics. However, when the curtain momentum flow of fines and air is introduced, the likelihood droplets adhere to the opposite wall is expected to reduce because the spray will be directed downwards and away from the wall by the fines stream. This is expected that product yield should increase to above 50% thus achieving successful drying.

7.2 Preliminary Experiments using a Powder Curtain

Forced agglomeration involved the impact of a curtain of fine particles and a sheet of spray droplets using the small scale equipment designed in Chapter 5. The preliminary experiments were designed to determine the agglomeration performance of the drier and the conditions required to improve droplet – particle impact. Preliminary experiments focussed on several key areas to assess agglomeration performance; the position of the nozzle relative to the fines curtain (P1 and P2), and manipulation of operating parameters (P3 to P5). Experiment P6 aimed to improve the probability of droplet – particle impact. The operating conditions used to perform these experiments and resulting agglomeration efficiencies have been included in Table 7.2.

In experiment P1 the nozzle was placed 50 mm from the front of the powder curtain. However, as the thickness of the powder curtain was changed, the front edge of the powder curtain also varied between experiments to maintain consistency, subsequent experiments placed the nozzle 50 mm from the centre of the curtain which provided better overlap (as discussed in §5.3.2). Experiment P2 also showed that moving the nozzle 15 mm closer to the curtain had little effect on ξ_h.

Experiments P3, P4 and P5 were carried out to investigate the effect of operating variables on the agglomerated product (see Table 7.2). ξ_h increases with each set of changes and indicates that Experiment P5 exhibits the most agglomeration. The particle size distributions of the dried droplets, fines curtain are included in Figure 7.11. However, the PSD of the agglomerates does not demonstrate the shift observed industrially (§6.4) and ξ_h indicates much lower levels of agglomeration than calculated for industrial powders.

Table 7.2: Agglomeration index results for preliminary experiments.

Exp	S	F	$D_{f,4,3}$	TS	P	D	FS	N	ξ_g	ξ_h
Units	(kg h^{-1})	(kg h^{-1})	(µm)	(wt%)	(bar)	(mm)		(mm)		
P1	2.0	1.0	30	42.3	1.5	30	N	65	0.108	0.118
P2	2.1	1.1	30	40.9	1.5	30	N	50	0.092	0.117
P3	2.1	2.1	58.8	47.5	2.5	10	N	50	0.011	0.099
P4	1.4	1.0	30	41.2	2.5	30	N	50	0.023	0.169
P5	2.1	2.0	30	41.3	1.5	30	N	50	0.018	0.184
P6	1.4	1.1	30	41.6	2.5	30	Y	50	0.025	0.175

S = concentrate spray flow rate, F = fines flow rate, $D_{f,4,3}$= volume weighted mean particle size of fines, TS = total solids of concentrate, P = atomisation pressure, D = curtain depth, FS = fines shroud, N = nozzle distance from centre of curtain, ξ_g = agglomeration efficiency, ξ_h = efficiency excluding fines from product.

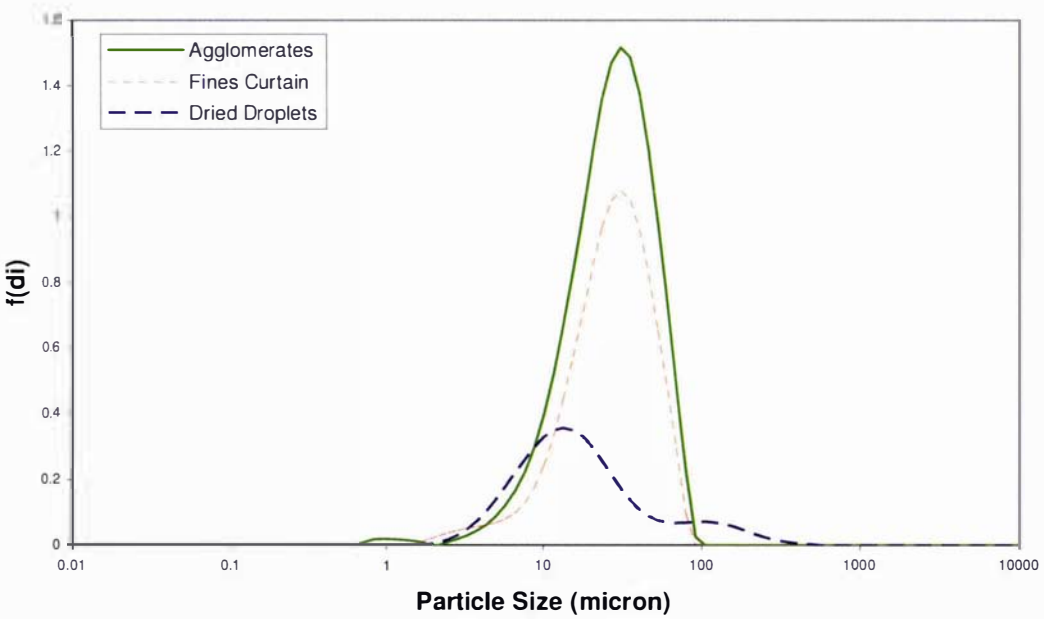

Figure 7.11: Comparing the weighted PSDs for P5.

It was observed that fines were dispersed by the drying air flow after entering the top of the drier, thus reducing the concentration of fines at the point of impact with the spray. The curtain distributor or 'chute' was modified to shroud the fines from the drying air as close to the spray interaction zone as possible. Experiment P6 was carried out by reducing the distance between the fines entrance and the spray zone from 80 mm to 25 mm (as discussed in §5.2.2). The experimental conditions are identical to those used for P4, the highest agglomerating case of the preliminary experiments (when assessing agglomeration using the *g* efficiency).

As discussed in Chapter 6, the ξ_g agglomeration index was originally assessed to be the best to determine agglomeration performance, however, the later development of the ξ_h proved to be a better method and will be used in all future assessments of agglomeration performance. No discernable difference was observed in agglomeration performance; the ξ_g increased marginally from 0.023 to 0.025 and ξ_h increased from 0.169 to 0.175. The section below addresses the design improvements that were required to improve the agglomeration performance of the small scale equipment.

7.3 Improving the Design

The preliminary experiments identified that the initial small scale equipment design did not appear to agglomerate to the extent exhibited industrially. The experimental programme carried out in this section aimed to improve the equipment design and increase agglomeration. This programme is outlined in §5.4.3 and is represented by trials D1 – 8. These experiments are described below in a chronological order stages 1 to 4 following:

- *Stage 1* – Experiments D1 to D5, where the design issues below are discussed:
    1. Fines dispersion
    2. Droplet dispersion and stickiness
    3. Agglomerate breakdown

- *Stage 2* – Experiment D6 is treated separately because it considers the previous design alterations and aims to optimise agglomeration.

- *Stage 3* – Experiments D7 and D8, the operating conditions of previous trials are discussed with respect to the *h* efficiency and D7 – 8 represent one further permutation of the design configuration.

- *Stage 4* – Experiment U1, where the self-cleaning two-fluid nozzle was replaced by an ultrasonic nozzle.

7.3.1 Stage 1 – Experiments D1 to D5

A series of design improvements were carried out. The four main areas are investigated here and indicated on Figure 7.12:

1. Fines dispersion
2. Droplet dispersion and stickiness
3. Agglomerate breakdown

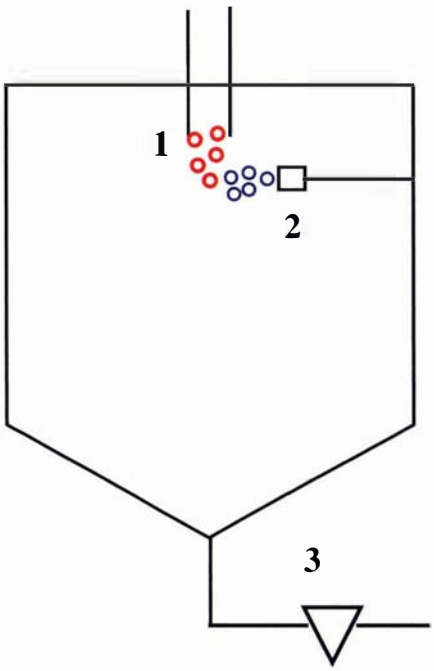

Figure 7.12: Schematic of small scale drier indicating improvement points.

Fines Dispersion (D1 & D2)

Experiments D1 and D2 qualitatively observed the shape of the fines curtain. D1 observed the curtain with no spray or atomising air but with cool drying air. Figure 7.13 is a representation of what was observed and shows the fines curtain dispersing. The curtain remained intact for the first 1 cm into the drier. After this point the fines were pulled away from the curtain and dispersed by the drying air and at 3 cm from the entrance into the drier the curtain has disappeared entirely. The fines in the centre of the curtain are the last to be dispersed. This meant that when the spray hit the fines curtain 2.5 cm below the entrance the number concentration of fines was very low.

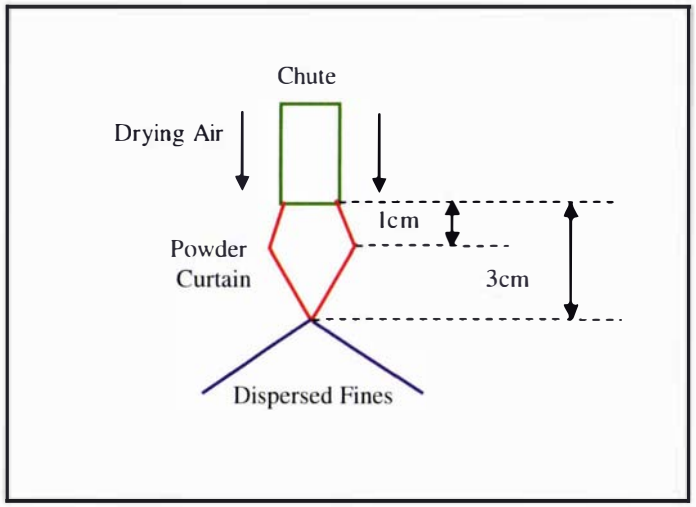

Figure 7.13: Experiment D1 showing dispersion of fines.

To reduce the dispersion of the fines by the drying air and to maintain a high particle concentration in the collision zone, deflector wings were attached. Experiment D2a, run under the same conditions, demonstrates that the deflector preserves the curtain shape past the point where the spray sheet would contact the fines (Figure 7.14). This implies that most of the fines pass through the collision zone. Experiment D2b includes atomising air at 1.5 bar, but no spray droplets. Here, the shape of the powder curtain changes and particles are transported towards the wall (Figure 7.15). Therefore the benefit of the deflector wings in the presence of atomising air is uncertain.

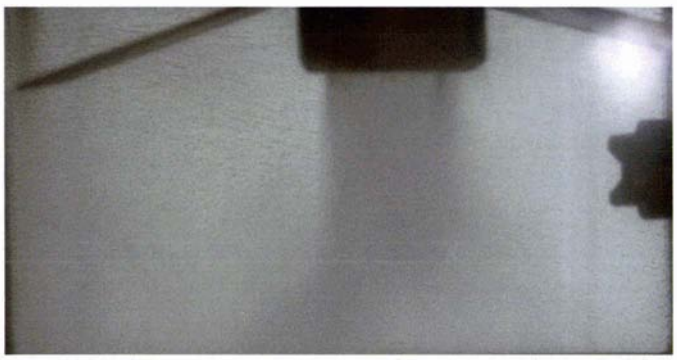

Figure 7.14: Fines curtain shape with no atomiser air (D2a).

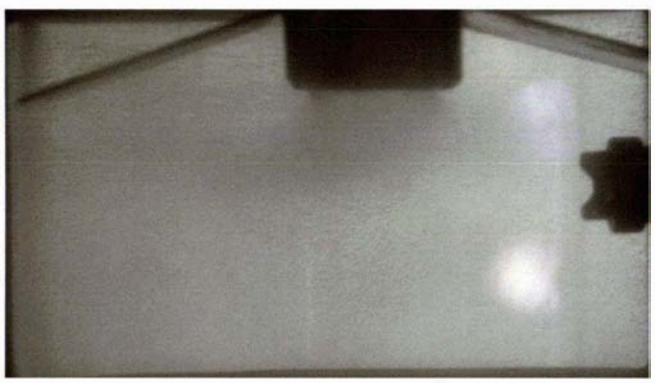

Figure 7.15: Fines curtain shape with 1.5 bar atomiser air (D2b).

Droplet Dispersion and Stickiness (D3)

The two-fluid nozzle used in this study affects the dispersion and stickiness of droplets. Dispersion occurs as the atomising air expands from the nozzle and entrains surrounding air into the flow stream. Although the flow was turbulent, the droplets dispersed away from each other. This dispersion also affected the particles in the fines curtain. Later, an ultrasonic nozzle was trialled to avoid this dispersion after experiments P1 – 6 and D1 – 8 were completed, as discussed in §7.3.4.

Droplets are dried as they travel through the drying air and their surfaces go through a period of stickiness as discussed in §2.4.3. Colliding droplets will only adhere to one another or other particles if they are sticky, which depends on the surface moisture content, and temperatures. These properties at the time of impact with fines are influenced by nozzle distance from the collision zone, solids concentration and the drying air temperature. The relative humidity of air surrounding the droplets also affects the surface stickiness; therefore spraying water into the collision zone should increase surface stickiness and promote agglomeration.

Experiment D3 sprayed water through the two-fluid nozzle with the intention to wet the powder in the curtain to make it surface sticky and this promotes agglomeration. Results show that almost no agglomeration occurred (Figure 7.16) indicated by the agglomeration efficiency of 0.006. This trial does not give a conclusive result, because either the fines particles were not wetted sufficiently (or became too wet to become sticky or, as explained above, the atomising and drying airflows dispersed the droplets and fines to such an extend that wetted fines did not collide with sufficient frequency to create agglomerates.

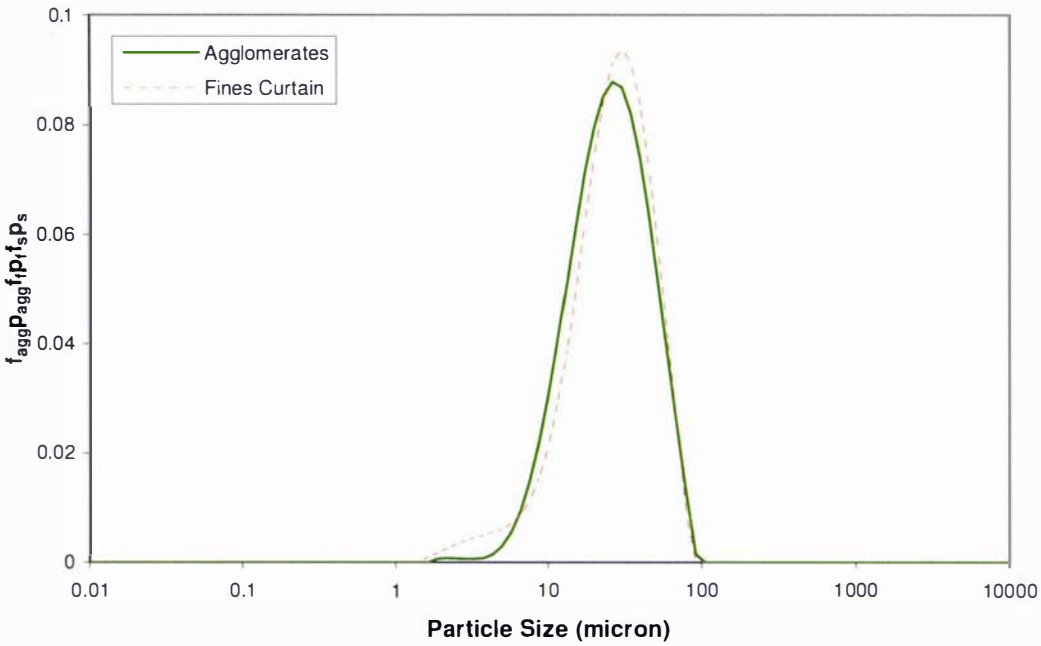

Figure 7.16: Comparing the weighted PSDs for D3.

Agglomerate breakdown (D4 and D5)

It is possible that some agglomerates forming in the drier are subsequently broken down in the collection cyclone. Experiment D4 was a repeat of the preliminary experiment P6, without the deflector wings but with the powder collected before the cyclone using a sieve placed in the bottom of the drier, onto which falling particles were collected. The sieve was a stack of two sieves, with a mesh size of 45 and 90 µm, placed in the bottom of the cone of the drier. The drying air had to pass through both sieves to exit the drier. The air flow rate decreased as the powder built up on the sieves. Although air flow rate was not measured the outlet air temperature dropped, from 64°C to 58°C, indicating that less inlet air was being heated.

Figure 7.17 shows that the cyclone particle size distribution was similar in size to the sample collected on the 90 µm sieve although slightly smaller. There could be several reasons for this difference, the larger particles may have inertial effects causing them to travel closer to the drier wall and are collected in the cone of the drier before being transported to the cyclone through the gaps available between the sieve and the drier wall, and/or the particles may agglomeration in the cyclone. The agglomeration indices show a high level of agglomeration (Figure 7.18) *g* efficiency = 0.045 and *h* efficiency = 0.361.

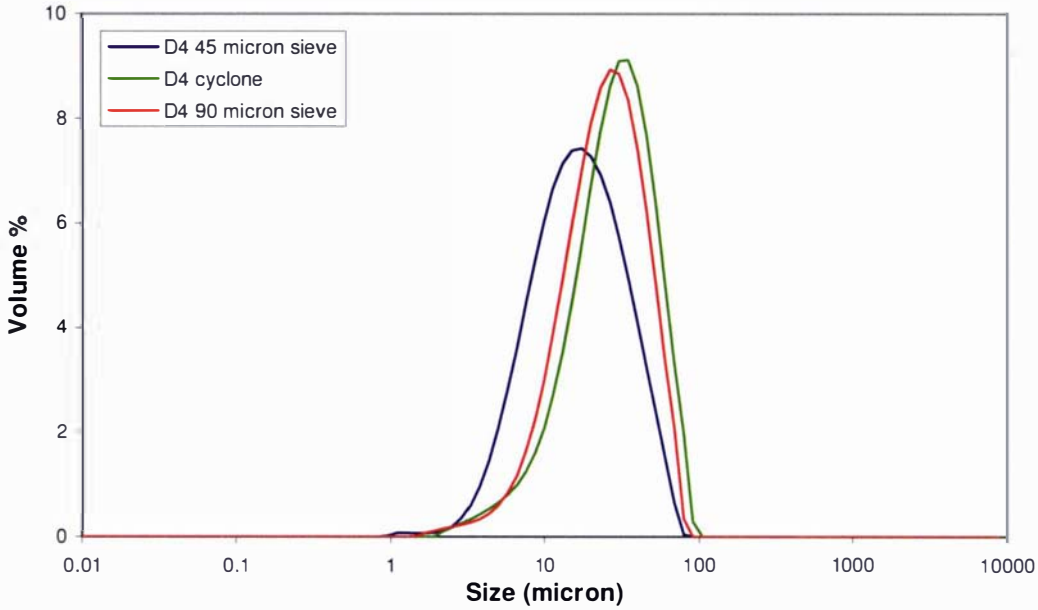

Figure 7.17: Comparing the PSDs from the sieves and cyclones for D4.

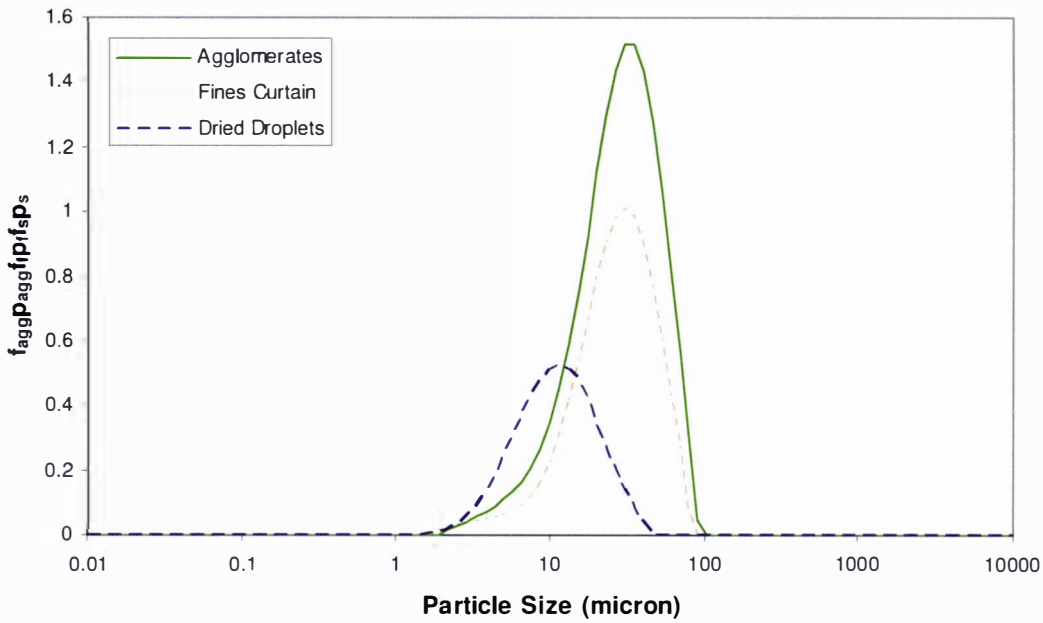

Figure 7.18: Comparing the weighted PSDs for D4.

Differential interference contrast microscopy (DIC) was used to view the product of the drier on the 90 µm sieve, the product of after the cyclone and compare these to the fines input into the drier (Figure 7.19(a – f)). The fines images (a) and (b) indicate clearly defined separate particles with some finer particles attached to the surface. The images in (c) to (f) clearly identify agglomerates present in the product from the drier and in the cyclone. This implies that although the previous experiments were thought to only produce coated particles some agglomerates were produced as well. Due to the large

number of non-agglomerated particles present in powder sample, the agglomerates present are unable to be detected in the particle size distribution.

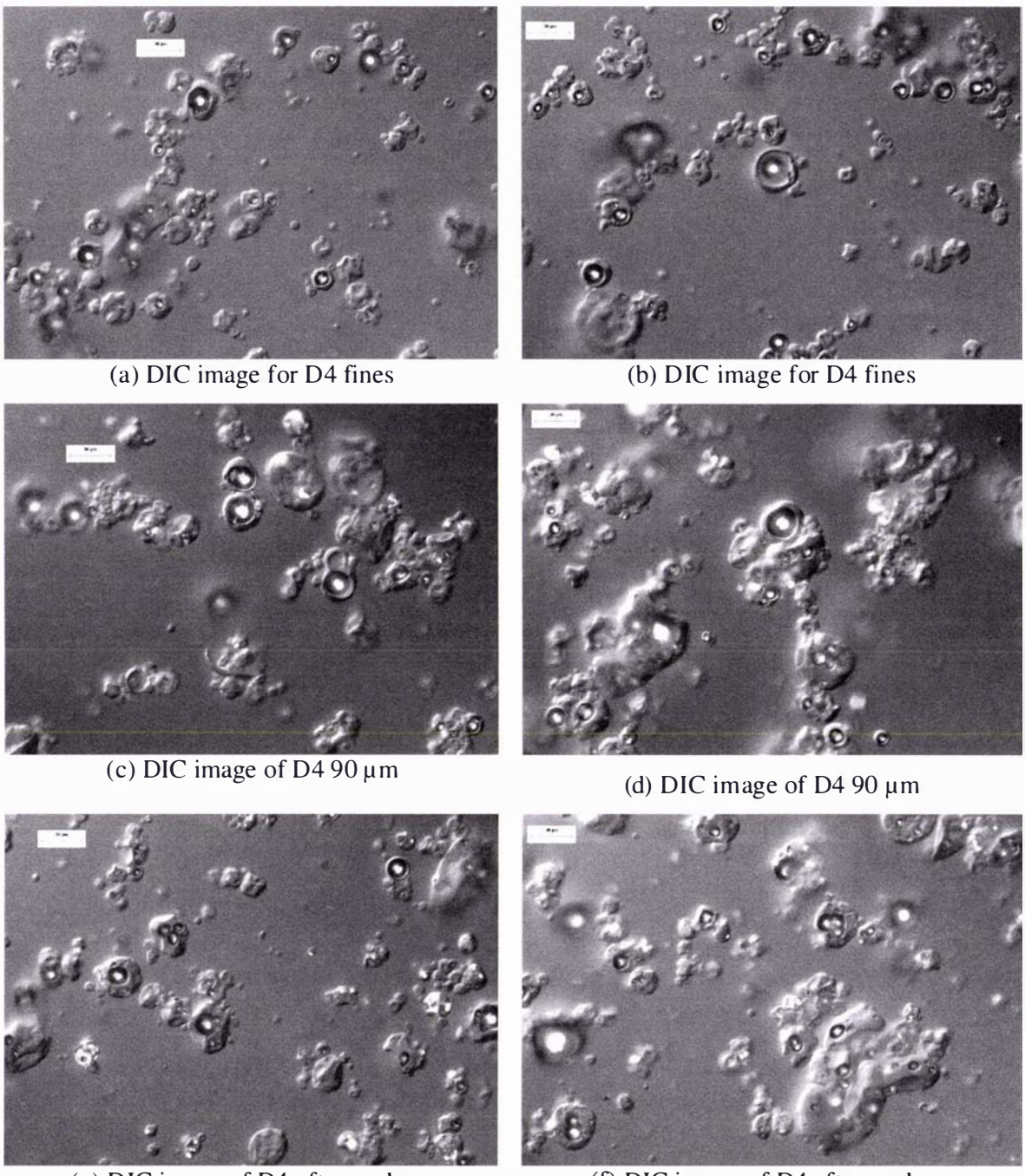

(a) DIC image for D4 fines (b) DIC image for D4 fines

(c) DIC image of D4 90 µm (d) DIC image of D4 90 µm

(e) DIC image of D4 after cyclone (f) DIC image of D4 after cyclone

Figure 7.19: DIC Images for D4 90 µm sieve, after cyclone and fines.

Experiment D5 repeated D4 using deflector wings, and the sieve stack was replaced by a single sieve supported on a stand so that the drying air flow rate was unaffected. A very low yield of 10 g was obtained on the sieve. The drier product collected in the sieve seems to be more agglomerated than the cyclone product (Figure 7.20). However this sample is a very small percentage of the total product so may not be the best

representation. The large particles (~1 mm) observed in the PSD are likely to be from deposits which have built up on the delivery chute and fallen on to the sieve. Also, particles less than 10 μm are more likely to follow the air flow into the cyclone. The *g* and *h* efficiencies for this experiment were 0.004 and 0.031 respectively. The sieve collector is not a suitable collection method for powder from the drier and as no agglomeration breakdown was observed in the cyclone, this mode of collection was used without sieves in latter experiments.

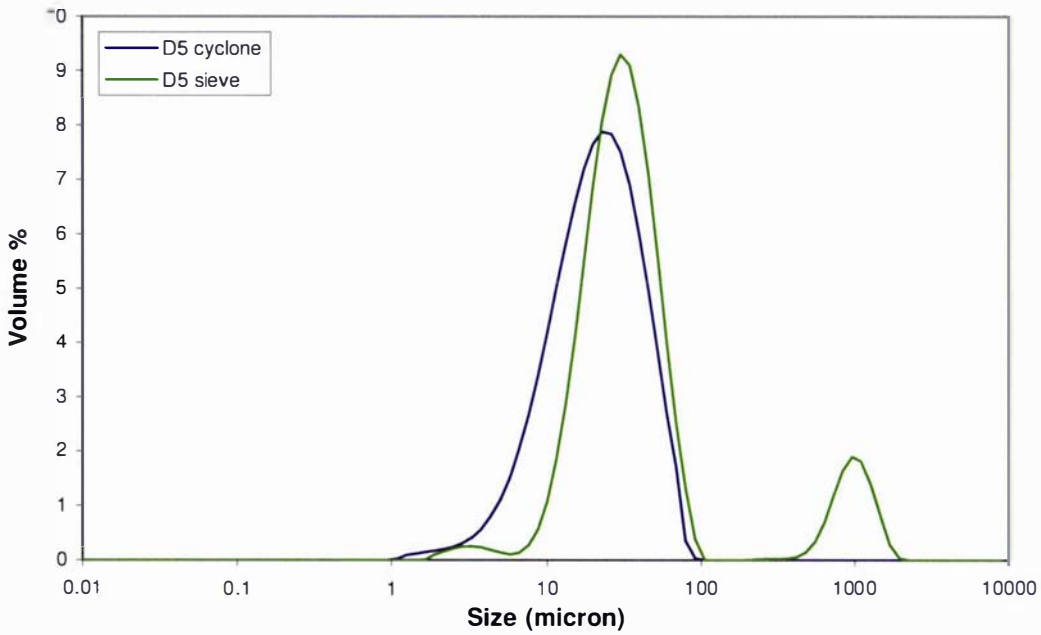

Figure 7.20: Comparison of PSDs for cyclone and sieve powders for D5.

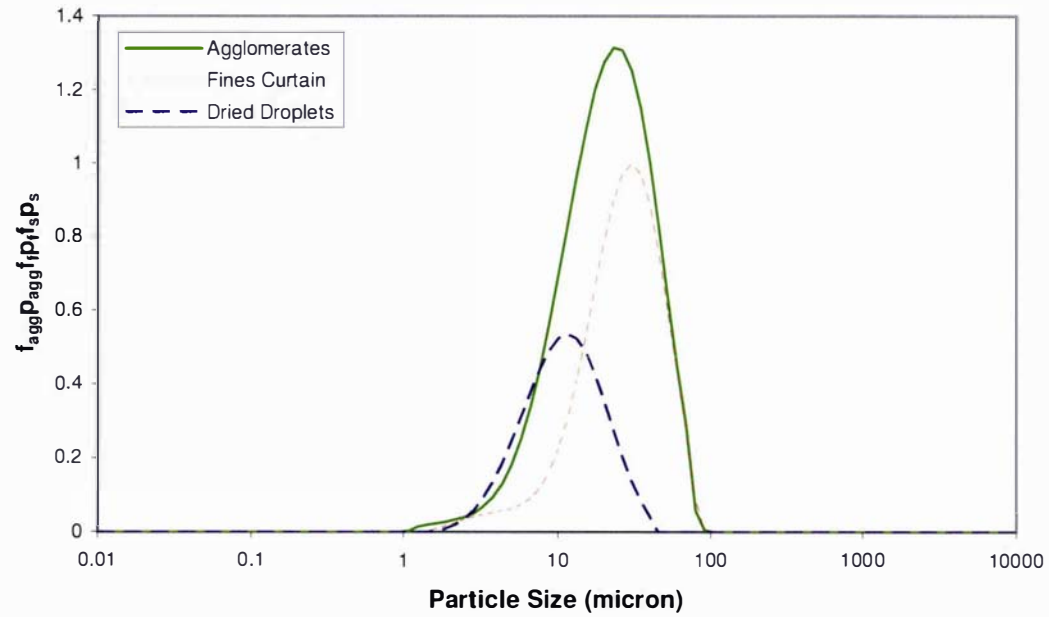

Figure 7.21: Comparing the weighted PSDs for D5.

7.3.2 Stage 2 – Experiment D6

The knowledge gained from previous experiments is used to optimise agglomeration performance. Relevant literature was also used to determine the optimum operating conditions to promote agglomeration. The flux number (FN) concept is discussed in Chapter 2 and Boerefijn and Hounslow (2005) use it as a guide to determine whether granulation or coating occurs in fluidised beds. This approach indicates that at high solids to spray ratio there is a boundary between granulation and coating. This is similar to the approach discussed by Litster et al. (2001) and Hapgood (2003) which used a binder spray flux to understand the influence of spray rate on nucleation.

Appendix Q calculates that there are more droplets than particles in the collision zone under the current conditions. Increasing the number flow rate of droplets would increase the area of the wetted particle surface. The atomiser air affects the trajectory of the curtain particles as well as dispersing the particles and droplets in the collision zone. Schelling and Reh (1999) found that increasing atomising air flow rate has little effect on air entrainment into the spray but would contribute towards increasing the overall spray velocity. It is this high induced air flow rate surrounding the spray which may contribute to the dispersion of fine particles in the collision zone. It may be necessary to reduce the velocity of the spray while still atomising effectively if the level of turbulence provided by the two-fluid nozzle is too high for agglomerates to survive after formation. The experimental work confirmed the importance of increasing the fines concentration in the collision zone (P6). Collecting powder at the base of the drier was necessary to establish that attrition in the cyclone was minimal.

Collisions occur between droplets and particles in the collision zone to produce wetted particles which also collide. The velocity of these subsequent collisions must be low enough to prevent rebound. The droplets should also be sticky enough to ensure the formation of liquid bridges between particles. The use of Stokes' law to determine the likelihood of coalescence is discussed in §2.5.1. This approach was used to determine the maximum collision velocity, 3.9 m s^{-1}. The calculations are included in Appendix Q and highlight the importance of reducing the collision velocity, maximising the thickness of the liquid layer and increasing the droplet viscosity to ensure coalescence and not rebound occurs when two wetted fines particles collide. The conditions given in Table 7.3 were deduced to optimise agglomeration based on the preliminary experiments P1 – 6 and the design improvement trials D1 – 5. These calculated optimal conditions were used in experiment D6. However, the results show very little change was observed between the agglomerates, curtain and spray particle size distributions (Figure 7.22). The agglomeration efficiency improved marginally to g efficiency = 0.013 and h efficiency = 0.058.

Table 7.3: Conditions to optimise agglomeration.

Variable	Units	Level
Concentrate Flow rate	(kg h^{-1})	2
Total Solids	(%)	47
Atomisation Pressure	(bar)	1.5
Fines Particle Size $D_{4,3}$	(μm)	30
Fines Flow rate	(kg h^{-1})	1
Curtain Depth	(mm)	10

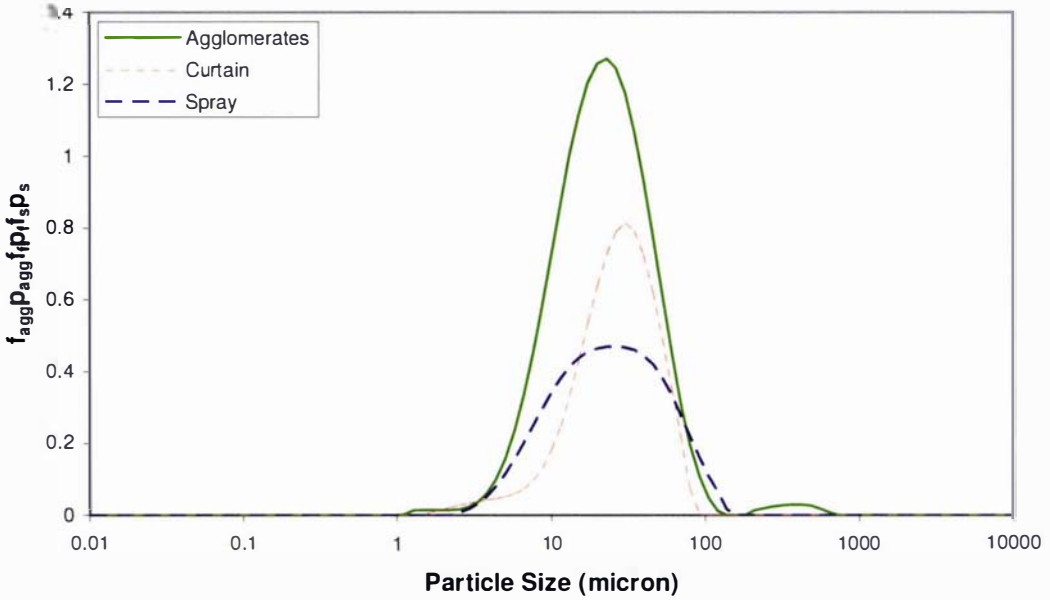

Figure 7.22: Comparing the weighted PSDs for D6.

7.3.3 Stage 3 – Experiments D7 and D8

This section discusses the results of Stage 1 (experiments D1 - 5) and 2 (experiment D6) and uses ξ_h to determine the optimum design for studying forced agglomeration on a small scale drier. Chapter 6 introduced the *h* efficiency as a better way to assess agglomeration performance. This *h* efficiency was developed following a pilot scale study and is based on the industrial situation where fines are recycled and so the extent of agglomeration needs to be defined in terms of changes experienced between the product and the spray. As discussed later in Chapter 8, although the small scale experiments have a low level of agglomeration observed in experiments P1 to P6 and D1 to D6, these efficiencies compare with those observed on a pilot scale drier which is discussed further in Chapter 8. The *g* and *h* efficiencies are compared for all small scale experiments in Table 7.4. The operating conditions have been included.

The efficiencies show that increasing the fines concentration increased agglomeration (by comparing P4 and P6) this was enhanced further by using a sieve collector to sample the product directly from the drier (D4). The D5 operating conditions resulted in the lowest level of agglomeration. This experiment repeated the operating conditions used for experiment D4 and used the deflector wings to further reduce fines dispersion. This low level of agglomeration may have been due to the build up of droplets on the opposite deflector. Subsequently, the length of this was reduced by 15 mm for further trials. Experiments P4, P5, P6 and D4 all show high levels of agglomeration at small particle sizes, low total solids and without the deflector wings.

Table 7.4: Comparing all small scale experiments with *g* and *h* efficiency.

Exp	S	F	$D_{f,4,3}$	TS	P	D	FS	SC	W	ξ_g	ξ_h
Unit	(kg h^{-1})		(µm)	(wt%)	(bar)	(mm)					
P1	2.0	1.0	30	42.3	1.5	30	No	No	No	0.108	0.118
P2	2.1	1.1	30	40.9	1.5	30	No	No	No	0.092	0.117
P3	2.1	2.1	58.8	47.5	2.5	10	No	No	No	0.011	0.099
P4	1.4	1.0	30	41.2	2.5	30	No	No	No	0.023	0.169
P5	2.1	2.0	30	41.3	1.5	30	No	No	No	0.018	0.184
P6	1.4	1.1	30	41.6	2.5	30	Yes	No	No	0.025	0.175
D1	1.2	25	30	-	-	30	Yes	No	No	-	-
D2a	1.2	25	30	-	1.5	30	Yes	No	Yes	-	-
D2b	1.2	25	30	-	2.5	30	Yes	No	Yes	-	-
D3	1.4	1.2	30	0.0	1.5	30	Yes	No	No	0.006	0.006
D4	1.4	1.1	30	41.7	2.5	30	Yes	Yes	No	0.045	0.361
D5	1.4	1.1	30	41.6	2.5	30	Yes	Yes	Yes	0.004	0.031
D6	2.1	1.1	20	47.3	1.5	10	Yes	No	Yes	0.013	0.058
D7	1.4	1.1	30	41.5	2.5	30	Yes	No	No	0.023	0.178
D8	1.4	1.2	30	41.6	2.5	30	Yes	No	Yes	0.028	0.236
U1	1.4	1.0	30	41.4	-	30	Yes	No	No	0.002	0.002

S = concentrate spray flow rate, F = fines flow rate, $D_{f,4,3}$= volume weighted mean particle size of fines, TS = total solids of concentrate, P = atomisation pressure, D = curtain depth, FS = fines shroud, Nozzle distance from centre of curtain = 65 mm (for P1) and 50 mm for all other experiments, W = deflector wings, SC = sieve collector, ξ_g = agglomeration efficiency, ξ_h = efficiency excluding fines from product..

The fines to spray mass flux ratio (discussed in §2.5) shown in Figure 7.23 for those experiments using small fines and low total solids concentrate, a linear relationship between the fines to spray flux ratio and the *h* efficiency. The two outliers do not follow this trend and these data points relate to the experiments where the sieve collector was used (D4 and D5). The two configurations of the sieve collector either blocked the exhaust which reduced the drying air flow rate (D4) or was ineffective at collecting a sufficient amount of product (D5). These two outlier data points are omitted from further discussions.

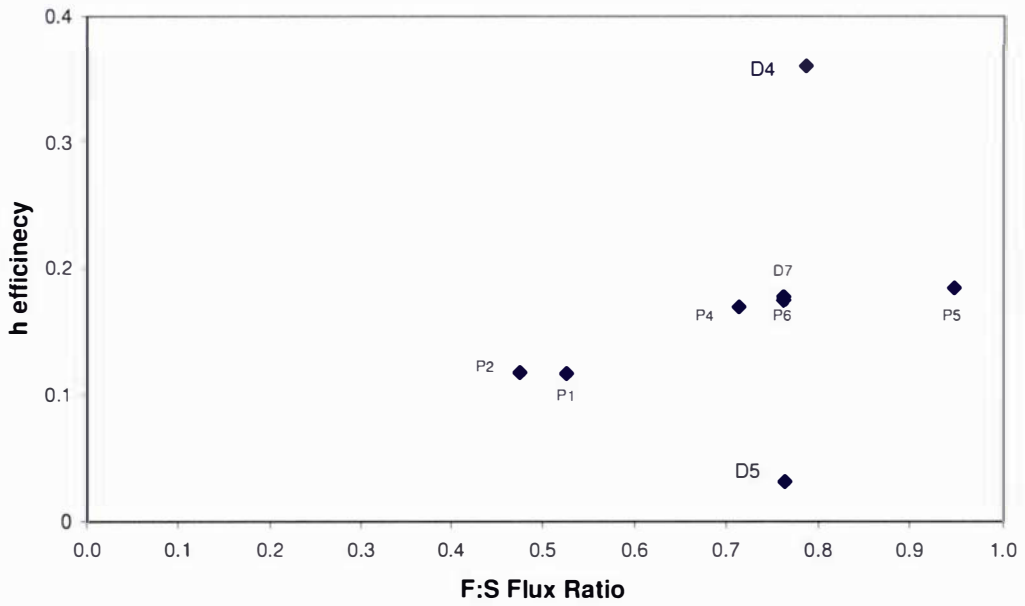

Figure 7.23: Mass Flux Ratio vs. *h* efficiency for small fines and low TS at small scale.

Figure 7.24 shows that D7 (same conditions as D4 without the sieve collector), has the same relationship. Experiment D8 repeated the conditions used in D7 (including deflector wings) and had a slightly increased agglomeration efficiency. The build-up of spray on the deflector wings reduced drier running time and decreased air/spray mixing meant the wings were not ideal. The equipment used to perform D7 was found to be the optimum design and was used in all further experimentation.

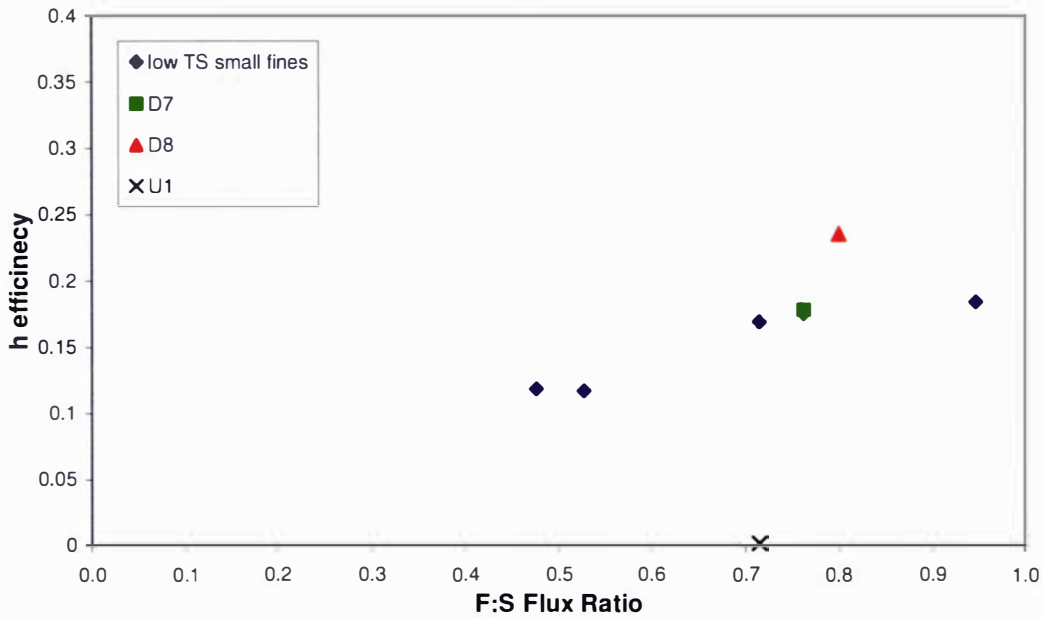

Figure 7.24: Mass flux ratio vs. *h* efficiency for small fines and low total solids

7.3.4 Stage 4 – Experiment U1

An ultrasonic nozzle was sourced to reduce the velocity of the spray. By eliminating the atomising air (see §7.3.1). This nozzle was found to atomise concentrate at the low flow rates required and did not foul or block easily during running unlike the two-fluid nozzle. The ultrasonic nozzle required a narrow power range to product an effective spray at a particular flow rate. Once this was achieved it was very difficult to collect enough powder to perform the required tests for the spray only case (~ 200 g) as a low yield of only 15 g per hour was achieved. The narrow spray pattern when atomising concentrate (significantly narrower than when atomising water) resulted in few fines particles being contacted by the spray droplets and the momentum difference between particles and droplets means it is unlikely that effective agglomeration occurred. In the assessment of agglomeration performance, the droplet size of the spray was ignored since such a small amount of the spray product could be collected. An agglomeration efficiency of 0.002 was obtained and as the figure below demonstrates there was no change observed between the fines and agglomerate particle size distributions.

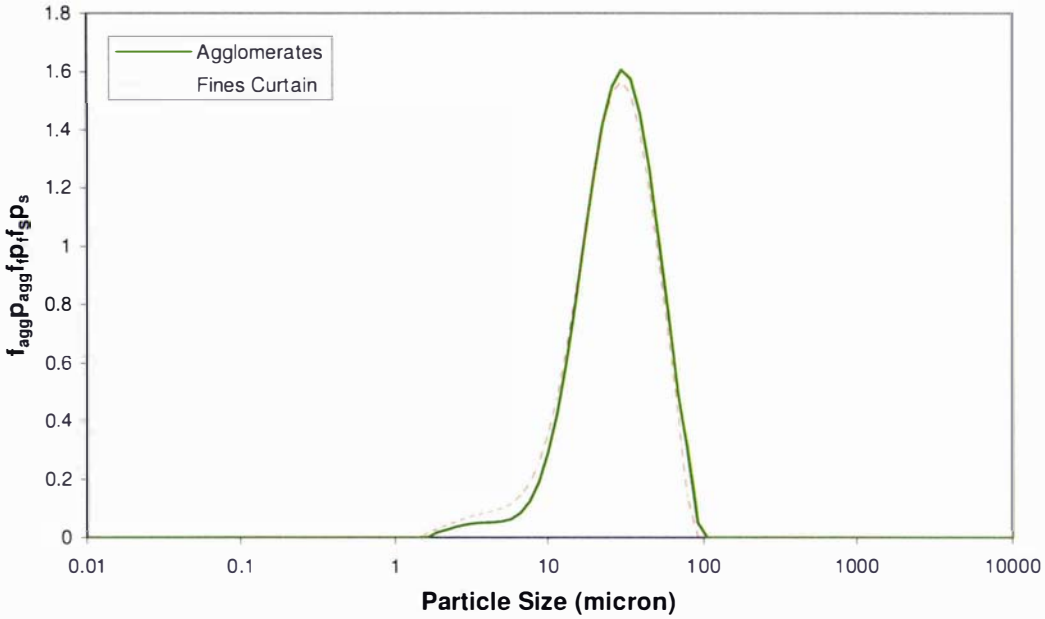

Figure 7.25: Comparing weighted PSDs for U1 - ultrasonic nozzle.

7.4 Forced Agglomeration Yield

Product yield was ~ 40 % for the natural agglomeration trials presented earlier, which is lower than the 50 % figure suggested by Bhandari et al. (1997) to indicate successful drying and below this yield is considered marginally successful. Figure 7.26 shows the yield for the forced agglomeration experiments from both the preliminary and design improvement experiments. This demonstrates that experiments with a powder curtain generally have yields that are higher than 50% which are also higher than the product yields from the spray-only, natural agglomeration experiments. Also, it is clear that spray drying milk concentrate at lower solids concentrations is more successful and produces higher yields.

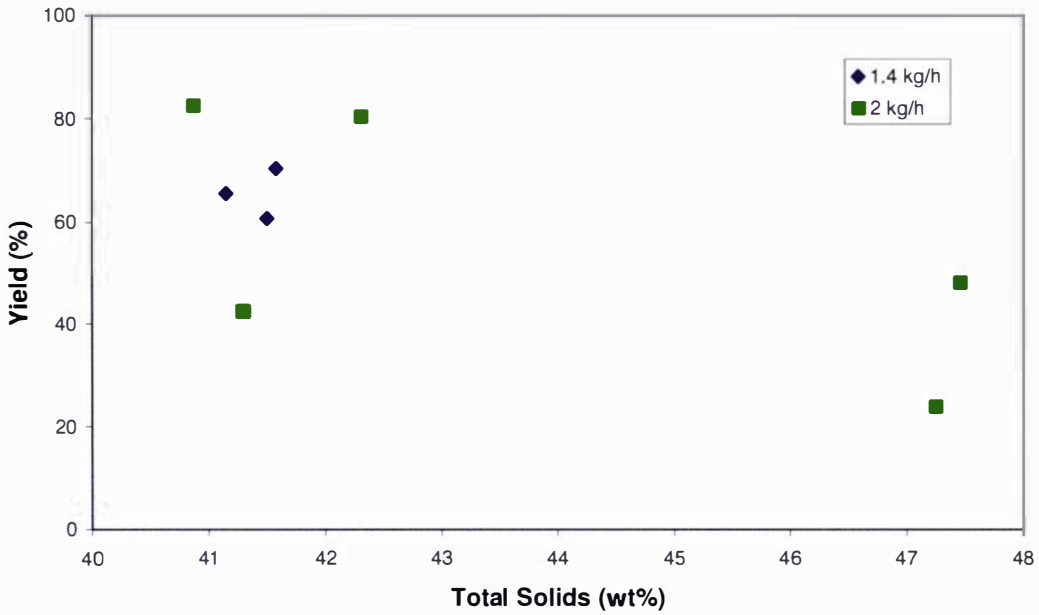

Figure 7.26: Product yield vs. total solids at several concentrate flow rates.

7.5 Forced Agglomeration Results

The final forced agglomeration experiments study the additional effect of fines to spray flux ratio and fines particle size on agglomeration efficiency. These were necessary to demonstrate the effect of two important variables on agglomeration efficiency using the optimised design. Experiment A1 had lower fines to spray mass flux ratio than previous experiments. Figure 7.27 shows that it lies on the same trend line as other experiments that had low total solids concentrate and small fines size ($D_{4,3}$ ~ 30 μm). Experiment A2 had identical operating conditions to experiment A1, but with larger fines ($D_{4,3}$ ~ 58.8 μm). Figure 7.27 shows that this gave a higher agglomeration efficiency when spraying low total solids concentrate. These results are compared to the pilot scale experimental results in §8.4.

Table 7.5: Experimental results for final agglomeration experiments.

Exp	S	F	$D_{f,4,3}$	TS	P	D	FS	SC	W	ξ_g	ξ_h
Unit	(kg h^{-1})		(μm)	(wt%)	(bar)	(mm)					
A1	2.1	0.8	30	42	2.5	30	Yes	No	No	0.027	0.098
A2	2.0	0.8	58.8	41	2.5	30	Yes	No	No	0.053	0.207

S = concentrate spray flow rate, F = fines flow rate, $D_{f,4,3}$= volume weighted mean particle size of fines, TS = total solids of concentrate, P = atomisation pressure, D = curtain depth, FS = fines shroud, Nozzle distance from centre of curtain = 50 mm, W = deflector wings, SC = sieve collector, ξ_g = agglomeration efficiency, ξ_h = efficiency excluding fines from product.

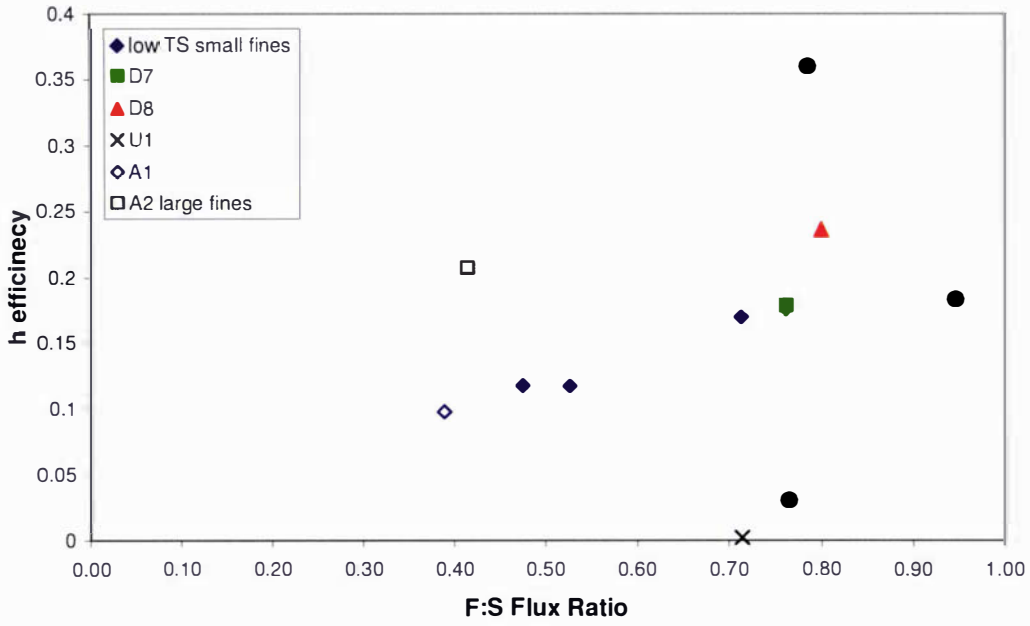

Figure 7.27: Mass flux ratio vs. *h* efficiency comparing low TS, small fines with final agglomeration experiments (A1 and A2).

7.6 Chapter Conclusions

This chapter investigated natural (without a fines curtain) and forced agglomeration (with a fines curtain) in a modified small scale Niro spray drier. The study of natural agglomeration identified a link between the particle size and bulk density of the product and observed that little natural agglomeration occurred between spray droplets in the small scale drier. The product yield was found to be unacceptably low (~40%) due to adhesion of spray droplets to the drying chamber wall. Product yield for the forced agglomeration experiments was found to be acceptable (> 50%) due to introduction of the fines curtain to collect spray droplets.

A series of preliminary experiments found that the agglomeration performance of the modified spray drier was lower than expected when delivering a fines curtain. A subsequent study optimised the equipment design by considering three key issues; fines dispersion, droplet dispersion and stickiness, and agglomerate breakdown. Deflector wings were designed to improve the fines curtain shape and reduce fines dispersion in the collision zone but were rejected because they reduced run times due to accumulation of deposits. A sieve collector was used to determine that agglomerate breakdown in the cyclone was minimal and was afterwards removed because as powder accumulated on the sieves the drying air flow rate decreased. An ultrasonic nozzle was trialled to eliminate droplet dispersion; however, its spray velocity was too low to promote collisions between droplets and particles. Further experiments then studied agglomeration at low fines to spray mass flux ratios and showed that increasing the fines size had a positive effect on agglomeration efficiency, ξ_h. Chapter 8 details the pilot scale study where the agglomeration efficiency is studied as a function of operating variables. The results at both scales are then compared and discussed with respect the relevant mechanisms of agglomeration.

CHAPTER 8

PILOT SCALE EXPERIMENTS

Chapter 7 concludes that small scale experiments design improvements enhanced agglomeration. It established that agglomeration performance on a small scale is much lower than in industry. The reason is not known but may relate to scale or to the mode of operation: the small scale trials had one pass of the fines powder through the spray zone whereas industrial scale operates with recycle. Here pilot scale agglomeration is studied as a function of operating parameters in both single pass and recycle operating modes. Three stages of pilot scale investigations were conducted: base case trials, production of fines and the experimental program. The base case trials established the operating ranges for the experimental study. Fines were needed for the sensitivity analysis conducted in the experimental programs. Each of these is discussed in the sections below.

8.1 Base Case Trials

The purpose of these base case investigates was to determine the extent of agglomeration when operating at standard conditions. The IFB drier at Fonterra Palmerston North was used (see §3.3.1). The drying runs are detailed below and relate to the running conditions included in Table 8.1. The only differences between the runs concern the delivery and collection of the fines stream.

1. Base Case 1 Recycle fines and collect product from the drier (see Figure 8.1).
2. Base Case 2 Eliminate fines recycle and collect from the cyclone (to estimate fines flow rate) and the drier (to find the spray only product) (see Figure 8.2).
3. Base Case 3 Deliver fines remotely and collect from the cyclone and drier to simulate a one pass agglomeration experiment (see Figure 8.3)

In order to conduct BC 3, a reliable fines metering system was needed. This is addressed below, after which the results are discussed.

Table 8.1: Running conditions for base case trials.

Run	Conc Flow Rate	Conc Pressure	Inlet Air Temp	Outlet Air Temp	Conc Temp	Conc density	Viscosity @ 1000 s^{-1}	Total Solids
Units	**(L h^{-1})**	**(kPa)**	**(°C)**	**(°C)**	**(°C)**	**(kg m^{-3})**	**(mPa s)**	**(%)**
BC 1	131	141	197	94	68.6	1207	46.5	48.0
BC 2a/b	129	140	197.1	95.3	69.7	1205	49.5	48.0
BC 3	114	141	197	96.7	69.8	1205	54.4	49.0

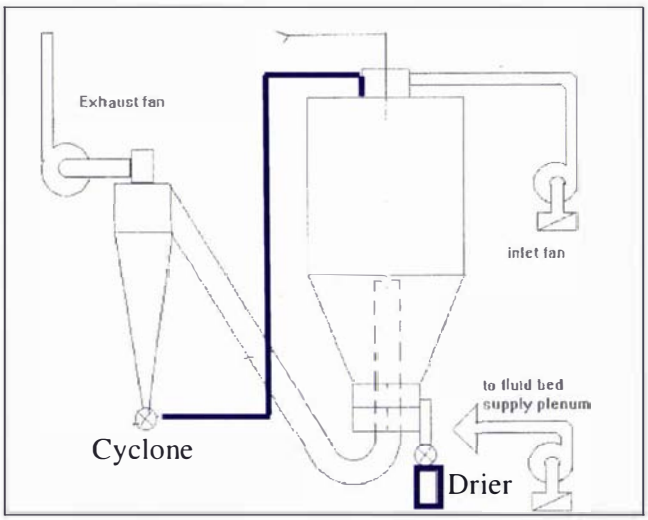

Figure 8.1: Schematic of IFB configuration for BC 1.

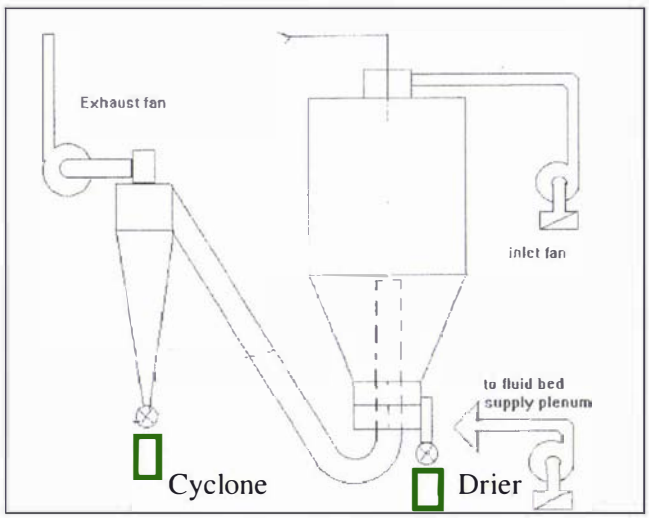

Figure 8.2: Schematic of IFB configuration for BC 2a and 2b.

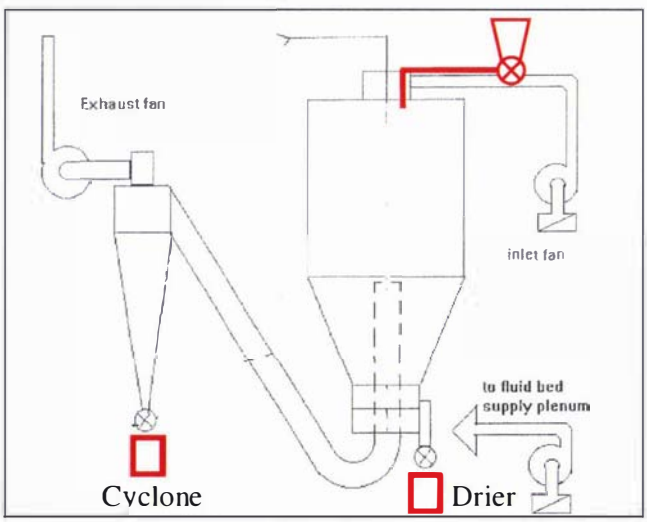

Figure 8.3: Schematic of IFB configuration for BC 3.

8.1.1 Calibration of Solids Feeder

The fines flow rate is a required experimental variable and Figure 8.3 shows a solids hopper and rotary value (4 vanes), which drops the powder into the blow line to deliver fines remotely to the drier. The solids feeder system was calibrated using standard skim milk powder produced on the IFB drier with a volume weighted mean particle size, $D_{4,3}$, of 70.5 μm. Figure 8.4 shows that the calibration for the solids feeder is linear and demonstrates that the current rotary valve can deliver a high powder flow rate. Air pulsing (25 p.s.i.) was used to aid powder flow from the solids hopper to the rotary valve, however, at low flows bridging occurred and a mallet was needed to vibrate the section before the rotary valve. As fines recycle rates were ~ 35 kg h^{-1}, which is at the low end of this calibration curve, later work required finer adjustment at the low end of the range and so the rotary valve was altered as discussed in §8.3.1.

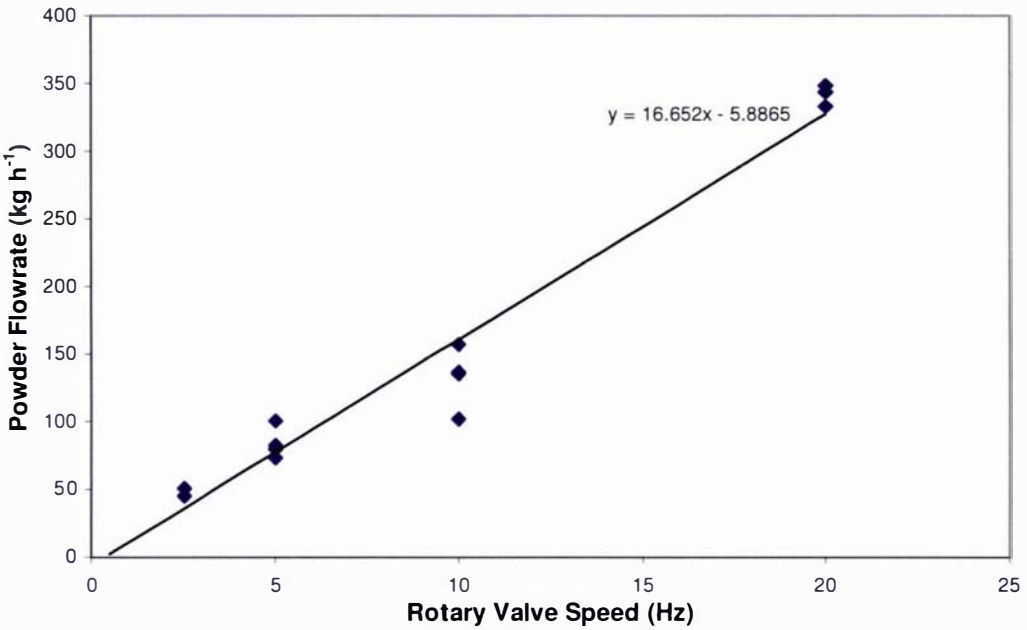

Figure 8.4: Calibration of solids feeder powder flow rate vs. rotary valve speed.

8.1.2 Product and Fines Properties

BC1 has the drier operating in recycle mode. BC 2a and b have the drier operating in spray only mode where the powder is collected both at the drier outlet and the cyclone (at a rate of ~34 kg h^{-1}). BC3 has the drier operating in single pass mode where fines are metered into the drier from a hopper (at a rate of 50 kg h^{-1} which is the lowest controllable delivery rate achievable using the 4 vane rotary valve) and collected at both the drier outlet and cyclone. The larger total mass flow of BC 3 in Figure 8.5 is due to the addition of fines. Figure 8.6 shows the rate of mass loss from the solids feeder hopper as recorded by the load cell. This shows that solids are being fed consistently at the calibrated rate of ~ 50 kg h^{-1} (0.0141 kg s^{-1}). From these preliminary trials, a fines addition rates of 35 kg h^{-1} was selected as the mid point for the experimental program in §8.3; 20 kg h^{-1} and 50 kg h^{-1} were selected as the low and high levels about the midpoint. The size distributions from BC 2a Cyclone and BC 2b Cyclone (which

represent the fines) are included below (Figure 8.7) and have volume weighted mean sizes of 53.5 and 52.6 μm respectively. As the fines were needed for later agglomeration experiment and so the above information is crucial for planning the mass of fines that need to be produced at each size (see §8.2). The mean particle sizes, particle and bulk densities are listed in Table 8.3.

Table 8.2: Flow rate measurements taken for BCs 1 to 3.

Run	Rep	Drier			Cyclone			Total
		Mass	Time	Flow	Mass	Time	Flow	Flow
		(kg)	(s)	(kg h^{-1})	(kg)	(s)	(kg h^{-1})	(kg h^{-1})
BC 1	1	6.295	300	75.5				
	2	6.245	300	74.9				
	3	6.04	300	72.5				
	4	6.015	300	72.2				
	Average			73.8				73.8
BC 2a	1	2.72	300	32.6	1.885	225	30.2	
	2	2.885	300	34.6	1.77	210	30.3	
	3	2.585	300	31.0	2.025	225	32.4	
	Average			43.0			31.0	74.0
BC 2b	1	3.315	315	37.9	2.595	210	44.5	
	2	2.495	300	29.9	1.565	180	31.3	
	3	2.5	300	30.0	2.455	220	40.2	
	4				2.075	240	31.1	
	Average			32.6			36.8	69.4
BC 3	1	5.16	300	61.9	2.465	180	49.3	
	2	4.855	300	58.3	2.63	180	52.6	
	3	4.56	300	54.7	2.345	180	46.9	
	Average			58.3			49.6	107.9

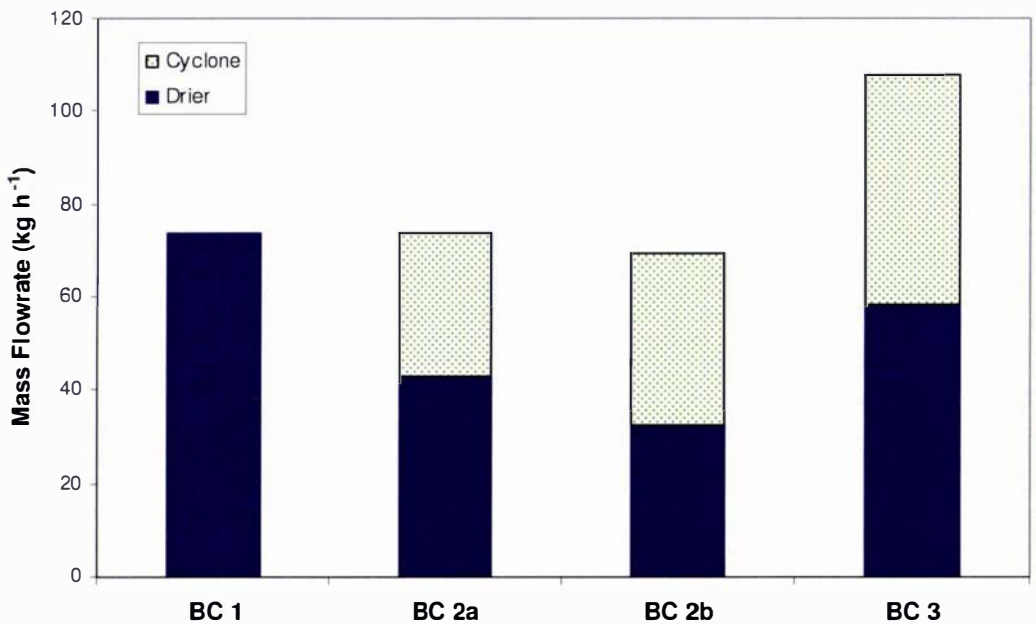

Figure 8.5: Drier and cyclone mass flow rates for BC 1 to 3.

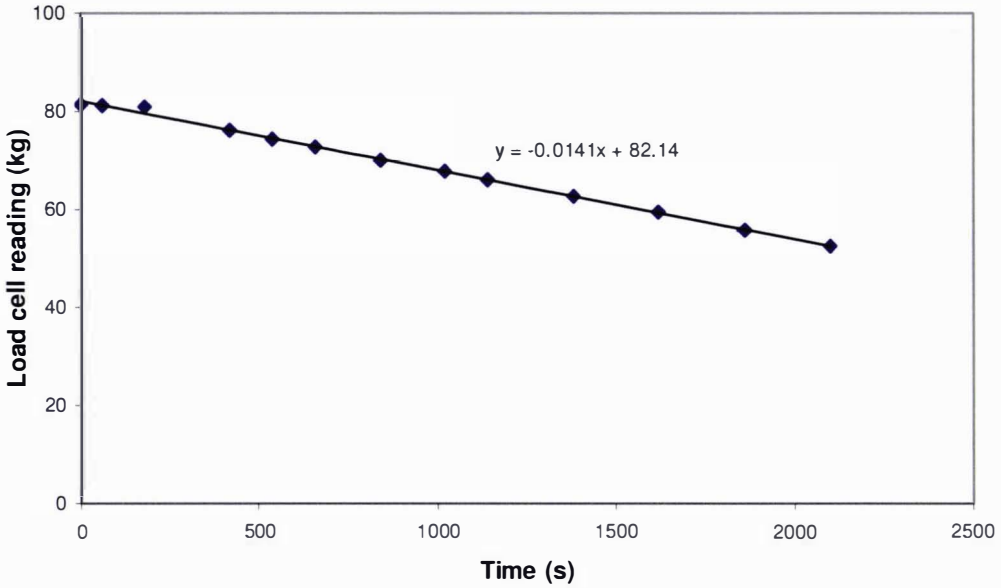

Figure 8.6: Load cell reading vs. time for solids feeder.

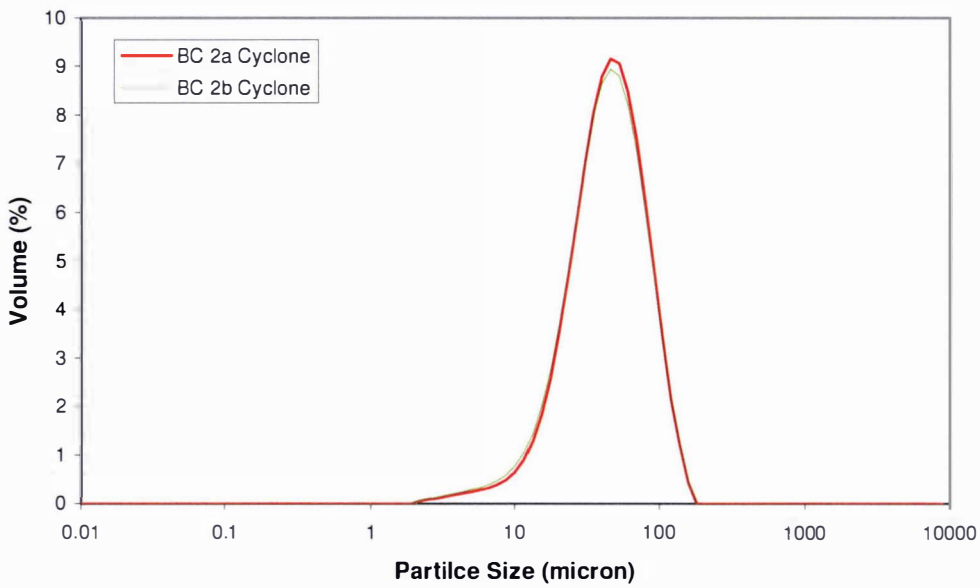

Figure 8.7: Comparing the PSDs of BC 2a Cyclone and BC 2b Cyclone.

Table 8.3: Mean sizes, particle and bulk densities from trial investigation.

Run	Drier			Cyclone		
	$D_{4,3}$	Particle Density	Bulk Density (100 taps)	$D_{4,3}$	Particle Density	Bulk Density (100 taps)
Units	(µm)	(g cm^{-3})	(g cm^{-3})	(µm)	(g cm^{-3})	(g cm^{-3})
BC 1	128.5	1.33	0.51			
BC 2a	97.0	1.26	0.66	53.5	1.31	0.66
BC 2b	91.4	1.30	0.67	52.6	1.32	0.71
BC 3	119.0	1.25	0.57	58.4	1.34	0.70
SMP	70.5	1.23	0.64			

8.1.3 Pilot Plant Droplet Size Estimation

As discussed in Chapter 4, droplet size was able to be measured by a range of commercial laser diffraction devices. The difficulty with spray sizing is to obtain a representative population of droplets from the spray, measurement of a pilot/industrial scale nozzle is even more difficult as the high droplet velocity and spray density means measurements may be inaccurate using standard laser diffraction measurement systems. Malvern have a specialty piece of equipment, the Spraytec system, which can measure these sprays, however, this can not be used in situ.

An implicit method of droplet sizing is to operate a single spray nozzle within a spray drier without any fine powder recycle. The collected dried droplets can be regarded as particles formed without any of the design or operating features that enhance agglomeration. This method is discussed further in §4.6 and was similarly used in the small scale study. Table 8.4 includes the shrinkage ratios for droplets dried in the IFB drier using the methods of Lin and Chen (2004) and Masters (1979). For BC 2b product, the mean particle size was determined by combining the streams from the cyclone and the drier. The mean droplet size obtained from this calculation is almost the same as the standard skim milk powder (SMP) which was used to calibrate the solids feeder in §8.1.1. From this calculation the mean droplet size for the IFB drier can be estimated as ~ 100 µm. Figure 8.8 shows the measured dried droplet distribution for BC 2b product and uses the shrinkage ratio calculated using Masters' approach to calculate a droplet size distribution.

Table 8.4: Estimated volume weighted droplet sizes.

BC	Particle Size	Shrinkage Rates		Droplet Size	
		Lin & Chen	Masters	Lin & Chen	Masters
	(µm)	(-)	(-)	(µm)	(µm)
BC 2b product	70.9	0.76	0.67	93	106
SMP	70.5	0.76	0.64	93	109

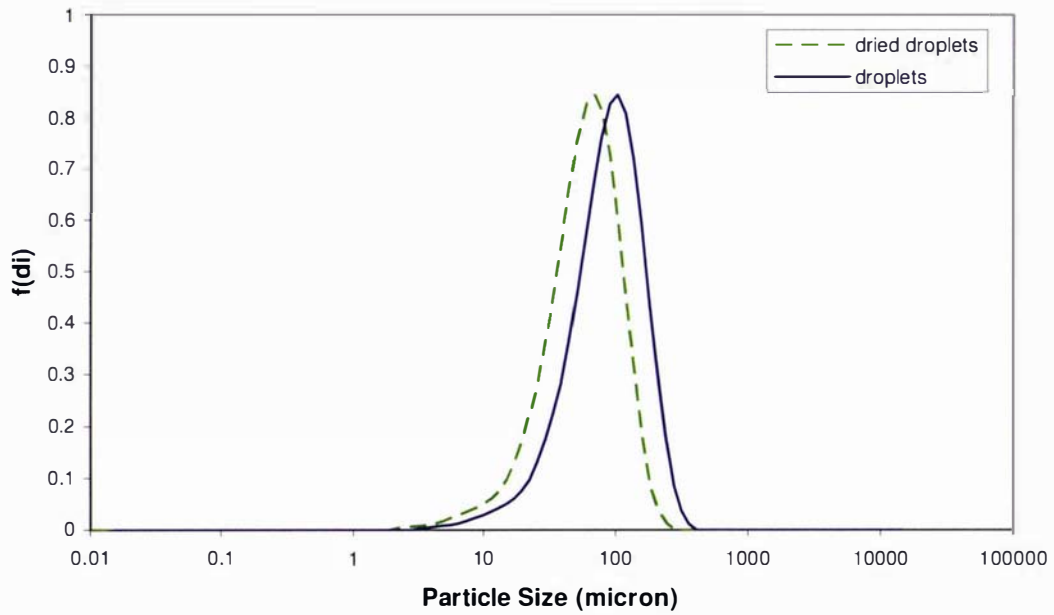

Figure 8.8: Measured dried droplet & calculated droplet distribution for BC 2b product.

8.1.4 Extent of Agglomeration

To determine the extent of agglomeration, the outlet streams are compared to the inlet streams. This is done differently depending on the configuration of the drier. In §6.5 the *h* efficiency, $\check{\zeta}_h$, is argued to be the best indicator of agglomeration extent. The configuration shown in Figure 8.9a) and b) correspond to those in Figure 6.6b) and c). The agglomeration efficiency for Figure 8.9a) is therefore a comparison of the size distributions between streams *d* and *s*. The *d* stream is the powder collected from the drier and the *s* stream is the spray (on dried droplet basis) obtained when operating the drier under spray only conditions. Under steady state conditions the flow of the recycle stream, c, and its size distribution are expected not to change. Section 6.5 shows the difference between the distributions (when weighted to their flow rates) yields a measure of the agglomeration. The formulae for the configurations are given by equations (6.21) to (6.24).

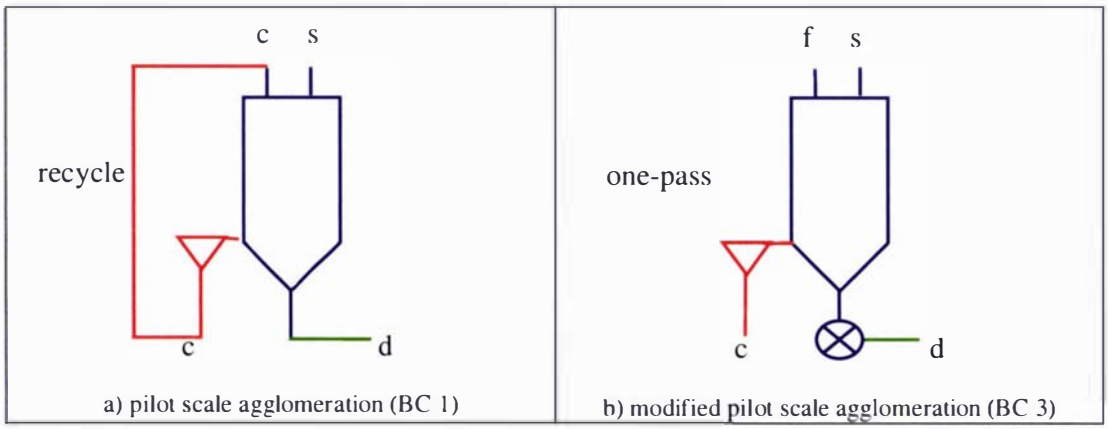

Figure 8.9: Equipment set up for the pilot and modified pilot scale experiments.

Figure 8.11 indicates a shift in particle size between the fines and agglomerates for the pilot scale recycle experiment (BC 1); however this was not observed in the one pass trial for BC 3 in Figure 8.12. It was postulated in Chapter 7 that the agglomerates that form when operating a drier under the one-pass design (at either pilot or small scale) are obscured by the fines present in the product and are not detected using the *g* method for the agglomeration efficiency index. To remove some of this obscuration it was proposed to remove the influence of the fines by censoring them from the agglomerated powder stream to give a better "view" of the agglomerates. This approach is derived from the industry situation where the fines are re-circulated in the system and assesses the transformation or agglomeration that has occurred from the spray to the product. This is referred to as the *h* efficiency, $\check{\zeta}_h$, and is discussed in §6.5.

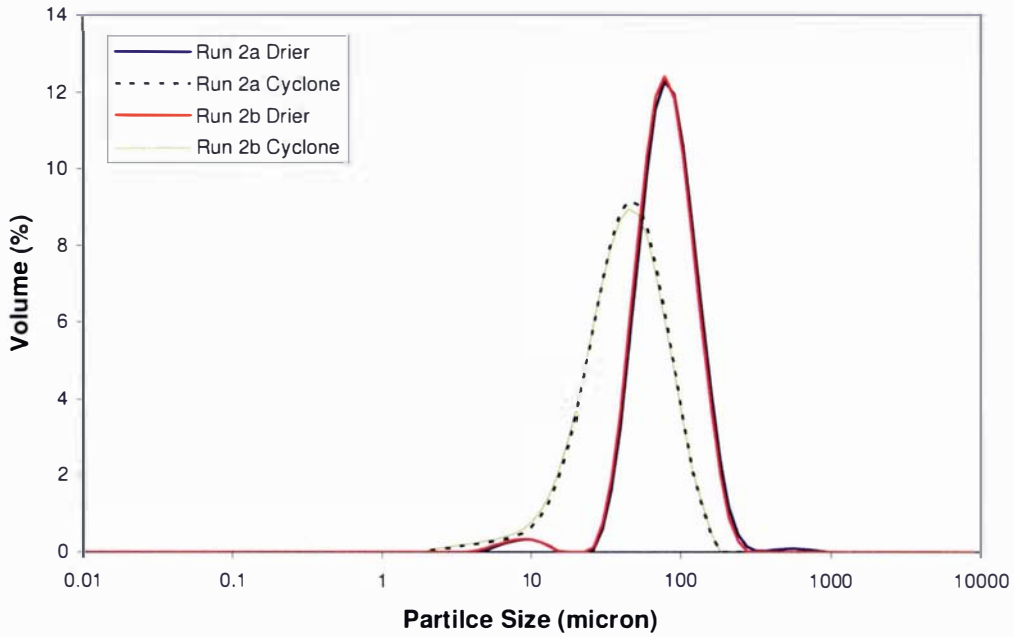

Figure 8.10: Comparing PSDs for BC 2a and BC 2b operated in spray only mode.

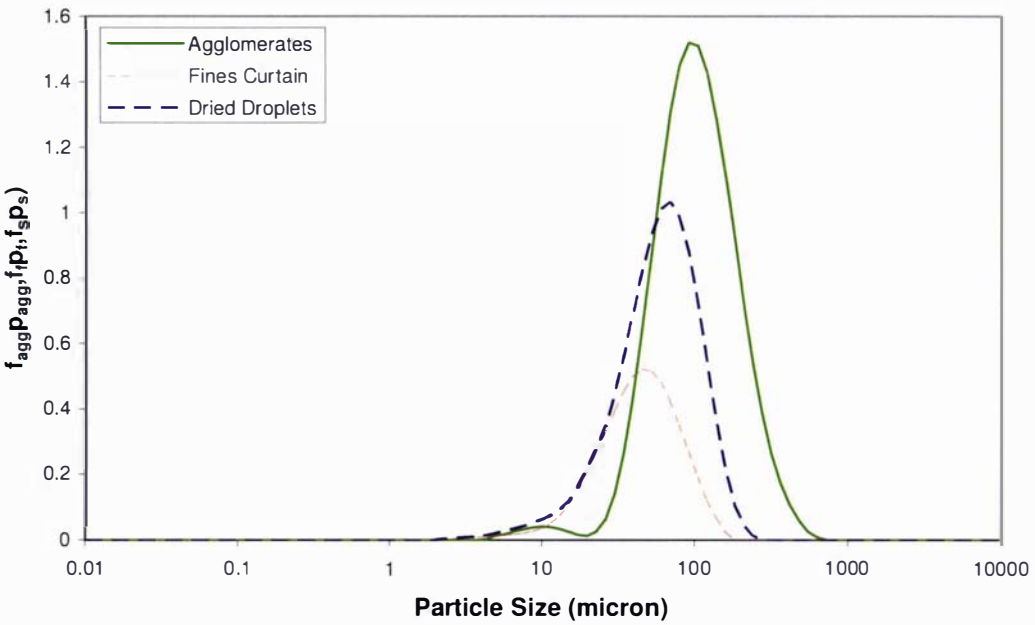

Figure 8.11: Comparing weighted PSDs for BC 1 operated in recycle mode.

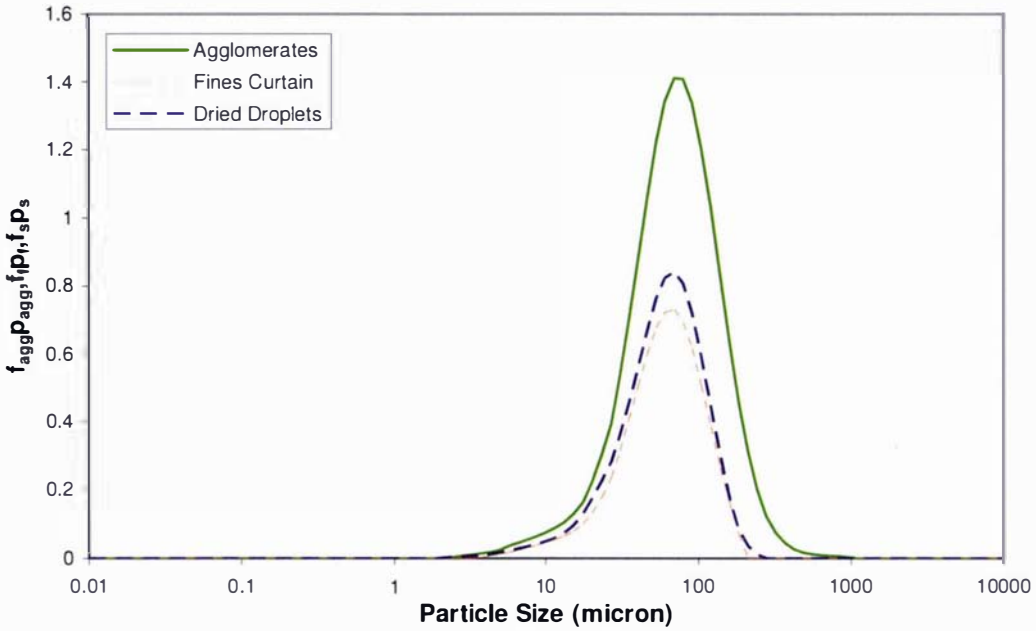

Figure 8.12: Comparing weighted PSDs for BC 3 operated in one-pass mode.

Table 8.5 compares all of the agglomeration indices with the new *h* efficiency across the different processing scales. The small scale and industry scale values are taken from Table 6.2 and Table 7.4. The *h* efficiency demonstrates that ISMP A and BC 1 are similar and D6 and BC 3 are similar. These findings also help us to conclude that the experiments carried out at small scale experienced a similar extent of agglomeration as observed using the modified pilot scale equipment when operated in one-pass mode, but when operated in the recycle mode the pilot scale drier performed similarly to the industrial scale drier. As justified (§6.5) the *h* efficiency is the better indicator of agglomeration and will be used in all future comparisons of agglomeration performance.

Table 8.5: Comparing agglomeration indices with *h* efficiency.

Scale	**Pilot Scale**		**Small Scale**	**Industry**
Reference	**BC 1**	**BC 3**	**D6**	**ISMP A**
Design	**Recycle**	**One-Pass**	**One-Pass**	**Recycle**
DoA	8.28	1.90	1.09	10.35
g efficiency	0.155	0.014	0.013	0.148
h efficiency	0.425	0.048	0.058	0.635
AP	2.25	1.09	1.54	0.84

*BCs 1 & 3 refer to the base case pilot plant investigation; D6 is a small scale experiment and ISMP A refers to the selected industrial powder

8.2 Fines Production

The more detailed experimental design explained in the next section requires three sizes of fine powder and three different flow rates. These are arranged as low medium and high about a medium centre point flowrate ~ 35 kg h^{-1} and size 53 µm. The experimental plan detailed in the next section shows that nearly 300 kg of fines are needed. The precise amounts of each size are shown in Table 8.6. It is difficult to predict what drying conditions are required to produce the three different sizes. Previous experience with the small scale experiments was used as a guide (§5.2.3). Fines of various sizes were collected from the cyclone and the drier. In FP 1 the drier was configured in one-pass design (no fines recycle) and in FP 2 the fines were returned to the fluid bed to mix with the drier powder. Table 8.7 shows the conditions used to produce the fines powder.

Table 8.6: Amount of fines to be produced for agglomeration experiments.

Size	Flow rate	Running time	Amount required	Mass to produce
(µm)	(kg h^{-1})	(h)	(kg)	(kg)
30	20	1	20	
30	50	1.5	75	95
50	35	3	105	105
70	20	1	20	
70	50	1.5	75	95
Total				295

Table 8.7: Actual running conditions used to produce fines.

Run	Conc Flow Rate	Conc P	Inlet Air Temp	Outlet Air Temp	Conc Temp	Conc density	Viscosity @ 1000 s^{-1}	TS	N
Units	(L h^{-1})	(kPa)	(°C)	(°C)	(°C)	(kg m^{-3})	(mPa s)	%	
FP1	103	220	193	96	70	1209	46.5	48.4	63/20
FP2	128	130	196	92	70	1218	54.3	50.9	56/17

The mean sizes, particle and bulk densities of the fine powders produced are included in Table 8.8 and the particle size distributions are included in Figure 8.13. Although the fines produced were larger than the size aimed for, there are still three clear sizes for the investigation. The different batches of fines are referred to as small, medium and large fines in the following sections.

Table 8.8: Mean sizes, particle and bulk densities from fines production.

Run	Drier			Cyclone		
	$D_{4,3}$	Particle Density	Bulk Density (100 taps)	$D_{4,3}$	Particle Density	Bulk Density (100 taps)
Units	(µm)	(g cm^{-3})	(g cm^{-3})	(µm)	(g cm^{-3})	(g cm^{-3})
FP 1	64.5	1.25	0.64	35.3	1.25	0.64
FP 2	101.4	1.28	0.57			

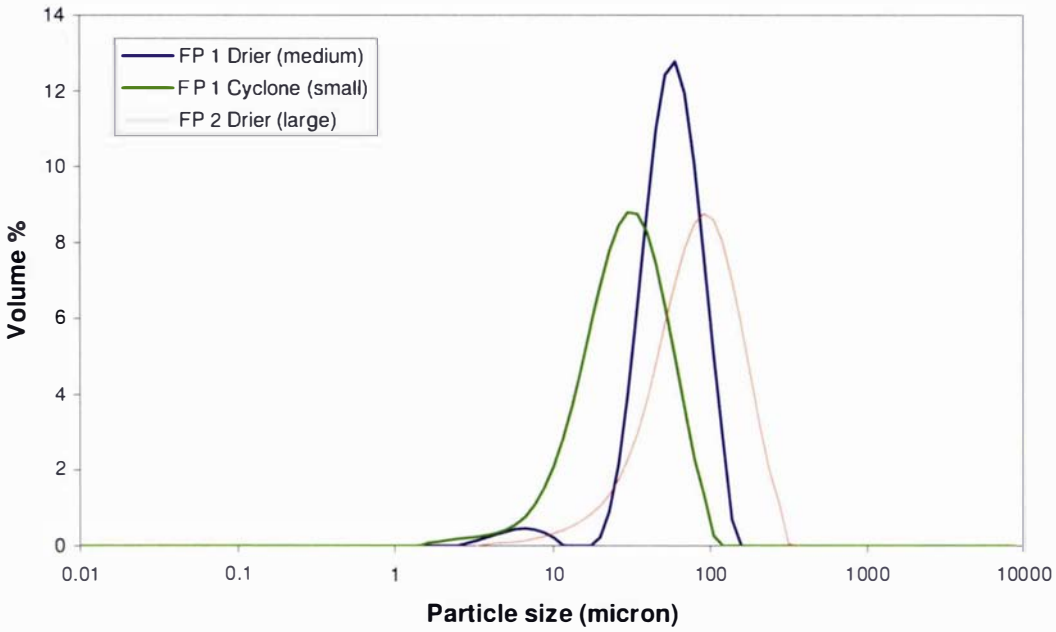

Figure 8.13: Particle size distributions of fines.

8.3 Agglomeration Experiments

This section presents a full experimental design about the base case conditions presented above. The purpose of these pilot scale experiments was to study the effect of spray drying operating parameters on agglomerate properties. The variables selected were the operating parameters most likely to have an effect on agglomeration performance. The knowledge gained during the small scale study was applied here although some variables are not easy to manipulate on the pilot scale spray drier. Unlike the small scale drier, this plant cannot independently vary the concentrate flow rate, droplet size and viscosity of the concentrate. Therefore, altering a single parameter may influence several variables.

8.3.1 Modification of the Solids Feeder

For the main agglomeration experiments, fines flow rates of 20, 35 and 50 kg h^{-1} were required which were lower than the solids feeder could deliver (Figure 8.4). Because fines flow rate was a key aspect of this study, the rotary valve was modified using plastic coving to reduce the volume of the vanes and increase the number of vanes to produce a continuous flow of powder (see Figure 8.14). The recalibration was carried out using powder with a $D_{4,3}$ particle size of 53.6 μm which is close to the actual fines size of BC 1. Figure 8.15 shows the calibration for the modified rotary valve; it was assumed to be linear in the same manner as that for the standard rotary valve. Despite reducing vane capacity, the valve was still running at the low end of the speed range and it was not easy to select a rotary valve speed in between 2.5 and 5 Hz. The two levels that were investigated in the agglomeration experiments were 27 kg h^{-1} and 52 kg h^{-1} corresponding to these speeds. Therefore the midpoint experiments were modified to 51.5 kg h^{-1} as this is similar to the fines flow rate delivered during BC 3.

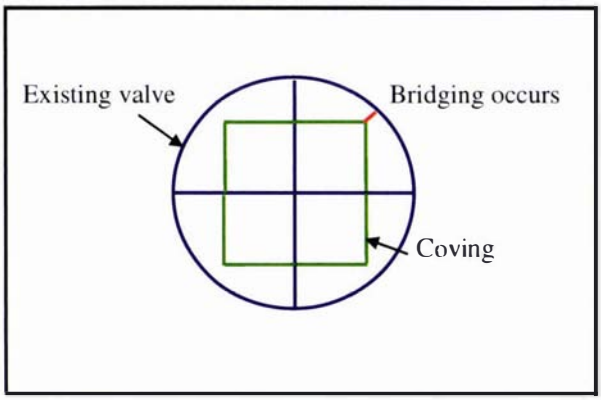

Figure 8.14: Modification of solids feeder rotary valve.

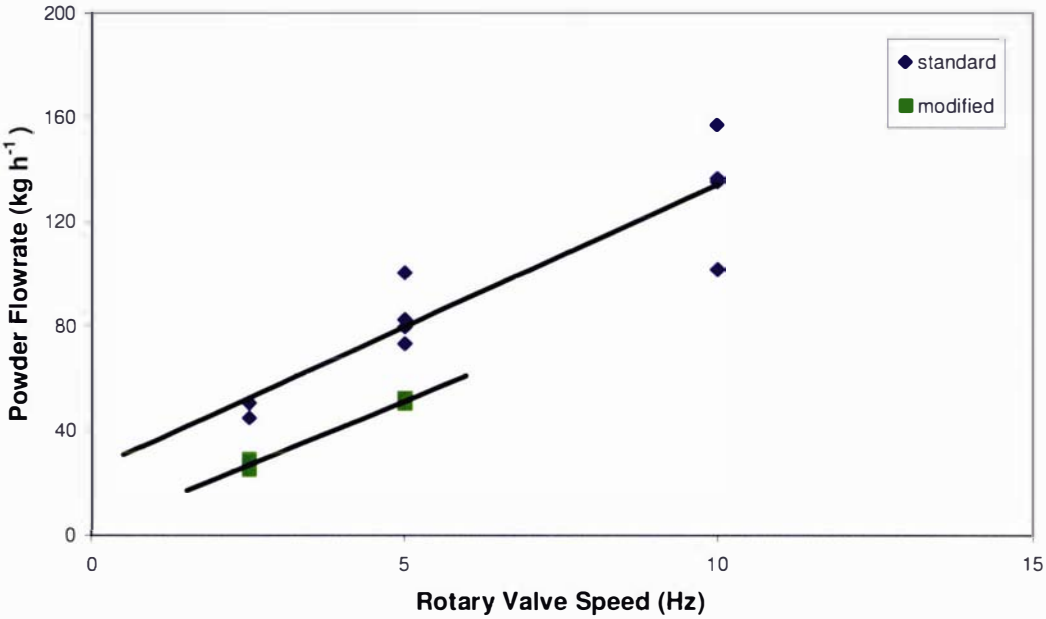

Figure 8.15: Calibration curve for the standard and modified rotary valves.

8.3.2 Experimental Design

Two levels of each operating variable were investigated, as shown in the design matrix below (Table 8.9). One midpoint (labelled M) experiment was carried out on each day to allow for differences between milk batches. It was not possible to do a full factorial experimental design due to potential atomisation problems. During atomisation using a pressure nozzle, the pressure, concentrate flow rate and nozzle orifice size are all dependent on one another and it was impossible to vary concentrate flow rate independently from the other operating parameters. For the same nozzle, a high flow rate with low solids at high pressure, results in very fine droplets, but conversely, a low concentrate flow rate with high solids at low pressure results in poor atomisation and a high moisture product. Instead, a constant flow was investigated on day 1 (Table 8.10) using one nozzle orifice, then on day 2 the high and low concentrate flows were investigated by changing the nozzle orifice size while holding all other variables constant (Table 8.11).

Table 8.9: Design matrix for agglomeration experiments.

Variable	Controlled	Mid	High	Low	Variable
Concentrate Flow rate	(L h^{-1})	120	130	110	1
Powder Flow rate	(kg h^{-1})	35	50	20	2
Solids Concentration	(%)	48	54	42	3
Particle Size $D_{4,3}$	(μm)	50	70	30	4

Table 8.10: Experimental design for agglomeration experiments (day 1).

Conc flow = 120 L h^{-1} pressure = 140 kPa Nozzle = 56/17			
Experiment	**Total Solids**	**Fines Flow rate**	**Fines Size**
M1a	M	M	
M1b	M	M	M
1a	L		
1b	L	L	L
2b	L	H	L
3b	L	L	H
4b	L	H	H
5a	H		
5b	H	L	H
6b	H	H	H
7b	H	L	L
8b	H	H	L

Table 8.11: Experimental design for agglomeration experiments (day 2).

TS = 48% Fines = 50 μm Pressure = 140 kPa			
Experiment	**Nozzle**	**Conc Flow rate**	**Fines Flow rate**
M2	56/17	M	M
9a	58/17	L	
9b	58/17	L	M
10a	55/17	H	
10b	55/17	H	M

Difficulties were experienced on day 1 when evaporating high solids milk concentrate (~ 55 wt%) and holding that concentrate for over an hour. Age thickening resulted meaning poor atomisation and limited pumping. Experiments 7b and 8b were completed on day 3 (Table 8.12) and experiment 5a was also repeated (7a) to determine the spray only conditions. During the repeat experiments, ~ 53 wt% concentrate was attained and the holding tank was stirred regularly.

Table 8.12: Experimental design for agglomeration experiments (day 3).

Conc flow = 120 L h^{-1} pressure = 140 kPa Nozzle = 56/17			
Experiment	**Total Solids**	**Fines Flow rate**	**Fines Size**
7a	H		
7b	H	L	L
8b	H	H	L

8.3.3 Experimental Results

Table 8.13 details the operating conditions used for each of the pilot scale experiments in chronological order. Table 8.14 to Table 8.16 shows the powder flow rates for the fines delivered to the top of the drier, and the flow of powder collected from the drier and cyclone. These flow rates, and the data included in Table 8.17, allowed calculation of the relevant agglomeration indices, which are presented in Table 8.18.

In order to analyse these results, some spot comparisons are first made, then the agglomeration efficiency, ξ_h, is related to the dimensionless flux ratios to provide mechanistic arguments to the analysis and a comparison to the literature. A statistical analysis is performed to extract the relationships between variables and the agglomeration efficiency.

Table 8.13: Operating conditions for agglomeration experiments.

Run	Conc Flow Rate	Conc P	T_{air} (in)	T_{air} (out)	Conc Temp	Conc density	Viscosity @ 1000 s^{-1}	Total Solids	Nozzle type
Units	**(L h^{-1})**	**(kPa)**	**(°C)**	**(°C)**	**(°C)**	**(kg m^{-3})**	**(mPa s)**	**(%)**	
M1a	126	140	197	91	70	1212	36.9	50.1	56/17
M1b	127	140	197	87.3	69.8	1212	36.9	50.1	56/17
1a	122	140	197	90	69.5	1184	11.5	42.0	56/17
1b	123	140	197	85.6	70	1184	11.5	42.0	56/17
2b	121.6	140	197.1	86.3	70.3	1184	11.5	42.0	56/17
3b	122.6	140	197	86.3	69.3	1184	11.5	42.0	56/17
4b	122	140	197	86	70	1184	11.5	42.0	56/17
5a	128	140	197	92.6	55	1240	166	55.3	56/17
5b	132	140	197	89.7	54.8	1240	166	55.3	56/17
6b	130	140	197	88.8	54.9	1240	166	55.3	56/17
M2	129	140	195	88	70.1	1208	36.9	47.8	56/17
9a	115	140	195.2	89.8	69.5	1208	44	47.0	58/17
9b	118	140	195.2	88.5	69.9	1208	44	47.0	58/17
10a	137	140	195.2	85.4	69.8	1208	29.7	47.0	55/17
10b	137	140	195.2	83.9	70.1	1208	29.7	47.0	55/17
7a	130.5	140	197	90.1	55	1230	92.9	52.3	56/17
7b	133	140	197	88.3	55	1230	92.9	52.3	56/17
8b	133	140	197.8	88.5	55	1230	92.9	52.3	56/17

Viscosity was measured at 50°C for all samples which was the delivery temperature of concentrate to the drier.

Table 8.14: Flow rates for agglomeration experiments (day 1).

Run	Rep	Drier			Cyclone			Total	Calc	Est	Load
		Mass	Time	Flow	Mass	Time	Flow	Flow	Fines	Fines	cell
Units		(kg)	(s)	(kg h^{-1})	(kg)	(s)	(kg h^{-1})	(kg h^{-1})	(kg h^{-1})	(kg h^{-1})	(kg h^{-1})
M1a	1	4.54	300	54.5	1.54	240	23.1				
	2	3.95	300	47.4	1.47	300	17.6				
	3	4.07	300	48.8	1.85	300	22.2				
Av				50.2			21.0	71.2	0.0	0	
M1b	1	4.65	300	55.8	8.9	480	66.8				
	2	5.45	300	65.4							
	3	4.39	300	52.7	4.695	300	56.3				
Av				58.0			61.5	119.5	48.3	52	
1a	1	2.74	300	32.9	2.07	300	24.8				
	2	2.54	300	30.5	2.2	300	26.4				
	3	2.53	300	30.4	2.17	300	26.0				
Av				31.2			25.8	57.0	0.0	0	
1b	1	4.15	300	49.8	3.34	300	40.1				
	2	3.84	300	46.1	3.275	300	39.3				
	3	3.63	300	43.6	3.085	300	37.0				
Av				46.5			38.8	85.3	28.3	27	29
2b	1	5.225	300	62.7	3.72	300	44.6				
	2	4.935	300	59.2	3.64	300	43.7				
	3	4.99	300	59.9	3.51	300	42.1				
Av				60.6			43.5	104.1	47.1	52	53
3b	1	3.81	300	45.7							
	2	3.49	300	41.9	2.74	300	32.9				
	3	3.48	300	41.8	2.75	300	33.0				
Av				43.1			32.9	76.1	19.1	27	25
4b	1	5.295	300	63.5	3.05	300	36.6				
	2	5.025	300	60.3	3.085	300	37.0				
	3	5.03	300	60.4	3.38	300	40.6				
Av				61.4			38.1	99.5	42.5	52	46
5a	1	4.925	300	59.1	2.26	300	27.1				
	2	4.85	300	58.2	2.185	300	26.2				
	3	4.82	300	57.8	2.06	300	24.7				
Av				58.4			26.0	84.4	0.0		
5b	1	6.095	300	73.1	3.49	300	41.9				
	2	5.435	300	65.2	3.06	300	36.7				
	3	6.095	330	66.5	3.305	330	36.1				
Av				68.3			38.2	106.5	22.1	27	20

The collection points are at the drier outlet and cyclone as shown in Figure 8.3. Fines flow rates are measured from the differential weight at the hopper load cell. They are estimated from the rotary valve speed and the previous calibration curve in Figure 8.15. Fines flow rates for 'b' runs are calculated from the difference between the total flow rate of a 'b' run and the total flow rate of the corresponding 'a' run.

Table 8.15: Flow rates for agglomeration experiments (day 2).

Run	Rep	Drier			Cyclone			Total	Calc	Est	Load
		Mass	Time	Flow	Mass	Time	Flow	Flow	Fines	Fines	cell
Units		(kg)	(s)	(kg h^{-1})	(kg)	(s)	(kg h^{-1})	(kg h^{-1})	(kg h^{-1})	(kg h^{-1})	(kg h^{-1})
M2	1	8.24	300	98.9	3.115	300	37.4				
	2	7.23	300	86.8	2.455	300	29.5				
	3	7.115	300	85.4	2.41	300	28.9				
Av				90.3			31.9	122.3	51.1	52	46
9a	1	4.105	300	49.3	1.84	300	22.1				
	2	4.005	300	48.1	1.545	300	18.5				
	3	4.085	300	49.0	1.405	300	16.9				
Av				48.8			19.2	67.9	0.0	0	0
9b	1	4.44	300	53.3	3.82	300	45.8				
	2	4.845	300	58.1	3.92	300	47.0				
	3	4.91	300	58.9	4.095	300	49.1				
Av				56.8			47.3	104.1	36.2	52	55
10a	1	4.87	300	58.4	2.23	300	26.8				
	2	4.36	300	52.3	1.815	300	21.8				
	3	4.33	300	52.0	2.01	300	24.1				
Av				54.2			24.2	78.5	0.0	0	0
10b	1	7.81	300	93.7	3.03	300	36.4				
	2	6.875	300	82.5	2.515	300	30.2				
	3	6.76	300	81.1	2.61	300	31.3				
Av				85.8			32.6	118.4	39.9	52	44

The collection points are at the drier outlet and cyclone as shown in Figure 8.3. Fines flow rates are measured from the differential weight at the hopper load cell. They are estimated from the rotary valve speed and the previous calibration curve in Figure 8.15. Fines flow rates for 'b' runs are calculated from the difference between the total flow rate of a 'b' run and the total flow rate of the corresponding 'a' run.

Table 8.16: Flow rates for agglomeration experiments (day 3).

Run	Rep	Drier			Cyclone			Total	Calc	Est	Load
		Mass	Time	Flow	Mass	Time	Flow	Flow	Fines	Fines	cell
Units		(kg)	(s)	(kg h^{-1})	(kg)	(s)	(kg h^{-1})	(kg h^{-1})	(kg h^{-1})	(kg h^{-1})	(kg h^{-1})
7a	1	5.41	300	64.9	1.785	300	21.4				
	2	5.04	300	60.5	1.58	300	19.0				
	3	5.115	300	61.4	1.485	300	17.8				
Av				62.3			19.4	81.7	0.0	0	0
7b	1	6.59	300	79.1	2.24	300	26.9				
	2	6.22	300	74.6	2.135	300	25.6				
	3	6.285	300	75.4	2.185	300	26.2				
Av				76.4			26.2	102.6	21.0	27	22
8b	1	7.96	300	95.5	2.915	300	35.0				
	2	7.09	300	85.1	2.745	300	32.9				
	3	7.31	300	87.7	3.01	300	36.1				
Av				89.4			34.7	124.1	42.5	52	46

The collection points are at the drier outlet and cyclone as shown in Figure 8.3. Fines flow rates are measured from the differential weight at the hopper load cell. They are estimated from the rotary valve speed and the previous calibration curve in Figure 8.15. Fines flow rates for 'b' runs are calculated from the difference between the total flow rate of a 'b' run and the total flow rate of the corresponding 'a' run.

Table 8.17: Size, particle and bulk density for agglomeration experiments.

Run	Drier			Cyclone		
	$D_{4,3}$	Particle Density	Bulk Density (100 taps)	$D_{4,3}$	Particle Density	Bulk Density (100 taps)
Units	(μm)	(g cm^{-3})	(g cm^{-3})	(μm)	(g cm^{-3})	(g cm^{-3})
M1a	85.3	1.31	0.69	56.6	1.31	0.70
M1b	145.2	1.30	0.63	55.2	1.32	0.76
1a	71.3	1.23	0.66	36.3	1.45	0.70
1b	106.1	1.32	0.59	41.9	1.31	0.71
2b	113.0	1.27	0.55	40.8	1.31	0.70
3b	137.9	1.31	0.64	48.8	1.42	0.73
4b	145.2	1.26	0.6	53.3	1.35	0.73
5a	124.3	1.14	0.52	68.3	1.26	0.66
5b	139.8	1.21	0.52	79.7	1.24	0.69
6b	155.3	1.18	0.45	85.1	1.25	0.67
M2b	143.4	1.30	0.66	51.8	1.31	0.74
9a	85.1	1.27	0.69	39.1	1.29	0.65
9b	149.0	1.28	0.61	61.9	1.33	0.75
10a	85.1	1.32	0.74	39.6	1.34	0.72
10b	155.3	1.28	0.65	51.9	1.36	0.74
7a	105.5	1.20	0.61	52.9	1.32	0.66
7b	107.5	1.22	0.58	54.7	1.33	0.68
8b	119.3	1.23	0.56	55.3	1.37	0.68
M1a	85.3	1.31	0.69	56.6	1.31	0.70
M1b	145.2	1.30	0.63	55.2	1.32	0.76

8.3.4 Extent of Agglomeration – Spot Comparisons

Table 8.18 shows that experiment 10b had the best operating conditions for agglomeration with an agglomeration efficiency, ξ_h, of 0.127. This experiment used the smaller nozzle orifice, a medium level of total solids, medium fines size with high fines flow rate and high concentrate flow rates. The mass flow rate weighted particle size distributions of the fines, dried droplets and agglomerates, included in Figure 8.16, show that agglomeration occurred. In contrast, experiment 5b had the lowest level of agglomeration, $\xi_h = 0.008$. This was produced using a medium size orifice, high total solids, large fines, low fines flow rate, and a medium concentrate flow rate. The weighted particle size distributions in Figure 8.17 show that agglomeration did not occur. It is difficult to determine why agglomeration occurred in experiment 10b and not experiment 5b as five variables were changed. However, it is significant that different levels of agglomeration (moderate and low) can be achieved at pilot scale.

For the spray-only experiments, Figure 8.18 compares experiments 5a and 7a. Initially 7a was intended to be a repeat of 5a (although carried out on a different day), however the solids level of the concentrate was lower than intended, 53% instead of 55%. Experiment 5a, with a higher solids, produces powders with a larger size. This is postulated to be caused by a higher droplet size distribution at higher solids concentration due to the higher viscosity.

Table 8.18: Key variables and agglomeration efficiency for each experiment.

Experiment	Conc Flow ($L\ h^{-1}$)	Nozzle	Total Solids (%)	Fines Flow ($kg\ h^{-1}$)	Fines Size (micron)	ξ_{sh}
M1b	127	56/17	50	52	64.5	0.062
1b	123	56/17	42	27	35.3	0.041
2b	122	56/17	42	52	35.3	0.121
3b	123	56/17	42	27	101.4	0.029
4b	122	56/17	42	52	101.4	0.057
5b	128	56/17	55	27	101.4	0.008
6b	132	56/17	55	52	101.4	0.019
M2b	129	56/17	48	52	64.5	0.094
7b	133	56/17	52	27	35.3	0.032
8b	133	56/17	52	52	35.3	0.106
9b	113	58/17	47	52	64.5	0.110
10b	137	55/17	47	52	64.5	0.127

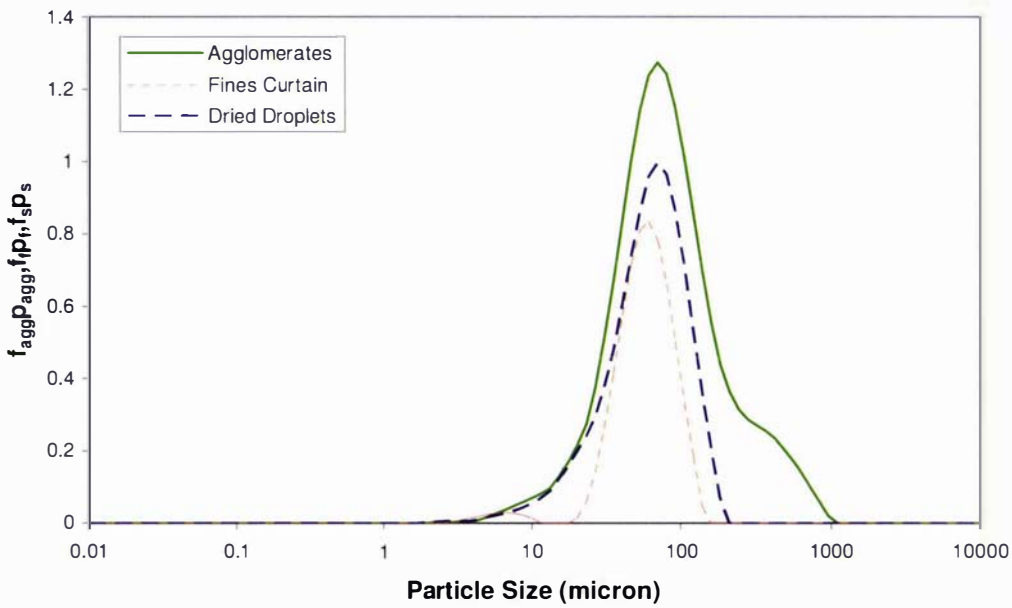

Figure 8.16: Comparing the weighted PSDs for experiment 10b (high concentrate flowrate, medium total solids, high fines flowrate and medium fines size).

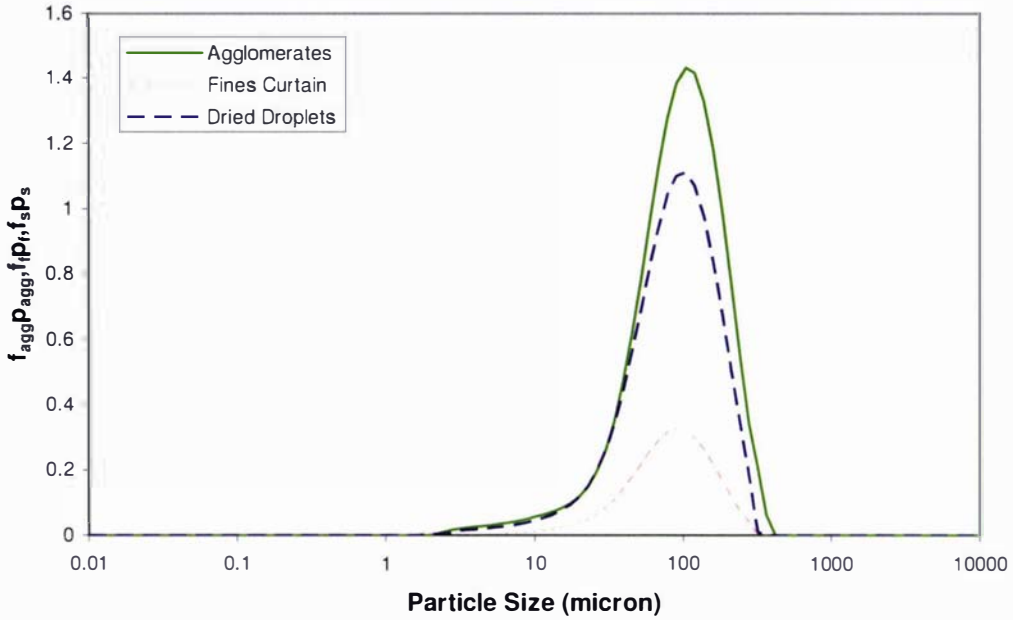

Figure 8.17: Comparing the weighted PSDs for experiment 5b (medium concentrate flowrate, high total solids, low fines flowrate and large fines size).

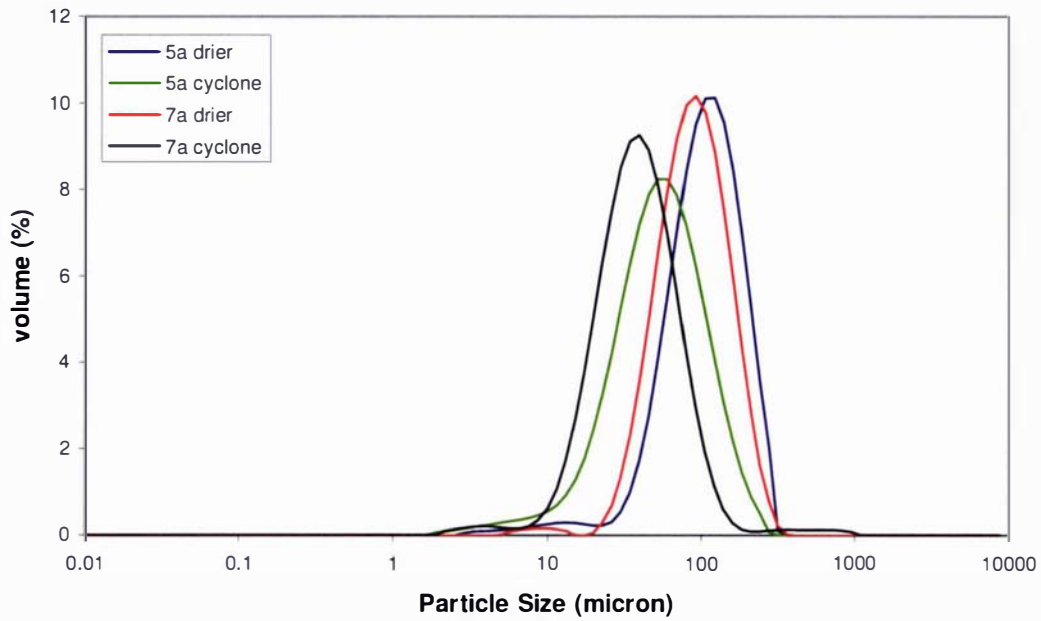

Figure 8.18: comparing 5a (55 wt% TS) and 7a (53 wt% TS) (spray only).

In the agglomeration experiments some differences can also be observed. In a spot comparison of experiments, 7b and 8b, fines flow rate is the only significant difference resulting in a higher agglomeration efficiency, ξ_h = 0.106 for experiment 8b (compared with ξ_h = 0.032 for 7b) which has a higher mass flow rate of fines delivered to the collision zone. Experiments 9b and 10b results differ significantly although only the concentrate flow rate was changed, however to achieve this, different nozzles were

used. Experiment 10b has only a slightly higher agglomeration efficiency compared to experiment 9b; it is difficult to determine if this is due to an increase in concentrate flow rate or a decrease in droplet size due to the smaller diameter of the nozzle orifice.

In summary, these spot comparisons are useful to isolate the influence of individual variables, but do not provide quantitative relationships. A list of the spot comparisons is contained in Table 8.19, along with possible explanations for the observed qualitative differences. It must be noted that, as only one replicate was performed for each experiment, some variability affects these explanations. To explore the quantitative relationships a statistical analysis is conducted later in §8.3.8. However, agglomeration efficiency is also examined as a function of dimensionless flux and this leads to a discussion of the mechanisms of agglomeration.

Table 8.19: Spot comparisons, variables and observed effects.

Experiments	Variable	Observed Effect of Increasing Variable
5b 10b	Five variables	Difficult to determine
5a 7a	Total solids	Increase in dried droplet size
7b 8b	Fines flow rate	Increase in agglomeration
9b 10b	Concentrate flow	Increase in agglomeration

8.3.5 Extent of Agglomeration – Dimensionless Flux

The dimensionless flux or flux ratio is a scaling parameter first developed by Hapgood (2001) and Litster et al. (2001) in reference to granulation where a spray is directed at a moving powder bed:

$$\Psi_a = \frac{3\dot{V}}{2\dot{A}D_d} \tag{8.1}$$

where $\dot{V}$ is the volumetric spray rate of the binder liquid [$m^3\ s^{-1}$], D_d is the droplet size [m] and $\dot{A}$ is the area flux of powder traversing the spray zone [$m^2\ s^{-1}$]. It is effectively the area of droplets divided by the area of the bed surface that sweeps through the spray zone. The dimensionless spray flux can be used to identify the nucleation regime of the system (Hapgood et al., 2003). Boerefijn and Hounslow (2005) found that for granulation to occur in a fluidised bed the flux number (FN) needs to be below 3.5 and above 2. The flux number is similar in principle to the dimensionless spray flux and allows for scale-up of growth rates from batch to continuous granulation:

$$FN = \log_{10}\left(\frac{\rho_p u_e A_{spray}}{q_b}\right) \tag{8.2}$$

where ρ_p denotes the particle density [kg m^{-3}], u_e the excess gas velocity [m s^{-1}], q_b the binder spray rate [kg s^{-1}], and A_{spray} is the spray-on foot print area of the nozzle onto the powder bed [m^2].

In a spray drier the configuration is different from the low or high shear granulator of Hapgood (2001) and the fluidised bed of Boerefijn and Hounslow (2005) whose work was reviewed earlier in §2.5. An agglomerating spray drier contains two dispersed

particle streams that intersect. A dimensionless flux can therefore be a ratio of either, (i) the volumetric flux of the spray droplets and fines particles, (ii) the number flux of fines particles and droplets, or (iii) the projected area flux of particles and droplets. The choice of ratio depends on which physical model is adopted. In the following paragraphs the influence of each dimensionless flux ratio is first determined after which the results are discussed in relation to the physical processes.

The volumetric flux ratio is almost equivalent to the mass flux ratio because here the spray flow rate is reported on a solids basis and its size distribution is measured on a 'dried droplet' basis. Therefore, the density of the spray stream can be assumed to be equal to that of the fines stream (see discussion in §6.2.3). Figure 8.19 shows the influence of fines to spray mass flux ratio, F:S, on the agglomeration efficiency, ξ_h. The number flux ratio, F_N:S_N is calculated from the particle size distribution information used to determine the agglomeration efficiency. At the i^{th} size interval there are $f_{n,i}$ fines particles per (dry basis) kilogram of feed which includes the spray and the fines.

$$f_{n,i} = \frac{p_f f(\log D_{f,i})}{\rho_f \alpha_f D_{f,i}^3} \tag{8.3}$$

where p_f = proportion of powder leaving the drier as fines, ρ_f = particle density of fines, α_f = shape factor (assuming spherical particles = $\pi/6$), and D_f = fines size. The quantity $f(log\ D_{f,i})$ represents the proportion of fines size distribution represented in the i^{th} size interval, noting that the i^{th} interval is on a log scale of size. Summing over the entire distribution gives the total number of fines, F_N, and spray, S_N, on a dry mass basis.

$$F_N = \sum_i \frac{p_f f(\log D_{f,i})}{\rho_f \alpha_f D_{f,i}^3} \tag{8.4}$$

$$S_N = \sum_i \frac{p_s f(\log D_{s,i})}{\rho_s \alpha_s D_{s,i}^3} \tag{8.5}$$

Figure 8.20 shows the influence of number flux ratio F_N:S_N on agglomeration efficiency, ξ_h. The same approach is used to calculate a projected area ratio F_{PA}:S_{PA}. Summing over the distribution gives the total projected area of fines, F_{PA} and the total projected area of spray, S_{PA}. Figure 8.21 shows the influence of the projected area flux ratio F_{PA}:S_{PA} on the agglomeration efficiency, ξ_h.

$$F_{PA} = \sum_i \frac{p_f \pi/4 D_{f,i}^2 f(\log D_{f,i})}{\rho_f \alpha_f D_{f,i}^3} \tag{8.6}$$

$$S_{PA} = \sum_i \frac{p_s \pi/4 D_{s,i}^2 f(\log D_{s,i})}{\rho_s \alpha_s D_{s,i}^3} \tag{8.7}$$

Figure 8.19, 8.20 and 8.21 all show that higher dimensionless flux ratios produce more agglomeration. These plots also indicate that the effect of fines size and total solids level where the concentrate and fines flow rates are maintained at their medium level

(see Table 8.10 to Table 8.12). Generally small fines and low total solids results in more agglomeration, however, the precise influence depends on the dimensionless flux. It is necessary to determine the physical meaning of the flux ratios and select the ratio which most represents the agglomeration process.

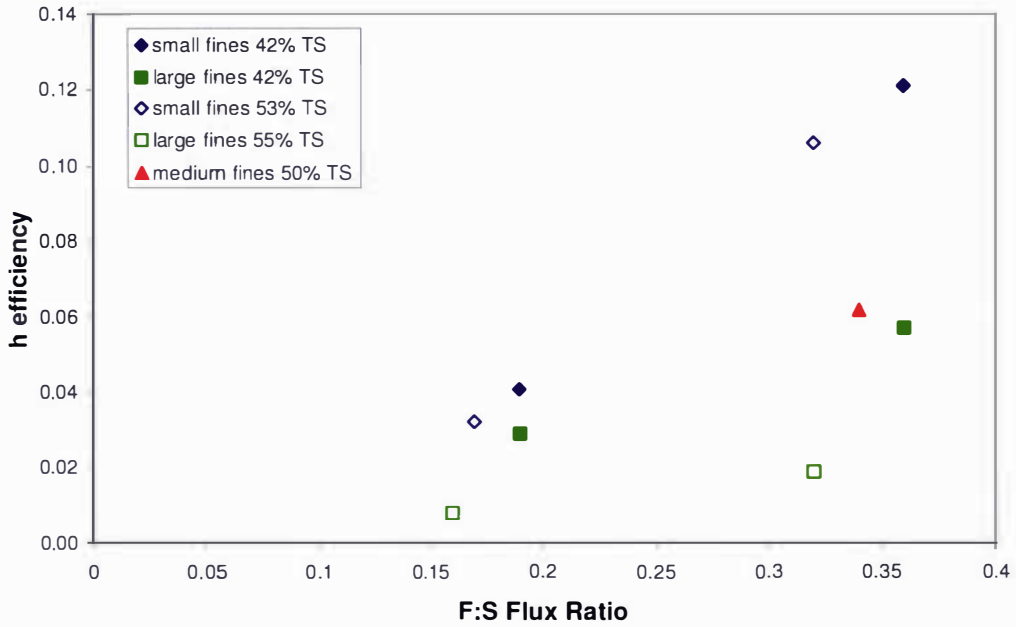

Figure 8.19: Fines to spray mass flow rate ratio vs. h efficiency.

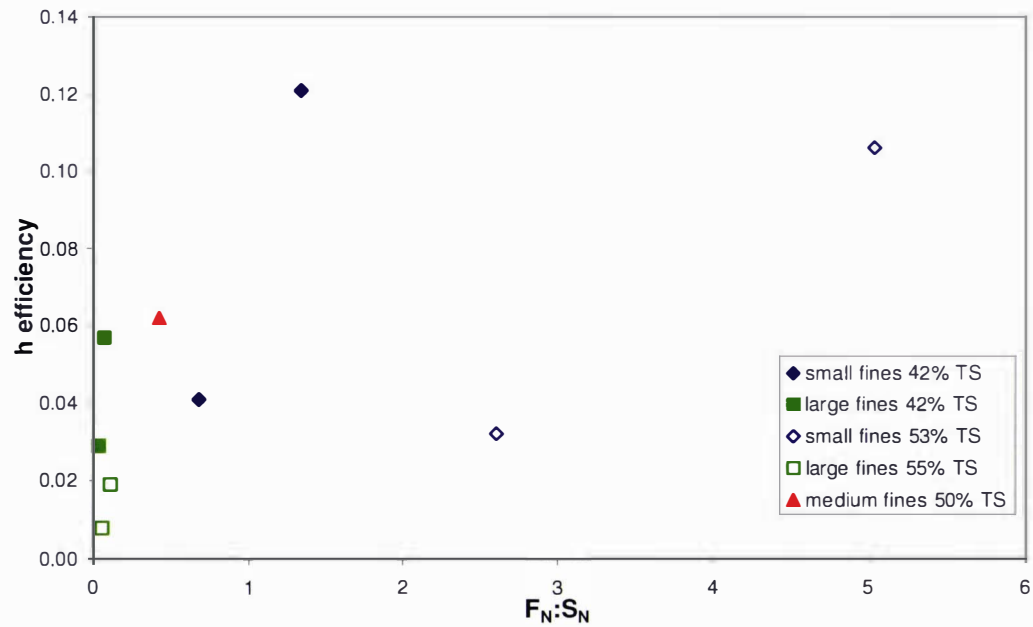

Figure 8.20: *h* efficiency vs. F_N:S_N.

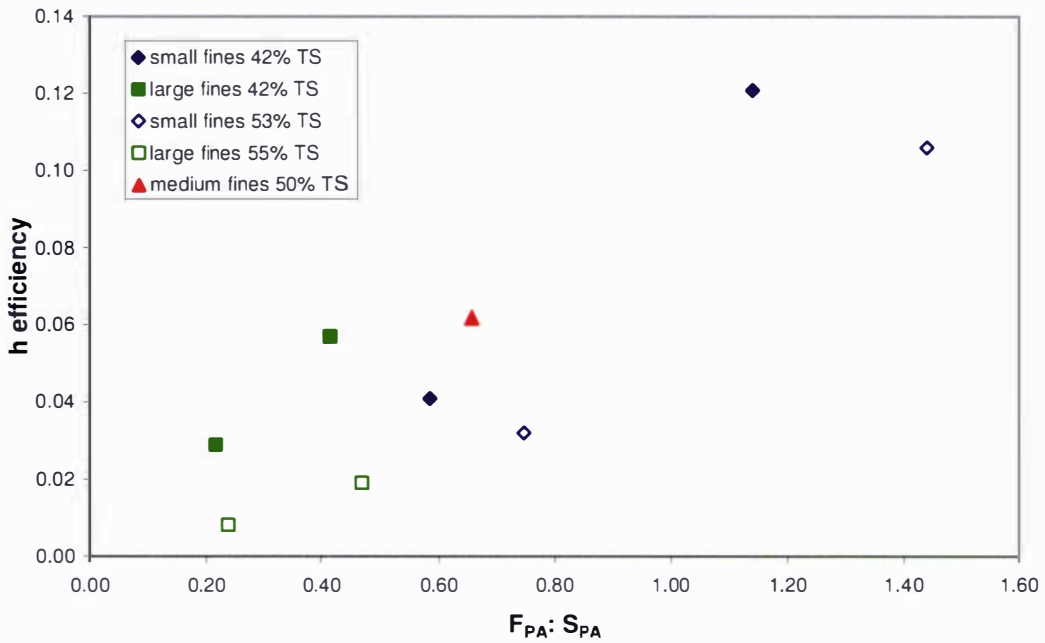

Figure 8.21: *h* efficiency vs. F_{PA}:S_{PA}.

Jones (2005) describes the interaction of droplets and particles in the contact zone at the top of the spray drier as a spray sheet contacting a powder curtain ignoring the effect of turbulence. The probability that collision will occur within the interaction zone can be calculated given the properties of size, velocity and spatial number-flux density. This approach identifies that if the rate of particles and/or droplets entering the collision zone increases, then the likelihood of a collision occurring will also increase. Providing these two particles can adhere, the collision will be the first step that will lead to further processes resulting in agglomerate formation. If the mass flow rate of fines entering the contact zone is increased then a greater proportion of droplets will be captured by fines. Similarly, if fines decrease in size, the spatial number-flux density of fines will increase and a greater proportion of droplets will be captured. Jones (2005) takes a simplistic limit of either droplet or fines dominated inertia, so droplets collect fines or fines collect droplets. The argument of Jones is based on the overlapping of swept volumes of droplets and particles which suggests that F_{PA}:S_{PA} is a suitable dimensionless flux ratio.

Verdurmen et al. (2004) modelled agglomeration in spray dryers using CFD to determine particle and droplet trajectories. Their drying sub model predicts droplet size, temperature and moisture content; the collision sub model uses the approach of Sommerfeld (2001) (based on Abrahamson (1975)) to predict the collision probability; and the agglomeration sub model determines whether adhesion occurs following adhesion and is based on stickiness information of the droplets and particles. The collision frequency of the particles in the interaction zone is a key issue so the dimensionless mass flux and the ratio of projected areas are relevant for discussion.

The above discussion of collision mechanism and the selection of the most appropriate dimensionless flux ratio ignored whether the colliding particles actually adhere. Successful adherence relates to the critical Stokes number developed by Ennis (1991) and Liu et al. (2000) which is a function of the liquid layer thickness, asperity height (on the colliding particles), the viscosity of the liquid and the energy involved in the

collision (see §2.5). If the kinetic energy of the collision is able to be absorbed by viscous dissipation then adhesion occurs. Some particles may absorb the collision energy by deformation and Iveson et al. (2001) use a Stokes deformation number to describe the threshold for deformation adherence. This number measures the ratio of impact kinetic energy to the plastic energy absorbed per unit strain.

$$St_{def} = \frac{\rho_p U_c^2}{2Y_g} \tag{8.8}$$

where U_c = collision velocity [m s^{-1}], ρ_p = particle density [kg m^{-3}] and Y_g = dynamic yield stress. Practically, not all variables needed to define the Stokes or Stokes deformation numbers are measurable. In this experimental study, the two easily measured quantities are the size of the droplets and the viscosity of the concentrate; it is not possible to directly measure the velocity of the fines and droplets before collision. The collision Stokes number shows that smaller particles agglomerate better. This is clearly observed in Figures 8.19 – 8.21. There are several reasons: as size decreases, the number density of fines increases, which means the projected area of collection increases; large fines have higher inertia and are less likely to coalesce given the same liquid bridging conditions; and drag influences smaller particles more meaning that there is less kinetic energy to dissipate in the liquid bridge between particles. This means that for smaller particles the binder layer thickness need not be as large and the viscosity of the bridge will not need to be as high as for two larger particles to coalesce.

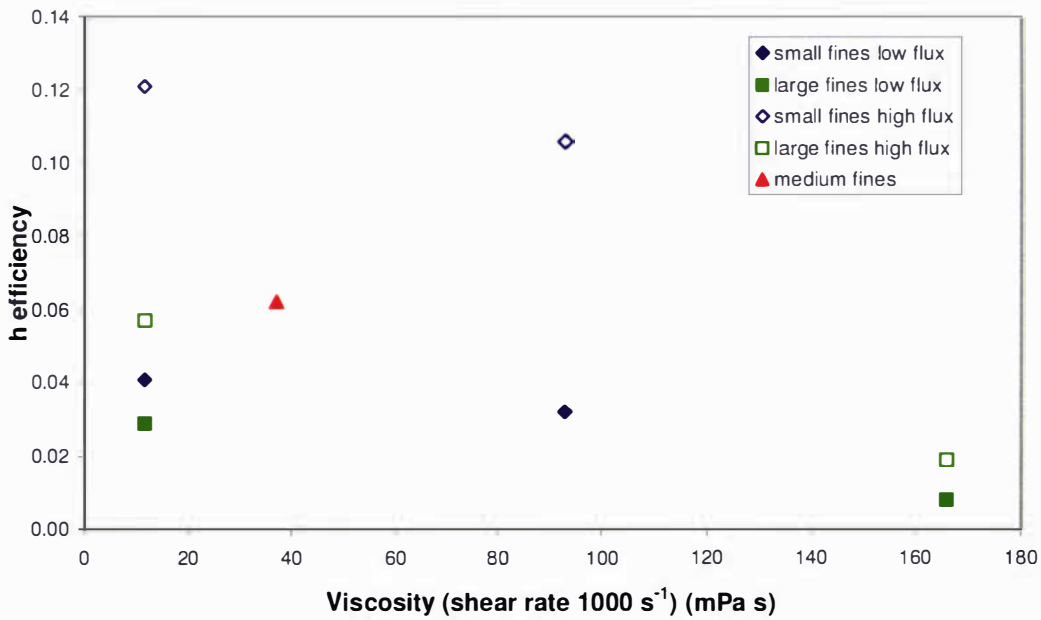

Figure 8.22: Concentrate viscosity vs. *h* efficiency.

The effect of viscosity on agglomeration efficiency is plotted in Figure 8.22. In these experiments, increasing solids concentration reduces the agglomeration efficiency, but this is less obvious than the effect caused by fines size and fines flow rate. The reason for the observed trend that agglomeration decreases with an increase in viscosity may relate to the drying environment. A more viscous concentrate will result in larger

droplets at atomisation which have a higher inertia and therefore more energy must be dissipated during collision for adhesion to occur. Also, the higher viscosity droplets will be surface-dry faster and may not adhere to particles in the collision zone. Werner (2005) studied surface drying of polymer solutions and showed that the surface of a droplet can become dry despite high bulk moisture contents. Therefore the bulk properties used to calculate the Stokes number may not represent the surface conditions that are needed to define whether the particles or droplets are adhesive.

The stickiness of a surface is material specific and for dairy powders which undergo humidification, the onset of stickiness is a rapid process (Chatterjee, 2004; Murti, 2006; Zuo, 2004). For the reverse process, the drying of a droplet, the onset of stickiness has only been quantified for a few substances (Adhikari et al., 2003a, 2003b; Adhikari et al., 2005; Truong et al., 2005a; van der Hoeven et al., 2006). So it is necessary to define an indicator of a solution's potential to become sticky or surface dry. One measure examined by Wemer (2005), is the mass transfer Biot number:

$$Bi_m = \frac{Sh}{2}\left(\frac{D_v}{D_w}\right) \tag{8.9}$$

where $Sh = 2 + 0.6\mathrm{Re}^{1/2}\mathrm{Sc}^{1/3}$ (Ranz and Marshall, 1952), $Re = \rho_a U_a D_d/\mu_a$, $Sc = \mu_a/D_v\rho_a$, and D_v and D_w = diffusion coefficients of water vapour in air and through the droplet.

D_w can be described as a function of the moisture content and temperature (Luyben, Liou, & Bruin, 1982). Sano and Keey (1982) showed that for skim milk, this quantity varies by seven orders of magnitude as milk dries from 90% moisture to fully dry. This means Bi_m tends towards infinity as drying occurs. The Biot number at the nozzle may be an indirect indicator of adhesion; a higher Biot number indicates a surface that will more rapidly dry to a non adhesive state. Kentish et al. (2005) reported the correlations for the diffusion coefficient of water through skim milk powder in the literature, including the method used by Sano and Keey (1982) which used the binary diffusion coefficient of Wijlhuizen et al. (1979) included in equation (8.10).

$$D_w = \exp\left[-\frac{38.912 + 323.39\omega_l}{1 + 15.84\omega_l} - \frac{4300\omega_l^{-0.445}}{1.987} \times \left(\frac{1}{T} - \frac{1}{303}\right)\right] \tag{8.10}$$

where ω_l = mass fraction of moisture [kg kg^{-1}]. This approach is used for the typical total solids concentrations used here; solution diffusion coefficient changes from 3.9×10^{-10} m^2 s^{-1} at 42% total solids, to 2.6×10^{-10} m^2 s^{-1} at 55% total solids. A lower diffusivity means a higher Biot number; i.e. a maximum total solids for agglomeration.

Another measure of surface stickiness was used by Verdurmen et al. (2004) when modelling agglomeration. The approach of Blei and Sommerfeld (2003) is used, three types of particles are defined that exist at the top of the spray drier:

- Surface tension dominated (STD) droplets
- Viscous forces dominated (VD) droplets
- Dry (DRY) particles

The relative importance of the viscous and surface tension forces defined by calculating the Ohnesorge number, Oh^2, (see Equation (8.11), when $Oh^2 < 1$, the viscosity is low and droplets are STD.

$$Oh = \frac{\mu}{\sqrt{\sigma \rho D}} \tag{8.11}$$

where Oh = Ohnesorge number, D = drop diameter [m], ρ = density of liquid [kg m^{-3}], μ = viscosity of liquid [Pa s] and σ = surface tension of liquid [N m^{-1}].

The boundary between VD droplets and DRY particles is determined by the sticky point temperature which is above the glass transition temperature for lactose containing powders (see §2.4.3). Verdurmen gives the threshold for the VD/DRY transition as 20 K above the glass transition temperature of lactose from direct measurements and the work of Bhandari et al. (1997). Above the sticky point temperature the surface of the fluid is viscous and sticky, below this temperature the surface is classed as dry. Murti (2006) used the particle gun technique to find the sticky point temperature of skim milk powder (similar in composition to ISMP A) to be 32°C above the glass transition temperature of lactose.

Collisions can therefore arise between particles in the following manner:

- STD-STD – occurs just after atomisation and results in a larger spherical droplet
- VD-STD or DRY-STD
- VD-VD or VD-DRY
- between DRY particles

In agglomeration Verdurmen et al. (2004) state that VD collisions are the decisive events and that form ideal agglomerate structures where the energy of the impact acts to deform the droplets which makes them partially penetrate each other to produce loosely bonded particles upon drying. Verdurmen et al. considers the successful adhesion of two colliding droplets or particles (VD-VD or VD-DRY collisions) to depend on the penetration depth and the amount of dissipated kinetic energy during the collision. Rebound will occur if the distance between particles is greater than the average of the two diameters and the relative velocity is greater than zero. Coalescence and agglomeration occurs if all of the kinetic energy is dissipated during the collision: coalescence occurs if penetration is > 50% of the smallest particle diameter and agglomeration occurs if the penetration is < 50% of the smallest particle diameter. The Ohnesorge number for the concentrate droplets in these experiments is directly proportional to the viscosity given minor differences exist between solution densities and droplet sizes across the range. Therefore, the relationship between Oh and agglomeration efficiency will be similar to that in Figure 8.22 where a weak dependence exists.

The mass transfer Biot number and the Ohnesorge numbers are both indicators of successful adherence but they are not direct measures. More research is required before adherence in droplet – particle systems is understood and efforts are now being directed at surface properties rather than bulk properties (e.g. (Adhikari et al., 2005; Werner, 2005)).

8.3.6 Extent of Agglomeration – Effect of flow rate

The spatial number flux density of droplets and fines is expected to be important in agglomeration processes. Figure 8.23 shows no significant effect of concentrate flow rate (for constant fines flow rate) on *h* efficiency. Although the nozzle orifice was changed to achieve the different concentrate flow rates, Figure 8.24 indicates that the dried droplet size distributions were also unchanged. This indicates that despite changing nozzles the spray has the same size distributions for all concentrate flow rates. Figure 8.25 includes the effect of fines flow rate (for constant concentrate flow rate) on agglomeration efficiency. Fines flow rate has a significant effect on the *h* efficiency compared to the concentrate flow rate.

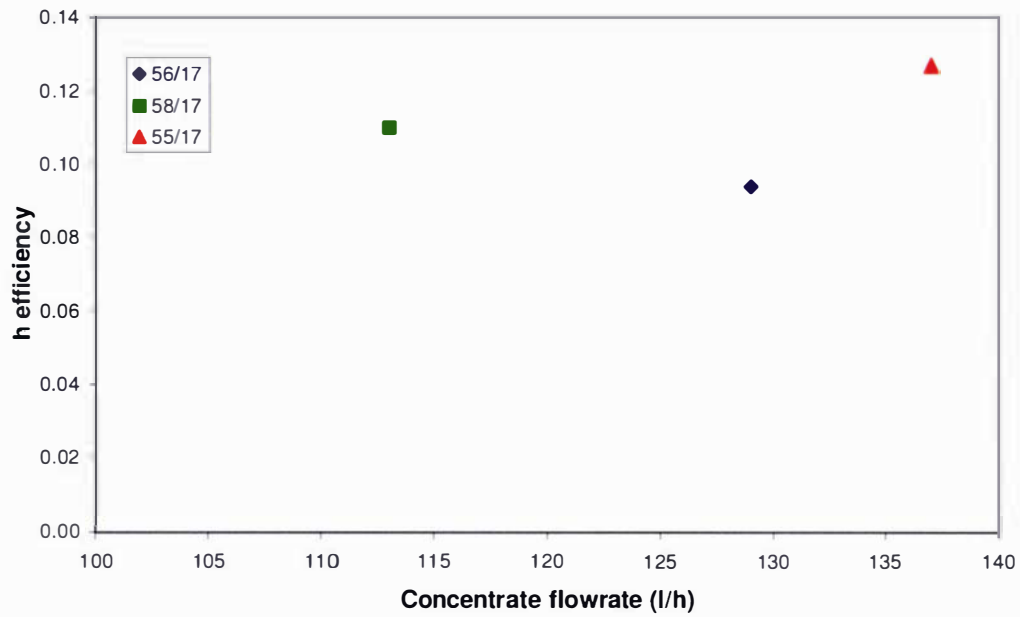

Figure 8.23: Effect of concentrate flow rate and nozzle type on *h* efficiency.

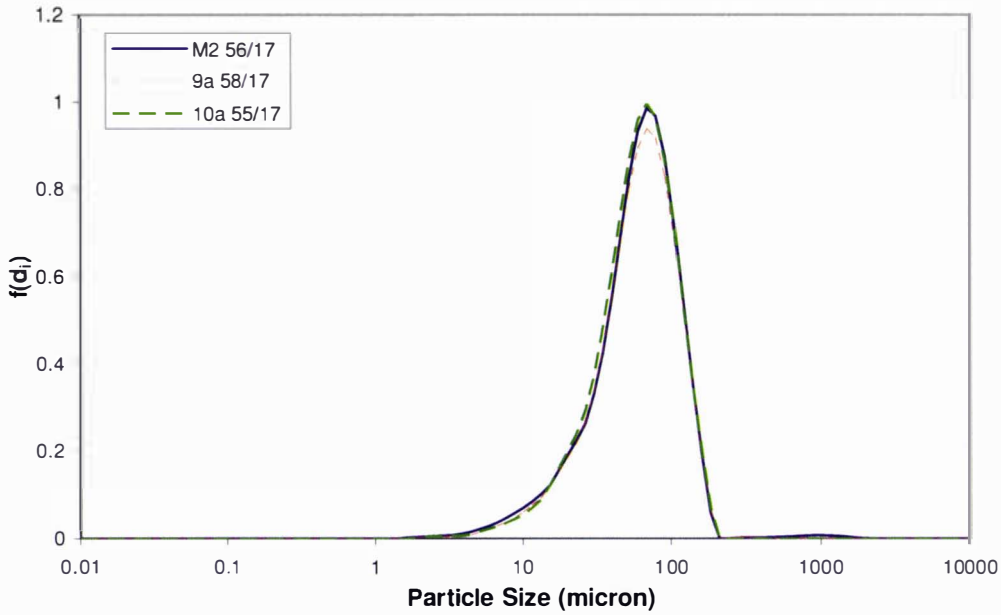

Figure 8.24: Comparing the PSDs of dried droplets for different nozzles.

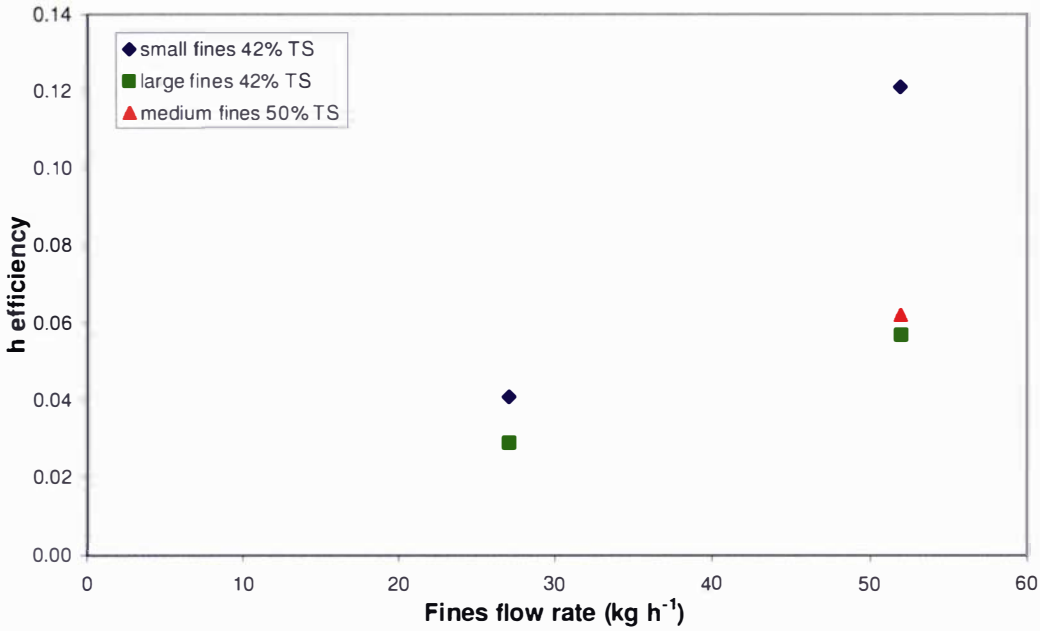

Figure 8.25: Effect of fines flow rate on *h* efficiency.

8.3.7 Extent of Agglomeration – Comparison to Literature

There is little information on agglomeration in spray driers in the literature to allow a comparison with these experimental results. While there are many recent studies that look at the influence of spray drying operating parameters on powder properties (Birchal et al., 2005; Chegini & Ghobadian, 2005; Goula et al., 2004; Huntington, 2004; Nijdam & Langrish, 2005), none of these aim to study agglomeration between fines and droplets at the top of the spray drier.

Verdurmen et al. (2004) modelled agglomeration in a spray drier and found increasing droplet viscosity lead to an increased agglomeration rate and a more homogeneous agglomeration population with improved powder properties. Their approach used CFD modelling, collision probabilities as discussed above and Ohnesorge criteria to establish a surface stickiness to produce agglomerates. During the agglomeration process droplets undergo time-dependent changes during drying; the property that changes the most is the viscosity and this impacts significantly on the collision mechanism which occurs. Verdurmen et al. (2004) also validated their simulation of agglomeration using a pilot scale drier with a chamber diameter of 4.3 m and ~ 275 kg h^{-1} water evaporation. Despite Verdurmen et al.'s (2004) prediction and validation of the effect of droplet viscosity being opposite to that observed here, both results may be valid if, in Verdurmen et al. (2004)'s experiments, the droplets partially dried to become sticky but in this work the high total solids droplets became surface dry.

Some of Verdurmen et al. (2004)'s findings agree with those reported here; introduction of fines has a strong influence on the extent of agglomeration. They also found that altering the drier outlet air humidity did not have an effect on agglomeration. This is expected as altering the outlet conditions will affect the final powder moisture content and stickiness, but it is not likely to significantly affect the initial droplet drying process.

8.3.8 Statistical Analysis of Agglomeration Efficiency

The pilot scale experiments were designed using a full factorial approach which investigated two levels of each of the 3 variables (total solids, fines flow rate, fines size) and included two centre points. This makes 10 runs ($2^3 + 2 = 10$). The previous section discusses the results of these experiments using an engineering approach to look at the relationships individually and discusses how these findings relate to the relevant mechanisms of agglomeration. It is also essential to analyse the results obtained statistically to understand how the interacting variables influence the response variables, in this case the h agglomeration efficiency. As the scatter plot in Figure 8.26 demonstrates, there does not seem to be any environmental affect or dependency of the response variable on the run order of the experiments.

Figure 8.27 shows the main effects for each of the variables on the response and demonstrates that an increase in fines flow increases agglomeration, small fines size increases agglomeration, a decrease in total solids increases agglomeration, but there was also a local maximum at 48 wt% total solids. This solids concentration probably represents the point of maximum stickiness before droplets become surface dry and non-adhesive.

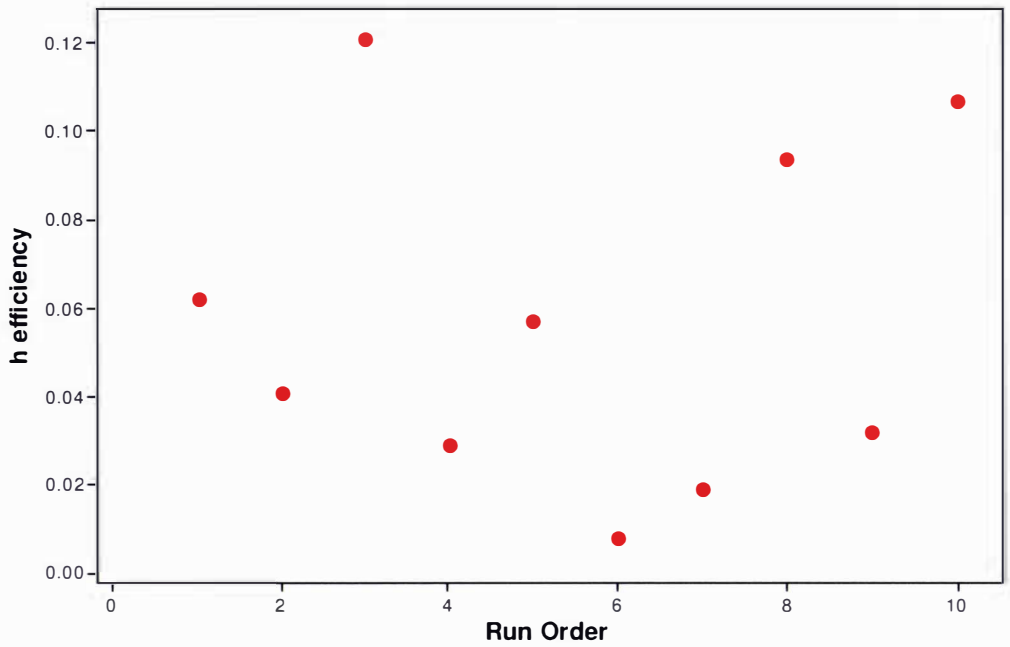

Figure 8.26: Scatter plot of *h* efficiency vs. run order for all pilot scale experiments.

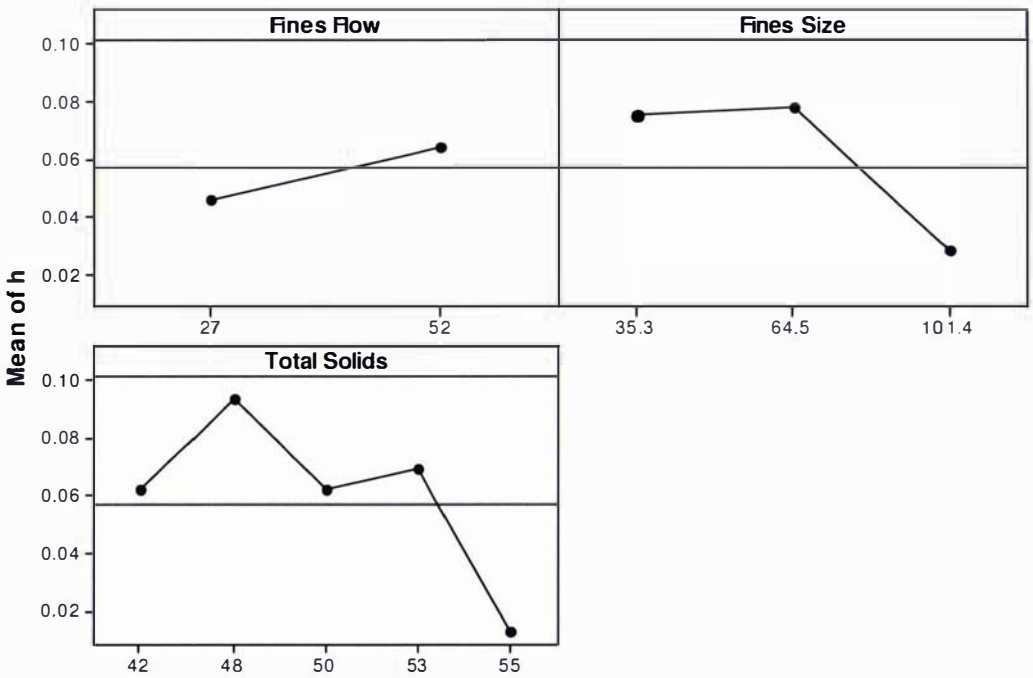

Figure 8.27: The main effects plot for *h* efficiency.

A simple regression analysis gives equation (8.12) which links fines flow (FF), fines size (FS) and total solids (TS) to the *h* efficiency. The p values indicate that none of the variables affect the h efficiency significantly (all are above 0.05). The adjusted R^2 value is 19.3% and S (pooled standard deviation) is 0.035.

$$h = 0.159 - 0.000696FS - 0.00176TS + 0.000704FF \quad (8.12)$$

Better fit is obtained using a response surface analysis, which takes into account quadratic terms and interactions between variables. Response surface methods (RSM) are used to examine the relationship between response variables and a set of quantitative experimental variables or factors. A response surface regression was carried out which also looked at the interacting effects of most variables. Data analysis using RSM is an iterative process starting with the initial operating variables. The non-significant terms are then removed, one at a time, until the model only includes significant terms (P<0.10).

The final model will have a higher adjusted R-squared value and a smaller pooled standard deviation than the full model, indicating that the data fit has improved. Two different sets of variables are investigated here: total solids, fines size (which have a significant effect on the agglomeration efficiency as indicated in previous sections), and either fines to spray mass flux ratio (F:S) or the fines to spray projected area ratio (F:S PA) are included instead of the individual flow rates. Flow rate can be dropped from the analysis as the concentrate flow rate and dried spray droplet size distribution are constant in this factorial design. The final model using F:S has been included in Table 8.20 and the model for F:S PA is included in Table 8.21. The lower S value and higher adjusted R^2 indicates that the model using the F:S ratio best fits the experimental data.

Table 8.20: Final model estimated regression coefficients for *h* using F:S.

Term	Coefficient	P
Constant	0.142	0.01
Fines Size	-0.020	0.005
TS	-0.163	0.021
F:S	0.023	0.007
F:S*F:S	-0.144	0.032
Fines Size*F:S	-0.017	0.012
Total Solids*F:S	-0.052	0.03

S = 0.0072 R^2 = 98.8% R^2 (adj) = 96.5%

Table 8.21: Final model estimated regression coefficients for *h* using F:S PA.

Term	Coefficient	P
Constant	0.098	0
Fines Size	0.017	0.091
TS	-0.023	0.01
F:S PA	0.067	0.003
TS*TS	-0.032	0.055

S = 0.0137 R^2 = 93.0% R^2 (adj) = 87.3%

As both RSM models have fit the data well, each model was used to generate contour plots to help understand the relationships between the factors and the response variable, the *h* efficiency. The shape of the contours represents any significant interactions and quadratic effects. Figure 8.28 confirms the findings from the previous section and

demonstrates the sensitivity of the F:S ratio in particular *h* efficiency for other operating conditions. Agglomeration efficiency (*h*) is maximized at medium to high F:S values (*i.e.* 0.24 to 0.30). Within that range, the effects of fines size and total solids were small and of no practical relevance. At high F:S values, agglomeration efficiency is maximised for low total solids and low fines size. Maximum agglomeration efficiency was not possible for low F:S values. Figure 8.29 demonstrates the sensitivity of the *h* efficiency to F_{PA}:S_{PA} (F:S PA). Agglomeration efficiency (*h*) is maximized at high F:S PA values. At low F:S PA ratios there is an optimum TS level to ensure agglomeration and increasing fines size increases agglomeration.

This statistical analysis gives a visual picture of the relationships that have been identified earlier. Although it is apparent that there is an optimum level of total solids and fines size for a specific fines to spray flow ratio. This leads to a clearer mechanistic understanding of the significant issues during agglomeration. It is clear that the flux of droplets and particles into the contact zone (both on a mass and projected area basis) is a key aspect to ensure agglomeration, second to this is the mechanism of adherence which is where the size and stickiness of colliding particles becomes important.

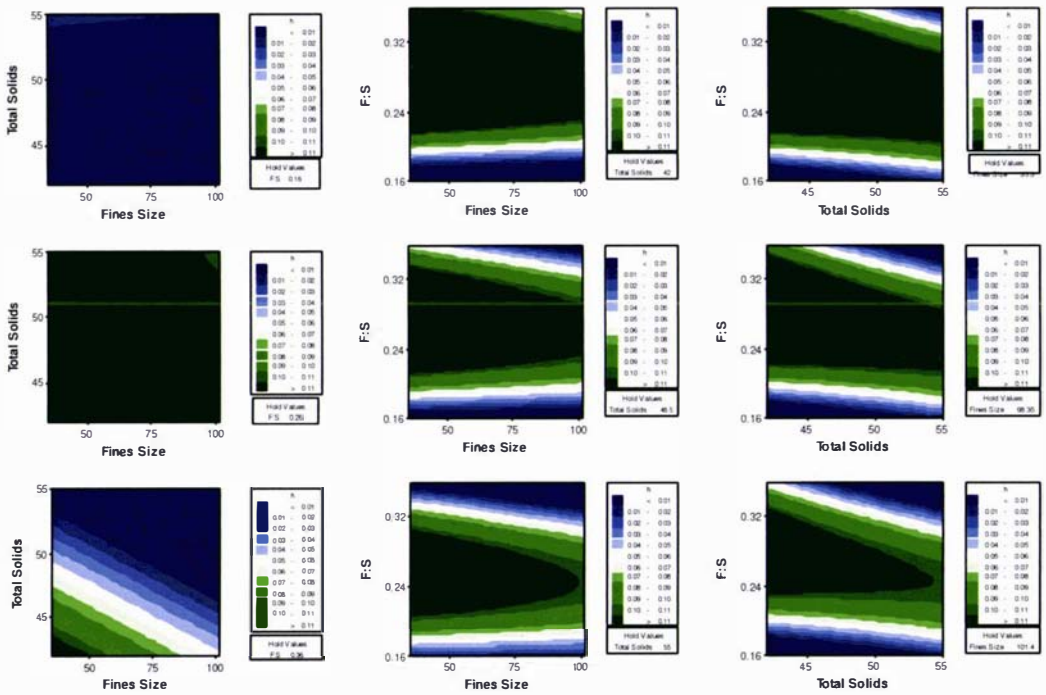

Figure 8.28: Contour plots of total solids, fines size and fines to spray mass flux ratio (F:S) vs. *h* efficiency using model

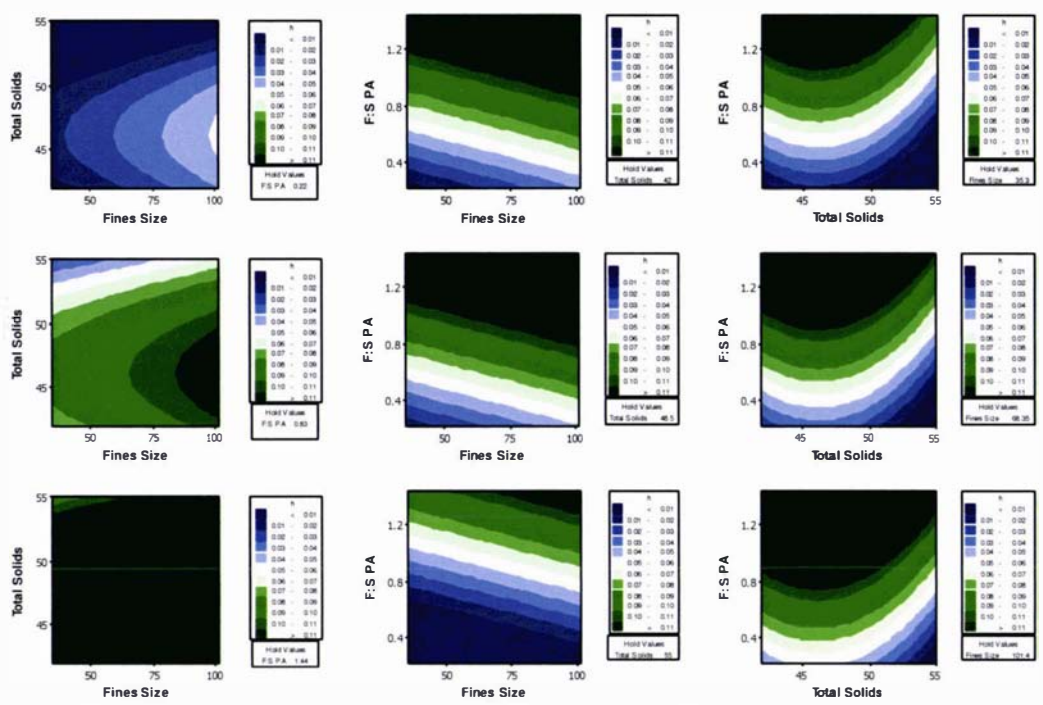

Figure 8.29: Contour plots of total solids, fines size and fines to spray projected area ratio (F:S PA) vs. *h* efficiency using model

8.4 Comparing Small Scale and Pilot Scale Agglomeration Experiments

The pilot scale results are compared to the earlier study on a small scale drier. From this discussion, practical tips are suggested for enhancing and controlling agglomeration in commercial spray driers (§9.2). The *h* efficiency, ξ_h, was previously argued to be the best index to describe the extent of agglomeration across all the processing scales. Table 8.22 shows that the ξ_h values were significantly higher for the two driers operated with fines recycle than for delivery of fines in one-pass mode. Very few conditions were different between the operation modes (one-pass and recycle). The total solids of milk concentrates, the spraying conditions, and the transport of fines to the top of the drier were all similar. Although the internal recirculation inside the drier was unknown this was likely to be quite small compared to the forced recirculation/fines delivery rates and should be identical irrespective of drier operation.

The main differences are in the fines, their size, properties and residence time. In recycle mode, fines are likely to be smaller and they may also have different bulk moisture contents. It is possible that some fines particles were not completely dried whereas fines delivered remotely were manufactured specifically for the purpose and dried to below 4% moisture to ensure acceptable storage conditions. Measurement of the moisture contents of in Table 8.23 demonstrates that there was very little difference between the recycled and manufactured fines moisture content levels. In the recycling systems the residence time was greater than in the one-pass designs; however the difference was not quantifiable and means that the one-pass results cannot be directly compared to the recycle results.

Table 8.22: Comparing between scales and experimental designs.

Experimental Design	*h* efficiency
Industry (Recycle)	0.545
Pilot Scale (Recycle)	0.425
Pilot Scale (One pass)	0.008 – 0.127
Small Scale (One pass)	0.006 – 0.207

Table 8.23: Comparing moisture content of fines.

Moisture Content Units	Fines (%)
Recycle (Run 1)	3.68
One Pass (Run 3)	2.75
Small Fines	2.44
Medium Fines	3.57
Large Fines	3.61

Figure 8.30 and Figure 8.31 directly compare the one-pass experiments for small scale and pilot scale experiments as a function of dimensionless fluxes. The most significant finding was that the small scale experiments can be compared to pilot scale agglomeration. The small scale experiments generally have larger agglomeration efficiencies than the pilot scale experiments due to the higher fines to spray flux ratios although some overlap indicates the same trend was observed. The small scale experiments were carried out using spray droplets of 42% TS and small fines size ($D_{4,3}$ = 30 μm). The highest data point was carried out with the same processing conditions as the other small scale with fines of a medium size ($D_{4,3}$ = 58.8 μm). This result on the small scale was opposite to that observed in the pilot scale experiments, which showed the increase the size of the fines decreased the extent of agglomeration.

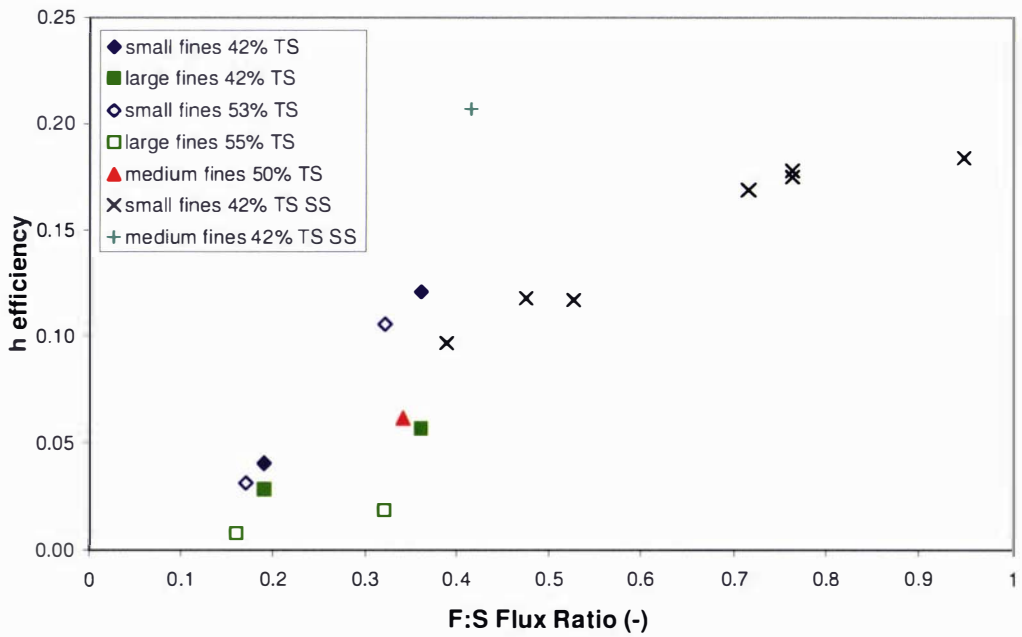

Figure 8.30: F:S flux ratio vs. *h* efficiency for pilot and small scale (SS).

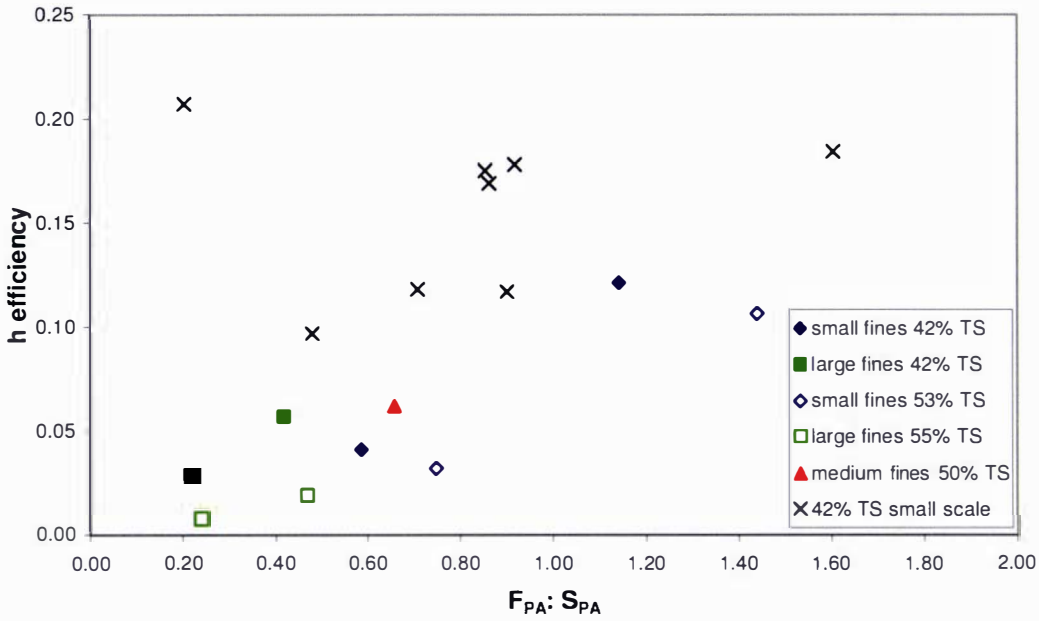

Figure 8.31: F_{PA}:S_{PA} flux ratio vs. h efficiency for pilot and small scale (SS).

While a clear relationship is shown between the dimensionless flux and the extent of agglomeration, the level of turbulence in the collision zone will also be important. Turbulence in this zone was not measured in these experiments but it is likely to be influenced most by the atomisation pressure. Above a certain atomisation pressure droplet size is not changed so the extra energy will be dissipated in turbulent eddies. This will not necessarily translate into more collisions and more agglomeration however as the droplets will also have a lower number concentration due to increased air to droplet ratio in the collision zone. The influence of atomisation pressure on turbulence will also likely be different for the different scales. This is due to the two fluid nozzle producing a flat spray utilised in the small scale experiments and a high pressure nozzle generating a hollow cone spray in pilot and industrial driers.

8.5 Chapter Conclusions

This chapter discussed the effect of operating parameters on agglomeration efficiency on the pilot scale. Some equipment modification was required to allow delivery of fines remotely to the top of the pilot plant spray drier. The key variables, total solids, concentrate and fines flow rate, and fines size were manipulated and the results of this study were discussed with respect to the key mechanisms. A dimensionless flux approach was used to explain the experimental results. The fines to spray mass flux ratio and the projected area flux ratio were found to be the most suitable to represent the physical processes during agglomeration.

Experimental results showed that a higher dimensionless flux resulted in more agglomeration and as did smaller fines size and lower solids concentrate. This finding was explained by a survey of recent literature on collision probability and coalescence. The critical Stokes number explained how viscous dissipation in the liquid bridge of the kinetic energy was critical for coalescence to occur. This highlights the importance of particle size and collision velocity on the outcome of the collision as well as the importance of stickiness on adherence following the collision.

A statistical analysis of the experimental results used response surface methods to confirm the previous observations. The model which included the F:S ratio gave a better fit to the data than the model using the projected area flux ratio. The contour plots generated from these models enabled a clearer mechanistic understanding. It is clear that the mass and projected area flux of droplets and particles through the contact zone strongly influences agglomeration. Practical findings from this research can have a significant impact on successful spray drying operation for instant powders. It will enable improved operation of spray drying and agglomeration equipment to improve product quality and plant productivity.

CHAPTER 9

CONCLUSIONS AND RECOMMENDATIONS

9.1 Conclusions

There is little understanding of the agglomeration processes that occur in the top of a spray drier during instant milk powder production. The complex interaction of variables makes it difficult to predict product properties from the controllable operating parameters. This thesis aimed to understand the effect of key droplet and fines properties on the extent of agglomeration to allow a mechanistic understanding of the process.

A survey of operators showed that control of instant milk powder production to influence bulk density is highly intuitive. Making precise measurements on industrial driers is difficult as there are many interacting and often only semi-controllable variables. Fines recycle rates were expected to be important in control of agglomeration processes and were estimated on a specific plant by using the pressure drop measured in the fines return line. Current models under-predict the pressure drop due to solids so a calibration curve must be generated for each specific drier. Fines recycle rates were found to be significantly higher than expected (95 – 130 % of production capacity compared to 50%).

Measurement of density and viscosity of milk concentrates showed that data agreed with existing models. Experimental results showed that the surface tensions of concentrated milks were within the same range as literature values for standard milks below 60°C, but were significantly higher for milk at above 60°C. This was linked to the Wilhelmy plate technique which requires time to lower and raise the plate, for the solution must drain from the plate and this allows a skin to form. The mechanism that causes this is not known precisely but appears to relate to disulphide cross linking as there is an increased tendency for skin formation at high temperatures and concentrations.

The velocity and droplet size of sprays determine the outcome of a collision with a fines particle in the interaction zone. These properties are difficult to measure and were measured using laser diffraction and a high speed camera. Atomisation pressure was found to have a larger effect on droplet size than the fluid flow rate. For the droplet velocity no relationship between atomisation pressure or fluid type was seen within the error limits.

To carry out a small scale study effectively, it must link to the industrial situation. A small scale agglomerating spray drier was designed to alter droplet and particle properties by delivering a fines particle curtain and spray sheet to the collision zone. An agglomeration index determined the extent of agglomeration between the feed (fines recycle and spray streams) and the product stream (the agglomerated powder). It was found that the presence of fines in the product of the one-pass design obscured the

agglomerates formed. The agglomeration efficiency, ξ_g, was modified to ξ_h to remove obscuration of agglomeration by fines by subtracting them from the agglomerated product distribution. This *h* efficiency was derived from the industrial situation and allows for better comparison between scales.

An experimental study on the small scale equipment investigated natural and forced agglomeration. Little natural agglomeration occurred between spray droplets and a link between the particle size and bulk density of the product was observed. The product yield was found to be unacceptably low (~ 40%) due to adhesion of spray droplets to the drying chamber wall, however yield increased (> 50%) for forced agglomeration experiments due to introduction of the fines curtain to collect spray droplets. A series of preliminary experiments found that the agglomeration performance of the modified spray drier was lower than expected when delivering a fines curtain. A subsequent study optimised the equipment design by considering three key issues; fines dispersion, droplet dispersion and stickiness, and agglomerate breakdown. Final experiments studied agglomeration at low fines to spray mass flux ratios and showed that increasing the fines size had a positive effect on agglomeration efficiency, ξ_h.

The agglomeration study on the pilot scale identified the effect of key variables, total solids, concentrate and fines flow rate, and fines size on the agglomeration efficiency. A dimensionless flux approach was used to explain the experimental results when concentrate flow rate was kept constant. The fines to spray mass flux ratio and the projected area flux ratio were found to be the most suitable to represent the physical processes during agglomeration. Experimental results showed that more agglomeration was obtained with higher dimensionless fluxes, small fines size and atomising low solids concentrate. The critical Stokes number highlighted the importance of particle size and collision velocity on the outcome of the collision. The near surface viscosity is generally unknown, but affects the stickiness of droplets as they dry, as well as the importance of stickiness on adherence following the collision. A statistical analysis established a model for predicting the agglomeration efficiency based on fines size, total solids and the fines to spray mass flux ratio. This project has gained insight into the agglomeration processes during spray drying and knowledge about how to determine the extent of agglomeration. Practical findings from this research can have a significant impact on successful spray drying operating for instant powders.

This work indicates that there is an optimum solids concentration for successful agglomeration. In this situation the fines/spray impact point must be manipulated to ensure droplets of higher viscosity but also acceptable stickiness collide with fine particles. As a droplet dries the bulk and surface moisture content will decrease below this stickiness curve until finally the surface of the particle exhibits no sticky behaviour and droplets are classed as dry particles and rebound upon collision with other dry particles. Droplets with a higher initial solids concentration than other milk concentrate droplets will dry faster at the surface and will be less sticky when colliding with fines particles.

9.2 Practical Tools

From this work some practical tips for control of agglomeration processes can be identified. The results show that the fines to spray flux ratio has a significant effect on the extent of agglomeration. Therefore, it is essential that this ratio is controlled during drier operation. The delivery of milk concentrate to the nozzles is quite consistent during spray drying and is monitored consistently. In contrast the mass flow rate of fines delivered to the top of the drier is not monitored and often fluctuates. Monitoring the fines recycle flow rates is critical because even delivery of both the spray and fines streams can improve the consistency of product properties, e.g. bulk density.

Increasing the ratio of fines to concentrate is not necessarily easy in drier operation particularly if more smaller fines are delivered. Fines flow rates can be manipulated by varying the fluidised bed air flow rates. Increasing air flow would increase the mass flow rate of recycled fines but would also aspirate fines which are larger in size. It may be possible to create small fines through enhanced nozzle operation by either altering the droplet size distribution (through nozzle performance) or diverting a nozzle away from the contact zone; however this may have a negative effect on agglomeration within the drier.

9.3 Recommendations

There are many challenges that remain to be tackled in the area of milk powder agglomeration. There is a need to improve industrial awareness that agglomeration can be improved by monitoring the recycle fines stream. This work produces practical steps to be taken industrially to not only improve bulk density control but also to provide more information for researchers. Some critical measurements are required to allow links to be made between operating parameters and product properties:

- droplet sizes and distributions of industrial sprays
- measurement and control of fines recycle rates
- fines particle sizes (and how drier operating influences fines particle size)
- continuous measurement of vital product properties.

Experimental studies on a small scale are limited by the difficulties associated with atomisation of viscous fluids. It is a challenge for the current equipment design. This thesis has provided an initial experimental study of agglomeration in spray driers which can provide the base for other studies. This includes linking the quality indicators for instant milk powders to agglomerate properties such as size and structure and characterisation of surface stickiness of milk concentrate droplets as they dry.

There is a lack of understanding of the micro-processes that occur during agglomeration at the top of spray driers. Directing research to study each of the micro-processes will allow prediction of optimum operating conditions at small, pilot and finally production scale. The final stage is to close the gap between the understanding key mechanisms and translating this into a useful tool to improve product quality and plant productivity.

REFERENCES

Abrahamson, J. (1975). Collision rates of small particles in a vigorously turbulent fluid. *Chemical Engineering Science, 30*, 1371-1379.

Adhikari, B., Howes, T., Bhandari, B. R., & Truong, V. (2001). Stickiness in Foods: A Review of Mechanisms and Test Methods. *International Journal of Food Properties, 4*(1), 1-33.

Adhikari, B., Howes, T., Bhandari, B. R., & Truong, V. (2003a). In situ characterisation of stickiness of sugar-rich foods using a linear actuator driven stickiness testing device. *Journal of Food Engineering, 58*, 11-22.

Adhikari, B., Howes, T., Bhandari, B. R., & Truong, V. (2003b). Surface Stickiness of Drops of Carbohydrate and Organic Acid Solutions During Convective Drying: Experiments and Modeling. *21*(5), 839-873.

Adhikari, B., Howes, T., Lecomte, D., & Bhandari, B. R. (2005). A glass transition temperature approach for the prediction of the surface stickiness of a drying droplet during spray drying. *Powder Technology, 149*(2-3), 168-179.

Allen, T. (1981). In *Particle Size Measurement* (Vol. 3rd). London: Chapman and Hall.

Anema, S. G. (2000). Effect of milk concentration on the irreversible thermal denaturation and disulfide aggregation of beta-lactoglobulin. *Journal of Agriculture and Food Chemistry, 48*, 4168-4175.

Anema, S. G., & Lugt, F. E. (1998). (No. Fonterra Report NZDRI-1998-099).

Aziz, S. D., & Chandra, S. (2000). Impact, recoil and splashing of molten metal droplets. *International Journal of Heat and Mass Transfer, 43*, 2841-2857.

Bakker, H. H. C. (1988). *Control of particle size distributions in spray dryers with two-fluid nozzles.*, PhD Thesis, University of Canterbury, Christchurch, New Zealand.

Beekman, W. J., Meesters, G. M. H., Scarlett, B., & Becker, T. (2002). Measurement of Granule Attrition and Fatigue in a Vibrating Box. *Particle & Particle Systems Characterization, 19*(1), 5-11.

Berlin, E., Howard, N. M., & Pallansch, M. J. (1964). Specific Surface Areas of Milk Powders Produced by Different Drying Methods. *Journal of Dairy Science, 47*(2), 132-138.

Bertsch, A. J. (1983). Surface tension of whole and skim-milk between 18 and 135°C. *Journal of Dairy Research, 50*, 259-267.

Bertsch, A. J., Bimbenet, J. J., & Cerf, O. (1982). The density of milk and of cream from 65°C to 140°C. *Lait, 62*, 250-264.

Bertsch, A. J., & Cerf, O. (1983). Dynamic viscosities of milk and creams from 70 to 135°C. *Journal of Dairy Research, 50*, 193-200.

Betteridge, N. (1998). *NZDRI Report* (No. DIGTP-DLP-1998-001).

Bhandari, B., Datta, N., Crooks, R., Howes, T., & Rigby, S. (1997). A semi-empirical approach to optimize the quantity of drying aids required to spray dry sugar rich foods. *Drying Technology, 15*, 2509-2525.

Bhandari, B., Datta, N., & Howes, T. (1997). Problems associated with spray drying of sugar-rich foods. *Drying Technology, 15*(2), 671-687.

Bienvenue, A., Jimenez-Flores, R., & Singh, H. (2003). Rheological Properties of Concentrated Skim Milk: Importance of Soluble Minerals in the Changes in Viscosity During Storage. *J. Dairy Sci., 86*(12), 3813-3821.

Birchal, V. S., Huang, L., Mujumdar, A. S., & Passos, M. L. (2006). Spray Dryers: Modeling and Simulation. *Drying Technology, 24*(3), 359-371.

Birchal, V. S., Passos, M. L., Wildhagen, G. R. S., & Mujumdar, A. S. (2005). Effect of spray dryer operating variables on the whole milk powder properties. *Drying Technology, 23*(3), 611-636.

Blei, S., & Sommerfeld, M. (2003). *Lagrangian Modelling of Agglomeration During Spray Drying Processes.* Paper presented at the 9th International Conference on Liquid and Spray Systems, ICLASS, Sorrento, Italy.

Bloore, C. G., & Boag, I. F. (1981). Some factors affecting the viscosity of concentrated skim milk. *New Zealand Journal of Dairy Science and Technology, 16*, 143-154.

Boerefijn, R., & Hounslow, M. J. (2005). Studies of fluid bed granulation in an industrial R&D context. *Chemical Engineering Science, 60*, 3879-3890.

Boonyai, P., Howes, T., & Bhandari, B. (2006). Applications of the Cyclone Stickiness Test for Characterization of Stickiness in Food Powders. *24*(6), 703-709.

Bronlund, J. (1997). *The modelling of caking in bulk lactose.* PhD Thesis, Massey University, Palmerston North, New Zealand.

Brooks, G. E. (2000). *The sticking and crystallisation of amorphous lactose.* Master of Technology, Massey University, Palmerston North, New Zealand.

Brunauer, S., Emmett, P. H., & Teller, E. (1938). Adsorption of Gases in Multimolecular Layers. *Journal of American Chemistry Society, 60*, 309.

Buma, T. J. (1970). Determination of crystalline lactose in spray-dried milk products. *Netherlands Milk Dairy Journal*, 129-132.

Buma, T. J. (1971). Particle size, its estimation. *Netherlands Milk and Dairy Journal, 25*, 23-27.

Buma, T. J. (1980). Viscosity and Density of Concentrated Lactose Solutions and of Concentrated Cheese Whey. *Netherlands Milk Dairy Journal, 34*(65-68).

Bylund, G. (1995). *Dairy Processing Handbook*. Lund, Sweden: Tetra Pak Processing Systems AB.

Cabrejos, F. J., & Klinzing, G. E. (1992). *Novel solids pressure drop flow meter*. Paper presented at the ASME Winter Annual Meeting, Anaheim, CA.

Capes, C. E., & Darcovich, K. (1997). In *Kirk Othmer Encylopedia of Chemical Technology* (Vol. 4). New York, USA: John Wiley and Sons.

Caric, M. (2002). Types and Manufacture. In *Milk Powders* (pp. 1869-1874). Oxford: Elsevier Science Ltd.

Caric, M., & Milanovic, S. (2002). Physical and Functional Properties of Milk Powders. In *Milk Powders* (pp. 1874-1880). Oxford: Elsevier Science Ltd.

Chatterjee, R. (2004). *Characterising Stickiness of Dairy Powders*. Institute of Technology and Engineering, Massey University.

Chegini, G. R., & Ghobadian, B. (2005). Effect of spray-drying conditions on physical properties of orange juice powder. *Drying Technology, 23*(3), 657-668.

Chen, X. D. (1992). Whole Milk Powder Agglomeration - Principles and Practise. In *Milk Powders for the Future*. Palmerston North, New Zealand: Dunmore Press.

Chen, X. D. (1994). *Selected Fundamental Aspects of the Drying of Milk*. Palmerston North, New Zealand: Dunmore Press.

Chen, X. D., Rennie, P. R., & Mackereth, A. R. (2004). Combined Influences of Humidity and Temperature upon the Inter-Particle Stickiness of a Whole Milk Powder. *International Journal of Food Properties, 7*(3), 499-509.

Chuy, L. E., & Labuza, T. P. (1994). Caking and Stickiness of Dairy-Based Food Powders as Related to Glass Transition. *Journal of Food Science, 59*(1), 43-46.

Clement, K. H., Hallstrom, A., Dich, H. C., Le, C. M., Mortensen, J., & Thomsen, H. A. (1997). On the dynamic behaviour of spray driers. *Transactions of the Institution of Chemical Engineers, 69*(A), 245-252.

CODEX. (1999). *Milk powders and cream powder* (Vol. 207): Codex Alimentarius Commision, Rome.

Cryer, S. A. (1999). Modeling Agglomeration Processes in Fluid-Bed Granulation. *AIChE Journal, 45*(10), 2069-2078.

Dewettinck, K., & Huyghebaert, A. (1998). Top-Spray Fluidized Bed Coating: Effect of Process Variables on Coating Efficiency *Lebensmittel-Wissenschaft und-Technologie, 31*(6), 568-575.

Di Felice, R. (1994). The voidage function for fluid-particle interaction systems. *International Journal of Multiphase Flow, 20*(1), 153-159.

Downton, G. E., Flores-Luna, J. L., & King, C. J. (1982). Mechanism of Stickiness in Hygroscopic Amorphous Powders. *Industrial Engineering and Chemistry Fundamentals, 251*, 447-451.

Eilers, H. (1941). Die Viskosität von Emulsionen hochviskoser Stoffeals Funktion der Konzentration. *Kolloid-Z, 97*, 313.

Elversson, J., Millqvist-Fureby, A., Alderborn, G., & Elofsson, U. (2003). Droplet and Particle Size Relationship and Shell Thickness of Inhalable Lactose Particles during Spray Drying. *Journal of Pharmaceutical Sciences, 92*(4), 900-910.

Ennis, B. J., Tardos, G. I., & Pfeffer, R. (1991). A microlevel-based characterisation of granulation phenomena. *Powder Technology, 65*(2), 257-272.

Fairbrother, R. J., & Simons, S. J. R. (1998). Modelling of Binder-Induced Agglomeration. *Particle & Particle Systems Characterisation, 15*, 16-20.

Fan, L. S., & Zhu, C. (1998). *Principles of Gas-Solids Flows.* New York: Cambridge University Press.

Fernandez-Martin, F. (1972). Influence of temperature and composition on some physical properties of milk and milk concentrates. II Viscosity. *Journal of Dairy Research, 35*, 75-87.

Field-Mitchell, G. (2002). Granulation of Whole Milk Powder. *Masterate Theses, Massey University, Palmerston North, New Zealand.*

Fitzpatrick, J. J., & Ahrne, L. (2005). Food powder handling and processing: Industry problems, knowledge barriers and research opportunities: Pneumatic Conveying and Handling of Particulate Solids. *Chemical Engineering and Processing, 44*(2), 209-214.

Fitzpatrick, J. J., & Cuthbert, R. (2004). Effect of temperature on the reconstitution of milk powder to high solids content in a stirred tank. *Milchwissenschaft, 59*(1), 55-58.

Fletcher, D. F., Guo, B., Harvie, D. J. E., Langrish, T. A. G., Nijdam, J. J., & Williams, J. (2006). What is important in the simulation of spray dryer performance and how do current CFD models perform? *Applied Mathematical Modelling, In Press, Corrected Proof.*

Foster, K. D. (2002). *The prediction of sticking in dairy powders.* PhD Thesis, Massey University, Palmerston North, New Zealand.

Goldschmidt, M. J. V., Weijers, G. G. C., Boerefijn, R., & Kuipers, J. A. M. (2003). Discrete element modelling of fluidised bed spray granulation. *Powder Technology, 138*, 39-45.

Goula, A. M., Adamopoulos, K. G., & Kazakis, N. A. (2004). Influence of Spray Drying Conditions on Tomato Powder Properties. *Drying Technology, 22*(5), 1129-1151.

Guignon, B., Duquenoy, A., & Dumoulin, E. (2002). Fluid Bed Encapsulation of Particles: Principles and Practise. *Drying Technology, 20*(2), 419-447.

Guignon, B., Regalado, E., Duquenoy, A., & Dumoulin, E. (2003). Helping to choose operating parameters for a coating fluid bed process. *Powder Technology, 130*(1-3), 193-198.

Hapgood, K. P. (2001). *Nucleation and binder dispersion in wet granulation.* University of Queensland, Brisbane, Australia.

Hapgood, K. P., Litster, J. D., & Smith, R. (2003). Nucleation Regime Map for Liquid Bound Granules. *Particle Technology and Fluidization, 49*(2), 350-361.

Harvie, D. J. E., Langrish, T. A. G., & Fletcher, D. F. (2002). A computational fluid dynamics study of a tall form spray drier. *Trans IChemE, 80*(C), 163-175.

Hassan, H. M., & Mumford, C. J. (1993). Mechanisms of drying of skin forming materials III. droplet of natural products. *Drying Technology, 11*(7), 1765-1782.

Hennings, C., Kockel, T. K., & Langrish, T. A. G. (2001). New measurements of the sticky behaviour of skim milk powder. *Drying Technology, 10*(3/4), 471-484.

Henthorn, K. H., Park, K., & Curtis, J. S. (2005). Measurement and Prediction of Pressure Drop in Pneumatic Conveying: Effect of Particle Characteristics, Mass Loading, and Reynolds Number. *Ind. Eng. Chem. Res., 44*(14), 5090-5098.

Hettiaratchi, K., Woodhead, S. R., & Reed, A. R. (1998). Comparison between pressure drop in horizontal and vertical pneumatic conveying pipelines. *Powder Technology, 95*, 67-73.

Hinkle, B. L. (1953). *Acceleration of particles and pressure drops encountered in horizontal pneumatic conveying.* PhD Thesis, Georgia Institute of Technology.

Hla, P. K., & Hogekamp, S. (1999). Wetting behaviour of instantized cocoa beverage powders. *International Journal of Food Science and Technology, 34*, 335-342.

Ho, C. A., & Sommerfeld, M. (2002). Modelling of micro-particle agglomeration in turbulent flows. *Chemical Engineering Science, 57*(15), 3073-3084.

Hogekamp, S. (1999a). Steam-Jet Agglomeration - Part 2: Modelling Agglomerate Growth in a Modified Steam-Jet Agglomerator. *Chemical Engineering and Technology, 22*(6), 485-490.

Hogekamp, S. (1999b). Steam Jet Agglomeration - Part 1: Production of Redispersible Agglomerates by Steam Jet Agglomeration. *Chemical Engineering and Technology, 22*(5), 421-424.

Hogekamp, S., & Pohl, M. (2003). Porosity measurement of fragile agglomerates. *Powder Technology, 130*, 385-392.

Hogg, R. (1989). Role of Colloid and Interface science in agglomeration. *ICHEME 5th International Symposium on Agglomeration.*

Houska, M. (1994). *Milk, milk products and semiproducts: thermophysical and rheological properties of foods.* Prague: Institute of Agricultural and Food Information.

Hruby, J., Steeper, R., Evans, G., & Crow, C. (1988). An experimental and numerical study of flow and convective heat transfer in a freely falling curtain of particles. *Journal of Fluids Engineering, 110*(2), 172-181.

Huang, L. X., Kumar, K., & Mujumdar, A. S. (2006). A comparative study of a spray dryer with rotary disc atomizer and pressure nozzle using computational fluid dynamic simulations. *Chemical Engineering and Processing, 45*, 461-470.

Huntington, D. H. (2004). The Influence of the Spray Drying Process on Product Properties. *Drying Technology, 22*(6), 1261-1287.

Ilari, J. L. (2002). Flow properties of industrial dairy powders. *Lait, 82*, 383-399.

Irvine, T. F., & Liley, P. E. (1984). *Steam and Gas Tables with Computer Equations.* USA: Academic Press.

Iveson, S. M., Beathe, J. A., & Page, N. W. (2002). The dynamic strength of partially saturated powder compacts: the effect of liquid properties. *Powder Technology, 127*(2), 149-161.

Iveson, S. M., Litster, J. D., & Ennis, B. J. (1996). Fundamental studies of granule consolidation Part 1: Effects of binder content and binder viscosity. *Powder Technology, 88*(1), 15-20.

Iveson, S. M., Litster, J. M., Hapgood, K., & Ennis, B. J. (2001). Nucleation, growth and breakage phenomena in agitated wet granulation processes: a review. *Powder Technology, 117*, 3-39.

Janal, R. S. L. (1975). The change in viscosity, electrical conductivity and surface tension with the fat content in milk (in Czech). *Prumysl potravin, 26*(4), 235-238.

Jones, D. (1992). *Investigation of the current straight-through agglomeration process for milk powder manufacture.* Massey University, Palmerston North, New Zealand.

Jones, J. R. (2005). *A Simplified Agglomeration Model.* Paper presented at the 8th International Symposium on Agglomeration, Bangkok, Thailand.

Joyner, L. G., Barrett, E. P., & Skold, R. (1951). The Determination of Pore Volume and Area Distributions in Porous Substances. II. Comparison between Nitrogen Isotherm and Mercury Porosimeter Methods. *Journal of American Chemical Society, 73*(3155-3158).

Kammler, H. K., Beaucage, G., Mueller, R., & Pratsinis, S. E. (2004). Structure of Flame-Made Silica Nanoparticles by Ultra-Small-Angle X-ray Scattering. *Langmuir, 20*, 1915-1921.

Kelly, P. M. (2006). Innovation in milk power technology. *International Journal of Dairy Technology, 59*(2), 70-75.

Keningley, S. T., Knight, P. C., & Marson, A. D. (1997). An investigation into the effects of binder viscosity on agglomeration behaviour. *Powder Technology, 91*, 95-103.

Kentish, S., Davidson, M., Hassan, H., & Bloore, C. (2005). Milk skin formation during drying. *Chemical Engineering Science, 60*(3), 635-646.

Kim, E. H. J., Chen, X. D., & Pearce, D. (2002). Surface characterisation of four industrial spray-dried dairy powders in relation to chemical composition, structure and wetting property. *Colloids and Surfaces B: Biointerfaces, 26*(3), 197-212.

Kim, E. H. J., Chen, X. D., & Pearce, D. (2003). On the Mechanisms of Surface Formation and the Surface Compositions of Industrial Milk Powders. *21*(2), 265-278.

Kim, W. T., Mitra, S. K., Li, X., Prociw, L. A., & Hu, T. C. J. (2003). A predictive model for the initial droplet size and velocity distributions in sprays and comparison with experiments. *Particle & Particle System Characterisation, 20*, 135-149.

Klinzing, G. E. (1980). *Gas–Solid Transport.* New York: McGraw-Hill.

Kockel, T. K., Allen, S., Hennigs, C., & Langrish, T. A. G. (2002). An experimental study of the equilibrium for skim milk powder at elevated temperatures. *Journal of Food Engineering, 51*(4), 291-297.

Konno, H., & Saito, S. (1969). Pneumatic Conveying of Solids Through Straight Pipes. *J. Chem. Eng. Jpn., 5*, 211.

Kristensen, D., Jensen, P. Y., Madsen, F., & Bird, K. S. (1997). Rheology and Surface Tension of Selected Processed Dairy Fluids: Influence of Temperature. *Journal of Dairy Science, 80*, 2282-2290.

Kudra, T. (2003). Sticky Region in Drying - Definition and Identification. *Drying Technology, 21*(8), 1457-1469.

Kuk, G. M. (1955). *Prozesse un Apparate in der Milchindustrie, Band 1.* Moscow: Verlag Lebensmittelindustrie.

Kwapinska, M., & Zbicinski, I. (2005). Prediction of Final Product Properties After Cocurrent Spray Drying. *23*(8), 1653-1665.

Langrish, T. A. G., & Fletcher, D. F. (2001). Spray drying of food ingredients and applications of CFD in spray drying. *Chemical Engineering and Processing, 40*, 345-354.

Langrish, T. A. G., & Kockel, T. K. (2001). The assessment of a characteristic drying curve for milk powder for use in computational fluid dynamics modelling. *Chemical Engineering Journal, 84*(1), 69-74.

Lech, M. (2001). Mass flowrate measurement in vertical pneumatic conveying of solid. *Powder Technology, 114*, 55-58.

Lin, S. X. Q., & Chen, X. D. (2002). Improving the glass-filament method for accurate measurement of drying kinetics of liquid droplets. *Transactions of the Institute of Chemical Engineers, 80.*

Lin, S. X. Q., & Chen, X. D. (2004). Changes in milk droplet diameter during drying under constant drying conditions investigated using the glass-filament method. *Transactions of IChemE, 82*(C3), 213-218.

Link, K. C., & Schlünder, E. (1996). A new method for the characterisation of the wettability of powders. *Chemical Engineering Technology, 19*, 423-437.

Link, K. C., & Schlünder, E. (1997). Fluidized bed spray granulation: Investigation of the coating process on a single sphere. *Chemical Engineering and Processing, 36*(6), 443-457.

Litster, J. D., Hapgood, K. P., Michaels, J. N., Sims, A., Roberts, M., Kameneni, S. K., et al. (2001). Liquid distribution in wet granulation: dimensionless spray flux. *Powder Technology, 114*, 32-39.

Liu, D. M., Lin, T. T., & Tuan, W. H. (1999). Interdependence between green compact property and powder agglomeration and their relation to the sintering behaviour of zirconia powder. *Ceramics International, 25*, 551-559.

Liu, H. (2000). *Science and Engineering of Droplets - Fundamentals and Applications.* Norwich, New York: William Andrew.

Liu, L. X., Litster, J. D., Iveson, S. M., & Ennis, B. J. (2000). Coalescence of Deformable Granules in Wet Granulation Processes. *AIChE Journal, 46*(3), 529-539.

Lloyd, R. J., Chen, X. D., & Hargreaves, J. B. (1996). Glass transition and caking of spray dried lactose. *International Journal of Food Science and Technology, 31*, 305-311.

Luyben, K. C. A. M., Liou, J. K., & Bruin, S. (1982). Enzyme degradation during drying. *Biotechnology and Bioengineering, 24*, 533-552.

Maa, Y.-F., Nguyen, P.-A., & Hsu, C. C. (1996). Spray-coating of rhDNase on lactose : effect of system design, operational parameters and protein formulation. *International Journal of Pharmaceutics 144*(1), 47-59.

Maa, Y.-F., Nguyen, P.-A., Sit, K., & HSU, C. C. (1998). Spray-Drying Performance of a Bench-Top Spray Dryer for Protein Aerosol Powder Preparation. *Biotechnology and Bioengineering, 60*(3), 301-309.

Mackereth, A. (1983). *NZDRI Report* (No. MP83R18).

Mackereth, A. R. (1985). *NZDRI Report* (No. MP85R9 DS 4741).

Mao, C. P., & Tate, R. (1997). In *Sprays* (Vol. 4). New York, USA.: John Wiley and Sons.

Masters, K. (1979). *Spray Drying Handbook*. New York: John Wiley and Sons.

Masters, K. (2002). *Spray Drying in Practise*. Denmark: SprayDryConsult International ApS.

Masters, K. (2004). Current Market-Driven Spray Drying Development Activities. *Drying Technology, 22*(6), 1351-1370.

McLeod, J. S., Jones, J. R., & Paterson, A. H. J. (2006). *A Preliminary Look at the Use of the Weibull Distribution for the Prediction of Growth Rate Dispersion in Lactose Crystals which have been Preselected Based on Size*. Paper presented at the Chemeca 2006, Auckland, New Zealand.

Middleton, J. (1996). *Physical Properties of Dairy Products*: New Zealand: MAF Quality Management, Ministry of Agriculture.

Muhkerjee, N., Bansal, B., & Chen, X. D. (2005). Measurement of Surface Tension of Homogenised Milks. *International Journal of Food Engineering, 1*(2).

Mujumdar, A. S. (1992). *Advances in Drying: Volume 5*. Washington.: Hemisphere.

Mujumdar, A. S. (2004). Research and Development in Drying: Recent Trends and Future Prospects. *Drying Technology, 33*(1 & 2), 1-26.

Murti, R. A. (2006). *The effect of lactose source on the stickiness of dairy powders*. Masters of Engineering, Massey University, Palmerston North, New Zealand.

Murti, R. A., Paterson, T., Pearce, D., & Bronlund, J. (2006). *Characterisation of the sticky point of dairy powders using the particle gun technique*, Orlando, Florida.

Namkung, W., & Minyoung, C. (2002). Pressure Drop in a Vertical Pneumatic Conveying of Iron Ore. *Ind. Eng. Chem. Res., 41*, 5316-5320.

Newstead, D. (1994). *Investigation of skin formation on heated milks*. New Zealand Dairy Research Institute, Palmerston North, New Zealand.

Nguyen, D. A., & Rhodes, M. J. (1998). Producing fine drops of water by twin-fluid atomisation. *Powder Technology, 99*, 285-292.

Nieuwenhuijse, J. A. W., Timmermans, W., & Walstra, P. (1988). Calcium and phosphate partitions during the manufacture of sterilized concentrated milk and their relations to the heat stability. *Netherlands Milk and Dairy Journal, 42*, 387-421.

Nijdam, J. J., Guo, B., Fletcher, D. F., & Langrish, T. A. G. (2003). *Lagrangian and Eulerian Models for Simulating Turbulent Dispersion and Agglomeration of Droplets within a Spray*.

Nijdam, J. J., Guo, B., Fletcher, D. F., & Langrish, T. A. G. (2004). Challenges of simulating droplet coalescence within a spray. *Drying Technology, 22*(6), 1463-1488.

Nijdam, J. J., & Langrish, T. A. G. (2005). An Investigation of Milk Powders Produced by a Laboratory-Scale Spray Dryer. *Drying Technology, 23*, 1043-1056.

Nijdam, J. J., & Langrish, T. A. G. (2006). The effect of surface composition on the functional properties of milk powders. *Journal of Food Engineering, 77*, 919-925.

Oakley, D. E. (2004). Spray dryer modeling in theory and practise. *Drying Technology, 22*(6), 1371-1402.

Ogata, K., Funatsu, K., & Tomita, Y. (2001). Experimental investigation of a free falling powder jet and the air entrainment. *Powder Technology, 115*, 90-95.

Ozkan, N., Walisinghe, N., & Chen, X. D. (2002). Characterisation of stickiness and cake formation in whole and skim milk powders. *Journal of Food Engineering, 55*, 293-303.

Ozmen, L., & Langrish, T. A. G. (2002). Comparison of Glass Transition Temperature and Sticky Point Temperature for Skim Milk Powder. *Drying Technology, 20*(6), 1177-1192.

Ozmen, L., & Langrish, T. A. G. (2003a). An Experimental Investigation of the Wall Deposition of Milk Powder in a Pilot-Scale Spray Dryer. *Drying Technology, 21*(7), 1253-1272.

Ozmen, L., & Langrish, T. A. G. (2003b). A Study of the Limitations to Spray Drier Outlet Performance. *Drying Technology, 21*(5), 895.

Palzer, S. (2005). The effect of glass transition on the desired and undesired agglomeration of amorphous food powders. *Chemical Engineering Science, 60*(3959-3968).

Panchagnula, M. V., & Sojka, P. E. (1999). Spatial droplet velocity and size profiles in effervescent atomizer-produced sprays. *Fuel, 78*(6), 729-741.

Panda, R. C., Zank, J., & Martin, H. (2001). Experimental investigation of droplet deposition on a single particle. *Chemical Engineering Journal, 83*, 1-5.

Papadakis, S. E., & Bahu, R. (1992). The sticky issues of drying. *Drying Technology, 10*(4), 817-837.

Papadakis, S. E., Bahu, R. E., McKenszie, K. A., & Kemp, I. C. (1993). Correlations for the equilibrium moisture content of solids. *Drying Technology, 11*(3), 543-553.

Paramalingam, S., Bakker, H. C., & Chen, H. (2002). *Physical Properties of Whey Products.* Paper presented at the 9th APCChE & Chemeca 2002, Christchurch, New Zealand.

Parker, B. R. (1978). *Atomisation of Spray-dryer feedstocks I: measurement of mean drop-size on full-scale plant and a comparison with the literature correlations* (No. RR5 R9040). Springs, UK: Separation Processes Service, Harwell/Warren.

Pasandideh-Fard, M., Chandra, S., & Mostaghimi, J. (2002). A three-dimensional model of droplet impact and solidification. *International Journal of Heat and Mass Transfer, 45*, 2229-2242.

Pasandideh-Fard, M., Qiao, Y. M., Chandra, S., & Mostaghimi, J. (1996). Capillary effects during droplet impact on a solid surface. *Physics of Fluids, 8*, 650-659.

Paterson, A. H. J., Brooks, G. F., Bronlund, J. E., & Foster, K. D. (2005). Development of stickiness in amorphous lactose at constant T - Tg. *International Dairy Journal, 15*, 513-519.

Perry, R. H., & Green, D. W. (1997). In *Perry's Chemical Engineers' Handbook, 7th Edition*: McGraw-Hill.

Petera, J., & Weatherley, L. R. (2001). Modelling of mass transfer from falling droplets. *Chemical Engineering Science, 56*, 4929-4947.

Pietsch, W. (2003). An interdisciplinary approach to size enlargement by agglomeration. *Powder Technology, 130*, 8-13.

Pisecky, J. (1978). Bulk density of milk powders. *Dairy Industries International*, 4-11.

Pisecky, J. (1997). *Handbook of Milk Powder Manufacture*. Copenhagen, Denmark.: Niro A/S.

Ranz, W. E., & Marshall, W. R. (1952). Evaporation from Drops: Parts 1 and 2. *Chemical Engineering Progress, 48*(3/4).

Rautiainen, A., & Sarkomaa, P. (1998). Solids friction factors in upward, lean gas-solids flows. *Powder Technology, 95*(1), 25-35.

Rautiainen, A., Stewart, G., Poikolainen, V., & Sarkomaa, P. (1999). An experimental study of vertical pneumatic conveying. *Powder Technology, 104*, 139-150.

Reineccius, G. A. (2004). The Spray Drying of Food Flavors. *22*(6), 1289-1324.

Renner, C. A. (1989). *Investigation of Instant Skim Milk Powder Agglomerate Fragility*, . Massey University, Palmerston North, New Zealand.

Rennie, P. R., Chen, X. D., Hargreaves, C., & Mackereth, A. R. (1999). A study of the cohesion of dairy powders. *Journal of Food Engineering, 39*, 277 284.

Retsina, T. (1988). Agglomeration: a process to improve fine powder handling. *Food Technology International*, 37-39.

Reynolds, G. K., Fu, J. S., Cheong, Y. S., Hounslow, M. J., & Salman, A. D. (2005). Breakage in granulation: A review. *Chemical Engineering Science, 60*(14), 3969-3992.

Rhodes, M. (1998). Pneumatic transport and standpipes. In *Introduction to Particle Technology* (pp. 139). England: John Wiley & Sons.

Roos, Y. H. (2002). Importance of glass transition and water activity to spray drying and stability of dairy powders. *Le Lait, 82*, 475-484.

Roosen, A., & Hausner, H. (1984). Sintering kinetics of zirconia powders. *Advances in Ceramics, 12*, 714-726.

Rumpf, H. (1990). *Particle Technology*. London: Chapman and Hall.

Samimi, A., Ghadiri, M., Boerefijn, R., Groot, A., & Kohlus, R. (2003). Effect of structural characteristics on impact breakage of agglomerates. *Powder Technology, 130*(1-3), 428-435.

Sano, Y., & Keey, B. (1982). The drying of a spherical particle containing colloidal material into a hollow sphere. *Chemical Engineering Science, 37*(6), 881–889.

Schelling, J., & Reh, L. (1999). Influence of atomiser design and coaxial gas velocity on gas entrainment into sprays. *Chemical Engineering and Processing, 38*(4-6), 383-393.

Schmid, H. J., Al-Zaitone, B., Artelt, C., & Peukert, W. (2006). Evolution of the fractal dimension for simultaneous coagulation and sintering. *Chemical Engineering Science, 61*, 293-305.

Schubert, H. (1987). Food particle technology, Part 1: Properties of particles and particulate food system. *Journal of Food Engineering, 6*, 1-32.

Schuchmann, H., Hogekamp, S., & Schubert, H. (1993). Jet agglomeration processes for instant foods. *Trends in Food Science and Technology, 4*, 179-183.

Schwartzbach, C., & Masters, K. (2001). Performance of Spray Dryer with Integrated Filter and Fluid Bed. *Drying Technology, 19*(8), 1909-1923.

Shakeri, S., & Chandra, S. (2002). Splashing of molten tin droplets on a rough steel surface. *International Journal of Heat and Mass Transfer, 45*, 4561-4575.

Simons, S. J. R., Seville, J. P. K., & Adams, M. J. (1994). An analysis of the rupture energy of pendular liquid bridges. *Chemical Engineering Science, 49*(14), 2331-2339.

Snoeren, T. H. M., Brinkhuis, J. A., Damman, A. J., & Klok, H. J. (1984). Viscosity and age-thickening of skim-milk concentrate. *Netherlands Milk Dairy, 38*, 45-53.

Snoeren, T. H. M., Damman, A. J., & Klok, H. J. (1981). Effect of concentrate viscosity on the properties of skim milk powder. *Zuivelzicht, 73*(47).

Snoeren, T. H. M., Damman, A. J., & Klok, H. J. (1982). The viscosity of skim milk concentrates. *Netherlands Milk Dairy Journal, 36*, 305-316.

Sommerfeld, M. (2001). Validation of a stochastic Lagrangian modelling approach for inter-particle collisions in homogeneous isotropic turbulence. *International Journal of Multiphase Flow, 27*(10), 1829-1858.

Sowersby, J. (2004). (No. TIF-2000-009).

Staiger, M., Bowen, P., Ketterer, J., & Bohonek, J. (2002). Particle Size Distribution Measurement and Assessment of Agglomeration of Commercial Nanosized Ceramic Particles. *Journal of Dispersion Science and Technology, 23*(5), 619-630.

Street, R. T. L., Watters, G. Z., & Vennard, J. K. (1996). *Elementary fluid mechanics* (Vol. 7th Edition): John Wiley and Sons. New York.

Tallon, S., & Davies, C. E. (2000). *Acoustic Sensing of Solids Flow in Pneumatic Conveying: a Development Perspective.* Paper presented at the Chemeca 2000, Perth, Australia.

Tardos, G. I., Khan, M. I., & Mort, P. R. (1997). Critical parameters and limiting conditions in binder granulation of fine powders. *Powder Technology, 94*(3), 245-258.

Tardos, G. I., & Talu, I. (2000). Agglomerate Growth and Break up in Wet Granulation of fine powders. *http://www-che.engr.ccny.cuny.edu/tardos/download/China-Paper-2000.pdf.*

Trinh, B., Haisman, D., & Trinh, K. T. (2002). *Design of recombination system for time-dependent food systems.* Paper presented at the APCChe Congress, Christchurch, New Zealand.

Trinh, B., Haisman, D., Trinh, K. T., Croy, R. J., & Hemar, Y. (2002). *Effect of total solids concentration and temperature on the rheology profile of reconstituted milk concentrates.* Paper presented at the APCChe Congress, Christchurch, New Zealand.

Truong, V., Bhandari, B. R., & Howes, T. (2005a). Optimization of co-current spray drying process of sugar-rich foods. Part I - Moisture and glass transition temperature profile during drying. *Journal of Food Engineering, 71*, 55-65.

Truong, V., Bhandari, B. R., & Howes, T. (2005b). Optimization of co-current spray drying process of sugar-rich foods. Part II - Optimization of spray drying process based on glass transition concept. *Journal of Food Engineering, 71*(66-72).

van der Hoeven, M. J., Litster, J. D., Cameron, I. T., Howes, T., Meesters, G. M. H., & Wildeboer, W. J. (2006). *Influence of surface tack of food products on agglomeration in spray drying.* Paper presented at the 5th World Congress on Particle Technology, Orlando, Florida, USA.

van Laarhoven, B., Wiers, S. C. A., Schaafsma, S. H., & Meesters, G. M. H. (2006). *Development of an Abrasion Tester for Testing Coated Granules.* Paper presented at the 5th World Congress on Particle Technology, Orlando, Florida.

Venkatasubramanian, S., Tashiro, H., Klinzing, G. E., & Mykelbust, K. (2000). Solids flow behaviour in bends: assessing fine solids buildup. *Powder Technology, 113*, 124-131.

Verdurmen, R. E. M., Houwelingen, G., Gunsing, M., Verschueren, M., & Straatsma, J. (2006). Agglomeration in Spray Drying Installations (The EDECAD Project): Stickiness Measurements and Simulation Results. *Drying Technology, 24*(6), 721-726.

Verdurmen, R. E. M., Menn, P., Ritzert, J., Blei, S., Nhumaio, G. C. S., Sorensen, T. S., et al. (2004). Simulation of agglomeration in spray drying installations: the EDECAD project. *Drying Technology, 22*(6), 1403-1461.

Verhey, J. G. P. (1973). Vacuole formation in spray powder particles: 3, atomisation and droplet drying. *Netherlands Milk Dairy Journal, 27*, 3-18.

Walstra, P. (1999). *Dairy Technology: Principles of Milk Properties and Processes*. New York, USA.: Marcel Dekker.

Walton, D. E., & Mumford, C. J. (1999). Spray dried products - characterization of particle morphology. *Trans IChemE, 77*(Part A).

Wardjiman, C., & Rhodes, M. (2006). *Shape of a Particle Curtain Falling into Stagnant Air*. Paper presented at the 5th World Congress on Particle Technology, Orlando, Florida.

Wardjiman, C., Wang, S., & Rhodes, M. (2005). *Behaviour of a Curtain of Particles Falling Through a Horizontal Gas Stream*. Paper presented at the Chemeca, Brisbane, Australia.

Watson, P. D. (1958). Effect of Variations in Fat and Temperature on the Surface Tension of Various Milks. *Journal of Dairy Science, 41*, 1693-1698.

Werner, S. R. L. (2005). *Air-suspension coating of dairy powders: a micro-level process approach*. PhD Thesis, Massey University, Palmerston North, New Zealand.

Werner, S. R. L., Jones, J. R., & Paterson, A. H. J. (2007a). Droplet impact and spreading droplet formulation effects. *Chemical Engineering Science, 62*, 2336 – 2345.

Werner, S. R. L., Jones, J. R., & Paterson, A. H. J. (2007b). Stickiness of maltodextrins using probe tack test during in-situ drying. *Journal of Food Engineering, 80*, 859-868.

Werner, S. R. L., Jones, J. R., Paterson, A. H. J., Archer, R. H., & Pearce, D. L. (2005). *Droplet impact and spreading in relation to air-suspension particle coating*.

Wesselingh, J. A., & Bollen, A. M. (1999). Single particles, bubbles and drops: their velocities and mass transfer coefficients. *Trans IChemE, 77*(A), 89-96.

Westermarck, S., Juppo, A. M., Kervinen, L., & Yliruusi, J. (1998). Pore structure and surface area of mannitol powder, granules and tablets determined with mercury porosimetry and nitrogen adsorption. *European Journal of Pharmaceutics and Biopharmaceutics, 46*(1), 61-68.

Westermarck, S., Juppo, A. M., Kervinen, L., & Yliruusi, J. (1999). Microcrystalline cellulose and its microstructure in pharmaceutical processing. *European Journal of Pharmaceutics and Biopharmaceutics, 48*(3), 199-206.

Wewala, A. R. (1992). Effect of Water Activity on Whole Milk Powder Storage Stability. In *Milk Powders for the Future.* Palmerston North, New Zealand: Dunmore Press.

Whitnah, C. H. (1959). The surface tension of milk. A review. *Journal of Dairy Science, 42*, 1437-1449.

Whitnah, C. H., Conrad, R. M., & Cook, G. L. (1949). Milk Surfaces. I. The Surface Tension of Fresh Surfaces of Milk and Certain Derivatives. *Journal of Dairy Science, 32*, 406-417.

Wijlhuizen, A. E., Kerkhof, P. J. A. M., & Bruin, S. (1979). Theoretical study of the inactivation of phosphatase during spray drying of skim-milk. *Chemical Engineering Science, 34*(651-660).

Wong, N. (1988). *Fundamentals of Dairy Chemistry.* New York: Van Nostrand Reihold Co.

Wood, P. W. (1996). *Physical Properties of Dairy Products.* Hamilton, New Zealand: MAF Quality Management, Ministry of Agriculture.

Yan, Y. (1996). Mass flow measurement of bulk solids in pneumatic pipelines. *Measurement Science Technology, 7*, 1687-1706.

Yang, W. C., Ekhardt, D. A., & Skriba, M. C. (1980). *Dilute phase pneumatic transport of fine nuclear fuel powders.* Paper presented at the Fifth International Conference on The Pneumatic Transport of Solid in Pipes, London.

York, D. W. (2003). An industrial user's perspective on agglomeration development. *Powder Technology, 130*(1-3), 14-17.

Yu, A. B., Standish, N., & Lu, L. (1995). Coal Agglomeration and its effect on bulk density. *Powder Technology, 82*, 177-189.

Zbicinski, I. (1995). Development and experimental verification of momentum, heat and mass transfer model in spray drying. *The Chemical Engineering Journal, 58*, 123-133.

Zuo, J. Y. (2004). *The stickiness curves of dairy powder.* Master of Technology in Bioprocess Engineering, Massey University.

APPENDICES

Appendix A Particle Size Measurement

Particle size measurements were carried out using either a Malvern Mastersizer S or 2000. Laser diffraction is commonly used to measure particle size of milk powders using a gas dispersion system. A Malvern Mastersizer (Model 2000, Malvern Instruments Limited, Malvern, Worcestershire, UK) was used to measure the particle size distributions of the dried milk powder particles and are delivered to the beam using a vibrating feeder (set at ~ 20% delivery) and dispersed using air (at 0.1 bar). When measuring powders 10 000 sweeps are used and the obscuration levels were set between 1 and 5%.

A Malvern Mastersizer (Model S) was also used to measure the particle size distributions of dried milk powder particles (and also droplet size of milk concentrate sprays as outlined in Section 4.6.3). The Mastersizer S has an alternative delivery method which uses a free fall feeder comprised of a vibrating chute which delivers powder particles directly into the path of the laser beam, and this is designed specifically for agglomerates and ensures the particles flow freely through the laser avoiding any agglomerate breakdown.

As Figure A.1 indicates, the free fall feeder is not suitable for measuring standard skim milks which have poor flowability and form clumps before passing through the laser. Fine, cohesive powders require some amount of mechanical breakdown prior to delivery to the laser beam for measurement such as that achieved in the gas dispersion system. For this reason, all particle size measurements were made using the Mastersizer 2000 for comparison purposes assuming that the agglomerates were treated identically and the small level of breakdown experienced would be identical for all powders.

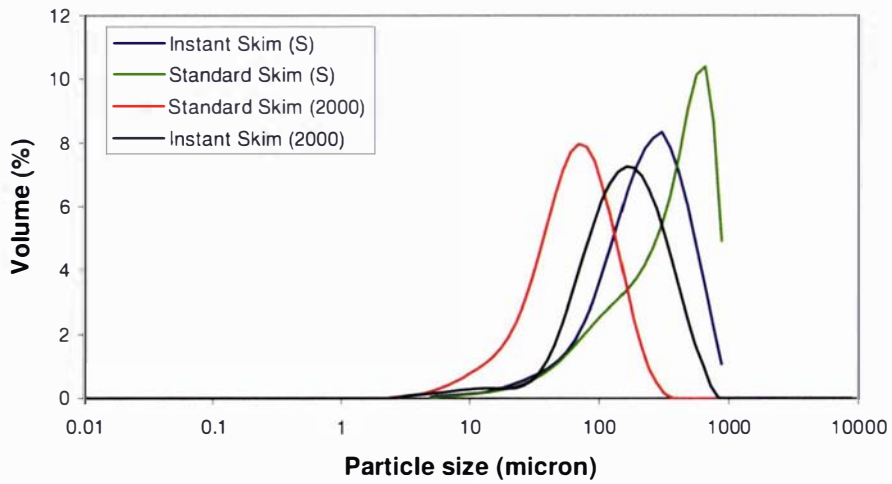

Figure A.1: Comparison between the Malvern Mastersizer S and 2000

Mastersizer S

HAZARD	RISK	EFFECTS OF HAZARD	MANAGEMENT OF HAZARD
Noise	Very High	Hearing damage	Wear earmuffs
Dust	High	Breathing problems	Wear face mask
Laser light	Moderate	Damage to eyes	Avoid exposure

Scope
Analysis of particle size measurement for milk powders.

Reference
Mastersizer S Manual

Principle
The light from a low power helium-neon laser is used to form a collimated and monochromatic beam of light. Sample particles presented to this beam will scatter the light at low angles. The scattered light is incident on to a receiver lens. This operates as a Fourier transform lens forming the far field diffraction pattern of the scattered light at its focal plane. Here the detector, in the form of a series of 31 concentric annular sectors, gathers the scattered light over a range of solid angles of scatter. The range lens configuration has the interesting and useful property that wherever the particle is in the analyser beam, its diffraction pattern is stationary and centred on the lens optical axis.

Safety Precautions
See Hazard Assessment.
Wear earmuffs and face mask for dusty samples.

Procedure
Use of Free Fall Feeder: For use with samples that will dissolve in water e.g. milk powders, blends etc

Step	Action
1	Remove 300RF lens - disconnect plug, unlock lens and store in case Remove "Wet" cell - unlock cell and remove from path of laser beam
2	Mount 1000 mm lens, at transmitter end of machine, align notches and press locking lever down
3	Mount "Dry" cell, lock cell into place over 1000 mm lens connecting hose to vacuum outlet
4	Position Free Fall Feeder so that the sample falls into the cell when the feeder is switched on
5	Plug the feeder into the vacuum cleaner. Plug the power cord from the SSU into the feeder Set the vibration speed low – will adjust during test
6	Hardware Setup: Range: 1000, Active Beam Length: 10mm, Sample Unit: MS66 Free Fall Feeder Unit Instrument Port: 1
7	Analysis Setup: Compressed, Kill Data Channels: Low 0 High 0 , Active Beam Length: 10.00

	Particle Density: 1.500
8	Presentation Setup: System: Standard Dry (3RHA) or can select by code (3RHA: 1.4500, 0.1000 in 1.0000)
9	Select Setup, from top tool bar
10	Select Experiment In the "Enable" box select All Change the Obscuration for "upper" from 100% to 30% and "lower" from 0% to 5% Malvern will now only accept data with an obscuration between these limits Change "sweeps" from 4000 to a greater figure, e.g. 30 000
11	Document sample and check alignment/background
12	Prepare sample and add to hopper. Thoroughly mix at least 100g of sample and sub sample 5 –10 g adding a small amount of Syloid
13	Measure "Inspect" Turn Feeder on. Increase vibration slowly until obscuration is in the orange/green
14	Run all prepared sample through hopper. As larger particles are vibrated to the top of the Hopper
15	Save and print data
16	Notes: Clean dry cell after each sample as particles may adhere to cell windows When finished dry samples change lens, cells and presentation back to setup for wet Sample Analysis
17	Obscuration Range % Obscuration Graph Colour Notes <5 Red Add more sample 5 – 10 Orange Low but usable 10 – 30 Green Ideal 30 – 50 Orange Usable but try to add more dispersant. Possibility of multiple scattering >50 Red Too High

Mastersizer S Manual
Report:results to 0.01
Repeatability: should agree within 1.0 %

Appendix B Method for using fluidisation device for the breakdown test

For agglomerate strength measurement, a fluidisation method exists; this was used as a comparative technique. The standard method requires bulk density measurements however these require large sample sizes and a total sample size of 1 kg is required for this method. This procedure was modified to suit this agglomeration study where small samples are produced due to the limited running time of the small scale drier. Figure B.1 shows that particle size can also be used infer agglomerate strength and this requires much less sample (10 g). In cases when the sample size of agglomerated powder available was below 1 kg, only one 150 g sample was fluidised for 5 minutes and then 5 particle size measurements were made using the Mastersizer 2000 as explained in Appendix A.

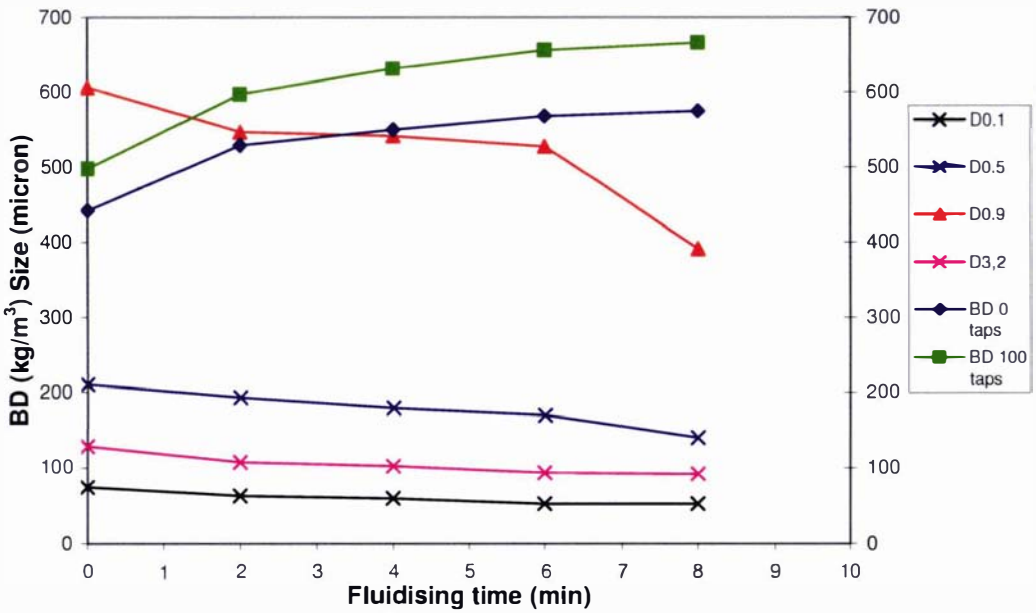

Figure B.1: Bulk density compared to size vs. fluidisation time

Appendix C Analysis Methods for Powders

Moisture content

Moisture content of milk powders is measured using a Karl Fischer Titrator (Metrohn KFP Titrino 784, Switzerland).

Bulk Density

The bulk density of milk powder is measured using a Stav 20003 Stampfvolumeter (J. Engelsmann AG, Ludwigshafen, Germany). The following procedure was used to measure the bulk densities:

1. First record the 0 taps mass of a level sample in the cylinder.
2. when weighing the sample brush the outside of the cylinder with a brush.
3. place the collar and top on the cylinder and fill powder to the top
4. place on machine for 100 taps
5. remove the top and collar, level the sample and record the mass.
6. BD g cm^{-3} = weight/99.4.

Method for Determining Particle Density

A Beckman Air Comparison Pycnometer (Model 930) was used to measure the particle density of powders. The particle density is that of the powder solids and the occluded air within the particles which influences the physical and functional properties of the powder. The pycnometer consists of two gas-tight pistons which are connected by a differential manometer and uses the principle of Boyle's Law ($P_1V_1 = P_2V_2$) and should be carried out at constant temperature. The procedure for measuring particle density using the Beckman Pycnometer has been included in Appendix M. Calculation of particle density (report to the nearest 0.01 g cm^{-3}):

X g cm^{-3} = Sample Weight (10 g) / (sample cm^3 – blank cm^3) (C.9.1)

Procedure

1. Ensure sample cup is clean on the top lip
2. Have both hand wheels at the anti-clockwise stop position and purge and coupling valves are open.
3. Place sample cup into the chamber and ensure the system is air tight.
4. close the purge valve
5. rotate the measuring piston clockwise to the starting number (side of the machine)
6. close coupling valve
7. keep the indicator need in the zero position as both hand wheels are rotated clockwise until the reference piston stops
8. After 3 minutes rotate the measuring piston hand wheel until the indictor need is exactly on zero (use mirror to avoid parallax) record this value as cm3
9. open coupling valve and purge valve until they stop, remove sample cup

Blank

This should be done first and between every 6 samples or every 30 minutes. Perform operations 1 to 9 with an empty sample cup, this will be a negative value (around – 0.35 cm^3) and is added to the sample value. Repeat until two consecutive values agree within 0.02 cm^3.

Calibration
Place the smallest ball (5.58 ± 0.02 cm^3) into the sample cup and repeat steps 1 to 9, repeat until two consecutive values agree within 0.05 cm^3.

Sample
Weigh 10 g of power into the sample cup and follow steps 1 to 9. Make sure no powder is on the lip of the cup as this will prevent a tight seal. Repeat until two consecutive values agree within 0.05 cm^3.

Appendix D Report on Solids Flow Measurement for Fines Returns Systems

Project Objectives:
The online continuous flow measurement of pneumatically conveyed solids has become increasingly important to achieve increased productivity, improved product quality and process efficiency. The area of flow measurement is a technically challenging area and many variables exist which may affect the response of a solids flow instrument including inhomogeneous distribution of solids over the pipe cross-section, irregular velocity profiles, variations in particles size, moisture content and deposition on the wall of the pipe. There are a number of different measurement principles which can be employed when establishing solids flow rates including the inferential approach or cross-correlation velocity measurement. Cross correlation refers to that used by some laser/microwave electrostatic or acoustic sensors, where an upstream and downstream signal is compared to find a velocity. The following methods have been identified as possibilities for measuring the solids flow rate at each stage of the project:

1. weighing and collecting
2. pressure drop on a vertical pipe
3. pressure drop on a bend
4. acoustic technique
5. optical technique
6. Electrostatic technique
7. Microwave

Weighing and Collecting
The accuracy of this process is limited by the number of times the measurement is taken and is likely to vary significantly during processing time. This technique would be suitable for the laboratory small scale experiments and may also be helpful for the pilot scale experiments carried out on the FRC plant. The fines returns lines could be diverted once the system reaches steady state after a step change and the flow volume can be reduced by using small cyclones and the fines can be collected for several minutes. This method is quite impractical for the industrial size plants.

Pressure Drop on a Vertical Pipe
Pressure drop as a measurement technique requires two pressure sensing devices positioned along a large vertical section of pipe. The pressure difference between these two measurements can be relating to the flow of solids through the pipe. This system is inexpensive and may cost less than $1000. The disadvantages far outweigh the benefits of this system; the pressure drop is likely to be affected by particle deposition and may be inaccurate for the dilute flows such as fines returns. This method would require in-situ calibration and correlation of the signal to flow rate. A large pipe section would need to be used for decent accuracy (friction can be a problem), the system would be subject to wear, and the probes are intrusive, interfere with the flow and are unlikely to cause problems for CIP processes.

Pressure Drop on a Bend
Similar to pressure drop on a vertical pipe, this measurement technique is cheap as it only requires two pressure sensors. Problems associated with this method are similar to those above regarding CIP, its intrusive nature and calibration would need to be in-situ. However pressure drop also depends on what form the flow is on the bend (roping may need to be dispersed before the pressure sensors) and friction can affect the pressure drop (although not as much as for a vertical pressure drop).

Acoustic Technique
This technique works on the basis of transmitting and receiving two different noise signals and relates the information directly to the velocity and concentration of the particles moving in a gaseous medium. An advantage of this device is it has already been designed and is in use at Unilever and is CIP capable, the method of calibration is straightforward and has been developed with this type of flow in mind. There is a possibility it may be affected by moisture and temperature. Cost ~ $30 – 40,000.

Optical Technique
A light sensor is used correlate the obscuration of light from a source to the solids flow rate. It requires that both windows are kept clean and will therefore be affected by solids deposition on the pipe walls and require airflow to keep these windows clean. The advantage of this technique is that it is not really affected by chemical composition or moisture and a product already exists (Teledyne light hawk) in the market and while it is cheap it is likely to be complicated to install. The main disadvantage of this technique is that it may not be appropriate for low solids concentrations (dilute flows), and can be affected by particle size.

Electrostatic Technique
The movement of particulate materials in pipelines generates an electrostatic charge when the powder comes into contact with the surface. Often these techniques use an intrusive probe but a ring can be used that will not intrude into the flow. This measurement technique takes advantage of the charge each particle carries from interacting with the system and converts this charge to a current. An advantage of this system is that a device is readily available however the leakage of charge from particles to the insulating material may be affected by moisture and humidity and is likely to be greatly affected by deposition of product on the walls. It is also affected by particle size, velocity, dielectric permittivity, chemical composition, temperature the pipeline material and the wall roughness. This product costs around $20,000 from PCME.

Microwave Technique
A transmitting injects low power microwave energy into the flow filed and a receiving device deflects the signal back. The return signal can relate to the concentration of solids. Velocity measurements are only possible with an intrusive device. Multiple devices are required to cover the entire cross sectional area of the pipe. The disadvantages of this technique are that it is affected by deposition and by roping. As the output depends on the dielectric constant for the material is very sensitive to changes in chemical composition and moisture. Another consideration is that deposition on the walls of the pipe may be cooked and foul and contaminate the product. This technique can also cause wear of pipe materials if microwave energy is absorbed.

Technique	Weigh & Collect[1]	ΔP Vertical Pipe	ΔP on a Bend	Acoustic	Optical	Electro-static	Micro-wave	Ultra-sonic
Affected by:								
Moisture				Y		Y	Y	Y
Chemical Compostion						Y	Y	Y
Roping			Y			Y	Y	Y
Deposition	Y	Y	Y		Y	Y	Y	Y
Intrusive		Y	Y	Y[5]		Y[2]		
Problems for Dilute flow		Y	Y		Y	Y		Y
CIP Issues		Y	Y			Y	Y	
Installation only	Y							
Installation & Calibration				Y	Y	Y		Y
Minor Development							Y	
Major Development		Y	Y					
< $20 000	Y	Y	Y	Y[3]				
$20 - 50 000				Y[4]		Y		
> $50 000								
Trialled in Dairy Industry	Y			Y		Y		
Supplier				IRL Massey Millitronics	Teledyne	PCME		Thermo Ramsey

[1]Impractical for industrial plants may be suitable for laboratory scale or pilot scale trials.
[2]A section of plastic would be the insulating material to collect charge.
[3]Millitronics price
[4]Massey/IRL price
[5]Transceiver inserted into wall of pipe

Appendix E Modelling Fines Flow

Following on from equation (3.4) in the main body of this report, the difference between the total pressure drop and that due to air is approximately the loss due to presence of solids, where ΔP_T = total pressure drop [Pa].

$$\Delta P_T = \Delta P_s + \Delta P_g \tag{D.1}$$

The loss due to solids can be described by two components:

$$\Delta P_s = \Delta P_{fs} + \Delta P_{hus} \tag{D.2}$$

where ΔP_{fs} is the pressure loss due to friction of the solids in the pipe [Pa] and ΔP_{hus} is the pressure drop due to hold-up [Pa]. The first term is described by the Fanning equation,

$$\Delta P_{fs} = \frac{f_p \rho_p U_p^2 (1-\varepsilon) L}{2D} \tag{D.3}$$

where f_p is particles friction coefficient [-], ρ_p is the density of solid particle [kg m^{-3}], U_p is the velocity of solid particles [m s^{-1}], ε is voidage in transporting line [-], L is length between two pressure transducers, and D is inside diameter of the pipe [m]. The pressure due to hold up of solids is the mass of the solids in the pipe at any given time multiplied by acceleration, to give a force over the cross-sectional area of the pipe

$$\Delta P_{hus} = \frac{M_p L g}{U_p A} \tag{D.4}$$

where M_p is the mass flow rate of solid [kg s^{-1}], g = acceleration due to gravity [m s^{-2}] and A is the cross sectional area of the pipe [m^2]. The voidage, or air volume fraction, in the pipe can be simplified by equation (D.5) for dilute flows only

$$\varepsilon = \frac{V_g}{V_g + V_s} \approx 1 - \frac{M_p}{U_p A \rho_p} \tag{D.5}$$

where $\rho_g < \rho_p$, V_g is the volume of the gas [m^3], and V_s is the volume of the solid [m^3]. The particle friction coefficient f_p has been simplified by Lech (2001) from the proposed relationship by Yang, et al. (1980); Lech (2001) obtains a friction coefficient directly proportional to the solid volume fraction. The total pressure drop due to solids in vertical transport of solids is then equation (D.7).

$$f_p = 0.0108 + 0.066(1-\varepsilon) \tag{D.6}$$

$$\Delta P_s = \frac{M_p U_p g L}{A}\left(\frac{f_p}{2Dg} + \frac{1}{U_p^2}\right) \tag{D.7}$$

This can then be used in analysis of the experimentally observed pressure drop as a function of powder addition rate.

Appendix F Pressure Recordings for Fines Flow Estimation

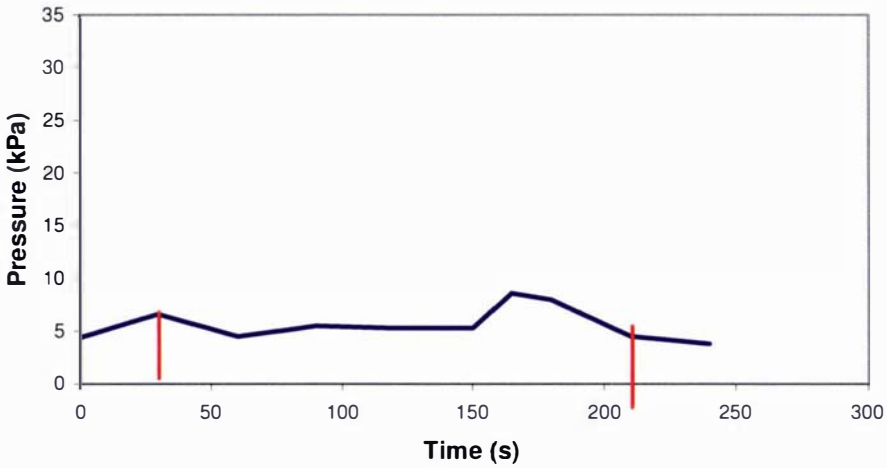

Trial 1 – 375 kg/h

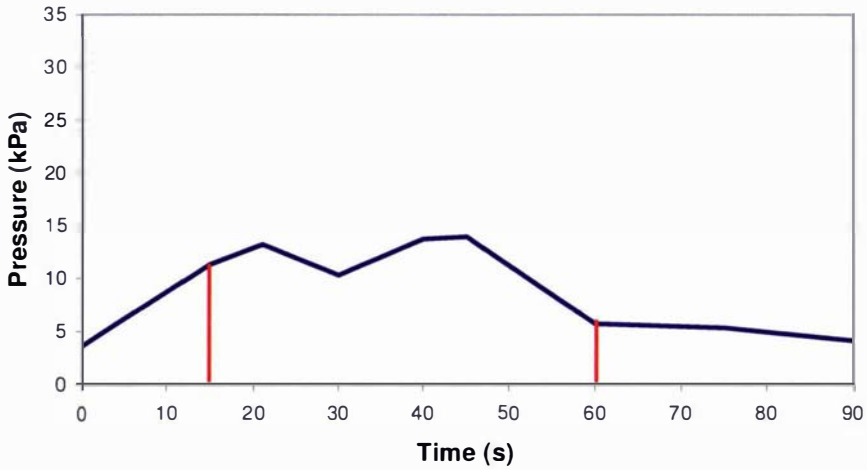

Trial 2 – 2000 kg/h

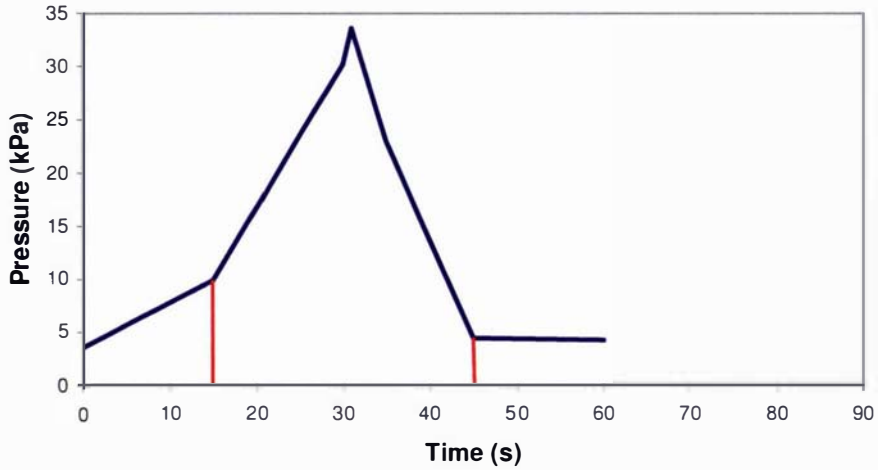

Trial 3 – 3000 kg/h

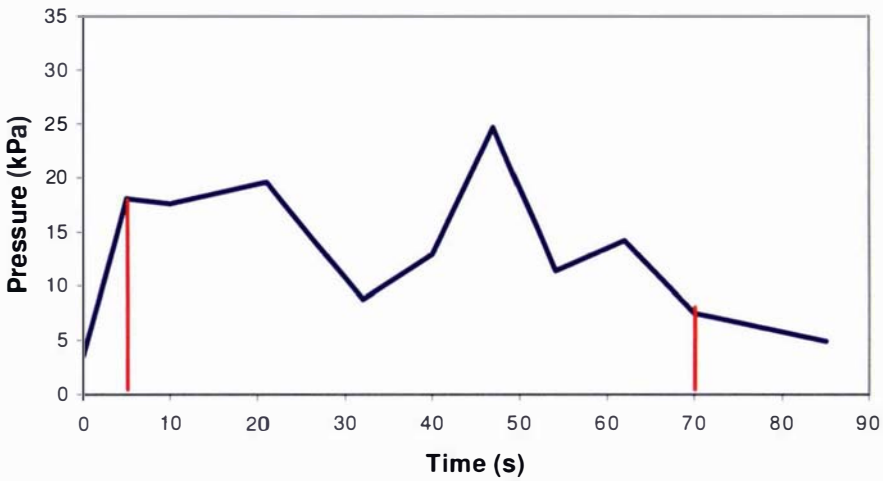

Trial 4 – 2118 kg/h

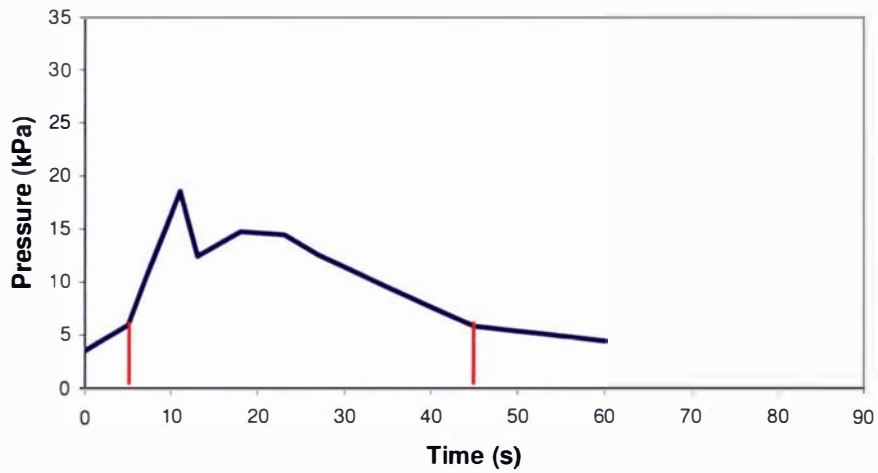

Trial 5 – 2570 kg/h

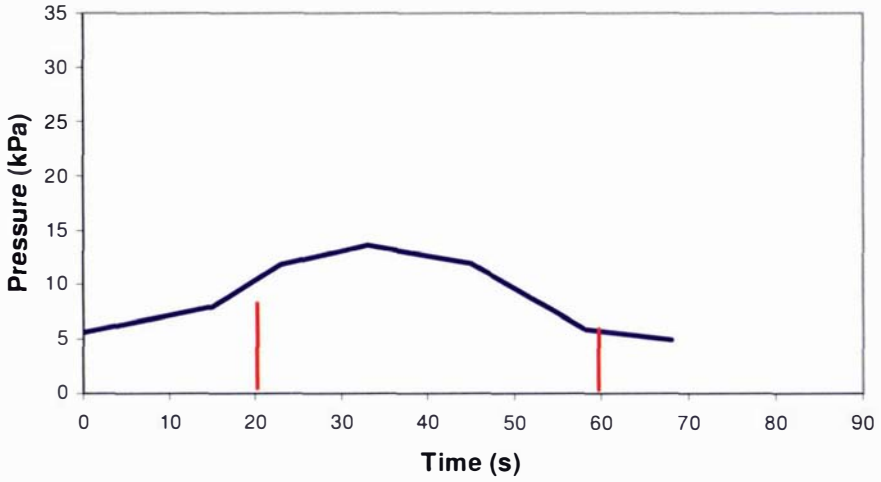

Trail 6 – 1915 kg/h

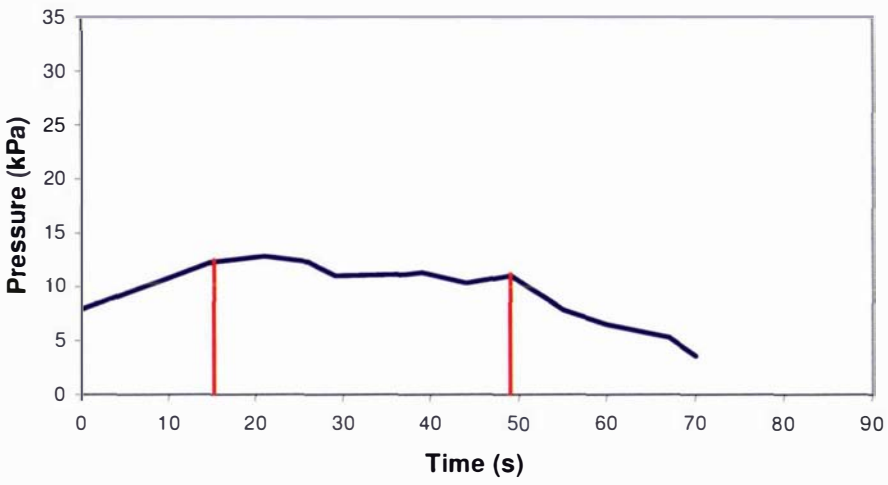

Trial 7 – 1915 kg/h

Appendix G Blower Performance Curve

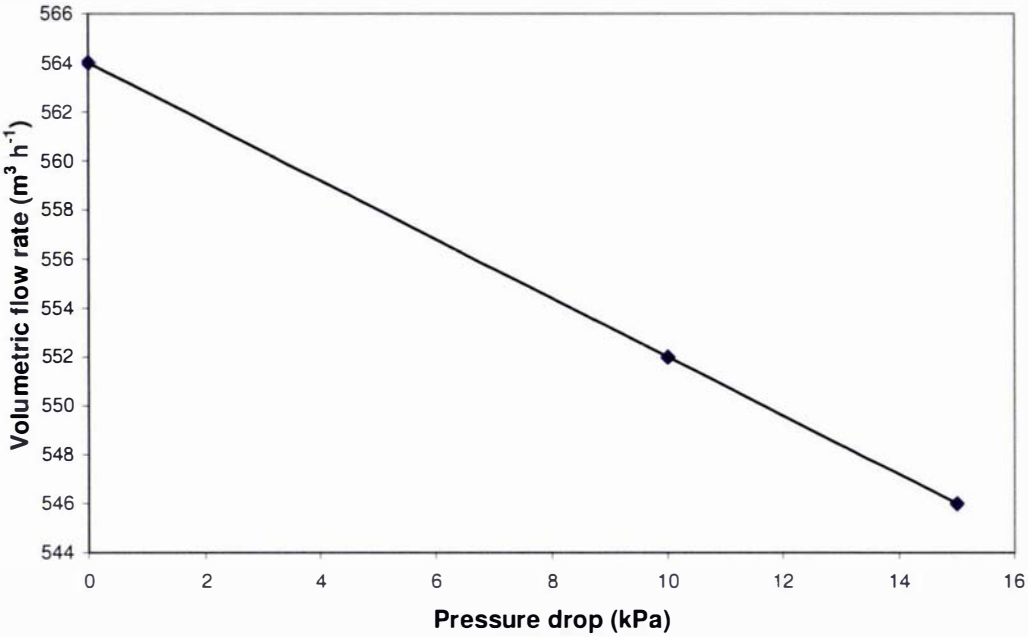

Figure G.1: Effect of pressure drop on volumetric air flow rate at 2960 rpm taken from the Robuschi blower test curves

Appendix H Method for Paar Viscometer

Procedure for using the Paar Physica MC1 operating with US200 software (v2.30):

1. Open US200
2. Open the work book extremelin.ctx
3. Settings – 6 samples, 10 points over 6 s, interval 60 s
4. Options – Start diagnostic – turn on viscometer – remote
5. Options – measuring device – setup – select measuring system
    a. Z1 DIN (double gap) for low solids
    b. 23.1 DIN (25 mm) for high solids
6. File – datapool – new – start button – enter sample name
7. samples:
    a. place in water bath at measurement temperature
    b. pour in sample to just cover internal cylinder for double gap, and up to the line for the high solids cylinder
    c. insert measurement cylinder into viscometer
8. press save on software, one sample takes 6 minutes
9. after measurement clean out the measuring cylinder with water

Appendix I Method for Surface Tension Measurement of Milk Concentrates

HAZARD	RISK	EFFECTS OF HAZARD	MANAGEMENT OF HAZARD
Chromic Acid	Moderate risk	Severe Burns	Wear nitrile gloves and goggles when handling
Ethanol	Low risk	Flammable, irritant	Wear gloves, goggles
Acetone	Moderate risk	Irritant to eyes and skin, flammable	Wear gloves, goggles, keep away from ignition sources
Isopropanol	Low Risk	Irritant, flammable	Wear gloves, goggles
Boiling water	Low Risk	Burns	Use tongs when handling sample vessels

Scope
To measure the surface tension of liquids, principally milk concentrates of varying solids contents and temperature.

Reference
Krüss Tensiometer K12 Manual

Quality Control
Before carrying out a measurement, the system must be calibrated following the calibration instructions. The validity of the calibration can be measured using a mass to imitate surface tension. The final check is carried out using water (RO or Tap) at 20°C a reading of greater than 71.5 mN m^{-1} should be achievable and a literature value of 72.7 mN m^{-1} is desirable. The calibration should be calibrated only after the balance has been levelled correctly.

Sample Preparation
The sample vessels and plates/ring used should be thoroughly cleaned before any measurement. Full details on various cleaning and handling procedures can found in the surface tension manual and the cleaning procedures included further in these instructions. The general procedure followed for handling is included below:

Important handling information
1. When handling ring/plate never touch the surface, to remove from storage container, gently invert and pull off base so that the plate rests in the felt-lined lid.
2. Hold the ring/plate by the shaft and clean before use as explained below.
3. To store the ring/plate, guide the shaft carefully into the wooden storage box and gently let it fall into place. Never force the ring/plate and always clean before storage.
4. If the ring/plate is suspected to be damaged, consult the manual and cleaning instructions for confirmation.
5. If incorrect results are obtained, first consider cleaning the sample vessels with Chromic Acid as the most common cause is sample contamination.

Platinum Device (Plate/Ring) Cleaning Procedure

1. Before use, clean with RO water and flame to red hot.
2. Wait for the device to cool before use or storage.
3. After use with an aqueous solution, simply rinse with RO water thoroughly before cleaning and flaming.
4. After use with milk solutions rinse thoroughly with hot water to remove excess milk. Follow by rinsing with RO water, then isopropanol to remove any proteins from the surface, followed by acetone before rinsing with RO water and flaming to red hot.
5. The ring/plate should NOT be flamed if any milk residue remains on the platinum surface. The device should be rinsed carefully with chromic acid for several minutes before a final rinse of RO water, repeat if necessary. Once the surface appears clean the plate/ring can be flamed to red hot and stored.
6. If the platinum surface becomes contaminated by flaming of milk residue onto the surface the plate/ring can be carefully placed in a beaker of chromic acid for ~ 2hrs before rinsing with RO water and flaming to red hot. This will remove the contaminant from the platinum surface and will not damage the surface properties.
7. The device should be cleaned between each measurement to maintain constant surface conditions.

Sample Vessel Cleaning Procedure

After use in aqueous solutions the glass sample vessel can be cleaned by rinsing with water, then acetone and flaming. However it is important that the sample vessel is very clean and should be handled wearing gloves to avoid contaminating with oil or other substances. For work with milk products it is recommended that the following steps be taken before use:

1. Completely immerse vessel in Chromic Acid for 3 minutes.
2. Rinse with MilliQ water into another beaker.
3. Boil in a 500mL beaker of water for 3 minutes
4. Flame using a Bunsen burner
5. Place in a sealed plastic container face down.
6. Alternatively plastic vessels can be used, to test the suitability of a plastic vessel, simply leave water in the vessel for ten minutes before measurement and if within the acceptable limits, the vessel is suitable for use.
7. Size of the sample vessel is important in maintaining the appropriate temperature during the measurements, water or another heat transfer liquid can be used to surround a smaller container to avoid too much heat loss.

Procedure

1. Turn on K12 Tensiometer and water bath, set water bath to ~2°C above desired sample temperature.
2. Start stirrer using ↔ button.
3. Remove plate/ring from storage container, clean and insert into suspension (balance = locked).
4. Release balance lock to activate K12 device, ensure platform is above the lower limit.
5. Place clean sample vessel inside the thermostat vessel.
6. If the sample does not form a skin, 30 – 40 mL of sample can be gently poured into the vessel.

7. Press (9) for setup and (4) Temperature to check the temperature inside the thermostat vessel. This should hold at the required temperature, the sample temperature can then be checked.
8. Once the vessel temperature and sample temperature are equal to the measurement temperature the procedure can start.
9. Select ring or plate measurement, select surface tension measurement, select single or series of measurements.
10. After inputting the required details raise the vessel so the liquid surface sits 3 to 4 mm below the plate/ring.
11. Stop the stirrer.
12. Start measurement.
13. Samples that undergo skin formation need to be poured into the vessel once already at the desired measurement temperature and measurement should be started as soon as possible. There will always be some delay as the system prints and the platinum device is inserted into the sample. ~ 2 or 3 minutes.
14. For a series of measurements the sample temperature should be recorded with a thermometer before and after.
15. A new, clean sample vessel should be used for each measurement and the plate should be cleaned after each measurement and cooled to ambient temperature before carrying out a subsequent measurement.

Appendix J Repeatability Surface Tension Measurements

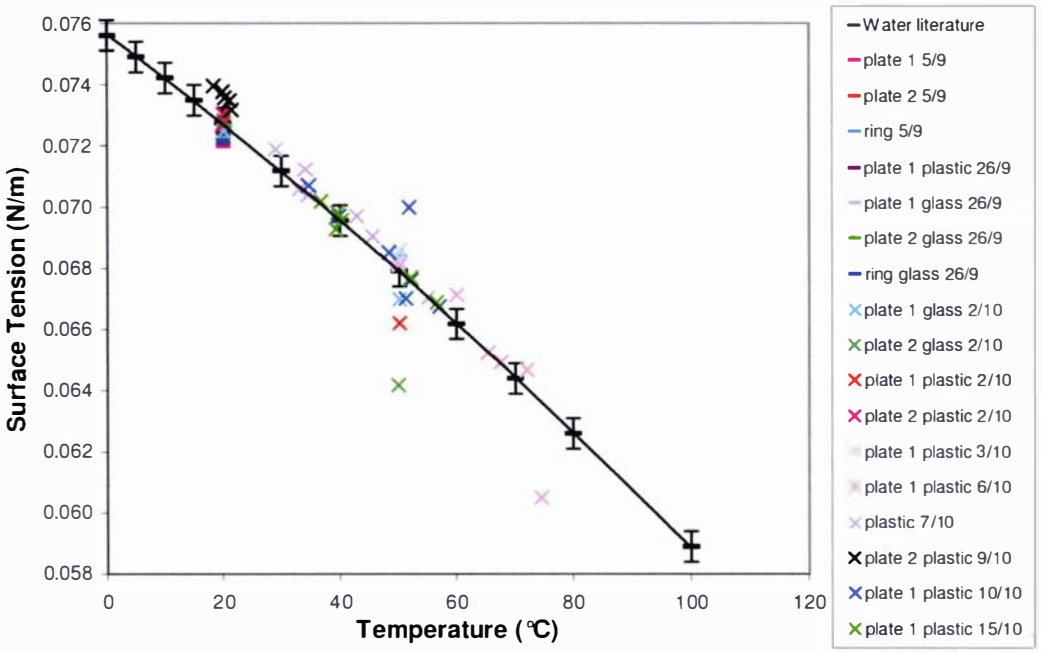

Figure J.1: Variability of surface tension measurements

Appendix K Influences to Plate measurements

The Wilhelmy plate method could be influenced by three major factors:
- The wetting properties of the plate changes (because of sample or the plate itself)
- The shape of the plate changes
- The viscosity of the sample

Changing of wetting properties
The theory of Wilhelmy requires complete wetting of the plate with liquid which can be prevented by two effects. The surface free energy of the plate can be reduced if the surface of the plate is altered (perhaps by improper cleaning) and the contact angle of the sample will change. The sample itself could prevent spreading too if cationic surfactants are used as a sample. Cationic surfactants have a hydrophilic end and a hydrophobic head like other surfactants. They build a layer around the plate and orientate with its hydrophobic head outside causing a hydrophobic layer around plate and prevent spreading as shown in Figure K.1.

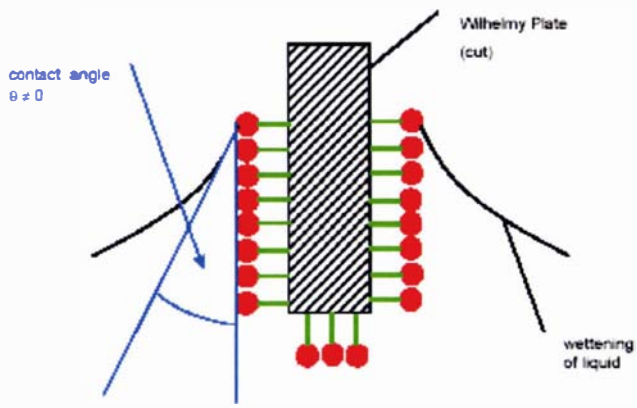

Figure K.1: How cationic surfactants prevent spreading

Changes in the shape of the plate
It is possible for the plate to change shape either through damage or over time; this is shown in Figure K.2 below. There is a liquid volume below the plate and the plate will get buoyancy because of this and the surface tension force is reduced.

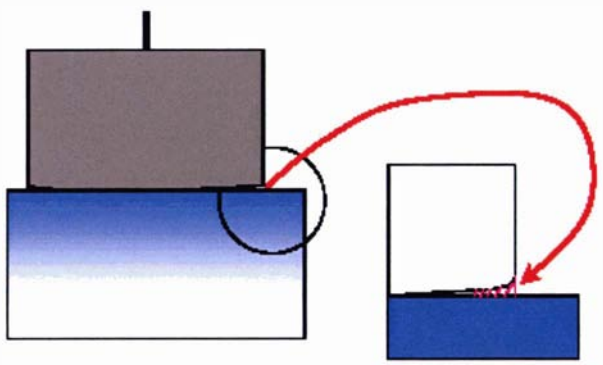
Figure K.2: Changes in plate shape

Viscosity of Samples

If the viscosity of the liquid is high a film of liquid will stick to the plate causing an increased load on the force measuring system which will be directly calculated into a increased surface tension. The film of liquid flows back into the sample vessel over time and the surface tension decreases to the actual value (see Figure K.3). Due to this effect it is best to wait until an equilibrium value is reached especially for samples with a high viscosity.

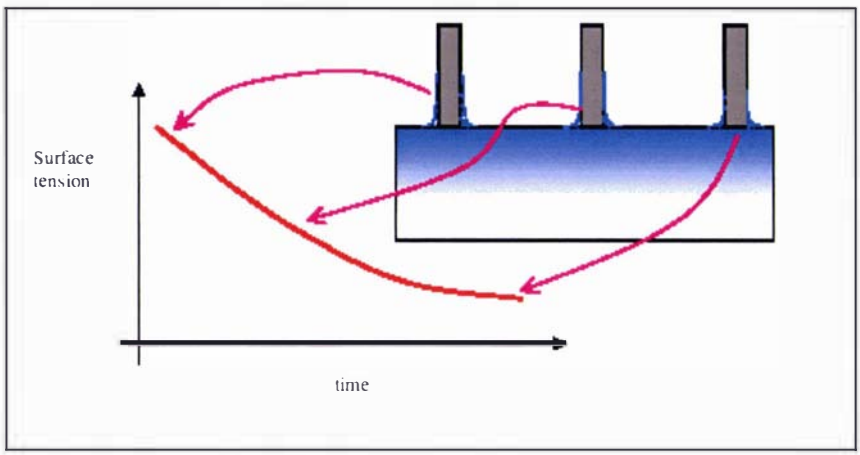

Figure K.3: Effect of high viscosity on surface tension measurements over time

Appendix L Calculation of Evaporation Rates

The rate of evaporation from the milk samples may affect the rate of skin formation and therefore the final surface tension value. The evaporation rate was established by using a heat transfer correlation for a horizontal flat surface to infer a mass transfer coefficient. The evaporation rate was found by using equation (L.1) below:

$$w = k_H A (H_{surface} - H_{air}) \tag{L.1}$$

where w = rate of evaporation [kg s^{-1}], k_H = mass transfer coefficient [kg $m^{-2}s^{-1}$], A = area of surface [m^2], $H_{surface}$ = humidity of surface [kg/kg], H_{air} = humidity of the air [kg/kg]. The relationship between the mass and heat transfer coefficient is approximated:

$$k_H \approx \frac{h}{C_p} \tag{L.2}$$

where h = heat transfer coefficient [W/m^2 K], C_p = specific heat capacity [J kg^{-1} K^{-1}]. The heat capacity of humid air is given by:

$$C_p = C_{p,air} + C_{p,steam} H_{air} \tag{L.3}$$

where $C_{p,air}$ = the specific heat capacity of air [J kg^{-1} K^{-1}], $C_{p,steam}$ = the specific heat capacity of steam [J kg^{-1} K^{-1}]. The heat transfer coefficient is obtained from the Nusselt number for natural convection from a flat horizontal surface (Perry and Green, 1997) as follows:

$$Nu = \frac{hD}{\lambda} = 0.54(Gr\,\mathrm{Pr})^{0.25} \tag{L.4}$$

where D = diameter of vessel [m], λ = thermal conductivity [W m^{-1} K^{-1}], Gr = Grashof number, Pr = Prandlt number. The dimensionless group used to define natural convection is the Grashof number, it is the ratio of buoyancy to viscous forces:

$$Gr = \frac{\beta g \rho^2 L^3 \Delta\theta}{\mu^2} \tag{L.5}$$

where β = coefficient of thermal expansion = $1/T$, ρ = density of air [kg m^{-3}], $\Delta\theta = |T_p - T_0|$ where T_p = surface temperature [°C] and T_0 = ambient air temperature [°C], L = diameter of vessel [m] and μ = viscosity of air [Pa s].

The Prandlt number defines the ratio of momentum and thermal diffusivities:

$$\mathrm{Pr} = \frac{\mu C_p}{\lambda} \tag{L.6}$$

To determine the evaporation rates, the air humidity and temperature was recorded in the chamber of the tensiometer at four different sample temperatures in four positions, directly above the sample, near the top of the chamber, to one side of the chamber and outside in the ambient air. This was done to estimate the evaporation rates experienced when conducting surface tension measurements, during this time the chamber doors are closed but are open when placing the sample. This means the humidity in the chamber is not constant during the experiment which makes it difficult to estimate a driving force from which to calculate evaporation.

Figure L.1 uses a driving force of ΔH, where $\Delta H = H_{surface} - H_{ambient}$ and shows the relationship between the rate of evaporation at the surface and the temperature of the sample being measured. The evaporation rate from the sample surface appears to be constant over a range of sample temperatures. Skin formation is significantly affected by temperature; therefore the formation of a skin does not depend on the rate on the evaporation from the surface. Skin formation is a temperature dependent phenomenon where a milk chemistry effect causes a high rate of skin formation above 60°C.

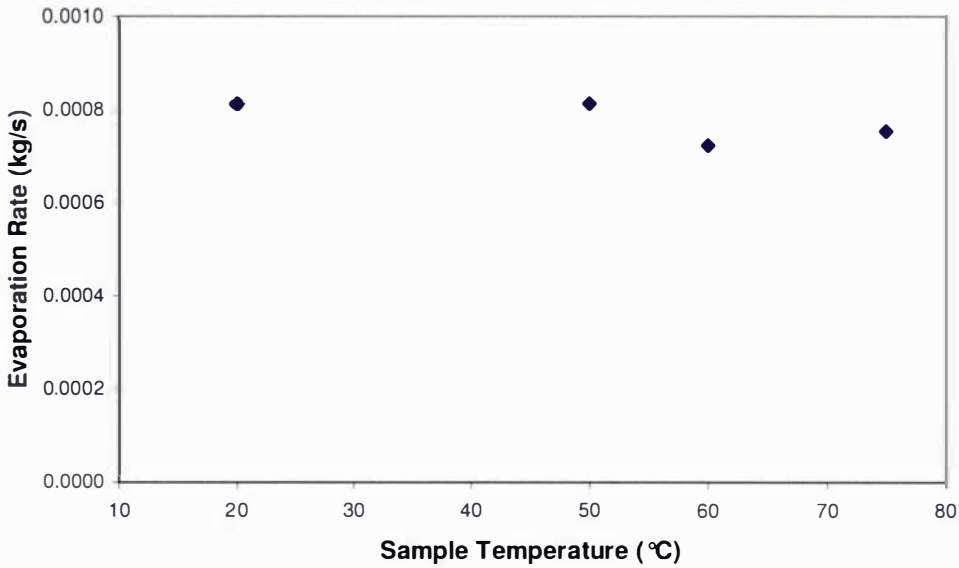

Figure L.1: Evaporation rate vs. sample temperature

Appendix M Drier Selection Criteria

Five criteria were used to evaluate the suitability of the available spray drying chambers for the agglomeration experiments. A spray drier chamber was considered necessary to contain the experiments and to enable the control of the same parameters that are important in an industrial situation. Four small scale spray drying units were available, two at Massey University and two at Fonterra Palmerston North. These driers only allow for spraying so the key modification required was to enable the supply of powder into the drying chamber for contact with the spray. The selection process has been included in Table M.1 and the criteria have been explained below:

- Availability refers to whether the drier was readily accessible
- Modification refers to the ease of adjusting the drier to allow fines delivery
- Concentrate refers to proximity to freshly produced milk concentrate
- Test access refers to proximity to the required apparatus to perform tests
- Initial setup refers to the amount of time required to make the drier operational

Table M.1: Drier Selection Criteria

Criteria	Massey (old)	Massey (new)	Fonterra (old)	Fonterra (new)
Availability	hard	moderate	easy	moderate
Modification	hard	hard	hard	moderate
Concentrate access	hard	hard	easy	easy
Test access	hard	hard	easy	easy
Initial set up	hard	hard	hard	easy

This suggests the most appropriate drier was the new Fonterra chamber. While it was only moderately available it was the easiest to modify due to large sight glasses. It is located in the pilot plant at Fonterra Palmerston North with easy access to concentrate and in close proximity to the tests required to be carried out. The only disadvantage of the old Fonterra chamber is the set up required. It needed new seals and had not been used for some time whereas the new Fonterra chamber was relatively new. The main reason the Massey spray driers were not selected was due to concentrate and tests access, also these driers have small sight glasses which would have made modifications difficult.

Appendix N Prediction of $(T-T_g)_{critical}$

It is important that powder collected in the cyclone of the small scale drier experiments avoid sintering. To assure this, the critical $T - T_g$ is calculated using Equation (2.18) from Palzer (2005) and the values from Murti (2006). Bronlund (1997) measured the surface tension of saturated lactose syrups between 17 and 40°C and fitted a linear relationship to this data. This linear relationship was extrapolated to the outlet air temperature of the drier (67.5°C) and surface tension was estimated to be 0.0631 N m^{-1}. The minimum $(T - T_g)_{critical}$ was calculated using the smallest $D_{4,3}$ dried droplet or fines particle size and the longest contact time and the maximum $(T - T_g)_{critical}$ value was calculated using the largest $D_{4,3}$ dried droplet or fines particle size and the shortest contact time. The mean $(T - T_g)_{critical}$ value is therefore 8.8°C.

Table N.1: Values used to calculate $(T - T_g)_{critical}$

Variable	Description	Minimum	Maximum
R	particle radius	0.0000065	0.000029
a	particle diameter	0.000013	0.000058
Ft	applied force	0	0
η_g	dynamic viscosity at glass transition	1E+12	1E+12
C	WLF constant for SMP Foster (2002)	-14.8	-14.8
B	WLF constant for SMP Foster (2002)	25.3	25.3
X/a	Palzer (2005)	0.1	0.1
γ	surface tension sat lactose 67.5°C	0.063	0.063
t	time	1200	600
T-Tg		**7.3**	**10.3**

Appendix O Chute dimensions

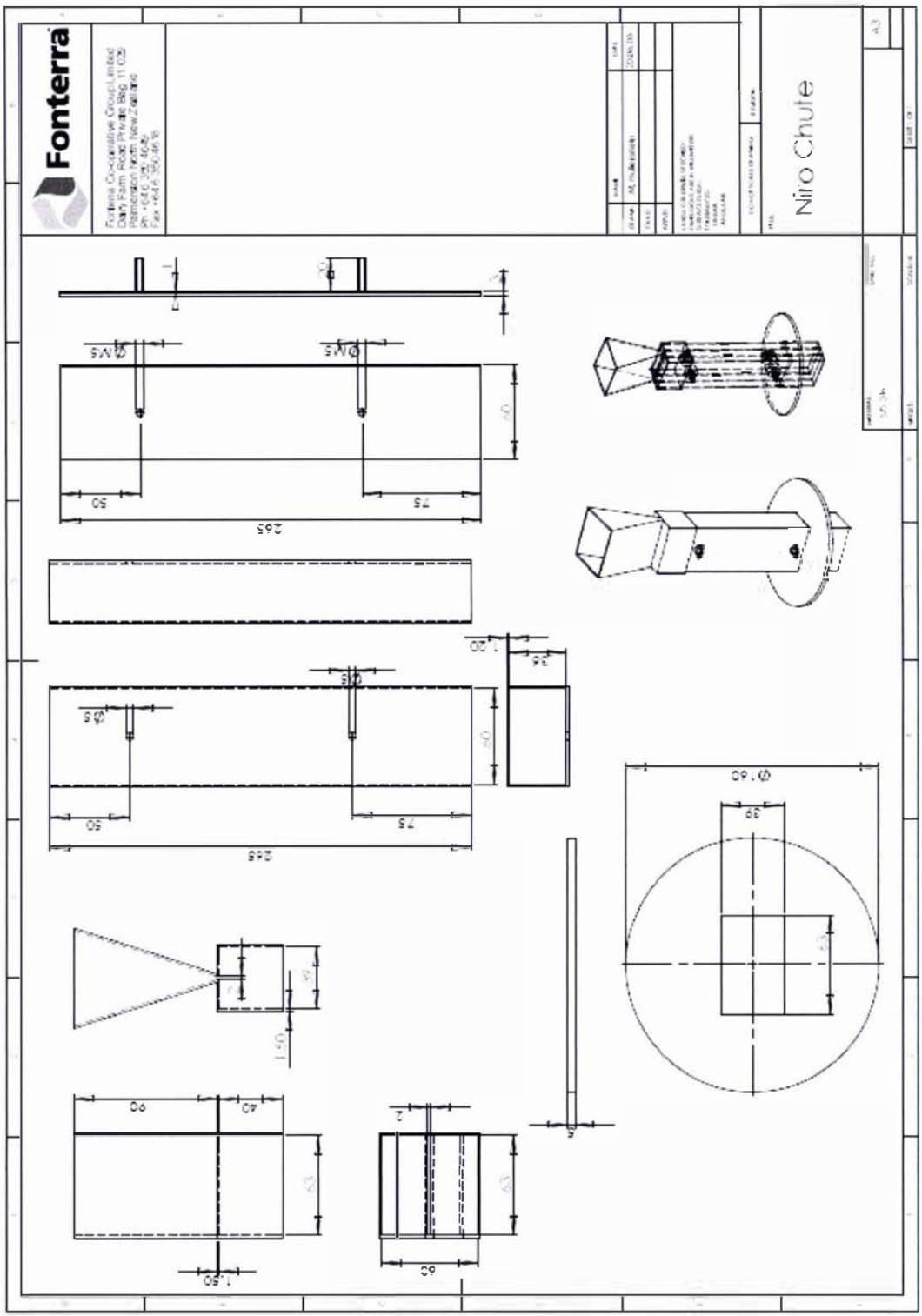

Appendix P Drawings for Niro Face Plate

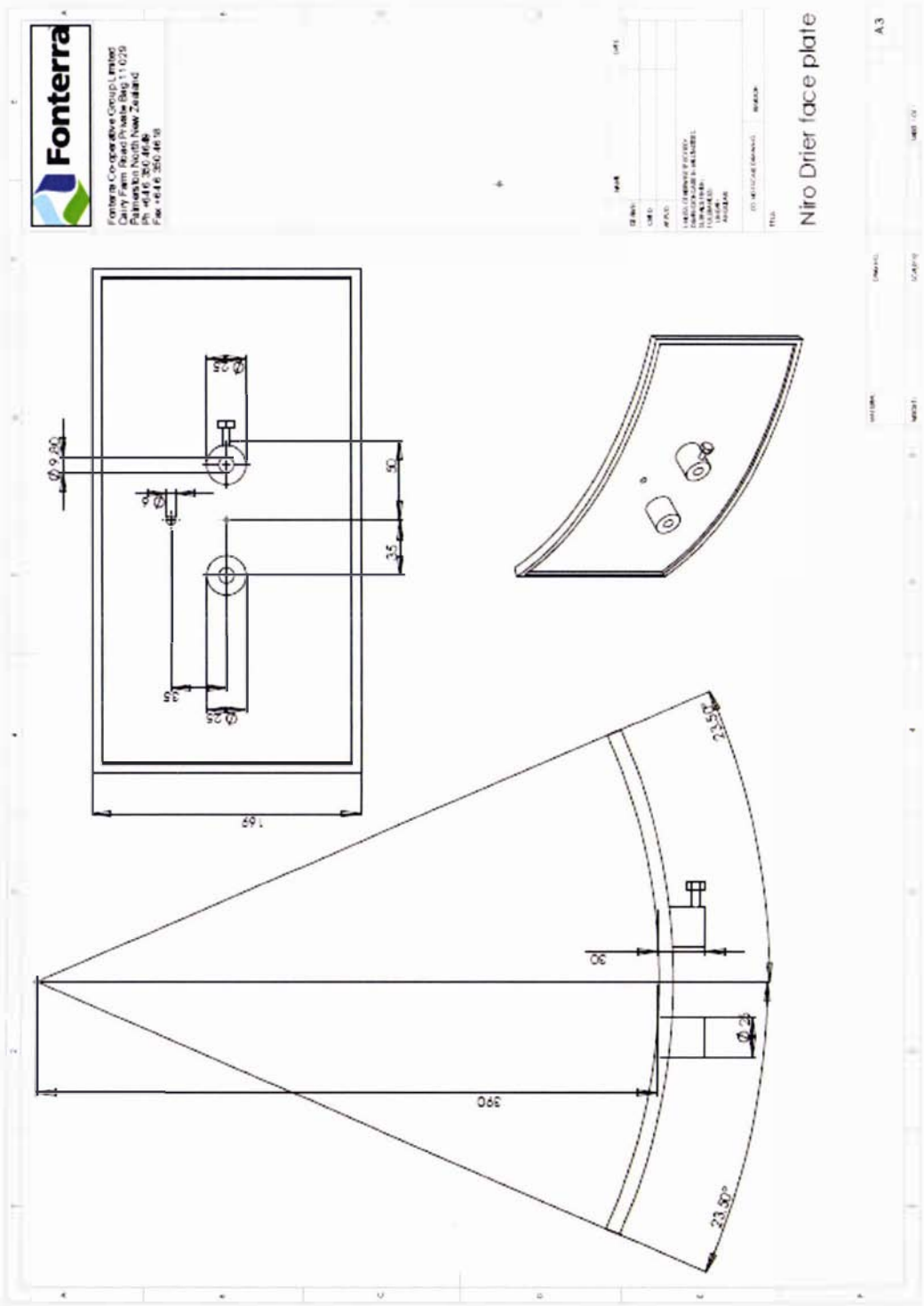

Appendix Q Small Scale Calculations

An agglomeration experiment involves the collision of droplets and fines in the collision zone at the top of the spray drier. In the small scale equipment typically 1.4 kg h^{-1} of spray droplets and 1 kg h^{-1} of fines particles are delivered to the collision zone. This section generally uses the lowest mass flow rates, small fines size and low solids concentration experiments to calculate:

i. the concentration of droplets and fines
ii. the number of particles and droplets in the collision zone
iii. the proposed trajectory of the agglomerates
iv. the likelihood of coalescence following droplet-particle collision.

Number concentration of fines and droplets in the collision zone

To calculate the number of fines particles and droplets in the collision zone, the concentration of droplets and particles must be calculated. This can be determined by calculating first the number concentration of fines, $\hat{N}_f$, and droplets, $\hat{N}_d$, which are included in Table R.1. This concentration is multiplied by the volume of the collision zone to give the number of particles or droplets available for collision:

$$\hat{N}_f = \frac{6M_f}{\rho_f \pi D_f Q_{a,c}} \qquad \text{(R.1)}$$

$$\hat{N}_d = \frac{6M_s}{\rho_d \pi D_d Q_{atm}} \qquad \text{(R.2)}$$

Table R.1: Concentration of droplets and fines

Droplets	Fines
1.4 kg/h = 9.6 x 10^{11}/m^3	1 kg/h = 1.9 x 10^{10}/ m^3
	Industry = 4.8 x 10^{10}/ m^3

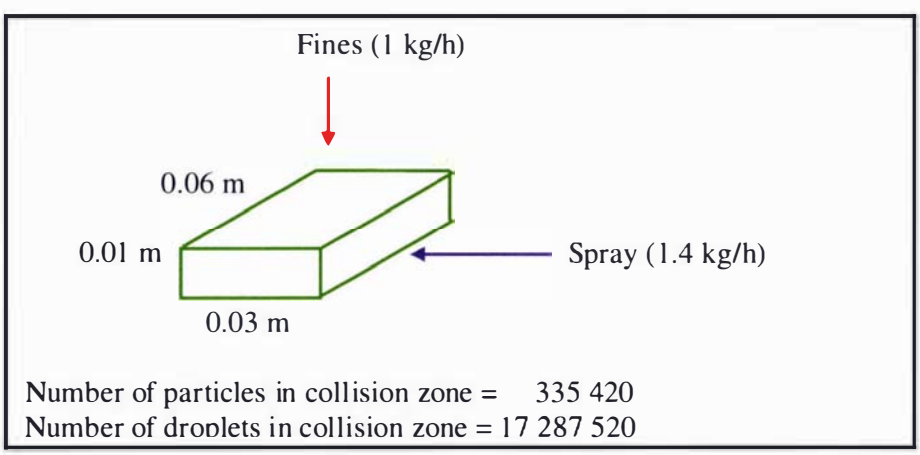

Figure R.1: Number of fines particles and spray droplets in the collision zone

Trajectory of agglomerates

A momentum balance can be used to determine the proposed product trajectory from the mass and velocity of the fines and spray prior to a collision in the contact zone. This is represented in the schematic in Figure R.2 where a, b and c can be calculated following the equations below:

Where *a* is the momentum of the spray, *b* is the momentum of the fines and *c* is the resultant momentum.

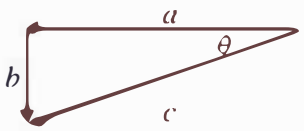

Figure R.2: Calculating the resultant momentum from the spray and fines properties

$$a = (M_s U_d) + (M_{atm} U_a) \quad \text{(R.3)}$$

$$b = (M_f U_f) \quad \text{(R.4)}$$

$$c = \sqrt{a^2 + b^2} \quad \text{(R.5)}$$

$$M_{agg} = M_s + M_f \quad \text{(R.6)}$$

$$U_{agg} = \frac{c}{M_{agg}} \quad \text{(R.7)}$$

Table R.2 Comparing spray velocities for the two-fluid nozzle

Inputs	Units	Low case with air	Low case no air	High case with air	High case no air
M_s	kg h^{-1}	1.4	1.4	2	2
U_d	m s^{-1}	7.2	7.2	7.2	7.2
M_{atm}	kg h^{-1}	0.36	0	0.66	0
U_a	m s^{-1}	30	0	50	0
M_f	kg h^{-1}	1	1	2	2
U_f	m s^{-1}	2.5	2.5	4	4
a		0.006	0.003	0.013	0.004
b		0.001	0.001	0.002	0.002
c		0.006	0.003	0.013	0.005
M_{agg}	kg h^{-1}	2.4	2.4	4.0	4.0
U_{agg}	m s^{-1}	8.8	4.3	12.0	4.1
θ	°	6.8	13.9	9.6	29.1

These calculations show that the curtain particles are removed by the spray droplets and any product is directed in a similar trajectory towards the opposite wall due to the small angle of the product stream. It is possible that some of the agglomerates formed may deposit on the chamber wall. The calculations also show that if the atomisation air could be removed from the system the spray would have less of an effect on agglomerate trajectory and the velocity of agglomerates would be reduced.

Critical Stokes

Ennis, et al. (1991) and Liu, et al (2000) have investigated collisions between two spherical particles with wetted surfaces and the forces involved. Following successful droplet-particle impact it is essential to establish what conditions are required for coalescence to occur. If it is assumed that all of the kinetic energy of the collision is dissipated in the pendular liquid bridge formed between particles the minimum velocity required for particles to rebound (or maximum velocity required for particle capture to occur) can be determined. Practically, both capillary and viscous dissipation mechanisms can occur simultaneously however viscous dissipation is dominant. The critical Stokes number for rebound is found using equation (2.27):

$$St^* = \frac{8\rho u_0 r}{9\mu} = \left(1+\frac{1}{e}\right)\ln\left(\frac{\delta}{h_a}\right) \tag{2.27}$$

where St_V = viscous Stokes' number, ρ = granule density [g cm^{-3}], u_0 = initial relative granule collisional velocity [cm s^{-1}], r = particle or granule radius [μm], μ = binder viscosity [Pa s], e = coefficient of restitution [–], δ = thickness of the liquid film on granule surface [m], and h_a = height of granule surface asperities [m].

This parameter can be used to establish the maximum velocity for a given binder viscosity and vice versa. In this case, the completely wetted spherical particles are considered an extreme case, and the coefficient of restitution is taken as 1 so particles are assumed to be rigid and perfectly elastic. This approach has many limitations (elastic, non porous wet particles, viscous effects not as large, breakage and consolidation) but is a good first step to understand the conditions that promote agglomeration.

The conditions for experiment P6 have been used as an example. First assume one drop hits a particle and covers the entire surface. The drop and particle are similar in size ($D_{4,3,p}$ = 30 μm, $D_{4,3,d}$ = 20 μm) however have different densities. If it is assumed the particle is spherical it will have a surface area = $4\pi r^2$ and the drop will have a volume = $4/3\ \pi r^3$. These two values can be used to find the thickness of the liquid layer assuming the droplet completely covers the liquid surface and does not have time to infiltrate the surface.

$$\delta = \frac{A_p}{V_d} \tag{R.8}$$

where A_p = particle surface area [m^2], V_d = volume of droplet [m^3] and δ = thickness of the liquid layer [m].

Observations of fines particle indicates that h_a the asperity height ranges from 1 to 5 micron however for the 30 μm particles investigated here they average ~ 2.5 μm. The viscosity of the binder layer is taken as the initial fluid viscosity prior to atomisation; this is measured to be 0.0147 Pa s at 50°C. The maximum velocity is predicted to be 1.5 m s^{-1} before rebound will occur, in this experiment the velocity of expected product of droplet-particle collision ~ 8.8 m s^{-1}. It is possible that the collision between wetted particles exceeded this limit.

Increasing the number of droplets to 4 per particle increases the droplet volume and therefore the thickness of the liquid layer increases the maximum velocity to 3.9 m s^{-1} before rebound occurs. However this maximum relative velocity depends on the properties of the colliding particles and the liquid layer and cannot be predicted for the distribution of different conditions that exist in reality.

If particle velocity is 8.8 m s^{-1} (calculated following the initial droplet-particle collision) a limiting viscosity can be established for one droplet of 0.0844 Pa s for capture to occur and 0.0333 Pa s for 4 droplets. This viscosity is similar to that measured for 47% total solids milk concentrate. It should be noted that the limiting viscosity is affected significantly by h_a which can only be roughly estimated.

Appendix R Agglomerate Morphology of Selected Pilot Scale Experiments

Agglomerate morphology can be assessed visually using microscopy techniques. The pilot scale experiments were characterised using both scanning electron microscopy (SEM) and stereoscope. Figure R.1 compares the stereoscope and SEM images for Run 1 and show that the stereoscope images effectively show the agglomerate structures formed more clearly than the SEMs. Images of Run 3 drier are compared in Figure R.2; both techniques demonstrate that not as many particles are present in the agglomerates compared to Run 1.

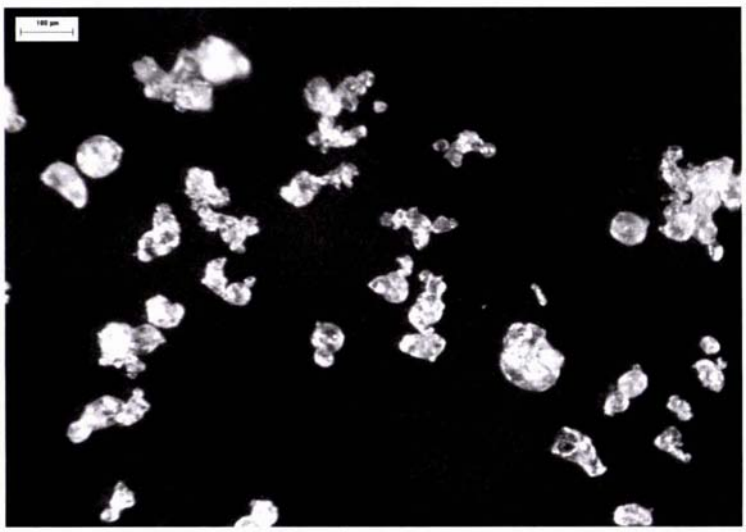

a) Run 1 stereoscope

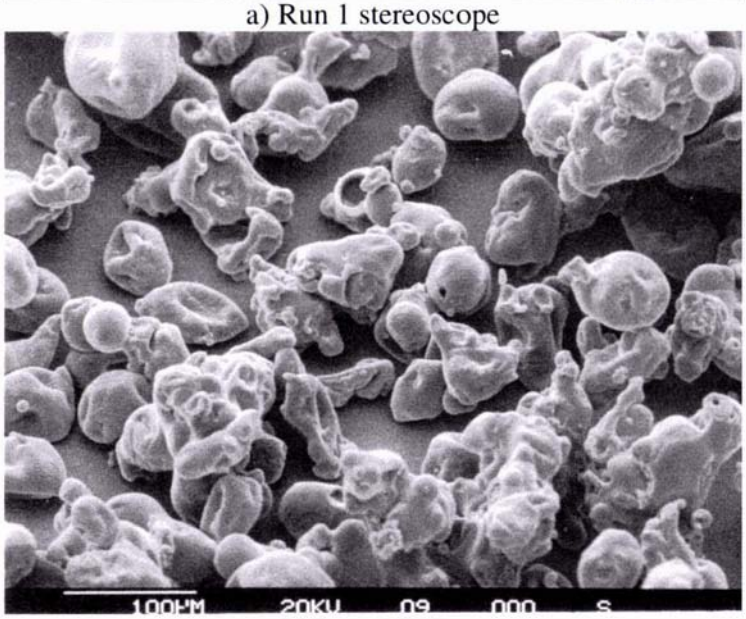

b) Run 1 SEM

Figure R.1: Comparing stereoscope and SEM images for Run 1

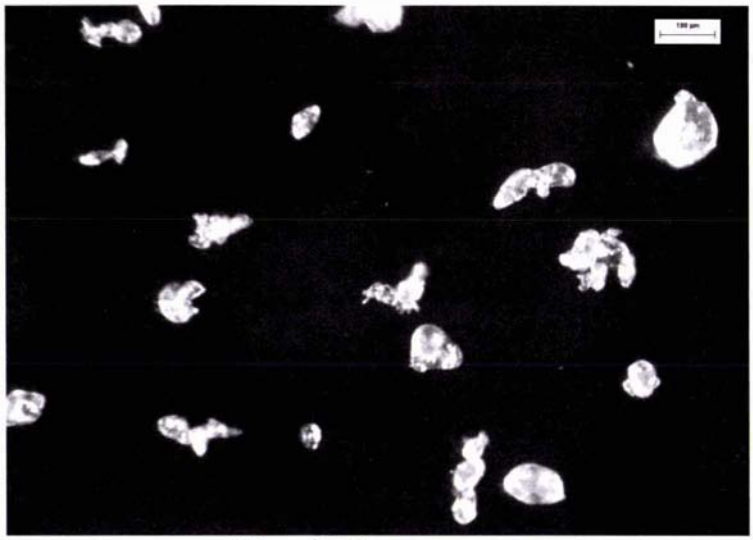

a) Run 3 drier stereoscope

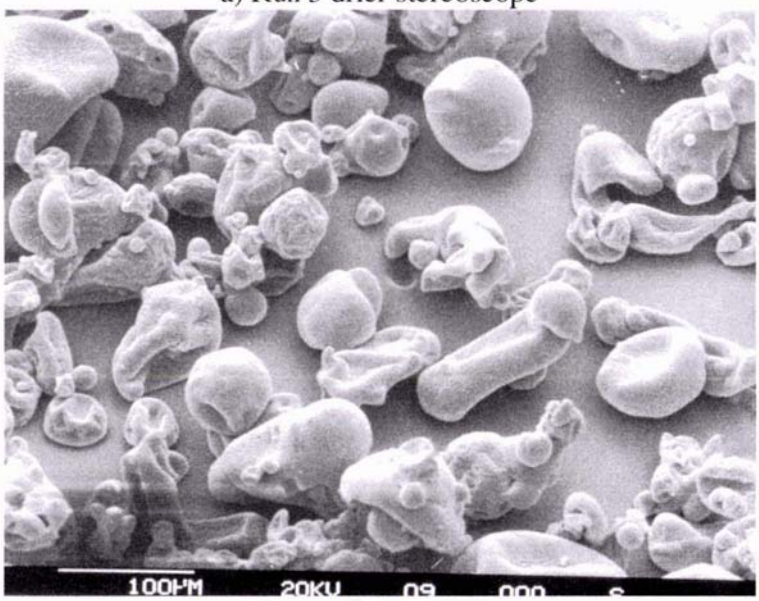

b) Run 3 drier SEM

Figure R.2: Comparing stereoscope and SEM images for Run 3 drier